Msx1 modulates the *Pax9*-null cardiovascular phenotype

Ramada Rateb Khasawneh

Submitted in accordance with the requirements for the degree of

Doctor of Philosophy

Institute of Genetic Medicine
Newcastle University

Supervisors

Dr. Simon D. Bamforth
Professor Helen M. Arthur

November 2016

ABSTRACT

Development of the aortic arch arteries from the pharyngeal arch arteries is a complex process requiring the interaction of several tissue types and tightly regulated gene expression during embryogenesis. In this work, the role of transcription factor *Pax9* in cardiovascular development was investigated using transgenic mice, imaging techniques and gene expression analysis. *Pax9* is specifically expressed in the pharyngeal endoderm at mid-embryogenesis, and *Pax9*-null mice die at birth from defects in the formation and remodeling of the 3rd and 4th pharyngeal arch arteries resulting in absent common carotid arteries, aberrant right subclavian artery and interrupted aortic arch.

The aim of the work presented in this thesis was to identify genes that potentially acting in the same genetic regulatory network as *Pax9* to control cardiovascular development. The transcription factor *Msx1* was selected as this was shown to interact with *Pax9* in tooth development, and transgenic mice lacking *Msx1* and *Msx2* display cardiovascular defects. Surprisingly, this analysis shows that mice simultaneously null for *Pax9* and heterozygous for *Msx1* have a significantly reduced incidence of aortic arch defects compared to *Pax9*$^{-/-}$ mice. Although Pax9 and Msx1 proteins can interact during tooth formation, the expression of these two genes does not overlap in the pharyngeal arches, with *Msx1* being expressed in neural crest cells.

Immunohistochemistry labelling revealed that more neural crest cells were present within the 3rd pharyngeal arch of *Pax9*$^{-/-}$*;Msx1*$^{+/-}$ embryos compared to *Pax9*$^{-/-}$ embryos, which suggesting a role for these cells in protecting the 3rd pharyngeal arch artery from regressing as observed in *Pax9*$^{-/-}$ embryos. In addition, a thick layer of smooth muscle around the 3rd PAA in *Pax9*$^{-/-}$*;Msx1*$^{+/-}$ embryos compared to *Pax9*$^{-/-}$ embryos was observed, , all together indicating that neural crest cells differentiate to smooth muscle in *Pax9*$^{-/-}$*;Msx1*$^{+/-}$ embryos and this help protect and support the 3rd PAA during remodeling.

Our data therefore show that *Msx1* heterozygosity appears to modulate the *Pax9*-null cardiovascular phenotype by a yet unrecognized mechanism.

ACKNOWLEDGEMENTS

Firstly, I would like to express my sincere gratitude to my supervisor Dr. Simon Bamforth for the continuous support of my Ph.D study and related research, for his patience, motivation, and immense knowledge. His guidance helped me in all the time of research and writing of this thesis. I could not have imagined having a better advisor and mentor for my Ph.D study. Additionally I would like to thank Prof. Helen Arthur for all her guidance in the project.

My sincere thanks also goes to Dr. Helen Phillips, Dr. Gavin Richardson, Dr. Alberto Briones-Leon, Dr. Rebecca Dodds, Kate Bailey, Ahlam Alqahtani, Catherine Stothard, Dr. Silvia Mazzotta and Emily Dookun for their continued help and support, for the stimulating discussions, and for their friendship. Also, I would like to extend this thanks to all, past and present, members of the Hanger Lab.

I would like to thank my family to whom I owe a great deal. To my late father Rateb, thank you for showing me that the key to life is enjoyment and patience, thank you for all your support. To my mother, who supported me all the way and allowed me to follow my dream. To my brothers and sister Rami, Raeda, Ronza, Razan and Riyed for supporting me throughout my life in general, thank you for putting your inheritance from our father at risk to allow me to get the scholarship from Yarmouk University; for that I am in your debt forever.

I have also had the good fortune to meet an amazing person: my husband Nedal, who stood next to me in my hardest time and who at opportune times offered me his wise counsel. I love you now and forever, thank you for being part of my life, thank you for being you.

Finally, I dedicate this thesis to my unborn child, may god bless you throughout your entire life.

ABBREVIATIONS

22q11DS	22q11 deletion syndrome
α-sma	α-smooth muscle actin
Ao	Aorta
AoA	Aortic arch
AD	Arterial duct
AP2α	Activator protein 2 α
ARSA	Anomalous right subclavian artery
ASD	Atrial septal defect
AV	Atrioventricular
BAV	Bicuspid aortic valve
BiFCo	Bimolecular fluorescence complementation assay
bp	Base pairs
BC	Brachiocephalic artery
B6-*Pax9*$^{+-}$	*Pax9*$^{+/-}$ mice on a congenic B6 background
cAo	Cervical aortic arch
CAT	Common arterial trunk
CD1-*Pax9*$^{+/-}$	*Pax9*$^{+/-}$ mice on a congenic CD1 background
CCVM	Congenital cardiovascular malformation
CHD	Congenital heart defects
cDNA	Complementary deoxyribose nucleic acid
cNCC	Cardiac neural crest
CP	Cleft palate
cRSA	Cervical origin of the right subclavian artery
Ct	Cycle threshold
dAo	Dorsal aorta
DEPC	Diethyl pyrocarbonate
ddH_2O	Double distilled water
DGS	DiGeorge syndrome
DIG	Digoxygenin
dNTP	Deoxyribonucleotide triphosphate
DORV	Double outlet right ventricle

E	Embryonic day
EDTA	Ethylenediaminetetraacetic acid
ES cells	Embryonic stem cells
EtBr	Ethidium bromide
eLCA	External left carotid artery
eRCA	External right carotid artery
FBS	Foetal bovine serum
FHF	First heart field
GAPDH	Glyceraldehyde 3-phosphate dehydrogenase
Gd-DTPA	Gadopentetate dimeglumine
H_2O_2	Hydrogen peroxide
H&E	haematoxylin and eosin
HCl	Hydrochloric acid
IAA	Interrupted aortic arch
IVC	Interventricular communication
IVS	Interventricular septum
iLCA	Internal left carotid artery
iRCA	Internal right carotid artery
JEG3 cells	Human placental choriocarcionoma cells
KCl	Potassium chloride
kDa	Kilo Dalton
LA	Left atrium
LB	Luria Bertani
LCC	Left common carotid
LiCl	Lithium chloride
LSA	Left subclavian artery
LV	Left ventricle
Mb	Mega base pair
$MgCl_2$	Magnesium chloride
MRI	Magnetic resonance imaging
n	Number
NaCl	Sodium chloride
NaOH	Sodium hydroxide

NCC	Neural crest cells
NGS	Normal goat serum
OFT	Outflow tract
P	Postnatal day
PA	Pulmonary artery
PAA	Pharyngeal arch artery
Pax	Paired box genes
Pax9$^{\Delta PE}$	*Pax9* deleted from the pharyngeal endoderm
PBS	Phosphate-buffered saline
PBT	Phosphate-buffered saline with Tween-20
PCR	Polymerase chain reaction
PFA	Paraformaldehyde
PT	Pulmonary trunk
PTA	Persistent truncus arteriosus
PVDF	Polyvinyl difluoride
PgE2	Prostaglandins E2
PgI2	Prostaglandins I2
qPCR	Quantitative polymerase chain reaction
RA	Right atrium
RCC	Right common carotid
RIPA	Radioimmunoprecipitation assay buffer
RNA	Ribose nucleic acid
RSA	Right subclavian artery
RV	Right ventricle
SDS	Sodium dodecyl sulphate
SHF	Secondary heart field
SSC	Saline Sodium Citrate
TAE	Tris-acetic acid-EDTA buffer
TBST	Tris-buffered saline with Tween-20
TBS-TX	Tris-buffered saline with Triton-X 100
TE	tris-EDTA buffer
TOF	tetralogy of Fallot
Tm	Melting temperature

V	Volts
VEC	Venus C terminal
VEN	Venus N terminal
VSD	Ventricular septal defect
v/v	Volume per volume
WB	Western blot
w/v	Weight per volume
WISH	Whole mount in situ hybridisation
YFP	Yellow fluorescent protein
µCT	Microcomputer tomography scan

Table of Contents

List of Figures

List of Tables

1 INTRODUCTION

1.1 HEART DEVELOPMENT IN MOUSE

Congenital heart defects (CHD), in which part of the heart fails to form properly before birth, are the most common type of birth defect. They cause changes to the normal flow of blood through the heart and occur in approximately 1% of the newborn as a result of genetic variations, environmental exposures, and other factors.

Heart development, or cardiogenesis, is the process by which the heart develops from the earliest specification of cardiac cells to the final four chambered heart, pumping blood through the body. Any deviation from the normal course results in a disastrous form of disease. Therefore, understanding normal heart development is important in order to understand CHD and the mechanisms involved in their etiology and pathogenesis.

The cardiovascular system is the first major system to become functional during early embryogenesis as it is required for providing oxygen and nutrients to the developing embryo. The heart is a muscular organ that pumps blood through blood vessels and into tissue via two circulatory systems; the pulmonary circulation, which takes deoxygenated blood to the lungs to be oxygenated; and the systemic circulation, which carries oxygenated blood to the various body tissues. It is important to understand heart development since a functional heart during early embryonic life is developed in order to support the growing embryo.

Heart organogenesis is a complex process starting with the formation of a grooved structure called primitive streak, within the epiblast at the posterior end of the embryo (Lawson and Schoenwolf, 2003). At around embryonic day 6 (E6) of the mouse development, the gastrulation process begins. The first mesodermal cells to migrate through the primitive streak are cells fated to become the heart (Garcia-Martinez and Schoenwolf, 1993; Psychoyos and Stern, 1996). These mesodermal cells migrate anteriorly and bilaterally to form bilateral paired cardiogenic plates or cardiogenic

area (Garcia-Martinez and Schoenwolf, 1993). Progeny of cells from this region will contribute to all layers of the heart tube, including endocardium, myocardium, and parietal pericardium (Lopez-Sanchez and Garcia-Martinez, 2011).

The origins of the heart tube are clusters of angiogenic cells, which are located in the cardiogenic plate. Cells of the cardiogenic area will arrange as longitudinal cellular strands called cardiogenic cords. The cords become canalized to form two thin walled endothelial tubes called endocardial heart tubes. As the lateral folds develop, the endocardial heart tubes gradually approach each other and coalesce to form a cardiac crescent in the midline of the embryo at E7.5 (Christoffels *et al*., 2000). The cardiac crescent then forms a linear tube at E8, at this stage the tube begins to beat (Figure 1-1). The cardiac progenitors cells present at the cardiac crescent, which give rise to the linear heart tube are called first heart field cells (FHF) (Garcia-Martinez and Schoenwolf, 1993).

The primitive heart tube is the first recognizable cardiac structure in all vertebrates (Lee *et al.*, 1994); it consists of an inner cell layer of endothelium (the primitive endocardium) and a single outer layer of myocardium, separated by an acellular layer of extracellular matrix, also known as the cardiac jelly.

At this stage, the heart can be subdivided into inflow tract, outflow tract, and a primitive-ventricular region and several regions in the heart tube can be distinguished. Starting from the venous pole, the heart tube consists of the sinus venosus, which is the inflow region, receiving blood from the veins and moving it to the primitive heart. Blood then flows from the truncus arteriosus, the outflow region, into the pharyngeal arches (Figure 1-2) (Mjaatvedt *et al.*, 2001; Savolainen *et al.*, 2009).

In order for the mature heart to form, myocardial cells from a second cardiogenic area contribute to the atrial pole development and the lengthening of the outflow tract. This myocardial progenitor field is located posterior to the dorsal wall of the developing pericardial cavity and it is known as the secondary heart field (Kelly *et al.*, 2001; Waldo *et al.*, 2001). Progenitors from the second heart field will later be incorporate into the inflow and outflow tract, the right ventricle and both atrial chambers (Meilhac *et al*., 2004).

The heart tube grows rapidly in length and looping to the right is observed to form the basic shape of the heart at E8.5. Through this process two loops are formed, with the cephalic portion of the tube bends in the ventral and caudal directions to the right, while the caudal atrial portion shifts in dorso-cranial direction to the left. By E10.5 the primary heart tube, now within the pericardial cavity, can be divided into atrial and ventricular components along with an inflow and outflow tracts (Figure 1-1) (Hiruma *et al*., 2002; Savolainen *et al.*, 2009).

In the inner heart wall of the atrioventricular canal and in the common outflow tract, localized swelling will arise to form the cardiac cushions at E9.5, which will participate in the septation of the heart (Mjaatvedt and Markwald, 1989). This process is necessary to produce the four heart chambers and for valve formation. Septation allows the remodeling of the heart from a single channel pump to four chambers. The dorsal and ventral atrioventricular cushion fuse to form the atrioventricular septum that separates atria from ventricles. Contrarily, the septation of the common atria and the common ventricle is much a more complex process (Savolainen *et al.*, 2009).

Myocardial development begins when the primitive heart tube is composed of an inner endothelial and outer myocardial cell layer. It is a process involving the formation of two different myocardial layers within the ventricular wall, the trabecular layer, and the subepicardium compact layer. After looping, the myocardial layer develops trabeculations to form a network of luminal projections called trabeculae; which consist of myocardial cells covered by the endocardial layer to increase surface area. This allows greater nutrient delivery to the growing myocardium in the absence of a coronary circulation (Liu *et al.*, 2010). Later the trabecular myocardium undergoes compaction. Further thickening and organization of the compact layer occurs during the later stages of gestation to form the architecture of the mature, multilayered myocardium (Sedmera and McQuinn, 2008).

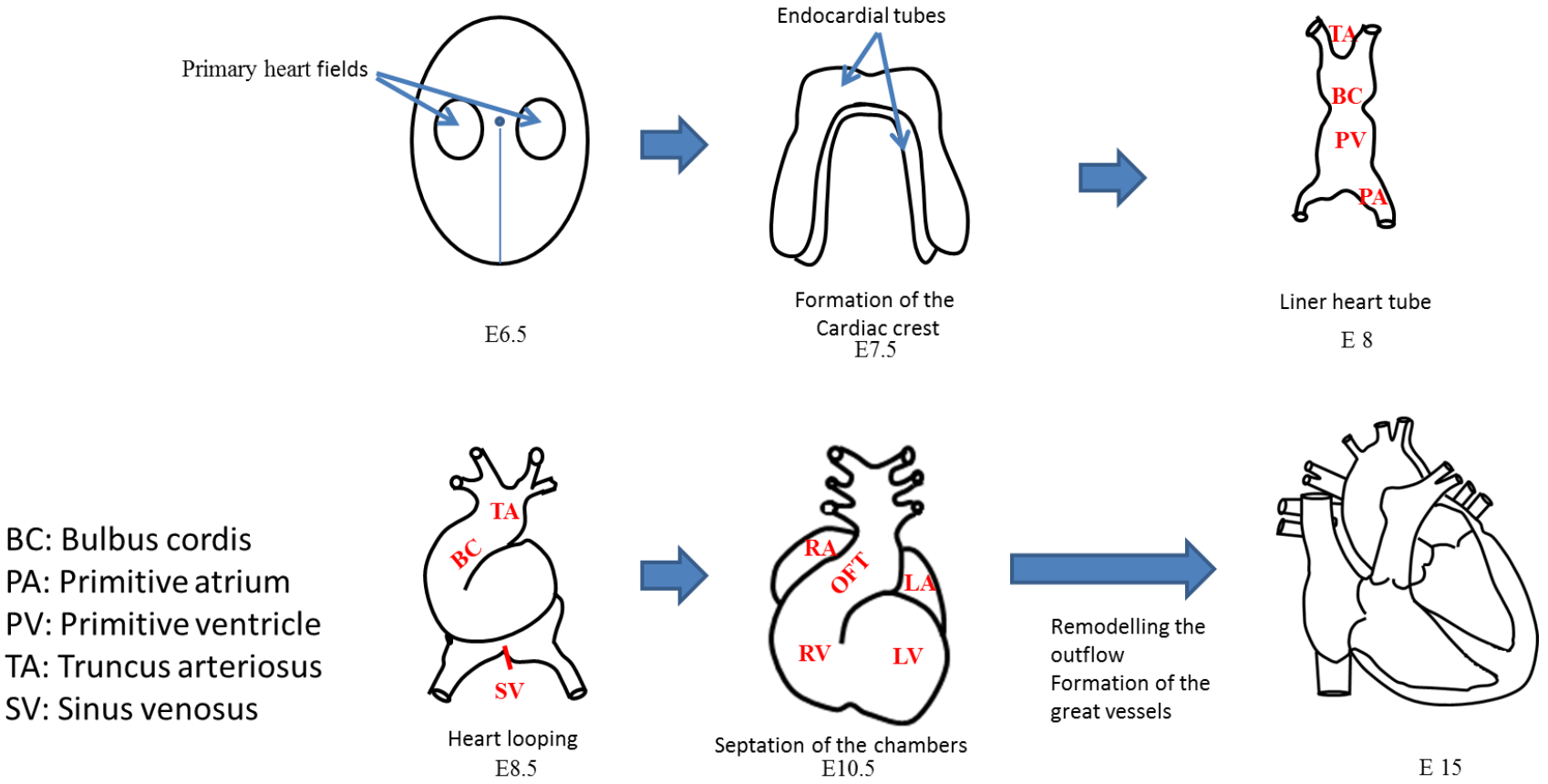

Figure 1-1: Stages of heart development.
At E6.5, myocardial progenitor cells derived from the primitive streak form the two cardiac plates. At E7.5, these two plates will form two elongated tubes, which will move closer to each other and fuse at the midline giving rise to a beating heart tube at E8. At E8.5, the linear tube bends rightward, and at the same time the atrial and ventricular chambers are formed along the outer curvature of the heart. At E14.5, the heart shows four fully septated chambers and a septated outflow tract connected to the pulmonary trunk and the dorsal aorta. By E15, the pulmonary trunk begins at the base of the right ventricle, and then branches into two pulmonary arteries, which deliver deoxygenated blood to the corresponding lung. The oxygenated blood enters the left atrium through the pulmonary veins, then the left ventricle pump the blood through the aorta to the systemic circulation. Adapted from (High and Epstein, 2008)
AOA, arch of aorta; AP, atrial pole; DA, ductus arteriosus; LA, left atrium; LV, left ventricle; RA, right atrium; RV, right ventricle; VP, ventricular pole.

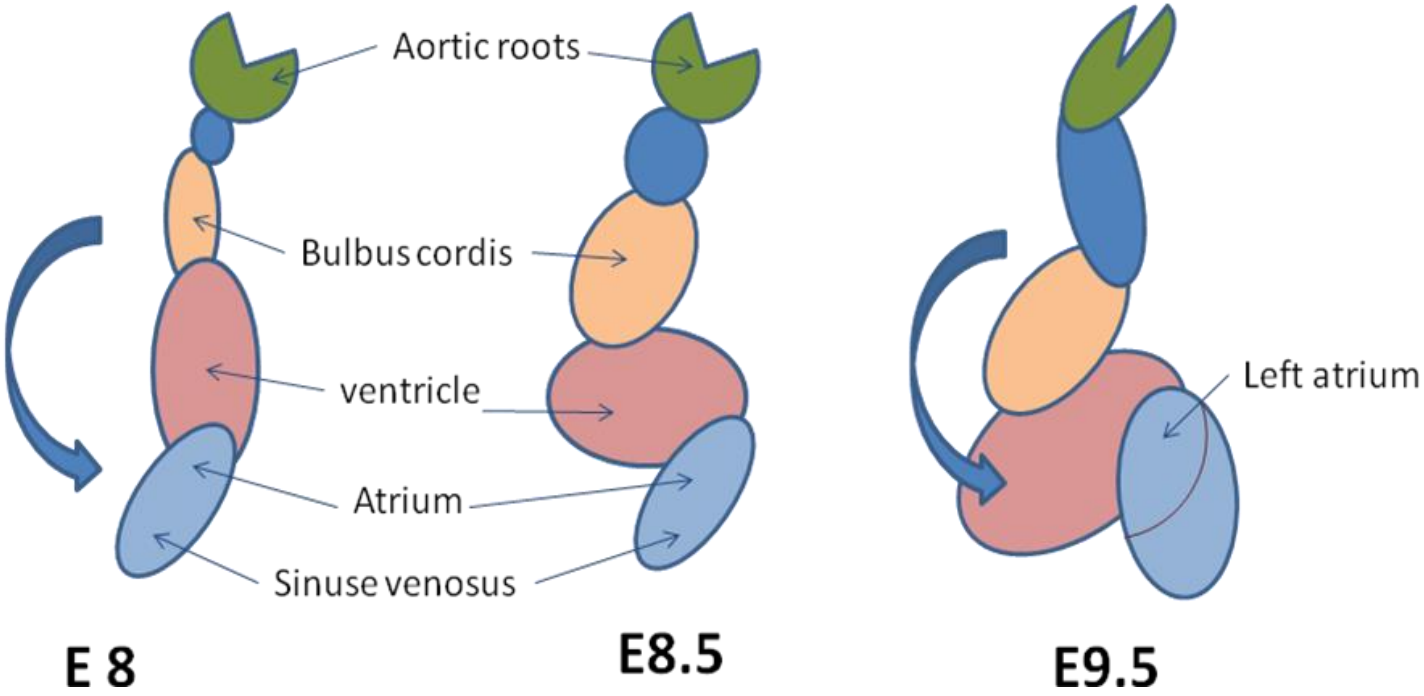

Figure 1-2 : Schematic representation of the heart tube undergoing the process of looping.
This illustration shows the heart undergoing the process of looping. At E8.0, cells from the cardiac crescent migrate to form a straight tube called the linear heart tube, which begins to elongate with simultaneous growth in the bulbus cordis and primitive ventricle. This will force the heart tube to start a rightward looping at E 8.5, this rotation will bring the bulbus cordis to the right, the venous pole will moves anteriorly, and the truncus arteriosus branches into aorta and pulmonary artery. At E9.5 the heart looping will bring atrial and ventricular chambers to their final position where the right ventricle lies anteriorly and the left atrium with the left ventricle lies posteriorly. As the heart develops, the sinus venosus becomes incorporated into the atrium, and the bulbus cordis becomes incorporate into the ventricle. Adapted from (Männer, 2009).

1.1.1 THE SECOND HEART FIELD

At mid-embryogenesis, the heart tube elongates by addition of progenitor cells to the arterial and venous pole. This group of cardiac precursor cells are known as the second heart field (SHF). They originate from the splanchnic mesoderm at the attachment site of the dorsal mesocardium (Waldo *et al.*, 2001) and reside in the anterior pharyngeal mesoderm during heart formation. These cells migrate and expand into cardiac chambers and the outflow tract after initial heart tube formation (Meilhac *et al.*, 2004).

The SHF can be identified by stage E7.5 in mice (Meilhac *et al.*, 2004). It is part of the cardiogenic fields but it segregates and contributes progressively to the growth of the heart after the linear heart tube stage when looping has started (Buckingham *et al.*, 2005; Mjaatvedt *et al.*, 2001; Waldo *et al.*, 2001).

It constitutes a source of myocardial precursor cells that gives rise to both the most distal outflow tract myocardium and the most proximal smooth muscle that forms the tunica media of the aortic sac (Savolainen *et al*., 2009). This lengthening of the primary heart tube appears to be an important process for the proper alignment of the inflow and outflow tracts prior to septation. If this process does not occur normally, ventricular septal defects and malpositioning of the aorta may occur (Kirby, 2002).

The SHF contributes to the endocardium of the right ventricle and proximal OFT, the smooth muscle of the OFT, and participates in the formation of both atria (Figure 1-3). Inside the heart, the SHF gives rise to the myocardium, endocardium and smooth muscle cells (Moretti *et al.,* 2006). Disturbances in the SHF during the early stage of their movement into the heart leads to congenital heart defects (Francou *et al.*, 2013; Meilhac *et al.*, 2004).

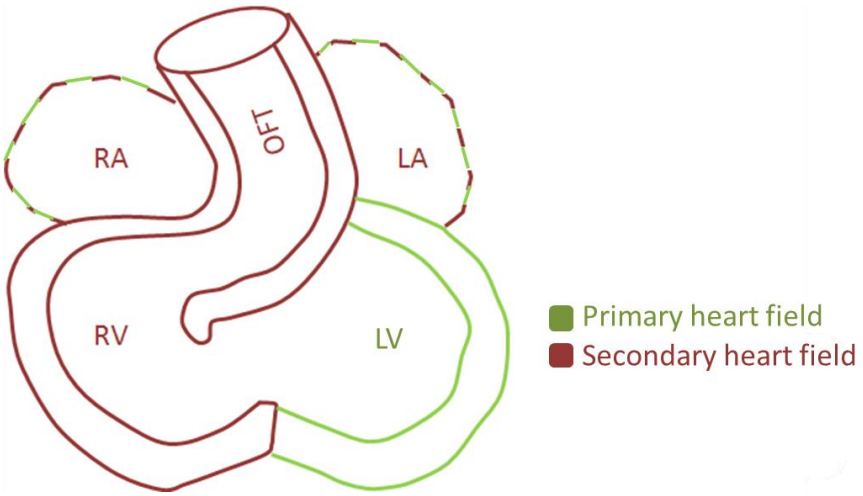

Figure 1-3: Schematic representation of the contribution of first (FHF) and second heart fields (SHF) to the developing heart.
SHF cells contribute to the formation of the OFT, the future right ventricle (RV), and participate in the formation of both atria (RA, LA). Conversely, the FHF forms the left ventricle (LV) and participates in the formation of the atria.

1.1.2 CARDIAC NEURAL CREST CELLS

The cardiac neural crest (cNCC) is an extracardiac population of cells that arises from the neural tube in the region of the first three somites up to the mid-otic placode level. cNCC migrate ventrally then pause in the circumpharyngeal ridge before continuing into the pharyngeal arches 3, 4, and 6 as each arch forms sequentially (Figure 1-4). Eventually the cNCC migrate into the developing outflow tract of the heart.

cNCC are necessary for the aorticopulmonary septation complex, and they form both the aortopulmonary and conotruncal portions of the outflow septation complex (Kirby and Waldo, 1990; Kramer, 1942). Moreover, cNCC surround the endothelial cells which form the arches arteries and help their patterning (Kuratani and Kirby, 1992). However, cNCC are not required for aortic arch artery formation, but only for its remodeling, since they will form the smooth muscle tunica media of the arteries (Bergwerff *et al*., 1998; Waldo *et al*., 1996). cNCC are also necessary for the formation of the anterior parasympathetic plexus, which contributes to cardiac innervation and the regulation of heart rate (Kirby *et al.*, 1983; Kirby *et al.*, 1985).

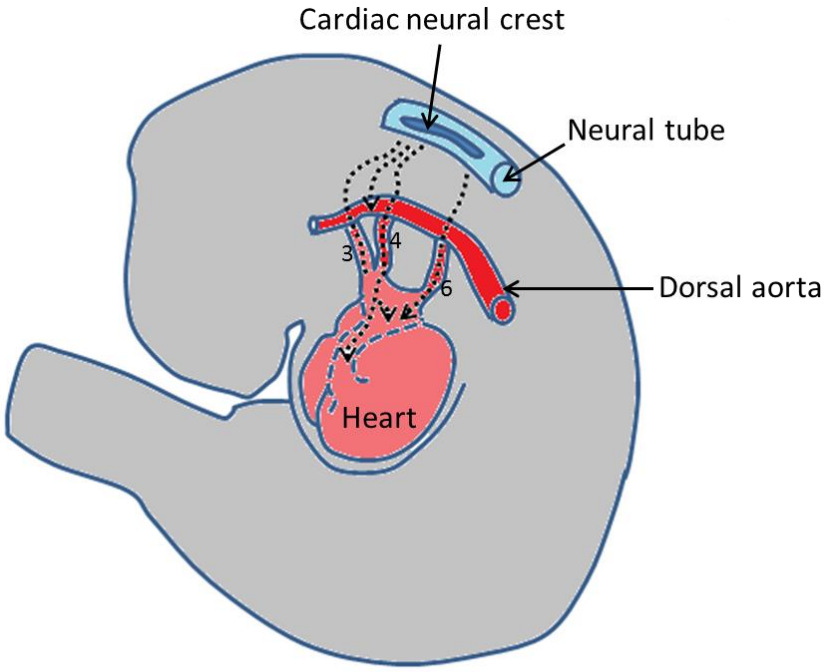

Figure 1-4: Schematic representation of the migration and distribution of cardiac neural crest cells (cNCC).
cNCC are multipotent migratory cells originate from the level of the otic placode and the third somite, and migrate through the pharyngeal arches 3, 4 and 6 to the outflow tract of the heart. Adapted from (Hutson and Kirby, 2007).

1.2 OUTFLOW TRACT DEVELOPMENT AND SEPTATION

The outflow tract (OFT) is a vital connection situated between contracting muscular heart chambers and a vast embryonic vascular network. Anatomical knowledge of the OFT can contribute to the understanding of the spectrum of complicated anomalies that arise from abnormal formation of the major vessels in this region.

The mature OFT is a short conduit derived from the SHF (Bajolle *et al*., 2006). During heart tube elongation, progenitors myocardium cells population derived from the SHF is progressively added to the arterial pole of the heart (Kelly *et al*., 2001; Waldo *et al.,* 2001). During OFT formation the arterial pole of the heart is displaced caudally in the pharyngeal region as pharyngeal arch morphogenesis and the formation of bilateral aortic arch arteries take place (Waldo *et al*., 2005). cNCC cells, derived from the dorsal neural tube, migrate through the caudal pharyngeal arches

into the OFT of the heart during formation of the distal region of the OFT (Hutson and Kirby, 2003).

The OFT begins as a single tube that connects the right and left ventricles to the pharyngeal arch arteries. The OFT can be further subdivided into a proximal region close to the ventricle and distal region close to the aortic sac, separated by a characteristic landmark called the dog-leg bend as a boundary between the two regions (Webb *et al.*, 2003).

Septation of the OFT also involves interactions between diverse cell types, including myocardium, endocardium, and cNCC (Waldo *et al.*, 2005). As described in section 1.1, during early embryogenesis the heart forms as a bi-layered tube. Within this tube, an acellular, extracellular matrix called “cardiac jelly” separates the myocardial and endocardial layers. Immediately following looping of the heart tube, the cardiac jelly expands, and concentrates itself into pairs of cushions lining the outflow tract.

Within the aortopulmonary septum are ridges of tissue that separate the 4th and the 6th aortic arches. The truncus ridges are formed at the area where the semilunar valves are destined to be formed, therefore forming the septum between the ascending aorta and the main pulmonary artery. The conus ridges form just below the semilunar valve and form the septation between the right and the left ventricular outflow tract (Van Mierop, 1979).

By E11.5 there is a rapid increase in the number of the cNCC, as a consequence of their migration into the outflow tract cushions and proliferation of the cells that are already in the cushions (Hutson and Kirby, 2007). The cNCC pack the distal outflow tract cushions and the dorsal wall of the aortic sac.

The four cushions from the outflow tract and from the aortic sac grow towards each other at a 180° angle. As the cushions grow and develop myocardium they fuse in a distal-to-proximal direction, resulting in the formation of the helical aorticopulmonary septum. This process will initiate OFT separation, and separation of the systemic circulation and the pulmonary circulation by forming a forming a spiral septum (Anderson *et al.,* 2003). This allows the cleavage of the distal portion of the OFT into aorta and pulmonary trunk. In addition, the spiraling nature of the cushions causes the pulmonary trunk to twist around the aorta (Figure 1-5). At this stage the OFT is

separated, with the aorta arising from the right- hand side and connecting to the left ventricle and the pulmonary trunk on the left-hand side connecting to the right ventricle. The formation of the aorta and the pulmonary artery involves the 4th and 6th aortic arches, respectively (Anderson *et al.*, 2012; Hurle *et al.*, 1980).

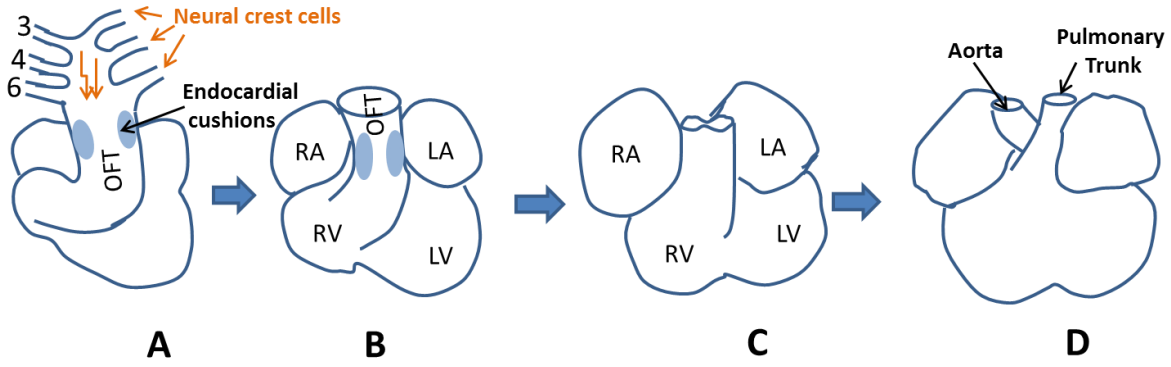

Figure 1-5: Schematic representation of the remodeling of the outflow tract (OFT). At E11.5 the OFT is connected to the 3rd, 4th, and 6th pharyngeal arch arteries (**A**), Following rightward looping of the heart tube, endocardial cushions form in the outflow tract (OFT) which are the precursors of the aorticopulmonary valves (**A, B**) also cardiac neural crest cells migrate into the OFT from the neural folds to septate the outflow **(A)**. At E14.5 the OFT septation is complete and the aorta is connected to the left ventricle and pulmonary trunk to the right ventricle **(D)** (Bajolle *et al.*, 2006).

1.3 PHARYNGEAL ARCH ARTERIES

1.3.1 DEVELOPMENT OF THE PHARYNGEAL ARCHES

The development of the vertebrate is a highly complex process involving tissues derived from all three germ layers whose development must be coordinated to generate the functional adult apparatus. Pharyngeal arches are bilaterally symmetric ventral structures that develop in a segmental fashion along the anteroposterior axis during embryogenesis (Graham, 2001; Hiruma *et al.*, 2002).

Five pairs of arches form during development, numbered 1-4 and 6, with however only four pairs of these arches visible externally (1-4). The 5th arch occasionally develops transiently and then is lost, it becomes part of the 4th pouches contributing to the thyroid formation. During embryogenesis, the pharyngeal arches enlarge to form a multitude of structures.

During the evolution of the vertebrate animals, the number of the pharyngeal arches reduces as some pharyngeal arches loss segmentation in the adult form, this lead to the reduction of the number of the blood vessels associated with it. This may be because the vertebrate no longer needs the structure formed by this arch, which may explain why human and mice do not have 5th pharyngeal arch.

The 6th pharyngeal arch remains rudimentary and not visible on the surface of the embryo (Grevellec and Tucker, 2010).

The pharyngeal arches consists of mesenchyme derived from the lateral plate mesoderm, covered externally by ectoderm and lined internally by endoderm (Graham, 2001). NCC migrate into the pharyngeal arches and surround the central core of the mesenchymal cells (Kameda, 2009). The mesenchyme will form muscles, arteries, connective tissue, cartilage and bones.

Fissures, called pharyngeal grooves or clefts, separate the pharyngeal arches from each other. These fissures are clefts between adjacent arches, they transient in nature (Graham, 2008). Only the 1st pharyngeal groove gives rise to a permanent structure; the external auditory meatus. The 2nd, 3rd, and 4th grooves are rapidly covered by a large outgrowth of the 2nd pharyngeal arch, the hyoid operculum, and obliterated (Graham, 2008).

As development continues, the endoderm inside of the pharyngeal apparatus invaginates to form pouches between the arches (Figure 1-6), which is the main event for the development of the pharyngeal arches.

The endoderm pouches are also transient in nature and give rise to many important structures. Since there are five pharyngeal arches, there are four pharyngeal pouches. The first pouch gives rise to the middle ear and the auditory tube (Mallo, 2001). The second pouch will form the palatine tonsil. The third pouch will form the inferior parathyroid glands and the thymus. The fourth and final pouch will form the superior parathyroid glands and the ultimobranchial bodies (Cordier and Haumont, 1980; Grevellec and Tucker, 2010).

It was shown that NCC play a less significant role than previously believed and that the endoderm is a major player in organizing pharyngeal development (Graham *et*

al., 2005; Graham and Richardson, 2012). The pharyngeal pouches will form and contact the ectoderm in the absence of NCC (Crump *et al.*, 2004). These pharyngeal segments are regionalized and have a sense of identity (Veitch *et al.*, 1999), which suggests that the NCC play a less important role than previously expected and that the endoderm plays the major role in the development of the pharyngeal arch.

In the pharyngeal arches, there are arteries, which connect the aortic sac at the distal end of the cardiac outflow tract with dorsal aorta; these are called the pharyngeal arch arteries (PAA; Figure 1-6).

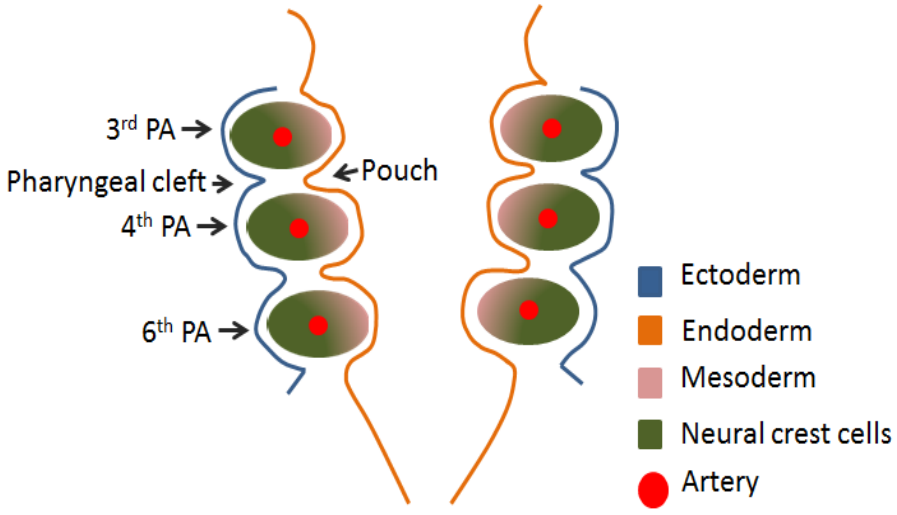

Figure 1-6: Schematic representation of the pharyngeal arches.
The pharyngeal arches consist of three layers; endoderm, ectoderm and mesoderm. Each arch has a specific nerve and blood vessel, the nerve will innervate the muscles that develop around the vessel; and a proportion of these arteries will form the adult vessels.

1.3.2 DERIVATIVES OF THE PHARYNGEAL ARCHES

The first three pharyngeal arches contribute to structures above the larynx, whereas the 4th and 6th pharyngeal arches contribute to the larynx and trachea (Waldo *et al.*, 1996)

The 1st arch will develop into maxillary and mandibular swellings, which will give rise to the midline of the face and lower face respectively (Table 1-1). The cartilage of the 1st arch in the maxillary swelling will form the incus (middle ear ossicle) and the alisphenoid (a small part of the greater wing of the sphenoid bone). The principal cartilage of the 1st arch, Meckel's cartilage, is a rod in the mandibular swelling. It will form the malleus (a second ossicle of the middle ear), and two ligaments, the sphenomandibular and anterior malleolar ligaments. The remainder of Meckel's cartilage disappears without a trace (Mallo, 2001). The musculature of the 1st pharyngeal arches form the muscle of mastication. The 1st pharyngeal pouches expand into an elongated tubotympanic recess and forms the endoderm that lines the future Eustachian tube, middle ear, mastoid antrum, and the inner layer of the tympanic membrane (Mallo, 2001).

The dorsal end of the 2nd arch (Table 1-1) cartilage, called Reichert's cartilage, ossifies to form the stapes (third ossicle of the middle ear) and the styloid process of the temporal bone. The ventral end of the 2nd arch cartilage ossifies to form the lesser horns of the hyoid bone, and will also form one ligament, the stylohyoid ligament. The musculature of the second pharyngeal arches will form the facial expression muscles. The pouches of the 2nd pharyngeal arches will differentiate into lymphatic tissue, which soon organizes into the lymphatic nodules of the palatine tonsil (Grevellec and Tucker, 2010).

The 3rd arch (Table 1-1) cartilage contributes to the hyoid body, the greater horns and the lower body of the hyoid. The musculature of the 3rd pharyngeal arches will form the stylopharyngeus muscle. The dorsal bulbar part of the cranial region of the third pharyngeal pouches will differentiate into the inferior parathyroid gland and the ventral part will form the thymus epithelium (Grevellec and Tucker, 2010).

The 4th and 6th arch (Table 1-1) cartilage contributes to the laryngeal cartilage, except the epiglottis. The musculature of the 4th and the 6th pharyngeal arches will form the cricothyroid and constrictors of the pharynx and the intrinsic muscle of the larynx respectively. The dorsal part of the 4th pouch forms a second pair of parathyroid glands known as the superior parathyroids (Hilfer and Brown, 1984).

The 5th pharyngeal arch is rudimentary and has no derivatives. The rudimentary 5th pharyngeal pouch becomes part of the 4th pharyngeal pouch and helps to form the ultimobranchial bodies (Hilfer and Brown, 1984).

Table 1-1: The fates of the pharyngeal arches and their derivatives.

Derivates from The Pharyngeal Cleft	PA Number	Aortic Arch	Cranial Nerve	Muscles	Skeletal Derivate	Derivates of Pharyngeal Pouch
External auditory meatus 1 2 3 4	1	Maxillary artery	Trigeminal	Muscle of mastication	-Meckel's cartilage -Malleus, incus -sphenomandibular and anterior malleolar ligaments	1 -Middle ear -Auditory tube
	2	Stapedial artery	Facial	Facial expression muscles	-Reichert's cartilage - Stapes -styloid process -stylohyoid ligament	2 Lymphatic nodules of the palatine tonsil
	3	common carotid arteries	Glosso-pharyngeal	Stylopharyngeus muscle	-Great horn of the hyoid -Part of the body of the hyoid	3 -Thymus -Inferior parathyroid gland
	4	-Right subclavian artery -Arch of aorta	Vagus	Pharynx and the intrinsic muscle of the larynx	Laryngeal cartilage	4 -Superior parathyroid glands -Ultimobranchial bodies

1.3.3 THE PHARYNGEAL ARCH ARTERIES

The pharyngeal arches develop around E8.5 to E9.0 (12 somite stage). Each arch contains an artery, called a pharyngeal arch artery (PAA), embedded in the mesenchyme. The PAA travels through the center of each pharyngeal arch (Graham, 2001; Hiruma *et al.,* 2002). There are five pairs of PAA extending from the aortic sac to the dorsal aorta at the distal end of the cardiac outflow (Figure 1-7).

The formation and transformation of the primitive aortic arches artery into mature blood vessels in the mouse occurs from E8.5 to E13.5 of gestation. The six paired vessels are not all present at the same time; instead they appear in a sequence moving toward the caudal end of the body. The 1st pair of PAA appear at E8.5 (12 somite stage), and develop as a loop between the bilaterally paired dorsal and ventral aorta. By late E9-9.5 the 2nd PAA appear as a sprout from the dorsal and ventral aorta and becomes fully formed at E9.5 stage (Figure 1-7). The 1st and the 2nd PAA will regress before E10.5 and the remaining parts will form the maxillary artery and the stapedial artery respectively (Hiruma *et al*., 2002). The 5th PAA appears to only exist transiently during embryologic growth (Bamforth *et al.*, 2013).

Around E9.5 (22 somite stage) the 3rd PAA appear, followed by the 4th PAA between late E9.5 and E10 (31-34 somite stage) and finally the 6th PAA by E10.5 (35-39 somite stage) (Hiruma *et al.*, 2002).

By E10.5 the 1st and 2nd PAA have already been transformed into other vessels and the 3rd, 4th, and 6th PAA are already formed, connecting the aortic sac with the dorsal aorta and showing bilateral symmetry within almost the same diameter (Figure 1-7) (Hiruma *et al.,* 2002).

The PAA form by both vasculogenesis and angiogenesis. The vasculogenes which is formation of new vessels by endothelial progenitors, independently of other vessels (Li *et al.*, 2012), is the mechanism that is responsible for the formation of the primitive PAA of the early embryo. The PAA are formed from a cluster of endothelial progenitor cells found between the dorsal and ventral aortae. This process is followed by angiogenesis, which is the process of creating new blood vessels from pre-existing blood vessels. The endothelial cluster cells grow out to join these

vessels, followed by luminisation. Both of these processes are required for the development of the PAA (Anderson *et al.*, 2008; Hiruma *et al.*, 2002).

From E11 the remodeling of the 3rd, 4th, and 6th PAA occurs to form the mature blood vessels of the cardiovascular system (Figure 1-7). The 3rd PAA become the common carotid arteries and the distal part of the internal carotid artery (Figure 1-7). The 4th PAA will form the part of the aortic arch that is located between the left common carotid (LCC) and left subclavian artery (LSA). The right 6th PAA forms the proximal part of the pulmonary artery, but the distal portion of the right side will disappear long before birth by apoptosis. However, the distal part of the left side remains and will form the arterial duct (AD), namely the blood vessel connecting the pulmonary trunk to the proximal descending aorta during the embryonic stage to allow the blood to bypass the non-functional lungs. The AD usually closes at or shortly after birth, allowing deoxygenated blood to the lungs (DeRuiter *et al.*, 1993; Hiruma *et al.*, 2002; Kameda, 2009).

Postnatal closure of the AD is affected by two factors: increase in oxygen tension and a decline in circulating prostaglandin E2 (PgE2) and I2 (PgI2). Oxygen and endothelin are very strong vasoconstrictors while PgE2 and PgI2 are strong vasodilators for the AD. Lower oxygen concentrations in utero and high circulating PgE2 and PgI2 levels help in keeping the ductus patent. The birth will cause a sudden increase in the oxygen level and fall in PgE2 and PgI2 level, which result in strong vasoconstriction and closure of the AD soon after birth (Coceani and Baragatti, 2012; Gournay, 2011; Schneider and Moore, 2006).

The proximal part of the aortic sac is divided into two horns and can be seen to be T-shaped, with the proximal part separated into aortic trunk and pulmonary trunk by E11.0 to E11.5. At this stage, the 3rd and 4th PAA connect to the aortic trunk while the 6th PAA connects to the pulmonary trunk. As the heart undergoes remodeling, asymmetry becomes prominent between the left and right 4th and 6th PAA. The spiral rotation of the OFT clockwise will reduce the length and diameter of the right side of the 6th PAA which will restrict the blood flow in this vessel. As a result, the right 6th PAA will regress by E13.5 and does not contribute to any mature blood vessels. Also the dorsal aorta below the left 6th PAA will regress and push blood to the left side (Hiruma *et al.*, 2002).

By E12.5 the portion of the paired dorsal aorta between the 3rd and 4th PAAs has completely regressed. At the same time a branch from the paired dorsal aorta has started to form, these branches will form the 7th intersegmental artery. This comes to be attached to the dorsal aorta near the attachment of the 4th PAA, it supplies the upper limb bud and is fated to be the subclavian artery.

The right dorsal aorta has completely regressed by E13.5. As a result, the left dorsal aorta becomes thick and the left 4th PAA forms the arch of aorta. At the same time, the right horn of the T-shape aortic sac becomes the brachiocephalic trunk and the right 4th PAA forms the proximal part of the right subclavian artery. By then, the 3rd PAA grow on both sides and form the common carotid arteries. Each 3rd PAA gives off a bud that grows cranially to form the external carotid artery. Finally, the right 7th intersegmental artery forms the distal portion of the RSA and the left 7th intersegmental artery has become the LSA (Figure 1-7).

The 5th PAA are considered rudimentary vessels that occasionally develop transiently and are lost shortly after formation. Some studies suggested that the 5th PAA do not form at all (Hiruma *et al.*, 2002), but a recent study has shown a bilateral collateral channel between the 4th and 6th PAA which is interpreted as transient 5th PAA (Bamforth *et al.,* 2013). The function of these transient vessels however is currently unknown.

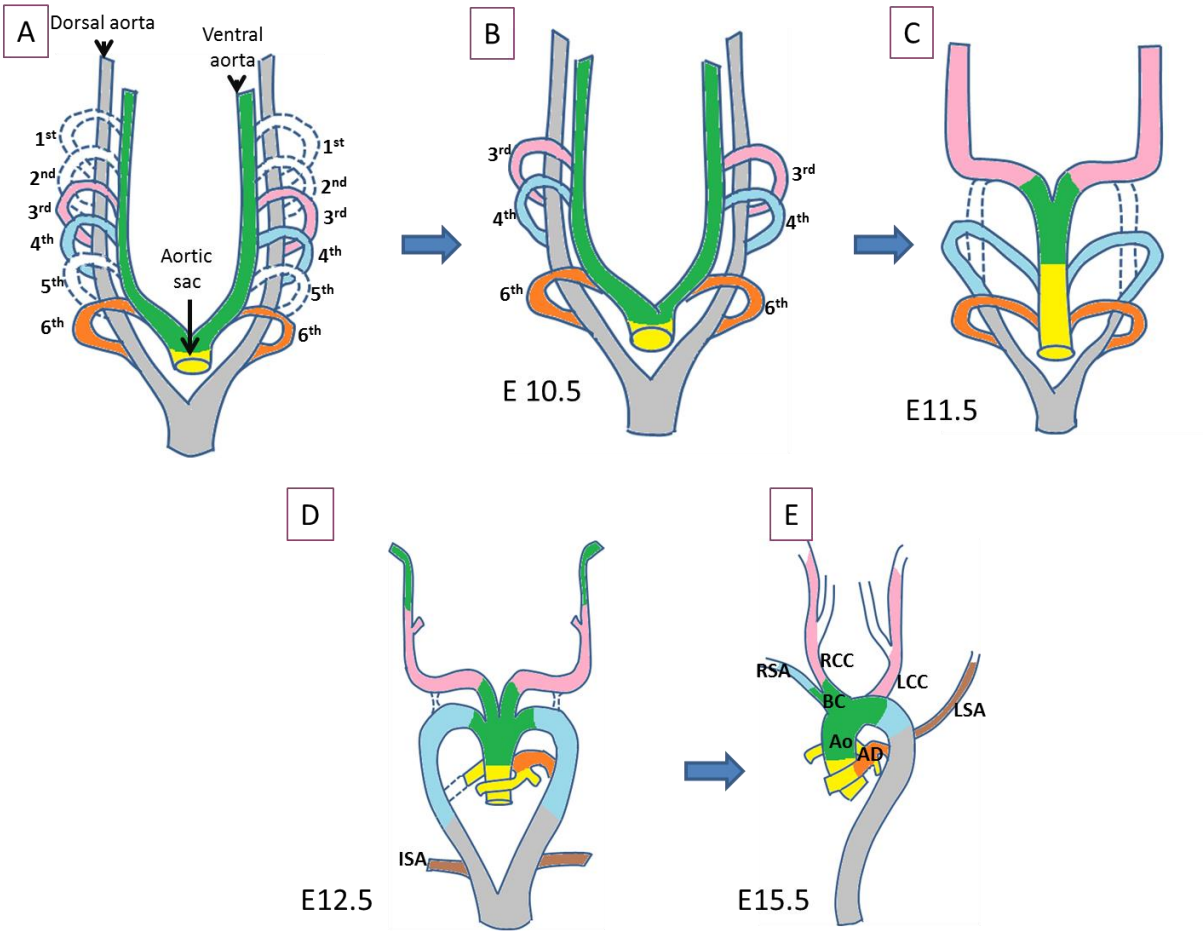

Figure 1-7: Schematic representation of the development of the pharyngeal arch arteries.
The pharyngeal arch arteries are five pairs in total. The 1st and 2nd PAA start developing but they soon regress. The 3rd, 4th and 6th PAAs appear in a craniocaudal sequence **(A)**. At E11.5, the dorsal aortic segments between the 3rd and the 4th PAA begin to regress. The aortic sac is separated into the aorta and pulmonary trunk **(C)**. By E12.5 the dorsal aorta between the 3rd and the 4th PAA has regressed and the 7th intersegmental arteries (ISA) enlarge and start to become the subclavian artery. The 3rd PAA has the same development on the right and left side, giving rise to the proximal portion of the left common carotid (LCC) and right common carotid arteries (RCC). The 4th PAA has different fates on the right and left side, on the left it forms the part of the arch of the aorta between LCC and left subclavian arteries (LSA). On the right, it forms the proximal segment of the right subclavian artery (RSA). The right 6th PAA regresses completely, on the left side the distal part persists as the arterial duct (AD) during intrauterine life.
Ao, aorta; AD, arterial duct; BC, brachiocephalic artery.

1.4 CONGENITAL HEART AND OUTFLOW TRACT MALFORMATIONS

1.4.1 CONGENITAL HEART DEFECT

Congenital heart defects is a general term for a range of birth defects that affect the normal function of the heart. It affects about twenty per 1000 live births (Savolainen, Foley *et al*. 2009). The etiology of CHD is multifactorial, possibly both genetic and environmental, although genetic components have only recently started to become understood and identified (Jenkins *et al.*, 2007).

Cyanotic congenital heart defects refer to a group of many different heart abnormalities that are present at birth and result in a low blood oxygen level. This defects cause the heart to work harder as well as low oxygen in the blood, which makes the skin look blue. Cyanotic heart defects are caused by malformation to various structures in the heart, which include the atrial septum, the ventricular septum and the heart valves. All forms of CHD in this section are considered to be cyanotic heart disease.

The so-called ventricular septal defect (VSD; Figure 1-8) is one of the most common congenital heart defects present at birth. It is caused by formation of a gap in the wall that separates the right and left ventricular chambers of the heart, which allows blood to pass from the left to the right side of the heart.

Formation of the interventricular septum is a complex process in which a single ventricular chamber is divided into two chambers. The division is accomplished by fusion of the muscular portion of the ventricular septum with the endocardial cushions and the bulbus cordis. The septation process begins with the appearance of a primordial muscular interventricular ridge developing in the floor of the ventricle. As either side of the ventricle grows and dilates, their medial walls fuse forming the prominent interventricular septum. The interventricular foramen, located between the cranial portion of the interventricular septum and the endocardial cushions, closes as the bulbar ridges fuse with the endocardial cushions. Sometimes the interventricular wall does not grow completely and the partitioning process does not occur completely leaving an opening in the ventricular septum (Morris, 1957; Zhang *et al.*,

2015). Therefore, oxygen-rich blood is pumped back to the lungs instead of out to the body (Figure 1-8).

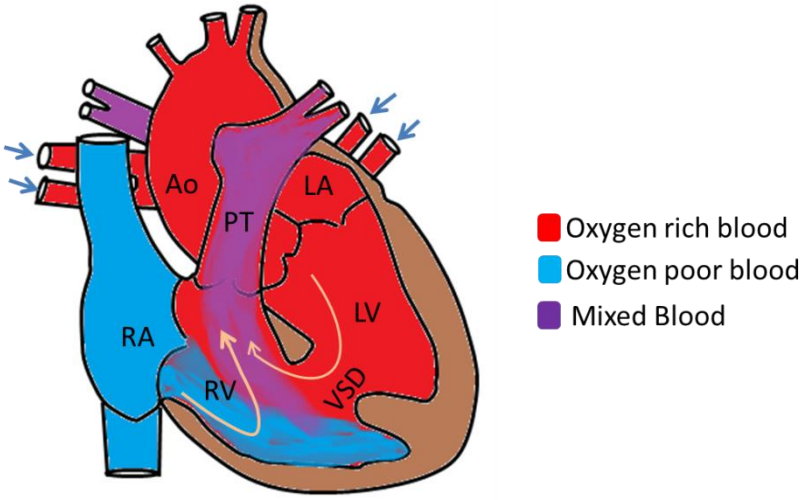

Figure 1-8: Schematic representation of ventricular septum defect (VSD).
A VSD is a hole in the wall of the septum that separates the left ventricle (LV) and right ventricle (RV). Normally, deoxygenated blood flows through the superior vena cava and inferior vena cava into the right atrium (RA), right ventricle, and pulmonary trunk (PT). When a VSD is present some oxygen-rich blood from the left ventricle mixes with deoxygenated blood through the defect and recirculates through the lungs.
Ao, aorta; left ventricle; LA, left atria.

During fetal life, an opening normally exists between the two atria to allow blood to bypass the non- functional lungs. This opening usually closes around the time the baby is born. When this partitioning process does not complete, it leaves a hole in the atrial septum call atrial septal defect (ASD; Figure 1-9). As a result, this defect will cause a large amount of oxygen-rich blood to leak from the heart's left side back to the right side.

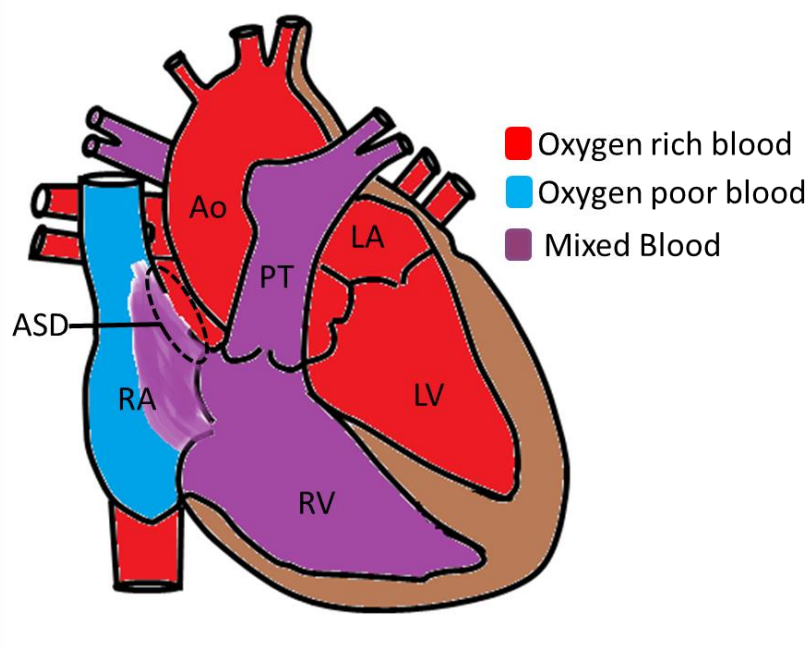

Figure 1-9 : Schematic representation of atrial septum defect (ASD).
An ASD is a hole that occurs when the septum separating the right atrium (RA) and left atrium (LA) does not close properly. This will allow oxygenated blood from the LA to flow and mix with deoxygentated blood in the RA, then back to the lung again.
Ao, aorta; LV, left ventricle; RV, right ventricle; PT, pulmonary trunk.

A bicuspid aortic valve (BAV) has been recognized as a common congenital abnormality for centuries, occurring in 14 per 1000 live births (Bruneau, 2008). The aortic valve is a one-way valve that regulates blood flow from the heart into the aorta. Normally, the aortic valve has three small flaps or leaflets that open widely and close securely to regulate blood flow, allowing blood to flow from the heart to the aorta and preventing blood from flowing backwards into the heart. A BAV is a heart deformity in which the aortic valve has only two leaflets and does not function perfectly (Tadros *et al.*, 2009). Although bicuspid aortic valve disease is present at birth, it is not usually diagnosed until adulthood because the defective valve can function for years without causing symptoms. When the leaflets of the valve fail to come together tightly when closing, regurgitation occurs in which blood leaks back into the heart (Figure 1-10) (Tadros *et al.*, 2009).

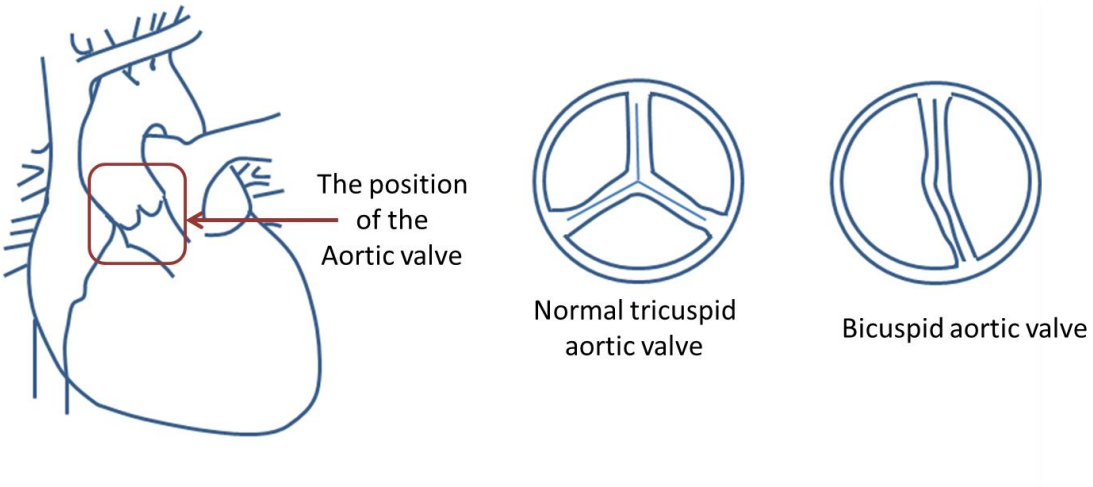

Figure 1-10: Schematic representation of the bicuspid aortic valve (BAV).
The normal aortic valve, as shown in the drawing, has three leaflets that move flexibly, opening and closing to control the flow of blood into the aorta from the left ventricle of the heart as it beats. When the cusps come together as the valve closes, the shape is that of a trisected circle. In contrast, a bicuspid aortic valve has only two leaflets, also shown in the diagram on the right.

Double outlet right ventricle (DORV; Figure 1-11) refers to a cardiac anomaly that occurs when both of the great arteries arise predominantly from the right ventricle and is associated with a VSD. Having the VSD is actually helpful in DORV because oxygen-rich blood is able to pass through the hole from the left ventricle into the right for circulation in the body so VSD is considered a haemodynamic necessity for the heart to function. DORV affects 0.09 cases per 1000 live births and represents 1.0% to1.5% of patients with CHD (Cetta *et al*., 2005). However, because the right ventricle normally collects oxygen-poor blood to pump to the lungs, the two types of blood mix and the embryo does not get sufficient levels of oxygenated blood. As a result, the heart must work harder to try to bring more oxygen-rich blood to the body.

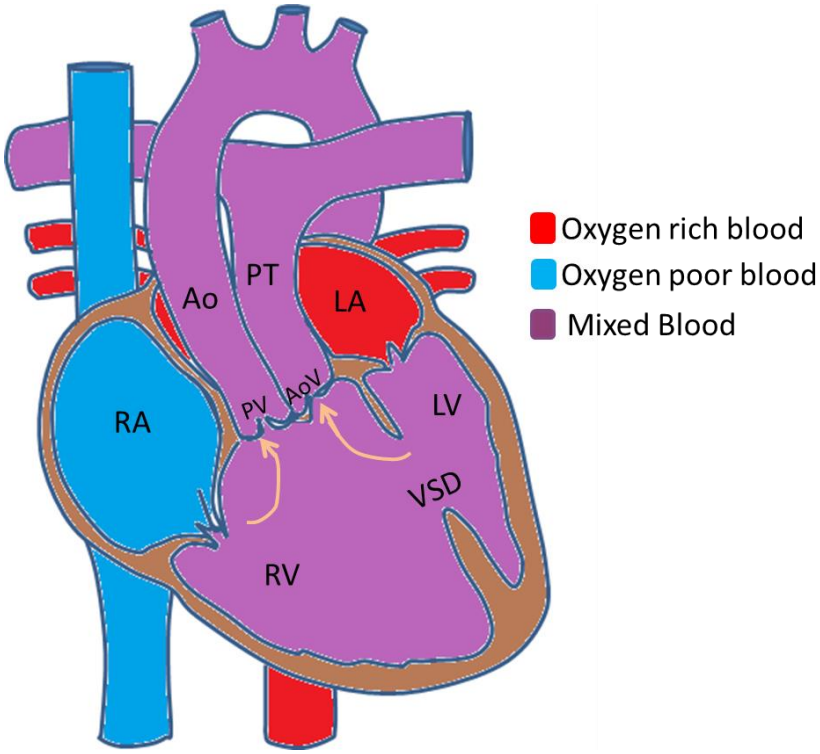

Figure 1-11: Schematic representation of double-outlet right ventricle (DORV).
DORV is a defect in which the aorta (Ao) connects to the right ventricle (RV) instead of the left ventricle (LV). Blood from the LV must exit through a large VSD. Most often, the great arteries (i.e. PT and Ao) are side by side and separated by the conus septum. In DORV, the pulmonary and aortic valves are at the same level.
AD, arterial duct; AoV, aortic valve; LA, left atrium; PV, polmonary valve; RA, right artium; VSD, ventricular septal defect.

Common arterial trunk (CAT) is a rare CHD that affects 0.03-0.056 per 1000 live births (Nagaraja *et al.*, 2015). This CHD occurs when the primitive truncus does not divide into the pulmonary artery and aorta, resulting in a single large blood vessel coming out of the heart and an overriding large VSD, instead of a separate aorta and a pulmonary trunk (Nishibatake *et al.,* 1987). Consequently, a mixture of oxygenated and deoxygenated blood enters the systemic, pulmonary, and coronary circulations. Patients with CAT require a surgical procedure to close the VSD and separate the pulmonary circulation from the systemic circulation.

1.4.2 PHARYNGEAL ARCH ARTERY DEFECTS

Congenital abnormalities of the great vessels, which take many forms, result from aberrant development of one or more components of the PAA system. Five pairs of PAA develop, forming the primitive vascular supply to the embryo. Any part of the embryonic aortic arch system can regress or persist abnormally, resulting in an extensive array of aortic arch abnormalities.

The 4th PAA defects are the commonly identified abnormalities. Derivatives of the 4th PAA contribute to a portion of definitive normal left aortic arch between the LCC and LSA and the proximal portion of the RSA. Under normal conditions, the aorta is the main blood vessel that carries oxygen-rich blood away from the heart to the organs of the body.

Interruption of the aortic arch (IAA; Figure 1-12) is a rare form of PAA defect, representing approximately 1% of congenital heart disease (Reardon *et al.*, 1984). With IAA, the part of the aorta located between the ascending aorta and the descending is absent which leads to severe obstruction to blood flow to the lower part of the body. This occurs through abnormal regression of the left dorsal aorta when the left 4th PAA is absent.

There are three types of IAA, which are classified according to the site of the interruption. Type A (Figure 1-12) is when the interruption occurs just beyond the left subclavian artery, and represents about 30% of IAA cases. The second and most common type is type B (Figure 1-12), in which the interruption occurs between the left carotid artery and the left subclavian artery. It accounts for about 53% of reported cases. The final type is type C (Figure 1-12); it is the most rare type occurring in about 4% of the reported cases.

Embryos carrying this malformation are often able to survive until birth and for a number of hours afterwards, as the AD provides blood to the dorsal aorta.

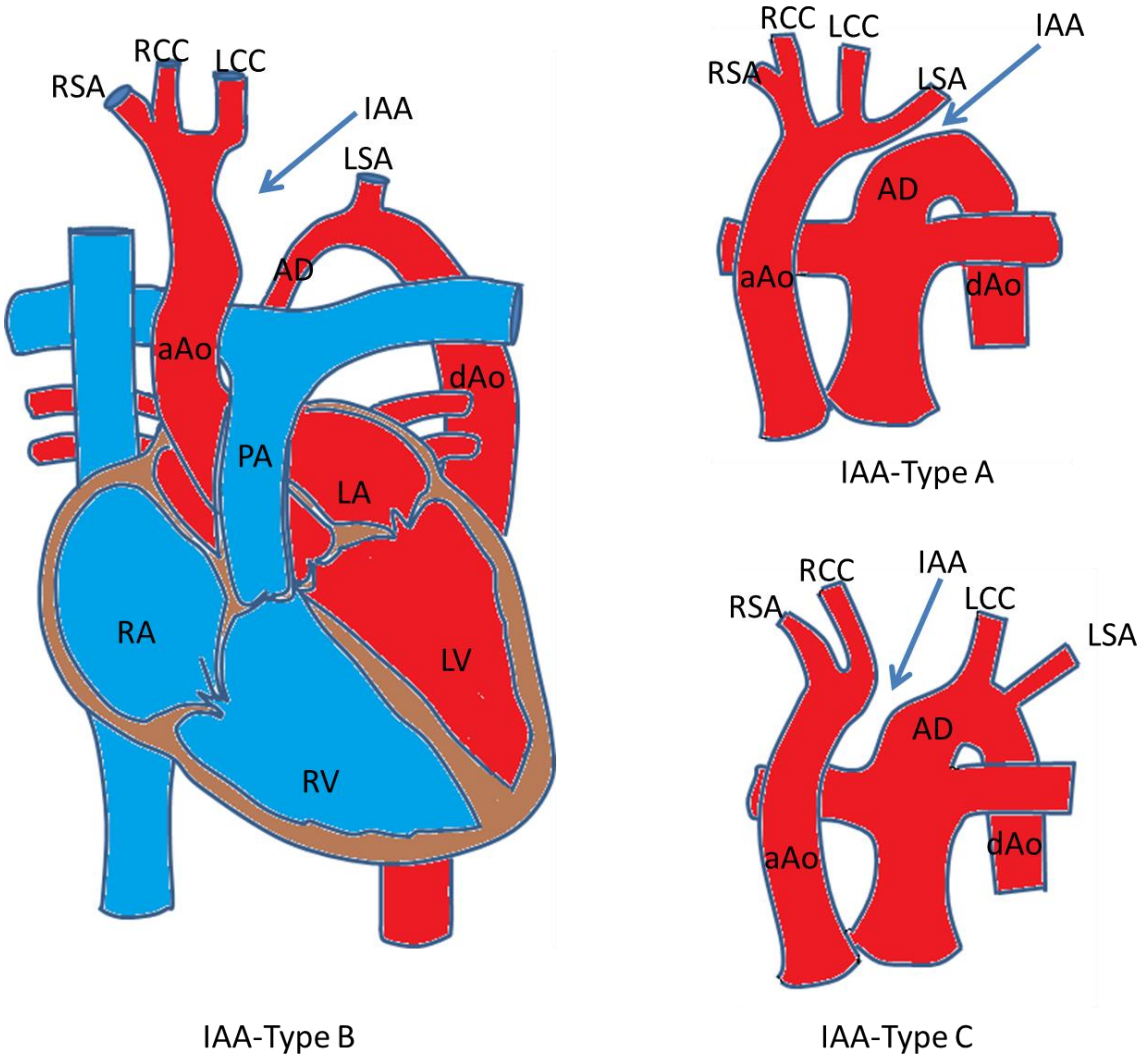

Figure 1-12: Schematic representation of the three types of aortic arch interruption.
Interruption of the aortic arch (IAA) is a defect in which part of the aortic arch is missing and there is no connection between the ascending aorta (aAo) and the descending aorta (dAo). Three types of IAA exist; type B is the most common interruption and occurs between the left common carotid arterial artery (LCC) and left subclavian artery (LSA) affecting 53% of the causes. Type A is the second most common form of IAA, it occurs distal to the LSA affecting 30% of the causes. Type C, which is the least common form affecting only 4% of the causes, it occurs distal to the brachiocephalic artery.
LA, left atrium; LV, left ventricle; PA, pulmonary artery; RA, right atrium; RCC, right common carotid artery; RV, right ventricle; RSA, right subclavian artery.

Anomalous origin of the RSA is common in type B aortic arch interruption. This anomaly results from either failure of the right 4th PAA to form or abnormal regression of the right 4th PAA between the carotid and subclavian arteries, rather than distal to the subclavian artery (Figure 1-13). This will cause the RSA to originate from an abnormal location, directly from the aortic arch distal to the left subclavian

instead of the normal originating from the brachiocephalic artery. As a result, the right subclavian artery will move to the right and cross the midline posterior to the esophagus (Hilfer and Brown, 1984) (Figure 1-13).

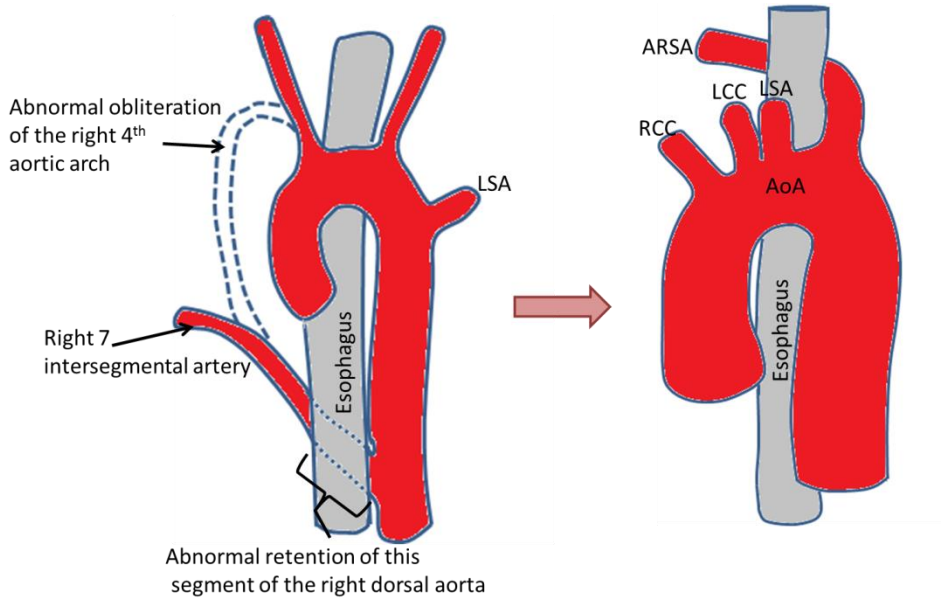

Figure 1-13: Regression of the right fourth arch results in an aberrant right subclavian artery (ARSA).
This artery has its root distal of the left subclavian artery and crosses the spinal column behind the esophagus.
AoA, arch of aorta; LCC, left carotid artery; LSC, left subclavian artery; RCC, right carotid artery.

Another defect which can result from the absence of the fourth left PAA is a cervical aortic arch (cAo). It is a very rare form of PAA defect with a prevalence of less than 0.01% (Turkvatan *et al.*, 2009). Cervical aortic arch occurs when the aorta arises normally from the left ventricle and extends in such a fashion that it is situated high in the neck (Figure 1-14). A cervical arch is considered to result from regression of the 4th PAA with persistence of the 3rd, which will cause the 3rd PAA to develop into the cervical arch (Shuford *et al.*, 1972; Tiraboschi *et al.*, 1980).

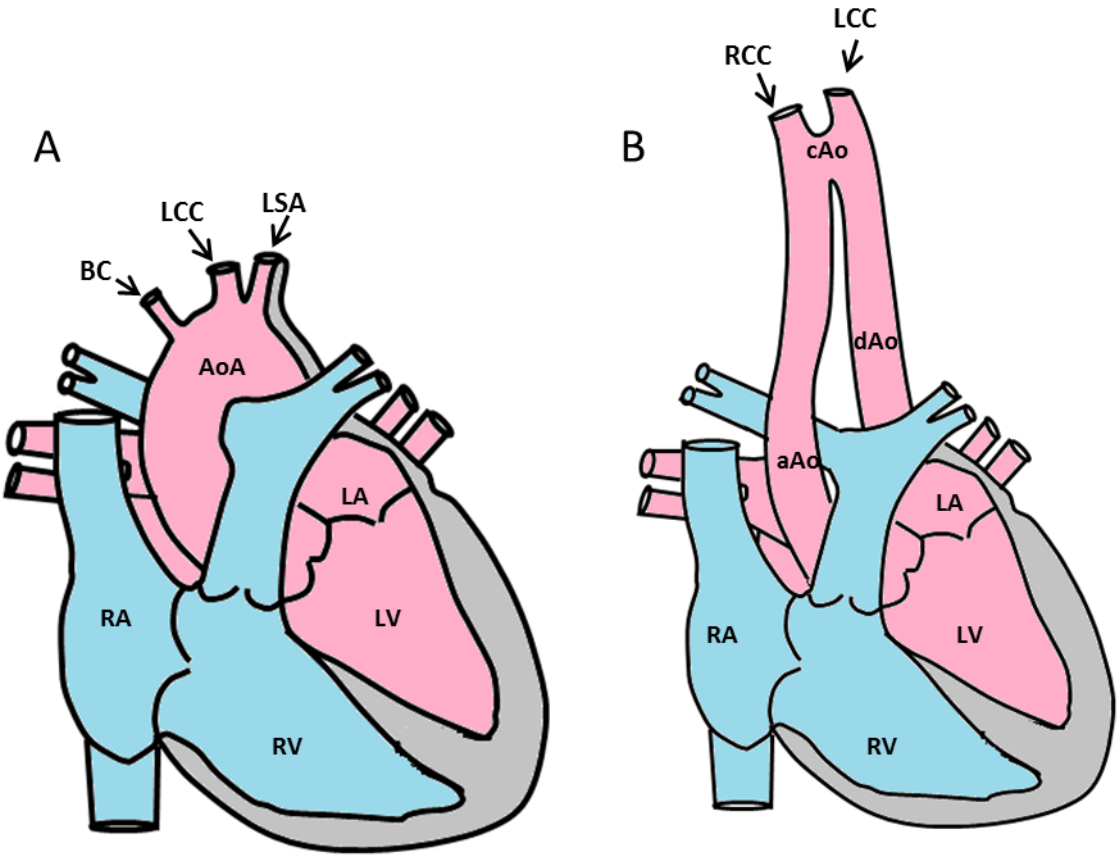

Figure 1-14: Schematic representation of the normal and cervical aortic arch (cAo).
(**A**) The normal shape of the aortic arch (AoA) arising from the left ventricle (LV), from this arch the three great vessels arise: the left subclavian artery (LSA), the left common carotid (LCC), and the brachiocephalic artery (BC). (**B**) The cAo with the left and right common carotid arteries arising as separate branches. This arch is different from the normal arch as it goes up to the cervical area then moves down to form the descending aorta (dAo).

Cervical right subclavian artery (cRSA) is not very common defect. The first case of this anomaly was described by Kutsche and Van Mierop (1984), and since then there have been a few reports of similar cases. This anomaly can be explained by the absence of right 4th PAA with the right subclavian artery arising from the right 3rd PAA. cRSA may be considered as a marker of 22q11 deletion syndrome as many patients show this defect (Sundaram *et al.*, 2014).

The identification of these anomalies has been given importance recently, especially the IAA. The presence of this entity has been described as a specific marker for the presence of monosomy 22q11, a chromosomal abnormality called DiGeorge syndrome, which is discussed in more detail in section 1.6.1.

1.5 THE MOUSE AS A MODEL TO STUDY CARDIOVASCULAR DEVELOPMENT

Transgenic animals are a powerful tool for modelling various diseases and identifying the molecular mechanisms and novel genes responsible for such diseases. The differences in the morphology of the heart within mammalian species are only subtle (Doevendans *et al*., 1998). In this work, the mouse model was used to investigate cardiac development and malformation.

A practical advantage of the mouse is the short gestation period and the low cost of breeding and housing compared to other mammalian models. In fact the gestation time of mice is 18-20 days, and heart formation begins as early as at embryonic day 7 (E7) and is completed at approximately E15.5 with the remodeling of the arch and the outflow tract, and eventually the heart septation into four chambers.

Additionally, the mouse turned out to be a species in which transgenic and gene targeting experiments could be performed with relative ease, it is in fact possible to create a genetic-null mice in which a certain gene will not expressed at all during development, which makes them a powerful tool to study a specific gene or disease (Olson and Schneider, 2003).

The first transgenic mouse was created by Rudolf Jaenisch in 1974 by inserting DNA into the mouse embryo during blastocyst stage. Currently, transgenic mice are usually created by two different techniques: inserting DNA into the pronucleus of zygotes and injection of embryonic stem cells into blastocysts (Gordon *et al*., 1980; Thomas and Capecchi, 1987).

The pronuclear microinjection method of producing a transgenic animal is based on the introduction of linear DNA sequences into the chromosomes of fertilized eggs. The foreign DNA must be integrated into the genome prior to the doubling of the genetic material that precedes the first cleavage in order for the animal to be born with a copy of this new information in every cell. The foreign DNA may be injected into the male pronucleus because it is slightly larger and closer to the oocyte surface. These oocytes are subsequently transferred into the uterus of pseudopregnant recipient animals (Gordon *et al*., 1980).

Embryonic stem cells (ES cells) are derived from the inner cell mass of blastocysts. These cells are pluripotent, which means that they can develop into almost any type of tissue. This technique makes it possible to insert as well as remove or modify DNA sequences. Knock-out, knock-in and conditional mutant mice can be produced with this method. The first step is the removal of ES cells from a blastocyst. After transfection of the ES cells, selection, cloning and screening methods make it possible to detect ES cell clones that demonstrate the desired, site-specific recombination. After microinjection of the genetically modified ES cells into blastocyst-stage embryos the ES cells divide and become part of the embryo. The resulting chimeric animals will subsequently transmit the recombinant genotype to their offspring, but only if the ES cells have contributed to their germ cells (Thomas and Capecchi, 1987).

Newer genetic engineering techniques allow the conditional inactivation of a gene spatially and/or temporally using site-directed recombination, such as the Cre-LoxP and FLP-FRT recombinases. These methods are most widely used to inactivate, inverse, or translocate a target gene in a conditional mutant mice, which make them a great tool for genetic manipulation.

The Cre-LoxP recombinase system can be used to excise a specific DNA fragment if flanked by loxP sequences. This is achieved by the expression of a site-specific DNA recombinase Cre in mice in conjunction with the introduction of two recombinase recognition sequences (loxP) into noncoding regions of the target gene (Sauer, 1998).

The FLP-FRT system is similar to the Cre-loxP system in which FLP recognizes a pair of FLP recombinase target (FRT) sequences that flank a genomic region of interest (Hoang *et al*., 1998).

Transgenic animals provide us with a privileged way of analyzing gene function in normal development and pathology as both gene deletion and replacement can be performed.

Heart development and structure are highly conserved between mouse and human. For example, regarding the heart structure, the mouse ventricles are similar to the human, presenting the same arrangement of the valves and trabeculations as the

human ventricles. On the other hand the most important difference between human and mouse in the cardiac structure are confined to the atrial and venous parts: in mouse the left superior caval vein persists and drains into the right atrium and the pulmonary vein has a single opening to the left atrium (Doevendans *et al.*, 1998). However the development of the great arteries are conserved between mouse and human (Bamforth *et al.,* 2013).

The human heart beats, on average, 60–70 times per minute. In contrast, the mouse has a heartbeat of around 500–600 times per minute. Moreover, the mouse heart has a shorter action potential duration during the repolarization stage than the human heart (Knollmann *et al.*, 2007).

On average, the protein-coding regions of the mouse and human genomes are 85% identical; some genes are 99% identical while others are only 60% identical (Batzoglou *et al.*, 2000). Also both species have 30,000 genes and a difference in approximately 300 genes, which is only 1% of the total genes (Emes *et al.*, 2003). One possible explanation for this difference is that it is derived from the changes in the non-coding and the coding sequences during evaluation. The coding sequence is conserved since it is required for function. Hence, the change would only be found in the non-coding sequence. The other possibility is that the difference is due to gene deletions and/or duplications specific to either of the lineages (Olson, 1999).

All together only minor differences can be observed when comparing mouse and humans; however these are far outweighed by the similarities to humans, making the mouse most accessible model with strong similarities to human, which makes it one of the best models to study heart development and defects.

1.5.1 GENETIC BACKGROUND

Using mouse models, researchers are studying various organs and diseases at the molecular level in order to identify essential regulators during development. In addition, using transgenic mice as a model helps in understanding how genetic mutations disrupt normal development. These studies could help develop new ways to prevent, diagnose and care for patients.

Usually the gene of interest can be maintained on one to several genetic backgrounds. This way, scientists take advantage of the different background, since some genetic backgrounds display the phenotype better than others. Many experiments may not have taken into account the potential strain effects on phenotype, and that the difference in phenotype may result from the influence of the genetic background of the mouse, not from the gene itself.

Outbred mice traditionally are considered to display high variability because they have been generated in random outcross way, in which the crossing occurs between genetically unrelated animals. This means the results may be much less reproducible (Festing, 2014). An increased number of animals are often required to overcome this. All of this discourages the use of outbred mice in some studies.

Researchers frequently use inbred strains of mice because of the greater homogeneity of these experimental animals (Vaickus *et al*., 2010). These mice can be used to replicate one's own experiments over time, and to compare results with other labs using genetically identical mice. However, mutations that have accumulated under laboratory conditions appear to be biologically atypical. Because the common laboratory mouse strains have generally been established from relatively small gene pools, common inbred mouse strains have limitations in their genetic polymorphisms and phenotypic variations.

Recently, there has been an increasing number of published evidence that the phenotype of a given single gene mutation in mice is modulated by the genetic background of the inbred strain in which the mutation is maintained. This has led to an awareness of the possible effects of modifying genes when transferring genes to a new strain background. Some modifying genes can totally suppress the phenotype effect of a mutant gene.

Sometimes using mice of different backgrounds may lead to a phenotype that can vary dramatically from the original phenotype, as reported in the literature (Sigmund, 2000). For example, two strains of mice were used to study the deficiency of ApoE in atherosclerosis; The FVB/NJ ApoE-deficient mouse and the C57BL/6J ApoE-deficient mouse. It was found that these two strains of mice have markedly different plasma lipoprotein profiles and susceptibility to atherosclerosis when fed either a low-fat chow or a high-fat Western-type diet (Lawrence F. Levin *et al*., 1999). Likewise, Hynes reported that fibronectin knockouts had considerable variation in phenotype which he attributed to the analyses being performed on embryos of a 129 and C57BL/6 background (George *et al.*, 1993).

In conclusion, although using transgenic animals will broaden our understanding of the complexities of gene function, care should be taken when using mice on different genetic backgrounds. The researcher should be aware that any phenotype could by influenced by this.

1.6 CHROMOSOMAL ABERRATIONS ASSOCIATED WITH CHD

The etiology of CHD is complex and is associated with both environmental and genetic causes. The genetic contribution to CHD has been significantly underestimated in the past. The morphogenetic events that are disrupted during cardiogenesis and that lead to CHD have started to be unravelled. However, whether these converge on discrete molecular programs involved in heart development is unknown.

1.6.1 22q11 DELETION SYNDROME AND THE TBX1 TRANSCRIPTION FACTOR

DiGeorge syndrome (DGS) is a disorder, which was first described in the 1960's by Dr. Angelo DiGeorge. It is one of the most common micro-deletion syndromes in humans affecting about one in 4000 live births (Burn and Goodship, 1996; Scambler, 2000).

DiGeorge syndrome, also called 22q11.2 deletion syndrome (22q11DS) is caused by a 1.5 to 3 megabase deletion on the long arm (q) of chromosome 22 (Figure 1-15). It results in the poor development of several body systems and is involved with

developmental anomalies of the 3rd and 4th pharyngeal arches (Kirby and Bockman, 1984). As a result, DGS is associated with the congenital absence of the thymus and parathyroid glands.

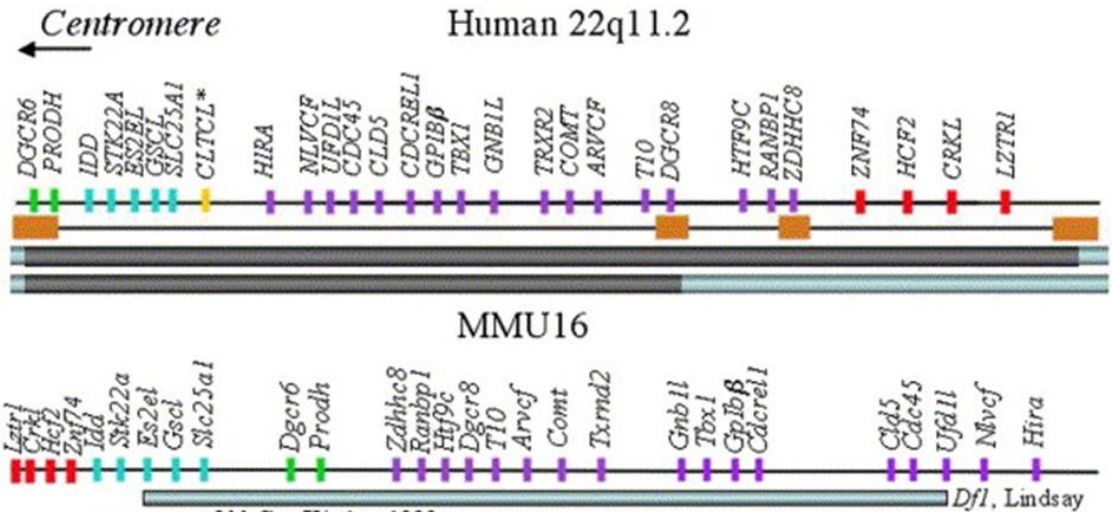

Figure 1-15: 22q11 deletion in human and mouse.
Schematic of human 22q11 and the syntenic mouse genomic region (MMU16). Grey bars indicate the common ~3 Mb deletion and the rarer ~1.5 Mb deletion found in 22q11DS patients. Note that in the mouse, there has been some reshuffling of gene order with respect to the syntenic human chromosomal region (shown by matching colours). Adapted from (Paylor and Lindsay, 2006).

About 75% of DGS patients suffer from cardiovascular defects including interruption of aortic arch (IAA) type B, double-outlet right ventricle (DORV), tetralogy of Fallot (TOF), ventricular septal defects (VSD), and aberrant of the right subclavian artery (ARSA). In addition to the cardiovascular defects, most of the patients have thymus and parathyroid abnormalities (Scambler, 2000). Clinical features also observed are cleft palate, cleft lip, renal agenesis and neural tube defects (Conley *et al.*, 1979).

Using Cre-LoxP chromosome engineering, Lindsay *et al.* (1999) created a mouse with cardiovascular defects similar to those seen in DGS. The mouse had a 1.2 Mb deletion, designated *Df1*, of chromosome 16 containing at least 20 genes that are most often deleted in DGS patients (Figure 1-15) (Lindsay *et al.*, 1999; Prescott *et al.*, 2005). However, 22q11 deletions result in heterozygosity for more than 30 genes deleted within the typical region suggesting the 22q11DS phenotype may result from complex genetic interactions.

A number of candidate genes that lie within the 22q11 region commonly deleted in DGS patients have been investigated in animal models to identify if a single gene from this region could be responsible for the clinical phenotype. For example, HIRA is expressed in the neural crest and in neural crest derived tissues, and was considered a good candidate as the 22q11DS phenotype was thought to derive from a failure in NCC development (Kochilas *et al.*, 2002). However, the mice that are heterozygous for *Hira* have not been reported to mimic the human 22q11deletion phenotype and the homozygous null mice die during early embryogenesis at E9.5 before the relevant structures have developed (Roberts *et al.*, 2002). Antisense attenuation of Hira expression in the cardiac neural crest during chick embryogenesis results in an increased incidence of common arterial trunk (Farrell *et al.*, 1999), although it was reported that this could be secondary to a non-specific effect of Hira downregulation on cellular differentiation rather than a specific effect within neural crest cells.

The *UFD1L* gene, which is also included in the DGS typically deleted region, was also excluded since some patients, who have cardiac defects, have deletions that do not include the region containing this gene, but on another part of chromosome 22 (Saitta *et al.*, 1999). Moreover, mice with hemizygous targeted mutations of *Ufd1l* were normal (Wadey *et al.,* 1999)

Another potential candidate gene located within the deleted region was *CRKL*. When *Crkl* was deleted from mice, cardiovascular defects occurred but the incidence of 4th PAA defect was low (Guris *et al*., 2001). Moreover, *Crkl* haploinsufficiency does not affect cardiovascular development (Guris *et al.*, 2006).

The gene that was finally identified as being the most likely candidate drivinig the 22q11DS phenotype, was TBX1(Merscher *et al*., 2001). Mouse models revealed that *Tbx1* haploinsufficiency causes cardiovascular defects (Lindsay *et al.*, 2001). Moreover, over-expression of *Tbx1* can rescue the DGS-like phenotype that is observed with haploinsufficiency (Merscher *et a*l., 2001). *Tbx1* plays an important role in the cardiovascular phenotypic features in DGS. The Df1 mouse deletion and the human 22q11 deletion both include *Tbx1*, which makes this gene the main candidate for the cardiovascular phenotype associated with DGS. Other genes in

this region however also contribute to the phenotype (Ilagan *et al.,* 2006; Jerome and Papaioannou, 2001).

Tbx1 is a member of a family of T-box transcription factors; a conserved family of genes that share a common DNA-binding domain (Papaioannou and Silver, 1998). It is expressed in head mesoderm, from as early as E7.5 then restricted to the pharyngeal endoderm, mesoderm and the otic vesicle by E9.5 (Chapman *et al.*, 1996; Yamagishi *et al.,* 2003). While *Tbx1* is not expressed in the neural crest cells that migrate to the pharyngeal arches and the OFT (Zhang e*t al.*, 2005), it is still required to control the cNCC migration (Zhang *et al*., 2006). *Tbx1* heterozygous mice show defects of the 4th PAA including IAA. It appears that *Tbx1* affects the 4th PAA, but not the patterning of the pharyngeal arches (Calmont *et al.*, 2009).

Tbx1 is required for the development of the pharyngeal arches and the PAA. *Tbx1*-null mice develop most of the clinical features of 22q11DS; including hypoplasia of the thymus and parathyroid, cardiac and outflow tract abnormalities, abnormal facial structures, abnormal vertebrae and cleft palate (Jerome and Papaioannou, 2001; Lindsay *et al*., 1999; Zhang *et al.*, 2006).

Moreover, *Tbx1* is shown to genetically interact with many genes including *Crkl*. *Tbx1;Crkl* double heterozygotes show both the aortic arch defect as well as the thymus and parathyroid defect compared to single heterozygotes (Guris *et al.*, 2001; Jerome and Papaioannou, 2001). In addition, *Tbx1* directly controls the SHF by controlling several genes, including *Fgf8* (Hu *et al.*, 2004) and *Wnt5a (*Stuart *et al., 1994)* (Chen *et al.*, 2012).

As previously mentioned, many genes are affected by homozygous loss of *Tbx1* in mouse embryos. Among those genes, the transcription factor *Pax9* was found significantly down-regulated by microarray of *Tbx1*-null embryos (Ivins *et al*., 2005). Analysing E8.5 *Tbx1*$^{-/-}$ embryos using *in situ* hybridization showed a down regulation of *Pax9* expression before the pharyngeal pouches had formed (Figure 1-16) (Ivins *et al.*, 2005). Also, quantitative PCR showed that *Pax9* is down-regulated in *Tbx1*-null embryos, and these two genes are expressed within the pharyngeal arches at the same time (Figure 1-16) (Ivins *et al*, 2005). In addition, there is evidence of a patient with congenital heart disease and chromosomal deletions that include *PAX9*

(see section 1.6.3) which suggests that the *PAX9* gene may play a role during normal cardiovascular development.

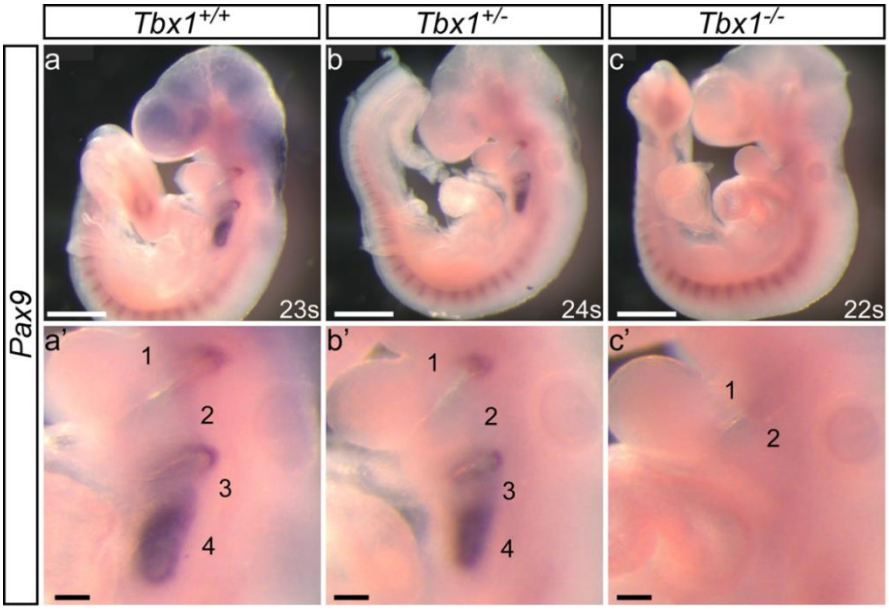

Figure 1-16: *Pax9* mRNA expression is reduced in *Tbx1*-null embryos.
Whole-mount *in situ* hybridisation using a Pax9 probe shows an obvious decrease of *Pax9* expression within the pharyngeal region of *Tbx1*-null embryos (**c**) compared to wild-type (**a**) and *Tbx1*$^{+/-}$ embryos (**b**) at E9.5. Scale bar 500µm (S. Bamforth data).

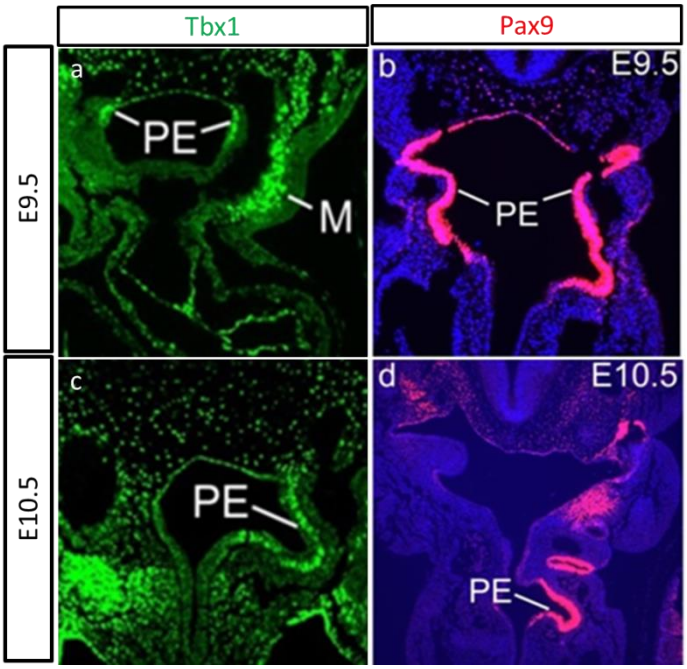

Figure 1-17: Expression of *Tbx1* and *Pax9* in the pharyngeal arches.
Immunofluorescence for *Tbx1* and *Pax9* expression in the pharyngeal arches of the mouse at E9.5 and E10.5. The staining shows that *Tbx1* and *Pax9* are both expressed in the endoderm and at the same time (S. Bamforth data).
M, mesoderm; PE, pharyngeal endoderm.

1.6.2 Pax GENE FAMILY

The Pax (Paired box) family of transcription factors was first found and isolated in Drosophila. The mammalian Pax transcription factors are characterized by a ~128-amino-acid DNA-binding paired domain that makes sequence-specific contacts with DNA (Dahl *et al.*, 1997).

To date, nine Pax genes have been isolated in human and mice. Mouse and human Pax genes are classified into four subgroups based on their structural similarity. This depends on the presence or absence of the following structural regions: a full homeodomain (60 amino acid helix-turn-helix), a partial homeodomain (first helix only), and an octapeptide motif (Stuart *et al.*, 1994). Pax genes contain a highly conserved DNA-binding domain called the paired domain. Although the paired domain contains three regions that are predicted to form an α-helix, there is no sequence similar to the helix-turn-helix motif presented in the homeodomain. Genes within a given class share specific intron/exon boundaries as well as additional sequences outside of the paired box domain (Walther *et al.*, 1991).

Pax3 and *Pax7* contain all of the above structural regions. *Pax4* and *Pax6* have a full homeodomain but no octapeptide motif. *Pax2, Pax5*, and *Pax8* have a partial homeodomain and an octapeptide motif. Finally, *Pax1* and *Pax9* have an octapeptide motif but no homeodomain (Stuart *et al*., 1994) (Figure 1-18). The carboxy portion of the protein has a specific sequence among the four Pax genes classes while the amino terminal is more conserved among them (Stuart *et al.*, 1994).

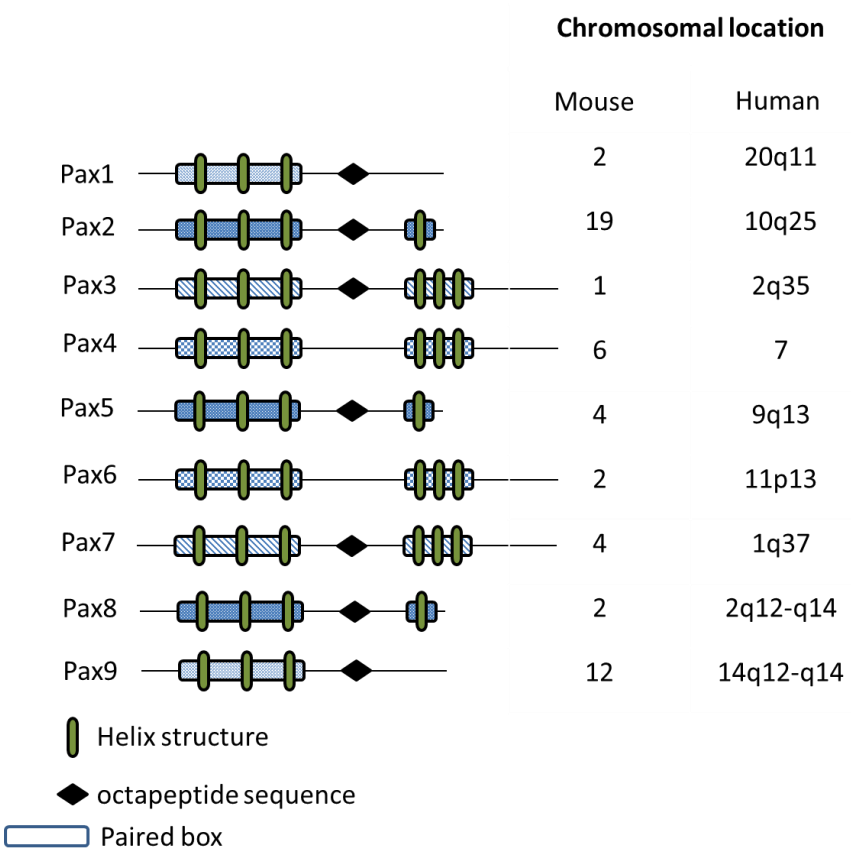

Figure 1-18: Structure of Pax proteins.
All of the Pax proteins contain a conserved DNA-binding domain of 128 amino acids at the NH2-terminal part, the paired box (Paired domain). The presence or absence of two other conserved domains, the octapeptide and a second DNA-binding domain called the paired-type homeodomain, define distinct groups of Pax proteins. In the schematic diagram above, Pax genes of a distinct group are labeled in the same way. These genes share a similar genomic organisation and a common expression pattern. Chromosomal location in both human and mouse is indicated. Adapted from (Stuart *et al.*, 1994).

The Pax transcription factors have a critical role in development. This is revealed by the observed defects caused by Pax gene mutations, in both mouse models and congenital human diseases.

Pax1 transcription factor is required for normal development of the vertebral column, the sternum, the scapula, pelvic girdle and in small fraction in the adult thymus. Mutation in this gene leads to defects in these skeletal elements (Sivakamasundari *et al.*, 2013) that are reminiscent of the human disorder Klippel-Feil syndrome (KFS). Screening 62 KFS patients showed a role for *PAX1* in this disorder (McGaughran *et al.*, 2003). Moreover, *Pax1* is important for normal T-cell maturation. Mutation in *Pax1* causes hypoplasia in the thymus (Wallin *et al.*, 1996). Also, *PAX1* shows hyper

methylation in cervical cancer (Lai *et al.*, 2008), indicating that it plays a role in cancer.

Pax2 transcription factor plays a critical role in the formation of tissues and organs during embryonic development. Heterozygous mutation of *PAX2* is associated with enal-coloboma syndrome (Nishimoto *et al.*, 2001). Also *Pax2*$^{-/-}$ mice have no kidneys, with the female mice also missing the Fallopian tubes (Winyard *et al*., 1996). Moreover, the ears of *Pax2*$^{-/-}$ mice often lack a distinct saccule, and the endolymphatic fluid (Burton *et al.*, 2004). *PAX2* is also expressed in some types of cancer including ovarian cancers, renal cell carcinomas and bladder carcinomas (Muratovska *et al.,* 2003).

Pax3 is expressed in the neural tube and neural crest cells during migration (Goulding *et al.*, 1991), which makes it important for delamination of the neural crest during embryogenesis (Sato *et al.*, 2005). Mutations in *PAX3* have been found in the waardenburg syndrome (Tassabehji *et al.*, 1993).

Pax4 is expressed during the development of the pancreas, where it is important for islet β- cell generation (Brun *et al.*, 2008). Mutation in this gene leads to type 2 diabetes (Brun *et al.*, 2008).

Pax5 is critical for the regulation of β-cell development, differentiation and function (Hamada *et al.*, 1998). *PAX5* haploinsufficiency acts with *STAT5* to induce acute lymphoblastic leukemia (Heltemes-Harris *et al.*, 2011).

Pax6 is essential for normal development of the eyes and nervous system (Van Heyningen and Williamson, 2002). *Pax6* mutation may cause cancer, such as alveolar rhabdomyosarcoma (Strachan and Read, 1994). Moreover *Pax6* mutation causes aniridia (Chograni *et al.*, 2014), a reduction in the cortical area of the brain (Yogarajah *et al*., 2016) and developmental disorders, for example autism (Umeda *et al.*, 2010).

Pax7 is expressed in the muscle satellite cells (Zammit *et al.*, 2006). *Pax7*$^{-/-}$ mice are born alive but smaller in size and the majority fail to grow, dying at approximately two weeks of age (Seale *et al.*, 2000) which suggests that *Pax7* is important for postnatal growth.

Pax8 is expressed in the adult thyroid and kidney. *Pax8* also regulates the expression of thyroglobulin and thyroperoxidase genes (Zannini *et al.*, 1992). *Pax8*$^{-/-}$ mice show a smaller thyroid gland than control animals, with a complete absence of follicular structures. Mutations in *Pax8* are associated with congenital hypothyroidism (Macchia *et al.*, 1998).

Pax9 plays important roles in development and organogenesis. In human dominant function mutations of *PAX9* cause selective tooth agenesis (Peters *et al*., 1998). More detail about *Pax9* transcription factor will be presented in the next section (1.6.3).

1.6.3 *Pax9* EXPRESSION DURING DEVELOPMENT

PAX9 is a member of the paired box-containing gene family. The cytogenetic location for *PAX9* in humans is 14q13.3 (Almeida *et al.*, 2010; Muller *et al.,* 1996; Santen *et al.*, 2012). The gene plays a critical role during fetal development and cancer growth. In mouse *Pax9* is located on the proximal part of chromosome 12 (Wallin *et al*., 1993).

The PAX9 sequence contains five exons (Figure 1-19); the first exon contains the start codon. Exon 3 had shown a variation over evolutionary time so human *PAX9* polymorphisms are limited to exon 3 only (Paixao-Cortes *et al.*, 2011b; Pereira *et al.,* 2006).

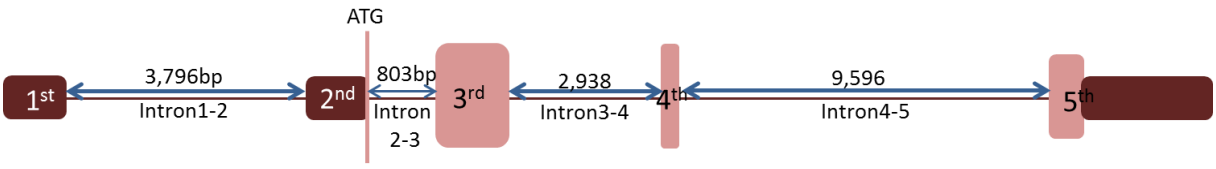

Figure 1-19: *Pax9* gene segments.
Pax9 transcription factor has 5 exons, the 1st exon is 33bp, the 2nd exon is 397bp, the 3rd exon is 627bp, the 4th exon is 140bp and the 5th exon is 1607bp in length. The starting codon (ATG) is located at the end of the second exon.

In humans, the first identified mutation of *Pax9* was a frameshift mutation in exon 2 of *Pax9* gene in a family. The affected individuals lacked almost all permanent molars and the majority lacked the permanent second premolars and lower permanent lateral incisors (Stockton *et al.*, 2000). The extensive study of *PAX9* in

human showed that it is commonly associated with the development of the teeth and mutations result in syndromic and non-syndromic oligodontia, hypodontia and tooth displacement anomalies (De Coster *et al.*, 2009).

Pax9 transcription factor has been found specifically in mesodermal tissues and the pharyngeal endoderm. In *Pax9*-null mice, teeth developments are arrested after bud stage as the mesenchyme fails to condense around the epithelial bud. This suggests a defect in the mesenchyme of *Pax9*$^{-/-}$ mice. According to Peters *et al.* (1998) the mesenchyme in *Pax9*$^{-/-}$ embryos show a down regulation of *Msx1* transcription factor as a result of the failed expression of *Bmp4*.

Wang *et al.* (2009) determined the structural and functional consequences of *PAX9* paired domain missense mutations and correlated findings with the associated dental phenotype variations. All mutant PAX9 proteins were localized in the nucleus of transfected cells and physically interacted with MSX1 protein.

During development, *Pax9* is expressed in a variety of organs and plays an essential role during mammalian embryogenesis. The expression of the *Pax9* transcription factor starts at E8.5 and becomes more evident at E9.5, exclusively in the pharyngeal endoderm (Figure 1-20). The pharyngeal endoderm is responsible for the formation of thymus, parathyroid glands and ultimobranchial bodies. The ulitmobranchial bodies are an outpocketing of the 4th pharyngeal pouch that fuses with the thyroid diverticulum, that give rise to calcitonin production. Later on, *Pax9* is expressed in the developing somites, specifically in the posterior ventrolateral region and the nasal process during the same period (Peters *et al.*, 1998).

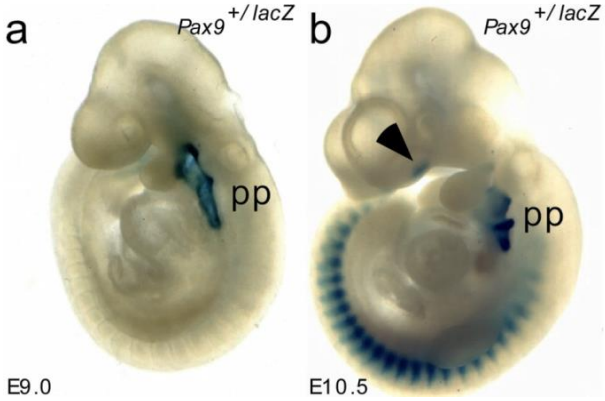

Figure 1-20: Expression of the *Pax9* gene during embryonic development.
Whole mount X-gal staining shows that *Pax9* starts to be expressed at E9 in the pharyngeal endoderm **(a)**. At E10.5 the expression of *Pax9* transcription factor extends to the somites and the craniofacial region **(b)** (Peters *et al*., 1998).

Furthermore, at E11.5, *Pax9* is expressed in the axial skeleton and in the neural crest derived mesenchyme required for craniofacial development. By the E16.5 stage of development, *Pax9* expression is found in the mesenchyme of the teeth, salivary glands and the tongue (Peters *et al.*, 1998).

The *Pax9* gene is involved in development of the pharyngeal arches. In *Pax9* mutant embryos, all of the pharyngeal arches develop normally until E11.5, at which point the 3rd and 4th pharyngeal arches stop developing. *Pax9*$^{-/-}$ pups lack the thymus, parathyroid glands, and ultimobranchial bodies that develop from these pouches. The pharyngeal arches are formed in *Pax9*-null mice, however most of the pharyngeal arch-derivatives are absent (Peters *et al*., 1998).

Pax9 knockout mice die immediately after birth. *Pax9*$^{-/-}$ mice are thought to die because of cleft palate defects; resulting in gasping respiration, which consequently leads to the development of a bloated abdomen. As *Pax9* is critical for tooth development, the pups also have an abnormal shaped mandible and missing teeth. They also present with a pre-axial digit duplication (Peters *et al.*, 1998).

Investigation of the role of *Pax9* in the NCC has been carried out in the mouse. Mouse *Pax9* is expressed in the cranial NCC, it is expressed in the nose, palate, and teeth, all of which are derived from NCC (Kist *et al*., 2007). Specific deletion of *Pax9* from the NCC using *Wnt1cre* causes the arrest of tooth development at the bud

stage. In addition to the missing teeth, the embryos showed craniofacial deformities including cleft palate, absent palatal processes of the premaxilla, absence of the alveolar bones and the coronoid process of the mandible (Kist *et al.,* 2007).

Searching the literature reveals three cases of patients that have been diagnosed with a mutation in the *PAX9* transcription factor and suffer from a cardiovascular defect. The first case recorded of a chromosome 14q13 deletion that included a *PAX9* deletion was reported in 1994 by Shapira *et al*., in which a female patient was born with patent foramen ovale and patent arterial duct. The patient died at the age of 14 months from cardiorespiratory arrest. The second case was recorded in 1999, for a male patient born with a patent arterial duct and pulmonary stenosis (Buckingham *et al.,* 2005).

The third case was a patient identified with congenital heart malformation including an interrupted arterial arch type B, bicuspid aortic valve, hypoplasia of the annulus of the aorta and a ventricular septum defect. The patient was later diagnosed with *PAX9* haploinsufficiency caused by chromosome14q13 deletions (Santen *et al.*, 2012). This cause is different from the first two causes since the deletion this patient had was a small deletion of only four genes. One of these genes was *NKX2-8*, but the sequencing results did not show any mutation in this gene. The tests excluded 22q11 deletion syndrome and *NOTCH1* mutation, which makes *Pax9* haploinsufficiency the main cause of the cardiovascular phenotype in this patient. However, until now, there are no other cases found with 14q13 deletion and a cardiovascular mutation (Santen *et al.*, 2012).

Pervious work in our lab checked the penetrance of the cardiovascular defects, analysing nineteen *Pax9*$^{-/-}$ embryos at E15.5 using magnetic resonance imaging (MRI) and haematoxylin and eosin staining (H & E). Table 1-2 show a summary of the penetrance of these defects in *Pax9*-null embryos. As shown in table 1-2 all *Pax9*-null embryos (19/19) suffered from pre-axial digit duplication, cleft palate and absence of the thymus. Also all *Pax9*$^{-/-}$ embryos displayed one or more forms of cardiovascular defects. The 3D reconstruction of the MRI data (Figure 1-21) and the H and E staining (Figure 1-22) sections revealed cardiovascular defects particularly those affecting the 4th pharyngeal arch artery and the outflow tract such as IAA, ARSA, DORV with interventricular communication (IVC), and isolated VSD (Figure

1-21, Table 1-2). The data suggests that *Pax9* is important during normal cardiovascular development, and it is required for normal PAA formation and/or remodeling.

Table 1-2: Incidence of cardiovascular defects in E15.5 *Pax9*-null embryos.

N	Phenotypes							
	Pre-axial digit duplication	Cleft palate	Absent thymus	VSD	DORV +IVC	IAA	ARSA	Carotids deformity
19	19	19	19	3	15	17	14	15
	100%	100%	100%	16%	79%	89%	74%	79%

Abbreviations: ARSA, aberrant right subclavian artery; DORV, double outlet right ventricle; IAA, interruption of the aortic arch; IVC, interventricular communication; VSD, ventricular septal defects. (S. Bamforth data).

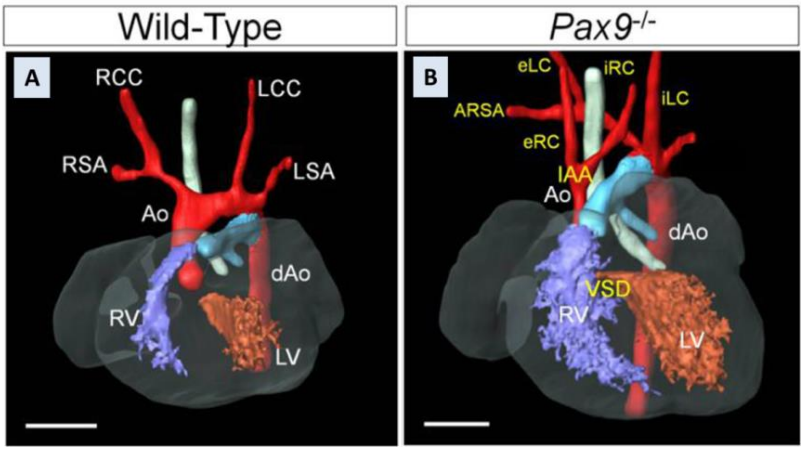

Figure 1-21: Cardiovascular phenotype of E15.5 *Pax9*-null embryos.
3D reconstruction of MRI data for a **(A)** wild type and a (**B**) *Pax9*$^{-/-}$ hearts. From the ventral view, the wild type embryo presented with normal branching of the great arteries where the aorta (Ao) arose from the left ventricle (LV) forming the aortic arch to connect with the descending aorta (dAo), the brachiocephalic artery, left common carotid (LCC) and the left subclavian artery (LSA) arose directly from the aortic arch. **(B)** *Pax9*$^{-/-}$ embryo presented with cardiovascular defects, including aberrant right subclavian artery (ARSA), ventricular septal defects (VSD), interruption of the aortic arch (IAA) type B and absence of both common carotid arteries, consequently causing the internal and external carotids to arise directly from the aorta (S. Bamforth data).
eLC, external left carotid artery; eRC, external right carotid artery; iLC, internal left carotid artery; iRC, internal right carotid artery; RSA, right subclavian artery; RCC, right common carotid artery; RV, right ventricle. Scale bar indicated a 500µm.

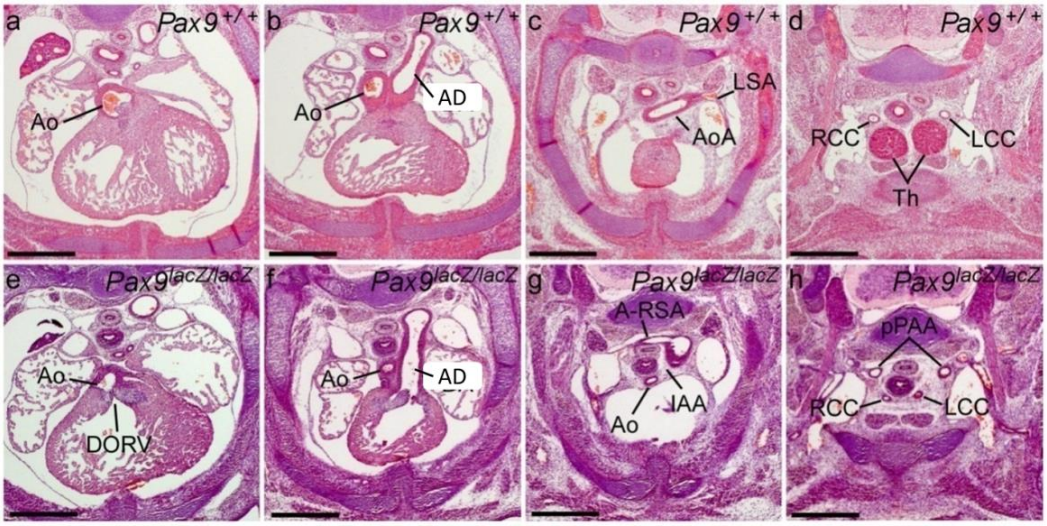

Figure 1-22 : Histological analysis of *Pax9*$^{-/-}$ embryos at E14.5.
Transverse section of E14.5 embryos using haematoxylin and eosin staining. **a – d,** Control embryo. A normal interventicular septum, normal aorta (Ao), and arterial duct (AD) connecting to the descending aorta are observed **(a, b)**. The aortic arch (AoA) and left subclavian artery (LSA; **c**) and the right and left common carotid arteries (RCC, LCC), as well as the thymus (Th) are indicated (**d**). **e – h**, *Pax9*$^{-/-}$ embryo. The aorta arises from the left ventricle, giving double-outlet right ventricle (DORV; **e**). The aorta is hypoplastic **(f)** and is also interrupted (IAA) and there is an aberrant right subclavian artery (A-RSA; **g**). Unusual presumed pharyngeal arch artery derivatives (pPAA) are seen dorsal to the RCC and LCC **(h)** (S. Bamforth data).
Scale bar, 500μM.

Furthermore, the development of the PAA were analysed in *Pax9*$^{-/-}$ embryos using intra-cardiac ink injections at E10.5 embryos (Figure 1-23). The wild type embryos showed normal PAA development in which the 1st and 2nd PAA had regressed and were no longer visible. The 3rd, 4th and 6th PAA displayed a normal pattern at both the left and right side. However, in *Pax9*-null embryos the formation of the PAA was disrupted with 100% showing 4th PAA defects, which included hypoplastic or complete absence of the vessels. Moreover, over half of the injected embryos showed a hypoplastic 3rd PAA. A number of the embryos had persistent 1st and 2nd PAA rather than the expected regression of these vessels. This is a sign of their late remodeling.

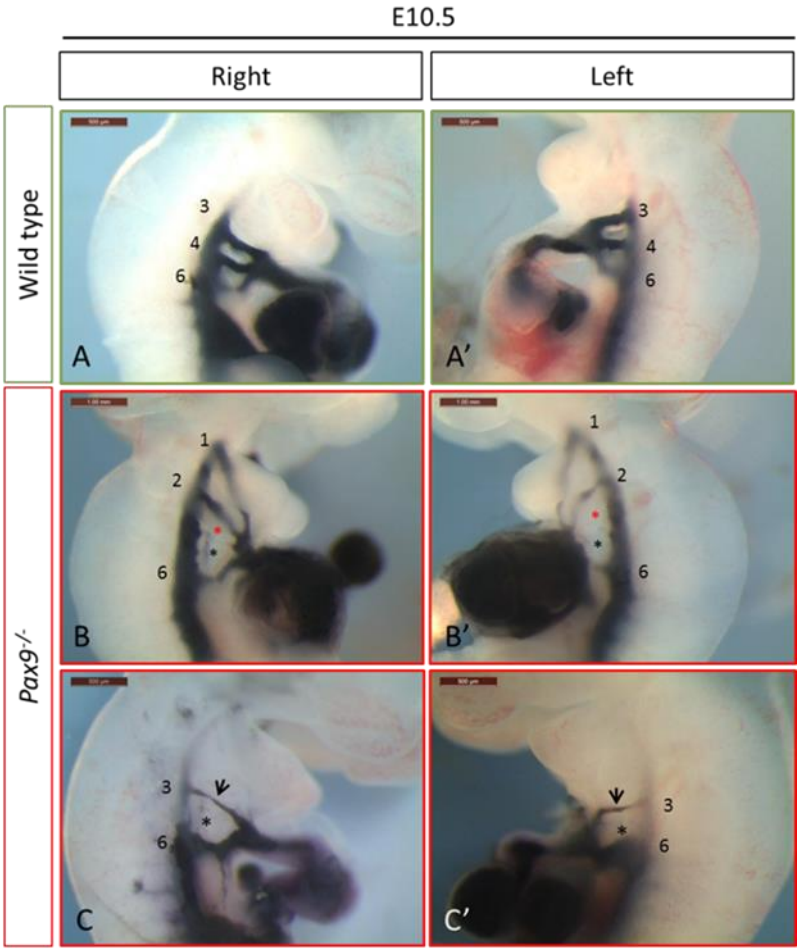

Figure 1-23: Abnormal morphology of the pharyngeal arch arteries in *Pax9*$^{-/-}$ embryos at E10.5 shown using ink injection.
Ink injection for E10.5 embryos showed the 3rd, 4th and 6th PAA **(A-A')** of a control embryo at both the right **(A)** and left **(A')** side. Whereas *Pax9*$^{-/-}$ embryos **(B-C')** showed abnormal patency of the persistent 1st and 2nd PAA on both sides at E10.5 **(B-B')** in a number of embryos, *Pax9*-null embryos also displayed missing (*red asterisk;* **B-B'**) or hypoplastic (*black arrow;* **C-C'**) 3rd PAA. The 4th PAA (*black asterisk*) is missing on both sides **(B-C')** in all *Pax9*-null embryos. Scale bar 500µm (S. Bamforth data).

1.6.4 Msx HOMEOBOX GENES FAMILY

MSX is a highly conserved family of homeobox genes (Tesfaye *et al.*, 2010). This family takes its name from the muscle segment homebox (*msh*) gene, and play important roles in transcriptional regulation during embryonic development.

In mouse the *Msx* gene family consists of 3 members, named *Msx1*, *Msx2*, and *Msx3* (Duncan, 1995; Robert *et al*., 1989). Two human *MSX* genes

(*MSX1* and *MSX2*) have been isolated, the third gene has been lost in human in early in vertebrate evolution (Hewitt *et al.*, 1991).

Msx2 is a protein coding gene, it provides instructions for producing a protein that is necessary for proper development of cells and tissues throughout the body (Satoh *et al.,* 2004). In addition, it plays an important role in mammary gland development. *MSX2* is important for craniofacial development in humans, mutations in this gene cause boston type craniosynostosis, a condition characterized by the premature fusion of the skull (Wilkie *et al.*, 2000). In mouse, knocking out *Msx2* showed a calvarial foramina similar to humans with *MSX2* haploinsufficiency (Liu *et al.*, 1995). *Msx2* gene is typically expressed in terminally differentiated osteoblasts, for example, collagen-I which is shown to be regulated by *Msx2* (Newberry *et al.*, 1997).

In mouse, *Msx3* is only expressed in the dorsal neural tube (Shimelda *et al.*, 1996). However, in developing mouse embryos, *Msx1* and *Msx2* are widely expressed in many organs including the neural tube, neural crest, facial processes and limb buds. *Msx1* and *Msx2* are particularly expressed at the sites where epithelial-mesenchymal interactions take place (Shimelda *et al*., 1996).

1.6.5 *Msx1* EXPRESSION DURING DEVELOPMENT

Msx1 (Figure 1-24) is member of the muscle segment homeobox gene family, which is expressed at multiple sites and induces tissue interactions during vertebrate embryonic development (Boogerd *et al.,* 2010; Ishii *et al.*, 2005; Nagel *et al.*, 2014).

Figure 1-24: *Msx1* gene segments.
Msx1 transcription factor consists of two exons, the 1st exon is 590bp while the 2nd exon is 1214bp in length. The two exons are separated by a 2107bp intron.

In humans, *MSX1* plays a crucial role in craniofacial morphogenesis, including development of the teeth and the craniofacial skeleton. It has been proposed to direct terminal cell differentiation. Mutations in this gene results in haploinsufficiency that contributes to non-syndromic forms of cleft lip and/or cleft palate and tooth agenesis (Lidral *et al.*, 1998). A similar phenotype was observed in newborn mice pups that are homozygous mutant for *Msx1.*

During mouse embryogenesis the first expression of *Msx1* is detected at E6.5 in extra-embryonic tissues (Robert *et al.*, 1989). Using whole mount *in situ* hybridization at E7.5 wild type mice embryos, *Msx1* was detected in the posterior lateral plate mesoderm (Catrona *et al.*, 1996). Then at E9.5, expression was found in the dorsal neural structures including; the dorsal neural tube and cranial neural crest (Bendall and Abate-Shen, 2000).

At E10.5, *Msx1* is detected in the mandibular arch. By E11.5, expression has expanded to the whole dental arch. At the same time *Msx1* expression is found in the cushion mesenchyme (Chen *et al.*, 2007; Ishii *et al.*, 2005). It is also expressed in the pericardium, amnion, allantois, umbilical vein, neural plate, brain, cranial neural crest, tooth and limb bud (Chakraborty *et al*., 2010; Chen *et al.*, 2007; Ishii *et al.,* 2005).

At E12.5, *Msx1* transcripts are detectable in the maxillary and mandibular prominences (Medio *et al*., 2012). In mutant embryos, expression of *Msx1* stops at E13.5, but by this time, the teeth have not progressed from the budding stage to the bell stage. Consequently, the teeth will remain in the bud stage and no further tooth growth will occur in the mutant embryos (Chen *et al.*, 1996). At E17.5, the expression is finally detected in the mesenchymal valve progenitor cells (Chakraborty *et al.*, 2010).

Msx1 and *Msx2* function redundantly in multiple tissues and organs during embryogenesis, including the heart. *Msx1* and *Msx2* expression in the heart was detected in the mesenchyme and the endocardium of the cardiac cushion (Boogerd *et al.*, 2010) and the outflow tract (Chen *et al.,* 2007). Also *Msx1* and *Msx2* show dynamic patterns in the dorsal neural tube and neural crest where they demarcate the area from which neural crest cells will migrate (Graham *et al.*, 1993).

Msx1;Msx2 double homozygous mutants die in the uterus at approximately E16, with profound defects in cranial neural crest development (Satokata and Maas, 1994)

Msx1-null embryos have a normal cardiovascular system, which means that *Msx1* by itself is not essential for normal heart development. However, studying *Msx1;Msx2* double homozygous mutants revealed that the embryos suffer from severe cardiovascular defects including VSD, DORV, TOF, persistent truncus arteriosus (Chen *et al.*, 2007). At the same time, they have a deformity in the atrioventricular valves (Boogerd *et al*., 2010). All together, these data suggest that *Msx1* and *Msx2* functions are redundant but fundamental for normal heart development.

1.6.6 Notch SIGNALING PATHWAY

Notch signaling, is a highly conserved transmembrane receptor mediator of short-range cell-cell communication, regulates various aspects of cell growth and differentiation (Weinmaster, 1998). The canonical Notch signaling pathway can be activated by one of five ligands (Delta ligand 1, 3, 4, Jagged1, 2) that interact with one of four Notch receptors (Notch1-4) (Gridley, 2003). After specific ligand binding, the receptor undergoes a series of cleavage events, triggering the release of the Notch intracellular domain (NICD); this translocates to the nucleus where it is able to regulate transcription through its interactions with Mastermind-like protein (MAML) and with recombination signal sequence-binding protein (JRBP-J; Figure 1-25) (Borggrefe and Oswald, 2009).

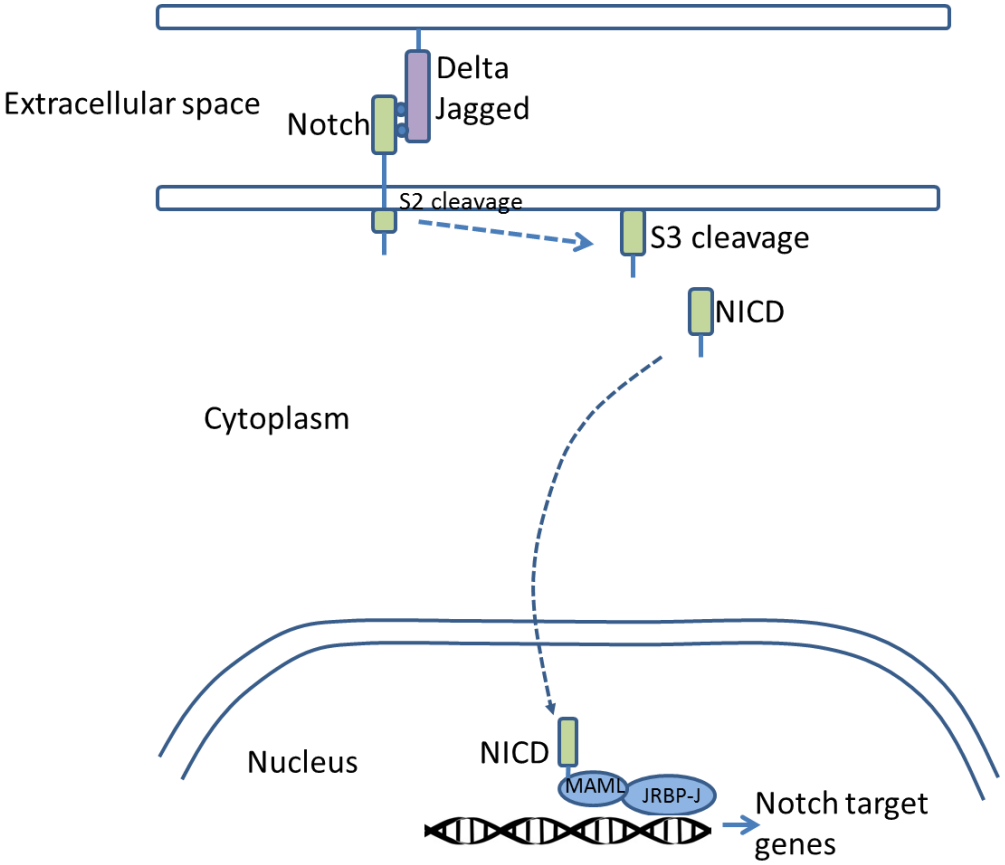

Figure 1-25: Simplified view for the notch signaling pathway.
Notch itself is a cell-surface receptor that transduces short-range signals by interacting with transmembrane ligands such as Delta and Jagged on neighboring cells. Ligand binding leads to cleavage and release of the Notch intracellular domain (NICD), which then travels to the nucleus to regulate transcriptional complexes containing the DNA-binding protein.

In both humans and mice, mutations in components of the Notch signaling pathway result in congenital heart disease characterized by cardiac outflow tract defects, all together strongly suggesting the implication of this signaling pathway in the process of cardiac and vascular development (Artavanis-Tsakonas *et al*., 1999).

In humans, the congenital disorder Alagille syndrome has been linked to haploinsufficiency of the Notch ligand Jagged1; this syndrome is a congenital heart disease affecting the cardiac outflow tract and great vessels, and causing, among others, stenosis of the pulmonary artery and its branches, VSD, and TOF (McCright *et al*., 2002). Similarly, mice deficient for the Notch target gene HRT2 develop VSD and pulmonary artery stenosis (Gessler *et al*., 2002).

Notch1 expression begins with the onset of blood flow but is pan-endothelial at the stage where erythroblasts enter circulation. Only by E9.5, after vascular remodeling has occurred, is Notch1 restricted to endothelial cells, which will contribute to arteries formation (Jahnsen *et al*., 2015). At E10.5, Notch signaling is important for NCC differentiation to smooth muscle around the PAA; consistently deficient cNCC migration, resulting in cardiac outflow tract malformations, occurs with increased or decreased Notch signaling in NCC (Mead and Yutzey, 2012).

There have been several *in vitro* studies indicating contradictory roles of Notch in smooth muscle cell differentiation. For example, Notch and its downstream target genes have been shown to inhibit myocardin-induced smooth muscle cell differentiation (Doi *et al*., 2006). Conversely, Notch has been shown to promote the formation of smooth muscle–like cells from peripheral nerve–derived neural crest stem cells *in vitro* (Morrison *et al*., 2000). Additionally, other *in vitro* studies have implicated Notch in regulation of smooth muscle cell proliferation and survival (Morrow *et al*., 2005). Moreover, Notch plays a critical role in remodeling of the aortic arch arteries (High *et al.,* 2007). Inhibition of Notch prevents the differentiation of cNCC precursors into smooth muscle cells *in vitro*. Gain or loss of Notch signaling in cNCC results in decreased smooth muscle cell differentiation of NCC derivative cells in multiple PAA (Mead and Yutzey, 2012).

All this demonstrates a critical cell-autonomous role for Notch within NCC during cardiovascular development and suggests regulation of NCC migration, proliferation, and differentiation in multiple derivative cell lineages by the Notch pathway. In addition, manipulation of Notch signaling *in vivo* results in cranial, cardiac, and enteric NCC deficiency with characteristic congenital malformations. Therefore, precise levels of Notch signaling are necessary for regulation of NCC-derived cell lineages in multiple tissues and organ systems (High *et al*., 2007; Mead and Yutzey, 2012).

1.7 HYPOTHESIS AND AIMS

In this thesis, it is hypothesized that the *Pax9*-null cardiovascular phenotype is modified by mutation in *Msx1*

The aims of this thesis:

- Identify if the *Pax9*-null cardiovascular defects observed on a C57Bl/6 genetic background are present on an outbred CD1 genetic background.
- Explore the potential genetic interaction between *Pax9* and *Msx1* in cardiovascular development
- Investigate the mechanism by which *Msx1* affects the remodeling of the pharyngeal arch arteries

2 MATERIALS AND METHODS

2.1 GENERAL REAGENTS

2.1.1 PHOSPHATE BUFFER SALINE

Phosphate buffered saline (PBS) was prepared from tablets (Oxoid, BR0014). 100 tablets were dissolved in 1 litre of double distilled water (ddH_2O) to make 10x PBS and autoclaved before use. 1X PBS was made by adding 100ml of 10X PBS to 900ml of ddH_2O.

2.1.2 RNase-FREE PBS

For work sensitive to RNase activity, 1X PBS was treated with 0.1% diethyl pyrocarbonate (DEPC) (1ml/1000ml) for 4 hours and then autoclaved.

2.1.3 PARAFORMALDEHYDE

4% weight per volume (w/v) paraformaldehyde (PFA) was made by dissolving 40g of PFA in one litre of 1x DEPC-PBS. This solution was used to fix all the embryos unless otherwise stated.

2.1.4 Tris-EDTA BUFFER

10ml of tris-EDTA buffer (TE) at pH 8.0 was prepared by adding 0.05 ml of 2M Tris with pH 8.0 and 0.1 ml of 0.5M EDTA with pH8.0 to 9.85 ml of ddH_2O.

2.1.5 SALINE SODIUM CITRATE

One litre of 20X Saline Sodium Citrate (SSC) was prepared by dissolving 175.35g NaCl and 88.23g sodium citrate in one litre of ddH2O.

2.1.6 Tris-acetic acid-EDTA BUFFER

Tris-acetic acid-EDTA buffer (TAE) is a basic laboratory buffer. It is used for making gels and as a buffer for electrophoresis. One litre of 50X TAE was prepared by adding 242g Trizma base, 57.1ml glacial acetic acid, 100ml of 0.5 M Ethylene diamine tetra acetic acid (EDTA) in one litre of ddH_2O. 1X TAE was made by adding 20ml of 50X TAE to 980ml of ddH_2O.

2.1.7 LURIA BROTH MEDIA

Luria broth (LB) media was prepared by adding 10g Sodium chloride, 10g tryptone and 5g yeast extract to one litre of ddH_2O and then autoclaved. Ampicillin (50 µg/ml) was added to the media when needed.

2.1.8 LURIA BROTH AGAR PLATES

Luria broth (LB) agar was prepared by adding 5g sodium chloride, 5g tryptone, 2.5g yeast extract and 7.5g agar to a 500ml of ddH_2O and then autoclaved.

After removing the solution from the autoclave, the agar solution was allowed to cool to 55°C then 50 µg/ml of ampicillin added to the media before pouring 20ml of the media into 10cm polystyrene petri dishes.

2.2 MOUSE LINES

All animals were handled in accordance with institutional and national guidelines for the care and use of laboratory animals the (Scientific Procedures) Act 1986 of the UK government. The protocol was approved by the Newcastle University animal ethics committee. Mice were maintained on a congenic CD1 genetic background, and intercrossed to produce embryos and neonates of the required genotypes. All adult mice were kept in individually ventilated cages and on a light/dark cycle for 12-hour for each cycle.

Throughout this study we either crossed *Pax9;Msx1* double heterozygous mice or *Pax9;Msx1* double heterozygous mice with *Pax9* heterozygous mice in order to generate mutant and control embryos between the ages of E9.5 and E15.5, and neonates. Embryonic age was calculated by noting the morning of vaginal plug detection as E0.5 based on the assumption that embryos were E0.5 at noon on the day of detection of vaginal plug.

2.2.1 *Pax9* and *Msx1* MICE

Pax9$^{+/Lacz}$ mice (Figure 2-1) have the insertion of a promoterless *Escherichia coli* ATG–lacZ–neomycin-poly (A) cassette into the coding sequence of the *Pax9* gene (Peters *et al.*, 1998)

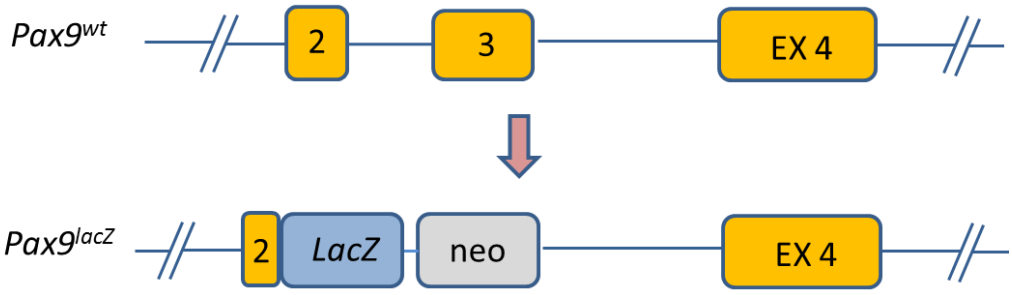

Figure 2-1: Schematic representation of the *Pax9*^{lacz} allele.
The *Pax9*$^{+/Lacz}$ mouse was generated by the introduction of a lacZ-neomycin cassette into the ATG-containing exon of *Pax9*, and the removal of the paired-box domain containing exon three. This disrupts the function of *Pax9* but allows for the expression of the lacZ gene from the endogenous Pax9 promoter.

Msx1 mice (Figure 2-2) have the insertion of a pMC1-neo cassette into the *Bgl*II site of the *Msx1* homeobox, eliminating this region (Satokata and Maas, 1994).

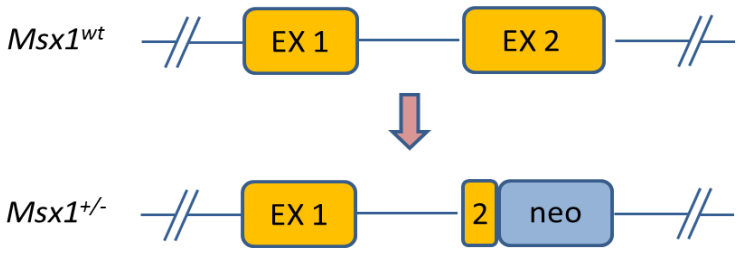

Figure 2-2 : Schematic representation of the *Msx1*$^{+/-}$ allele.
A neo cassette was inserted into the coding sequence of the *Msx1* locus by homologous recombination in ES cells. The interruption to the second exon, which contains the homobox domain, results in a loss of function of the *Msx1* gene.

2.2.2 *Pax9*^{Flox} MICE

Pax9^{flox} mice (Figure 2-3) have two loxP sites flanking exon 1 and exon 2 of the *Pax9* gene (Kist *et al.*, 2007).

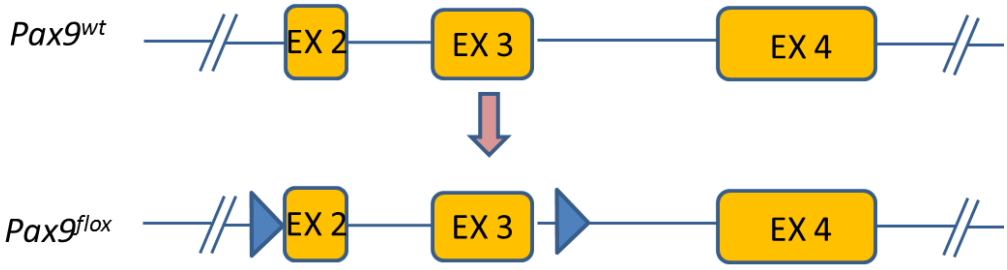

Figure 2-3 : Schematic representation of the *Pax9*^{flox} allele.
Two LoxP sites (blue triangles) flanking the *Pax9* exons 2 and 3, which include the start codon and the paired domain, respectively, were introduced into ES cells by homologous recombination.

2.2.3 *Pax9cre* MICE

*Pax9*cre mice were generated by inserting a *Cre* -mediated recombination to the ATG site of the *Pax9* gene (unpublished data).

2.2.4 *Isl1cre* MICE

Isl1cre mice were generated by *Cre* knocking into the endogenous *Isl1* locus, replacing the endogenous *Isl1* ATG (Yang *et al.*, 2006).

2.2.4.1 Genetic background.

Pax9$^{+/-}$, *Msx1*$^{+/-}$ and *Pax9*^{flox} mice were acquired from Dr Heiko Peters (Institute of Genetic Medicine) and had all been backcrossed for more than 10 generations on to CD1, which is considered to be >99% pure on the CD1 background. The *Pax9cre* mouse was imported from Dr Rene Maehr, University of Massachusetts and backcrossed on to the C57Bl/6 background for five generations, giving approximately 95% C57Bl/6 pure genetic background (Table 2-1).

The *Isl1cre* mouse was acquired from Prof Deborah Henderson and was on an unknown mixed genetic background. It was, outcrossed with a wild-type CD1 mouse to give *Isl1Cre* mice with 50% CD1 genetic background. These mice were subsequently crossed with *Pax9*$^{flox/flox}$ females (>99% CD1 background) to generate the male *Pax9;Isl1Cre* stud males used in this study (75% CD1 genetic background) (Table 2-1).

Table 2-1: Genetic background of the mice that were used during this study.

Mouse	Genetic background
Pax9$^{+/-}$	>99% CD1
Msx1$^{+/-}$	>99% CD1
Pax9^{Flox}	>99% CD1
Pax9cre	~95% C57Bl/6
Isl1cre	~75% CD1

2.3 EMBRYO DISSECTION

The pregnant dam was sacrificed by a schedule one method and the uterus was removed and flooded with PBS. Each embryo was removed from the uterus and the yolk sac was then dissected free and retained for genotyping. Embryo stage was confirmed by somite counting. Embryos were fixed in 4% paraformaldehyde (PFA). For E14.5 and E15.5 stage mice, slits were made in the skin beneath the forelimbs to allow sufficient penetration of the fixative.

Embryos for whole mount *in situ* hybridization were collected at E9.5 and E10.5 in ice-cold DEPC-PBS. Embryos were fixed in 4%DEPC-PFA overnight and dehydrated in methanol as described in section 2.14.2

Embryos for MRI were analysed at E14.5 and E15.5. They were collected and dissected in Hanks' balanced salt solution with 5mM EDTA warmed to 37ºC. The dissection procedure was performed on a heated mat to keep the embryo warm during the procedure. The presence of blood limits the contrast in MRI scans so the umbilical cord was cut to allow the embryo to fully bleed out, but for no longer than 20 minutes. The left forelimbs were removed and lysed for genotyping. Polymerase chain reaction was used to identify genotypes for *Pax9* and *Msx1* as described in 2.4.2. Embryos were fixed in 4% PFA for at least one week.

Embryos for micro computer tomography (µCT) were collected at E12.5 and E15.5. Embryos were collected and dissected in PBS at room temperature. For E12.5, the yolk sac was collected for genotyping but for E15.5 the left limb was collected. Embryos were rinsed with PBS and fixed in 4% PFA until they sent for scanning.

2.4 GENOTYPING

2.4.1 DNA EXTRACTION

DNA extraction from the yolk sac or limb was carried out using lysis buffer (50Mm KCL, 1.5 Mm MgCL2, 10Mm Tris PH 8.5, 0.45% NP40, 0.45% TWEEN-20) with proteinase K (concentration of 20µg/ml). The tissue was placed into a 1.5 ml centrifuge tube and incubated at 56ºC until the sample had completely lysed (from 30 minutes up to two hours). During the incubation, the samples were vortexed two to three times to ensure complete breakdown of the tissue, and release of the DNA. Proteinase K was heat inactivated by incubation at 95ºC for 10 minutes.

The lysed samples were centrifuged at full speed for 1 minute to collect any debris and then stored at 4ºC until used. The final volume of the lysis buffer and proteinase K prepared was dependent on the tissue piece that was used to extract DNA (Table 2-2).

Table 2-2 : Volumes of lysis buffer used in DNA extraction from various tissues.

The lysed sample	Volume of the lysis buffer
E8.5 yolk sac	30µl
E9.5 yolk sac	50µl
E10.5 yolk sac	100 µl
E11.5 yolk sac	200µl
E12.5 yolk sac	300µl
E13.5 yolk sac and E15.5 forelimb	400 µl
Ear notch	150 µl

2.4.2 POLYMERASE CHAIN REACTION

Adult mice and embryos were genotyped by polymerase chain reaction (PCR) on extracted DNA. PCR reactions were carried out using the following components: 1 unit GoTaq polymerase (Promega),1x GoTaq reaction buffer (contains 1.5 mM $MgCl_2$), 0.5 µl each deoxyribonucleotide triphosphate (dNTP; Fisher), 0.5 -1 µl forward primer, 0.5 -1 µl reverse primer (Table 2-3) and 2 µl cell lysate DNA prepared as above (section 2.4.1), with the final reaction volume made up to 20 µl with dH_2O.

For multiple PCR reactions, a master mix was made to minimize the pipetting error and reduce contamination. Then 2 µl of the template DNA and 18 µl of the master mix was then added to each tube. During the process, the primers, dNTPs, template DNA and the Go Taq polymerase were kept on ice to prevent degradation.

The PCR reaction was performed in a DNA Engine thermo-cycler (Gene flow) for 30 to 35 cycles with denaturation at 94ºC for 2 minutes, annealing at primer specific temperature for 30 to 40 sec and elongation at 72ºC for 30 to 40 sec. Primers used for each gene are described in table 2-2.

PCR products were analyzed by electrophoresis on a 2% agarose gel in 1X TAE buffer with ethidium bromide added to a final concentration of 0.5µg/ml. PCR products were run alongside a GeneRuler™ 100 bp or 1 kb DNA ladder (Fisher Scientific) at 100 volts for 30 - 40 minutes, until the bands had fully separated. Then the gel was imaged under ultraviolet (UV) light.

Table 2-3: Primer sequences used for genotyping by PCR.

Gene	Primer	Sequence	TM	Cycles per PCR	Product size
Pax9	P9-gen2-F1	ACTCACCGGCCTGCACCAATTAC	58ºC	35	WT 196bp Mutant 450bp
	P9-gen2-R1	TTGTTCTCACTGAGCCGGCCTGT			
	P9-gen2-R2	GGATGTGCTGCAAGGCGATTAAG			
Msx1	M1-F1b	CCTACGCAAGCACAAGACCAAC	58 ºC	35	WT 202bp Mutant 410bp
	M1-R1b	CTCCTGCAGTCTCTTGGCCTTA			
	M1-R2b	GGCCACACGCGTCACCTTAATA			
Pax9 flox-Lox1	P9-lox1-F	AGCGGAGACAAGGATGAAACCAC	56ºC	35	WT 305 bp Mutant 351bp
	P9-lox1-R	AGAGGAATCCCGATGTTCACCAG			
Pax9 flox -Lox2	Pax9-lox2-F	TTCGGCTGCTGTCTCTGGTT	54ºC	35	WT 200 bp Mutant 351bp
	Pax9-lox2-R	CCGGACTGTATGGTACAGAA			
S1Xcre	S1X-A	GCATAACCAGTGAAACAGCATTGCTG	55ºC	30	280bp
	S1X-B	GGACATGTTCAGGGATCGCCAGGCG			

2.5 HISTOLOGY

2.5.1 WAX EMBEDDING AND SECTIONING

Embryos were collected at the desired developmental stages and fixed in 4% paraformaldehyde (PFA) overnight at 4ºC. The embryos were dehydrated through a graded ethanol series (50%, 70% x 2, 90%, and 100% x 2) at room temperature. Embryos were incubated in histoclear, then a 1:1 solution of histoclear : paraffin wax at 60ºC. Embryos were then incubated in wax to allow the paraffin to penetrate the tissue before embedding in paraffin wax. The incubation times depended on the age of the embryo and are shown in table 2-4. E9.5 – E11.5 embryos were embedded to

be sectioned in a coronal orientation, while E15.5 embryos were embedded for sectioning in a transverse orientation.

Embryos were sectioned at 8 µm thickness using a Leica RM 2235 microtome. The sections were placed on a slide covered with water on a 37ºC hot plate (Thermo Scientific) to stretch the tissue sections. After the water dried, the sections were transferred to a 37ºC slide oven (Genlab Ltd) to ensure that the water had completely evaporated and the sections were firmly adhered to the slides.

Table 2-4: Protocol for dehydration and processing of embryos for histology.

	E9.5	**E10.5**	**E11.5**	**E12.5**	**E15.5**
4%PFA at 4 ºC	1 night	1 night	1 night	2 nights	2-3 nights
Wash with PBS					
50%EtOH	30 minutes	30 minutes	1 hour	2 hours	3 hours
70% EtOH	30 minutes	30 minutes	1 hour	2 hours	3 hours
	30 minutes	30 minutes	1 hour	Overnight	Overnight
95%EtOH	30 minutes	30 minutes	1hour	2hours	3 hours
100% EtOH	30 minutes	30 minutes	1 hour	2hours	3 hours
	30 minutes	1 hour	1hour	Overnight	Overnight
Histoclear	10 minutes	15 minutes	20 minutes	20 minutes	30 minutes
	10 minutes	15 minutes	20 minutes	20 minutes	30 minutes
Histoclear /Wax at 60 ºC	15 minutes	20 minutes	20 minutes	30 minutes	1 hour
Histoclear X ¾ at 60 ºC	20 minutes	30 minutes	40 minutes	1 hour	1 hour
	20 minutes	30 minutes	40 minutes	1 hour	1 hour
	20 minutes	30 minutes	40 minutes	1 hour	1 hour
					1 hour

2.5.2 HEMATOXYLIN AND EOSIN STAINING

Sections were stained with haematoxylin and eosin to examine histology. Haematoxylin stains the cell nuclei purple, while eosin stains the cytoplasm pink. Slides were dewaxed in histoclear (2 x 2 minutes) and then dehydrated in 100% EtOH twice for 3 minutes each time followed by immersing the slides in 90%, 70%, and 50% EtOH for 2 minutes each time. The slides were then rinsed in ddH_2O for 2 minutes.

The sections were stained in Harris' hematoxylin solution for 5 minutes followed by washing under running tap water for 5 minutes to remove the excess hematoxylin. The slides were then dipped 2-3 times in an acid alcohol solution (1% v/v

hydrochloric acid (HCl), 70% ethanol) to remove excess staining from the tissue except from the nucleus. The sections were then immediately rinsed in tap water for 5 minutes and then incubated in eosin (Fisher Scientific) for 3 minutes, the slides rinsed under running tap water for 5 minutes then dehydrated by dipping in 50%, 70%, 90% and 100% EtOH (x2) for 2 minutes each time, then incubated in histoclear (2 x 10 minutes).

Finally, the slides were mounted with a coverslip using histomount (National Diagnostics) and examined with a Zeiss Axioplan microscope equipped with Axiovision software (Carl Zeiss, Jena, Germany).

2.5.3 SLIDE IMMUNOHISTOCHEMISTRY: FLUORESCENCE

Immunofluorescence staining of embryos at E9.5, E10.5, E11.5 and E15.5 was performed on paraffin sections that had been generated as described in section 2.5.1. Antigen retrieval was performed in citric acid buffer inside a pressure cooker at 80kPa for 5 minutes, followed by 20 minutes waiting to cool down. The slides were then rinsed in tap water, and washed with Tris Buffered Saline with Triton-X100 (TBS-TX;Tris-HCl-pH7.5, 5M NaCl, Triton-100 X, ddH_2O) for 5 minutes.

Sections were blocked using 10% fetal calf serum (FCS) in TBS-TX for 30 minutes before 120 µl of a cocktail of primary antibodies in 2% FCS in TBS-TX was added to each slide. The slide was then covered with a piece of parafilm and incubated overnight at 4°C in a humidified chamber.

The next day slides were washed with TBS-TX for (3 x 5 minutes). Secondary antibodies diluted in 2% FCS in TBS-TX were added to each slide, covered with parafilm and incubated in a humid chamber for two hours at room temperature. They were then washed in TBS-TX (3 x 5 minutes) in dark, mounted in vectashield with 4',6-diamidino-2-phenylindole (DAPI, Vector laboratories LTD, H1500) and stored at 4ºC until analysed. The primary and secondary antibodies and the concentrations used are listed in table 2-5.

When probing with the AP-2α antibody, slides were blocked using TBS-TX, 5% donkey serum and 0.2% BSA for 30 minutes. The remaining Block was diluted 1:5 with TBS-TX. Mouse anti-AP-2α primary antibody was diluted in block diluted 1:5,

and 120 µl of primary antibodies was applied to each slide. Each slide was covered with a piece of parafilm and incubated overnight at 4ºC in a humidified chamber.

The next day primary antibody was removed by washing three times in TBS-TX for 5 minutes each. The slides were then incubated in secondary antibodies diluted TBS-TX for 2 hour at room temperature, in a humidified chamber. Slides were then washed three times in TBS-TX for 5 minutes each in dark before mounting in Vectashield with DAPI and stored at 4ºC until analysed.

Table 2-5: Primary and secondary antibodies used.

Primary antibody	Concentration	Secondary antibody	Concentration
Anti- alph-smooth muscle actin (Sigma, A5228)	1:500	Alexafluor 594 donkey anti-mouse IgG (Invitrogen, A21203)	1:200
Anti-AP-2α (3B5, Santa Cruz Biotechnology, sc-12726)	1:50	Alexafluor 594 donkey anti-mouse IgG (Invitrogen, A21203)	1:200
Cleaved Caspase3 (Asp175, Cell Signalling)	1:100	Alexafluor 594 donkey anti-rabbit IgG (Invitrogen, A21203)	1:200
Anti- ERG (Abcam, Ab92513)	1:750	Alexafluor 488 donkey anti-rabbit IgG (Invitrogen, A21203)	1:200
Anti-GFP (Abcam, ab13970)	1:200	Alexafluor 488 donkey anti-rabbit IgG (Invitrogen, A21203)	1:200

Anti Phospho-Histone H3 (Millipore, 06-570)	1:300	Alexafluor 594 donkey anti-rabbit IgG (Invitrogen, A21203)	1:200

2.5.4 SLIDE IMMUNOHISTOCHEMISTRY: FLUORESCENCE –USING TSA KIT

Tyramide signal amplification (TSA) kit (Perkin Elmer, Cat# NEL704A001KT) was used to amplify the fluorescent signal from immunohistochemistry. A weak signal can be caused by low levels of primary antibody expression. TSA kit improves the detection sensitivity and the fluorescent images.

Embryos were collected and fixed using 4% PFA overnight, then processed and wax embedded as described above (section 2.5.1). For staining, the slides were dewaxed in histoclear (2 x 10 minutes), followed by rehydration in an ethanol series (100% x2, 95%, 70% and 50% EtOH; 2 minutes each), then placed under running tap water for 2 minutes.

Slide immunohistochemistry for Cleaved Caspase 3 to label cells undergoing apoptosis was carried out on coronal sections of E9.5 and E10.5 embryos. Antigen retrieval was carried out using citric acid buffer inside a pressure cooker at 80kPa for five minutes, followed by 20 minutes waiting period to cool down.

The slides were washed (3 x 5 minutes) with TBS-TX. The sections were blocked with TNB blocking buffer (TNB; Perkin Elmer, Cat# NEL704A001KT) for 30 minutes. Purified cleaved caspase 3 antibody (Cell Signaling, 1661), diluted 1:100 in TNB buffer, was applied to each slide, the slides were covered with a piece of parafilm then incubated at 4ºC overnight in a humid chamber.

The next day, the slides were washed in TBS-TX (3 x 3 minutes), and then incubated with biotinylated goat anti-rabbit secondary antibody (Dako, 00094167), diluted 1:200 in TNB, for two hours at room temperature. The sections were washed with TBS-TX (3 x 5 minutes) followed by addition of anti-fluorescein-HRP (Perkin Elmer, Cat# NEL704A001KT) and incubation for 30 minutes. The sections were then washed with TBS-TX (3 x 3 minutes). The sections were incubated with 100µl of fluorescein-tyramide-plus solution, diluted 1:50 in the provided dilution buffer, for 10 minutes in

the dark at room temperature. The sections were then washed with TBS-TX (3 x 3 minutes) in dark. Cover slips were then mounted using Vectashield with DAPI (Vector laboratories LTD, H1500). The slides were examined with a Zeiss Axioimager microscope (Carl Zeiss, Jena, Germany).

2.6 CELL COUNTING AND STATISTICS

Cells were counted from coronal histological sections of the pharyngeal arch region stained with appropriate markers suitable for the purpose of the experiment. Three sections were analysed for each stained embryo (3 embryos at least in each group). Analysis was performed using Image J software (available from http://rsbweb.nih.gov/ij/) to calculate the number of the cells. Statistical significance ($P<0.05$) was determined by one-tailed ANOVA.

Statistical differences between the incidences of cardiovascular defects between two different genotypes were calculated using a two-paired T-test. One-tailed ANOVA test was used to determine whether there are any significant differences between the means of three independent groups, all these tests were carried out using the SPSS program. Statistical significance was considered when the p-value was <0.05.

2.7 WHOLE-MOUNT EMBRYO STAINING

2.7.1 BONE AND CARTILAGE STAINING

Bone and cartilage staining was performed of the whole skeletal system at Postnatal day 0 (P0) neonates. The neonate was either found dead in the breeding cages on the day of birth or euthanised using 200mg/ml of euthatal (Merial). First, the neonate was examined to check the external and internal phenotypes. Neonates were scalded in a 70ºC water bath for 30 seconds for easier maceration of the tissue later. The skin was peeled carefully away with forceps and the neonate eviscerated, removing all the peritoneal and pleural cavities, followed by fixation in 95% EtOH overnight at room temperature.

The neonate was transferred to acetone at room temperature for 48 hours to remove the fat. They were then rinsed in water for 5 minutes and stained for cartilage by incubating the neonate in 0.01% alcian blue (Sigma) for 8 days.

The neonates were then washed three times with 70% EtOH over 8 hours, and covered with 1% KOH overnight until the tissue was visibly cleared. Counterstaining of the bone was performed with 0.001% alizarin red (Sigma) overnight. The neonates were cleared by placing it in a 1% KOH/20% glycerol solution for 3 days which was then replaced with a glycerol series (50%, 80% and 100%) for 2 days each time. The neonates were then stored in 100% glycerol at room temperature until examined under a stereomicroscope (Leica, Stemi 2000).

2.7.2 LacZ STAINING

For visualisation of LacZ, embryos were collected at E9.5 in ice-cold PBS. The embryos were washed twice in 5ml of ice-cold PBS at 4ºC then fixed in 4% PFA for 5 minutes. The embryos were then washed again 3 times in PBS at room temperature, and the PBS was replaced with the staining solution (0. 2M K-ferrocyanide, 0.2M K-ferricyanide, 20mg/ml X-Gal) and stained overnight at room temperature in the dark.

On the following day, the embryos were washed twice with PBS for 5 minutes each time and fixed in 4% PFA overnight.

2.8 MAGNETIC RESONANCE IMAGING

Embryos for magnetic resonance imaging (MRI) were collected at E15.5 as previously described in section 2.3

2.8.1 PREPARING EMBRYOS FOR MRI

MRI tubes were prepared as described previously (Bamforth *et al.,* 2012). Before fixation embryos were washed with PBS. Slits were made in the skin beneath the forelimbs at the side of the abdomen to allow sufficient penetration of the fixative. Embryos were fixed with 4% PFA for at least one week at 4ºC. The embryos were then fixed in 4% PFA containing 4 µl/ml Magnevist (gadopentetate dimeglumine, Gd-DTPA) for a minimum of 4 days at 4ºC before loading into the MRI tube.

Fixed embryos were embedded in 1% agarose plus Gd-DTPA contrast agent (4µl/ml) in a glass tube (diameter 28mm; Fluorochem, UK), stacking the embryos in 8 layers of 4 embryos each layer for a total of 32 embryos per tube. The tube contained a teflon disk attached to a plastic rod to allow the embryos to be removed

from the tube after scanning. To identify each embryo in each layer, a different limb or the tail was removed; this data was recorded in a sheet with the ID number and the genotype of each embryo. The tube was sealed with a lid and parafilm and sent to Oxford for scanning (Dr Jürgen Schneider, British Heart Foundation MRI unit, University of Oxford, UK).

2.8.2 DATA ANALYSIS AND EMBRYO PROCESSING

Amira software (FEI Visualization Science Group) was used to reconstruct the collected data stacks as 3D models. The voxel size used was: X-25.4, Y-25.4, and Z-24.4. The images were cropped to the region of interest and the program was used to create 3D models for the heart. After the embryos were returned from Oxford, they were processed for histology as previously described (section 2.5.1) to obtain higher resolution images and check the fine detail that was not clear in the MRI images.

2.9 MICRO COMPUTER TOMOGRAPHY

Micro computer tomography (µCT) was carried out on E12.5 embryos, to investigate the morphological changes on the 3rd PAA and on E15.5 embryos to study the cardiovascular phenotype of mutants and control embryos.

Embryos were collected as previously described in section 2.3 and fixed in ice-cold 4% PFA at 4ºC until they were sent for scanning. Embryos were put in separate tubes with 4%PFA and sent to Oxford for scanning (Dr Jürgen Schneider; British Heart Foundation MRI unit, University of Oxford, UK).

2.10 INK INJECTION

For India ink injections, embryos were collected at E10.5. The India ink was diluted (1:1) in water. Embryos were harvested quickly, then dissected and transferred to a petri dish containing 1% agarose flooded with PBS. The embryos were pinned in the agarose and ink injected into the left ventricle while the circulation was still active using a pulled glass needle and a mouth pipette. The embryos were photographed from both right and left sides using a Leica MZ6 microscope (Leica).

2.11 BIMOLECULAR FLUORESCENCE COMPLEMENTATION (BiFCO) ASSAY

2.11.1 JEG-3 CELL CULTURE

Human placental choriocarcionoma cells (JEG3) were used for all *in vitro* experiments. Cells were cultured in high glucose Dulbecco's modified eagle medium (Life Technologies) supplemented with 10% (v/v) fetal bovine serum (FBS, Life Technologies) and 100units/mL of Penicillin and 100µg/mL of Streptomycin (Life Technologies). These cells were cultured at 37ºC in the presence of 5% CO_2 with high humidity. The culture media was changed every two to three days. Cells were checked under the microscope daily to ensure they were healthy and growing as expected.

The cells were passaged once a week when 80% confluent by incubating with 0.05% Trypsin in EDTA (Life Technologies) at 37ºC for 5 minutes to detach the cells. The trypsin reaction was stopped by the addition of culture media, and the cells were pelleted by centrifugation at 1000 g for 5 minutes. The pellet was re-suspended in 10ml warm complete growth medium and plated in a T75 flask, 100mm dishes or multiwell plates according to each experiment (Table 2-6).

Table 2-6: Number of cells plated for each vessel for each experiment.

Vessel	Seeding density
T75 flask	2.1×10^6
100mm dish	2.2×10^6
12 well plate	0.1×10^6

2.11.2 CLONING

Bimolecular fluorescence complementation (BiFCo) assay was performed to test for both a protein-protein interaction between Pax9 and Msx1 and direct visualisation of this interaction in living cells.

The Venus N terminal (VEN) and Venus C terminal (VEC) cloning vectors, and the VEN-GAL4 and VEC-GAL4 control plasmids, were generously provided to us by Dr. José Bragança (University of Algarve). Mouse *Msx1* and mouse *Pax9* cDNA were generated by PCR (see Table 2-7 for primer sequences and restriction enzyme sites

used) and sub-cloned into the VEN and VEC vectors respectively. Briefly, the PCR products were digested with the appropriate restriction enzyme and ligated into the cut vector, which was also dephosphorylated with Antarctic Phosphatase. All enzymatic reactions were carried out for one hour in a 37ºC water bath. Ligation of the DNA was performed with T4 DNA ligase (Promega) for one hour at room temperature and ligated constructs were subsequently transformed into DH5α competent cells and grown overnight in a 37ºC incubator. Plasmid DNA was purified using a QIAprep Spin Miniprep kit (QIAGEN) according to the manufacturer's instructions. Plasmid DNA was eluted using 30µl of dH_2O, and the concentration was estimated using the nanodrop spectrophotometer. The cloned fragments were verified by sequencing by GATC. Schematic representations of the VEC-Pax9 and VEN-Msx1 constructs are shown in figure 2-4 and figure 2-5.

Table 2-7: List of primers and restriction enzymes used for cloning.

Target	Oligo	Sequence	Restriction enzyme
VEC-Pax9	F	gggctcgagGAGCCAGCCTTCGGGGAGGTG	XhoI
	R	ggggcggccgcTCAGAGTGCAGAAGCGGTCACAG	NotI
VEN-Msx1	F	gggctcgagGCCCCGGCTGCTTGCTATG	XhoI
	R	ggggcggccgcGAGGTGACTCTGGACCCACCTAAG	NotI

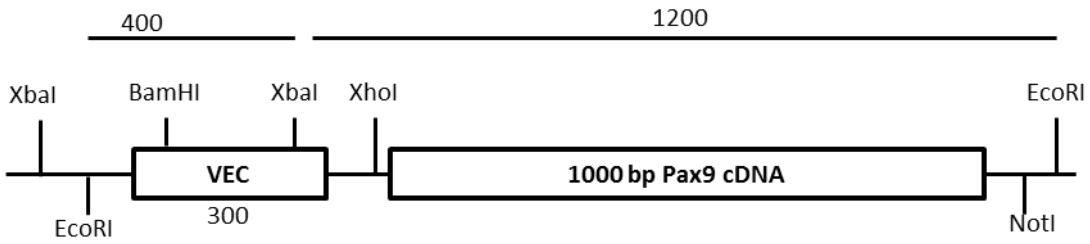

Figure 2-4: Strategy for construction of synthetic VEC-Pax9.
The VEC containing vector, and the Msx1 PCR fragment, were digested using XhoI and NotI. The vector was also dephosphorylated. The DNA was purified and ligated together. EcoRI and XbaI were used to perform a diagnostic digestion, which generated 400bp and 1200bp fragments.

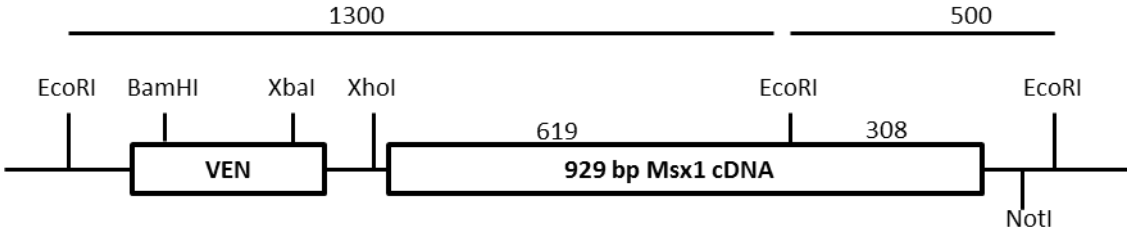

Figure 2-5: Strategy for construction of synthetic VEN-Msx1.
The vectors and the insert were serially digested using XhoI and NotI. The vector was also dephosphorylated. The DNA was purified and ligated together. To check the product XbaI and EcoRI used to perform a diagnostic digestion, which generated 400bp and 1200bp fragments.

JEG3 cells were plated at a density of $0.1x10^6$ cells per well in 12-well plates with complete medium one day prior to transfection. The following day, a transfection mix containing 1µg of plasmid DNA in 3µl of X-treme GENE 9 DNA transfecting reagent (Troche) and 47µl of PBS for a total of 50µl for each well of the 12 well plate.

Cells were transfected with VEC-*Pax9* and VEN-*Msx1* together. As a negative control for the experiment 1µg of VEN-GALA4 with 1µg VEC- Pax9 and 1µg of VEC-GALA4 with 1mg ofVEN-Msx1 were used. 50µl of the transfection mixture (1µg of the DNA-plasmid, XtremeGene9 transfection reagent (Roche) in a 3:1 ratio (µl transfection reagent: µg DNA) in 1x PBS (Life Technologies)) was added drop-wise to each well and incubated for 24 hours. Transfections were performed in triplicate for each group.

After 24 hours, the transfected cells were examined under a fluorescence microscope (Zeiss Axioimager) equipped with YFP filter. For a life cell imaging the culture media was removed, the cells rinsed three times with PBS and the cells placed in a media lacking indicator red dye. Culture media was removed from the culture plate, and cells were washed twice with PBS fixed using ice cold 4% PFA for 30 minutes at room temperature.

Finally, cells were mounted on 12 wells plate with 3 drops of vectashield PLUS DAPI (Vector laboratories LTD, H1500) and a round cover slip then left to dry overnight. Images were captured using the YFP filter on fluorescence microscope (Zeiss Axioimager).

2.11.3 INDIRECT IMMUNOHISTOCHEMISTRY

To visualise the Pax9 and Msx1 proteins, immunohistochemistry was performed. Transfected JEG3 cells were washed twice with ice cold PBS then fixed with ice cold 4% PFA for 30 minutes at room temperature. Cells were rinsed 3 times with PBS for 5 minutes each time with agitation. After that, they were blocked with 2% normal goat serum (NGS) in 1ml PBS for 20 minutes. The blocking solution was removed and the cultures were incubated with primary antibody diluted to a proper concentration in 1% Triton X-100 in PBS overnight at 4ºC.

The following day, the cells were rinsed 4 times for 20 minutes with PBS at room temperature then incubated with secondary antibody (diluted 1:200 in PBS) for 2 hours in dark at room temperature. The primary and the secondary antibodies used and concentrations are listed in table 2-8. Cells were washed again (4 x 20 minutes) with PBS in the dark at room temperature. Finally, cultures were mounted on 12 well plate with 3 drop of vectashield PLUS DAPI (Vector laboratories LTD, H1500) and a round cover slip then left to dry overnight. Images were captured using the YFP filter on the Zeiss Axioimager microscope.

Table 2-8: List of primary and secondary antibodies.

Primary Antibody	
Primary	**concentration**
Anti-Msx1antibody (Abcam, ab49153)	IP: 1µl/250µl
Ani-Pax9 antibody (Provided by Dr. Heiko Peters)	IP: 10µl/1ml WB:30µL/10ml
Secondary Antibody	
Mouse anti-rat IgG (Life Technologies, A-21208)	1:200
Rat anti-mouse IgG (Life Technologies, A-11029)	1:200

2.12 WESTERN BLOT

2.12.1 SAMPLE COLLECTION AND LYSIS

JEG3 cells were cultured in a 10 cm plate at a density of 2.2 x 10^6 cells for 24 hours then transfected with 100µl of VEC-*Pax9* and VEN-*Msx1 (*1µg/µl). 24 hours post transfection, cells were rinsed with ice cold PBS. To dissociate the cells 1ml of radioimmunoprecipitation assay buffer (RIPA buffer; 50mM Tris, 150mM NaCl, 0.1% SDS, 0.5% sodium deoxycholate, 1% Triton X) was added and the cells scraped from the plate using a cold plastic cell scraper. The cells were transferred to a cold microcentrifuge tube where they were maintained under constant agitation in a 4ºC cold room for 30 minutes. The tube was spun at 16,000 x g for 20 minutes in a 4ºC pre-cooled centrifuge. The supernatant, containing the protein, was transferred to a fresh tube and stored at -20ºC until required.

2.12.2 WESTERN BLOTTING

Commercially available pre-cast gels (Novex® Tris-Glycine Gel, Life Technologies) were used. The electrophoresis tank was filled with 1x running buffer (25mM Tris pH8.0, 190mM glycine, 0.1% SDS). Ten µl of each sample was loaded into a well, and 10 µl of protein ladder (Thermo Scientific) was loaded to run alongside the samples. The gel was run at 180 V for 90 minutes.

For protein transfer a polyvinyl difluoride (PVDF) membrane was activated by immersing in 100% methanol for 30 seconds, rinsed in dH_2O for 5 minutes, and then equilibrated in ice cold transfer buffer (48mM Tris, 39mM glycine, 0.04% SDS, 20% methanol) for 20 minutes. The protein gel was placed onto the membrane and a sandwich was created with the gel and the membrane between two sheets of blotting paper and sponge on either side. Transfer was carried out at 4ºC in the cold room, at a constant 100V for 1 hour. The transfer buffer was gently agitated with a magnetic flea throughout.

2.12.3 BLOCKING, IMMUNODETECTION AND DEVELOPMENT

The membrane was blocked in 5% skimmed milk in TBST (50mM Tris pH7.0, 150mM NaCl, 0.05% Tween-20) at room temperature for 1 hour with gentle agitation.

The membrane was then incubated with primary antibody at the appropriate dilution in 5% skimmed milk in TBST blocking solution and incubated overnight at 4ºC with gentle agitation.

On the following day, the membrane was washed with 5% skimmed- milk in TBST (4x 10 minutes) then replaced with horseradish peroxidase (HRP) linked- secondary antibody diluted 1:10,000 in 5% skimmed milk in TBST and incubated for 1 hour at room temperature. The secondary antibody was washed with 5% skimmed milk in TBST (4x10 minutes) followed with TBST for 10 minutes.

For detection of the bound secondary antibody the Super Signal West Dura Substrate (Thermo Scientific) was used. Solution A and B were mixed (1:1) and applied to the membrane for 5 minutes. Excess substrate was drained, and the membrane wrapped in a plastic sheet and exposed to an X-ray film sheet (Amersham Hyperfilm, GE Healthcare). The exposed film was developed in a film developer (Konica Minolta).

2.13 WHOLE-MOUNT *IN SITU* HYBRIDISATION

2.13.1 PROBE PREPARATION

In situ hybridisation was performed for *Msx1* using a self-made probe (Figure 2-6). All primers were designed using the NCBI Primer-BLAST tool (http://www.ncbi.nlm.nih.gov/tools/primer-blast). Primers were designed to amplify a 702 bp fragment from the *Msx1* gene (Table 2-9) using cDNA made from an E10.5 mouse embryo. The PCR product was purified using the QIAGEN PCR purification kit according to the manufacturer.

Table 2-9: Primer sequences used to generate a probe for *in situ* hybridization.

Primer	Sequence	TM	Product size
RK-Msx1-F	CACCCTACGCAAGCACAAGA	60ºC	702 bp
RK-Msx1-R	GGCCTCTGCACCCTTAGTTT		

The 702 bp *Msx1* PCR product was cloned into the pGEM-T-Easy bacterial vector (Promega). Following transformation of the ligated product into DH5α competent cells (Invitrogen), colonies were picked then screened using mini prep and a

diagnostic restriction enzyme digest. Following identification of a plasmid containing the correct insert; the plasmid confirmed by sequencing (GATC Biotech). The vector was linearised using Sac II to produce an antisense probe, and Sal I for the sense (control) probe. The linearised plasmid was purified using the QIAGEN PCR purification kit. DNA concentration was estimated using the nanodrop spectrophotometer and gel electrophoresis was used to check the quality of the probe. The DNA concentration was adjusted to 1µg/µl.

For whole mount *in situ* hybridization, both sense and antisense probes were labeled using a digoxygenin (DIG) RNA labeling kit (Roche). Size and yield were checked using gel electrophoresis. The concentration of the probe was then estimated using the nanodrop spectrophotometer. 250 ng of probe plasmid was mixed with 6X loading dye and run at 200V for 10 minutes.

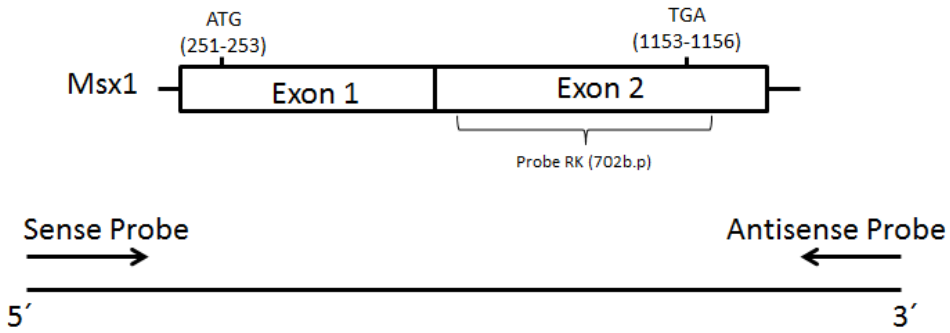

Figure 2-6: In situ hybridisation probe design.
Schematic representation of the *Msx1* transcription factor showing that Msx1 is comprised of two exons. The start (ATG) and stop (TGA) codons are indicated. The structure of the Msx1-antisense probe used for the in situ hybridizations is located within exon 2.

2.13.2 EMBRYO COLLECTION AND HYBRIDISATION

Wild type embryos were dissected at E9.5 and E10.5, in ice-cold DEPC-PBS. All tools and equipment were treated with RNase away (Fisher) to remove all traces of RNases that may degrade the RNA of interest. The brain cavities were opened with forceps to ensure the penetration of the probe during the hybridisation process. Embryos were prepared by fixing in 4% DEPC-PFA overnight, then rinsed in DEPC-PBS and dehydrated through a methanol series (25%, 50%, 75% and 100%), before being stored in methanol at -20ºC.

The embryos were rehydrated in a methanol series (75%, 50%, and 25%) and then rinsed twice in PBS. Embryos were bleached in 6% hydrogen peroxide in DEPC-PBT (DEPC-PBS, 20% tween) for one hour at room temperature and stepwise rehydrated to DEPC-PBS (phosphate buffered saline, 20% Tween-20).

After rehydration, embryos were further permeabilised by a 15 minutes incubation with 10µg/mL proteinase K (in PBT), and then rinsed in Glycine-PBT (2mg glycine for 1mL PBT) for 5 minutes to stop the reaction. Timing in this step was critical to prevent over-digestion of the embryos. Proteinase K activity was stoped by incubating embryos in 2mg/mL glycine (in PBT) for 5 minutes at room temperature, followed by two 5 minutes washes with PBT.

Afterwards the embryos were post-fixed for 20 minutes with 0.2% glutaraldehyde/4% PFA (in PBS) at room temperature followed by two 5 minutes washes with PBT.

Embryos were transferred to cryovials and prehybridisation for one hour at 70°C using pre-hybridisation solution (50% formamide, 5X SSC, 0.1% Tween, 50µg/ml Heparin, DEPC-H_2O) in an oven with gentle rocking.

The digoxigenin- labelled probes were mixed together in hybridisation buffer (50% Formamide, 5x SSC pH 4.5, 0.1% Tween-20, 50µg/mL heparin, 50µg/mL yeast tRNA, 100µg/mL salmon sperm DNA and 1µg/mL of denatured probe in DEPC-treated water) and hybridised simultaneously. Embryos were then incubated with the hybridisation solution at 70ºC overnight with gentle rocking.

The following day post-hybridisation washes were performed. First, embryos were washed twice in pre-warmed (70ºC) solution I (50% formamide, 4x SSC, 1% Sodium dodecyl sulphate (SDS, w/v) in DEPC-treated water) for 30 minutes at room temperature. This was followed by a 10 minutes wash in pre-warmed (70ºC) solution I/solution II mix (1:1 v/v; solution II: 0.5M sodium chloride, 0.01M Tris pH 7.5, 0.1% Tween-20) in the hybridisation oven with gentle agitation. Embryos were further washed three times for 5 minutes at room temperature in solution II, and then treated twice with 100µg/mL RNAse A (in solution II) for 30 minutes time at 37ºC.

Embryos then were washed for 5 minutes with solution II at room temperature, followed by a 5 min wash in solution III (50% formamide, 4x SSC, 0.2% SDS in

DEPC-treated water) at room temperature. After that, embryos were incubated in solution III for 30 min at 65ºC, twice. Embryos were transferred into glass vials, and washed three times with TBST (0.05M Tris pH7.5, 0.15M NaCl, 0.05% Tween-20) for 5 minutes at room temperature. Then blocked in blocking solution (10% Fetal calf serum (FCS) diluted in TBST (Tris-Buffered Saline with Tween 20) at room temperature for 2.5 hours. The blocking solution was replaced with 0.5µl/ml Anti-Digoxigenin-AP Fab fragments (Roche) diluted in 1%FBS/TBST and incubate overnight at 4ºC.

Embryos then underwent a series of washes using TBST solution at room temperature over a day, five times for 1 hour each followed by a final overnight wash at 4ºC. On the fourth day, the embryos were washed 5 times for 10 minutes each time at room temperature in NTMT solution (100M NaCl, 0.1M Tris pH 9.5, 0.1% Tween-20).

Embryos were developed using a developing solution (5M NaCL, 2M Tris pH 9.5, 100%Tween-20, 20µl/ml NBT/BCIP). Throughout the development reaction the samples kept covered with aluminum foil to protect them from light and the embryos were checked periodically to monitor the progress of the reaction. When the reaction was judged to be complete, embryos were washed for 10 minutes at room temperature twice with NTMT followed by a 10 minute wash with PBT pH 5.5 at room temperature. Embryos were photographed from both sides using a Leica MZ6 microscope (Leica).

3 THE EFFECT OF GENETIC BACKGROUND ON THE *Pax9*$^{-/-}$ CARDIOVASCULAR PHENOTYPE

3.1 INTRODUCTION

As the number of mouse strains and sub-strains increases, attention to genetic background is increasingly more important. Each strain has unique background alleles that may interact with and modify the expression of a mutation, transgene or other genetic insert. For example, an effect of genetic background has been described in the *Cited2*-null mouse in which there was a defect in left-right patterning observed on an altered genetic background; such as cardiac looping on a C57BL/6J background. The penetrance of this phenotype was reduced on a mixed background (Bamforth *et al.,* 2004). Likewise, a mutation of the diabetes-associated gene Leprdg on a C57Bl/6J background results in obesity with transient diabetes, but on a C57BlKS/J background, the same mutation results in obesity with overt diabetes (Greenhill, 2016).

Haploinsufficiency of the transcription factor *TBX1* is thought to be responsible for the cardiovascular phenotype in 22q11DS patients (Jerome and Papaioannou, 2001; Merscher *et al.,* 2001). Cardiovascular malformations in these patients are highly variable although the genetic insult is essentially the same. This raises questions as to whether variations in the 22q11DS phenotype are due to differences in the genetic background of an individual, and how this could influence the function of *TBX1*.

The *Tbx1* mutant mouse phenotype is also affected by the genetic background of animals (Taddei *et al*., 2001). Taddei *et al* (2001) showed a reduction in the penetrance of cardiovascular defects in 129SvEv Df1/+ genetic background embryos when compared to embryos on a C57BL/6;129SvEv mixed genetic background. In contrast, in C57BL/6 Df1/+ embryos, they found a much higher penetrance (50%) of cardiovascular defects compared to the other two genetic backgrounds.

Previous work in our lab has identified that *Pax9* potentially interacts with *Tbx1* during cardiovascular development (S. Bamforth, unpublished data). Mice doubly heterozygous for *Tbx1* and *Pax9* (i.e. *Tbx1*$^{+/-}$;*Pax9*$^{+/-}$) had a statistically significant

increase in the presentation of IAA when compared with *Tbx1*$^{+/-}$ mice. This data suggests that heterozygosity of *Pax9* is exacerbating the *Tbx1* heterozygous cardiovascular phenotype.

The *Pax9*-null cardiovascular phenotype is complex and includes outflow tract and aortic arch artery defects, these are described in detail in section 1.6.3. Because it is well recognised that transgenic mice can display altered phenotypes on different genetic backgrounds, the *Pax9*-null phenotype was examined on a congenic CD1 background and compared to the C57Bl/6J congenic background phenotype.

3.2 AIM OF CHAPTER

The aim of this chapter was to study the role of genetic background on the penetrance of the *Pax9*-null cardiovascular phenotype. The already described cardiovascular phenotype on a congenic C57Bl/6J (B6) genetic background was compared to *Pax9*-null mice on a congenic CD1 background.

3.3 RESULTS

3.3.1 *Pax9*$^{-/-}$ ON CD1 GENETIC BACKGROUND

Previous work in our group has described the cardiovascular defects that occur in *Pax9*-null mice on a congenic C57Bl/6 (B6) genetic background (B6-*Pax9*$^{-/-}$). To determine the effect of genetic background on the presentation of the *Pax9*-null cardiovascular phenotype, *Pax9*$^{+/-}$ mice on a congenic CD1 background (CD1-*Pax9*$^{+/-}$) were acquired (from Dr Heiko Peters). The mice were intercrossed and neonates at postnatal day 0 (P0) and embryos at E15.5 were collected and examined.

Externally at P0, the wild type neonates had normal hind limb digits and a normal palate that separated the oral cavity from the nasal cavity (Figure 3-1). Dissecting the wild type neonates showed two thymic lobes of normal appearance located in the anterior part of the chest directly behind the sternum but in front of the heart (Figure 3-1). Beneath the thymic lobes a normal cardiovascular system was present. The aortic arch connected the ascending aorta with the descending aorta and the three main great vessels branched directly from this arch: namely, the brachiocephalic artery, left common carotid artery, and the left subclavian artery (Figure 3-1).

Pax9$^{-/-}$ neonates on both B6 and CD1 genetic backgrounds have pre-axial digit duplication which has been previously described (Peters *et al*., 1998) (Figure 3-1). B6 -*Pax9*$^{-/-}$ and CD1-*Pax9*$^{-/-}$ neonates presented with a bloated abdomen, which is interpreted as a sign of respiratory insufficiency due to the cleft palate (Peters *et al.*, 1998). Dissecting these neonates showed that *Pax9*-null neonates on both genetic backgrounds presented with an absent thymus and cardiovascular defects including IAA, ARSA and absence of one or both common carotid arteries (Figure 3-1).

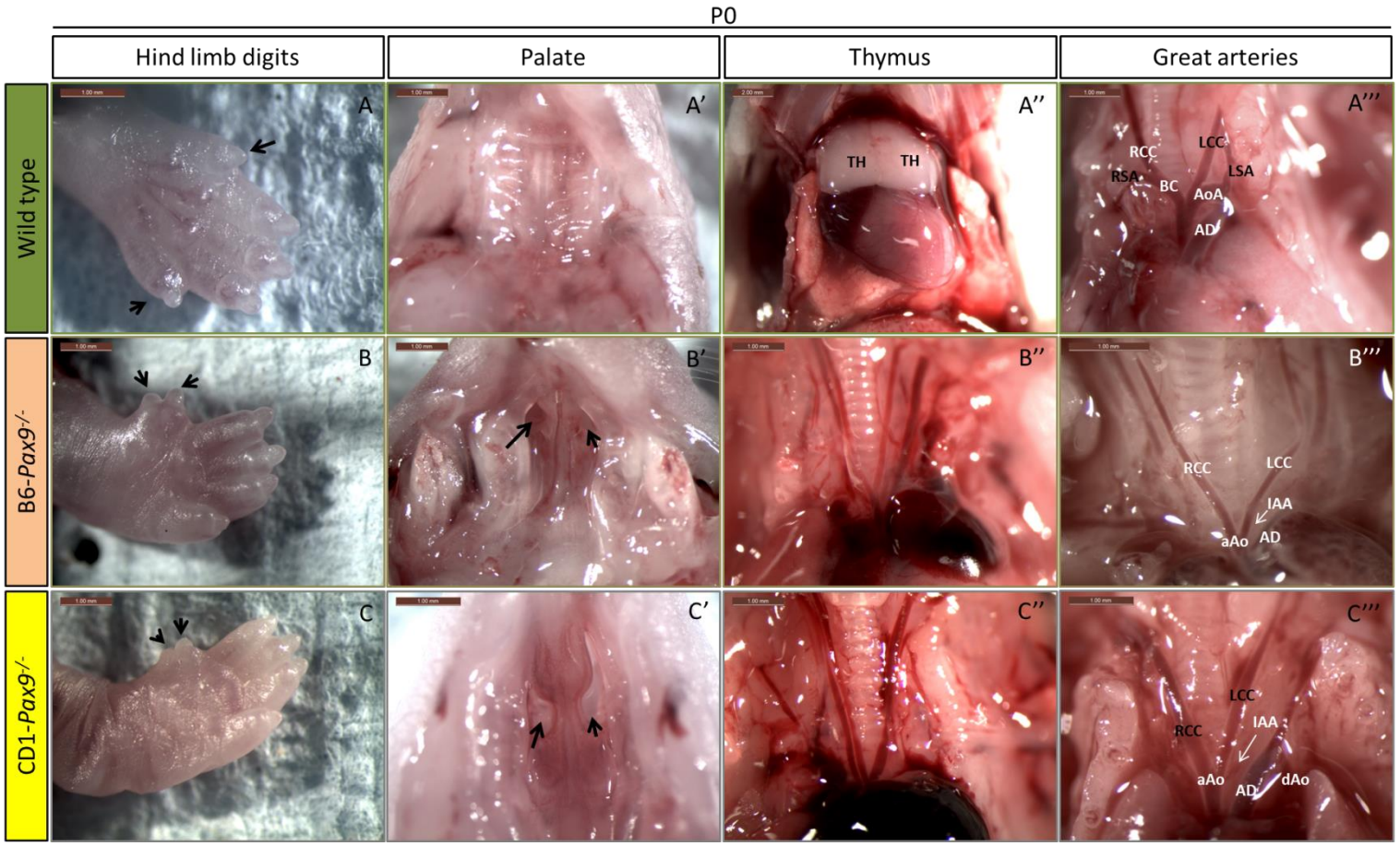

Figure 3-1: Comparison of neonatal *Pax9*-null phenotypes between wild type, C57Bl/6J and CD1 backgrounds.
All neonates were collected at P0. Wild type neonates presented with a normal hind limb digits **(A)**, normal palate **(A')**, and two identical lobes of the thymus **(A'')** located in the anterior part of the thoracic cavity, it extends from the inferior part of the neck to the superior mediastinum. **(A''')**The aortic arch (AoA) gave rise to the brachiocephalic artery (BC), the left common carotid artery (LCC) and the left subclavian artery (LSA). The arterial duct (AD) in this neonate is still patent **(A''')**. **(B-B''')** *Pax9*-null neonates on a congenic C57Bl/6J background (B6-*Pax9*$^{-/-}$) displayed pre-axial digit duplication **(B')**, cleft palate **(B')**, absent thymus **(B'')**, and the cardiovascular defect including interruption of the aortic arch (IAA) **(B''')**. **(C-C''')** *Pax9*-null neonates on a congenic CD1 background (CD1-*Pax9*$^{-/-}$) displayed the same phenotype as the B6-*Pax9*$^{-/-}$ neonates. Scale bars are given on each panel.

To analyse the phenotype in more detail, *Pax9*$^{-/-}$ embryos on a CD1 genetic background were collected at E15.5 and examined by MRI and H&E staining (n = 13). Externally these embryos did not appear different from B6-*Pax9*$^{-/-}$ embryos, as they exhibited pre-axial digit duplication (as shown in Figure 3-1).

The aligned image stacks generated by MRI were analysed with AMIRA software. This confirmed that the palate was cleft and the thymus absent in all CD1-*Pax9*$^{-/-}$ embryos (Figure 3-2 A-C). Using the Amira software, 3D representations of the cardiovascular system were made (Figure 3-2 A'-C'). In wild type embryos, the outflow tract was divided into the aorta, that takes oxygenated blood out from the left ventricle and delivers it to the body, and the pulmonary trunk which takes deoxygenated blood from the right ventricle to the lungs (Figure 3-2 A'). In B6-*Pax9*$^{-/-}$ embryos, the majority presented with DORV combined with an interventricular communication (15/19; 73%) (Table 3-1), in which the outflow tract vessels are misaligned, with both aberrantly arising from the right ventricle (Figure 3-2 B'). In contrast, however, only three cases of DORV with interventricular communication (23%) were observed in the CD1-*Pax9*$^{-/-}$ embryos (3/13).

The great arteries were also assessed. In wild type embryos, the ascending aorta was connected to the descending aorta by the aortic arch. From the arch of aorta, three arteries were observed: the brachiocephalic artery, which gives rise to the right subclavian artery and the right common carotid artery, the left common carotid artery, and the left subclavian artery. In B6-*Pax9*$^{-/-}$ embryos the ascending aorta was frequently hypoplastic (17/19; 89%), the arch was interrupted (17/19; 89%), the right subclavian artery was aberrant (14/19; 74%) and one or both common carotid arteries were missing (15/19; 79%) (Figure 3-2, Table 3-1). A similar incidence of most of these phenotypes was identified in the CD1-*Pax9*$^{-/-}$ embryos. The incidence of IAA (10/13; 77%), ARSA (13/13; 100%) and absent carotid arteries (10/13; 77%) were not significantly different to B6-*Pax9*$^{-/-}$ embryos ($p>0.05$). However, the incidence of hypoplastic aorta was significantly reduced in CD1-*Pax9*$^{-/-}$ embryos, it was only observed in one CD1-*Pax9*$^{-/-}$ embryo (8%) compared with 17 (89%) B6-*Pax9*$^{-/-}$ embryos (Table 3-1).

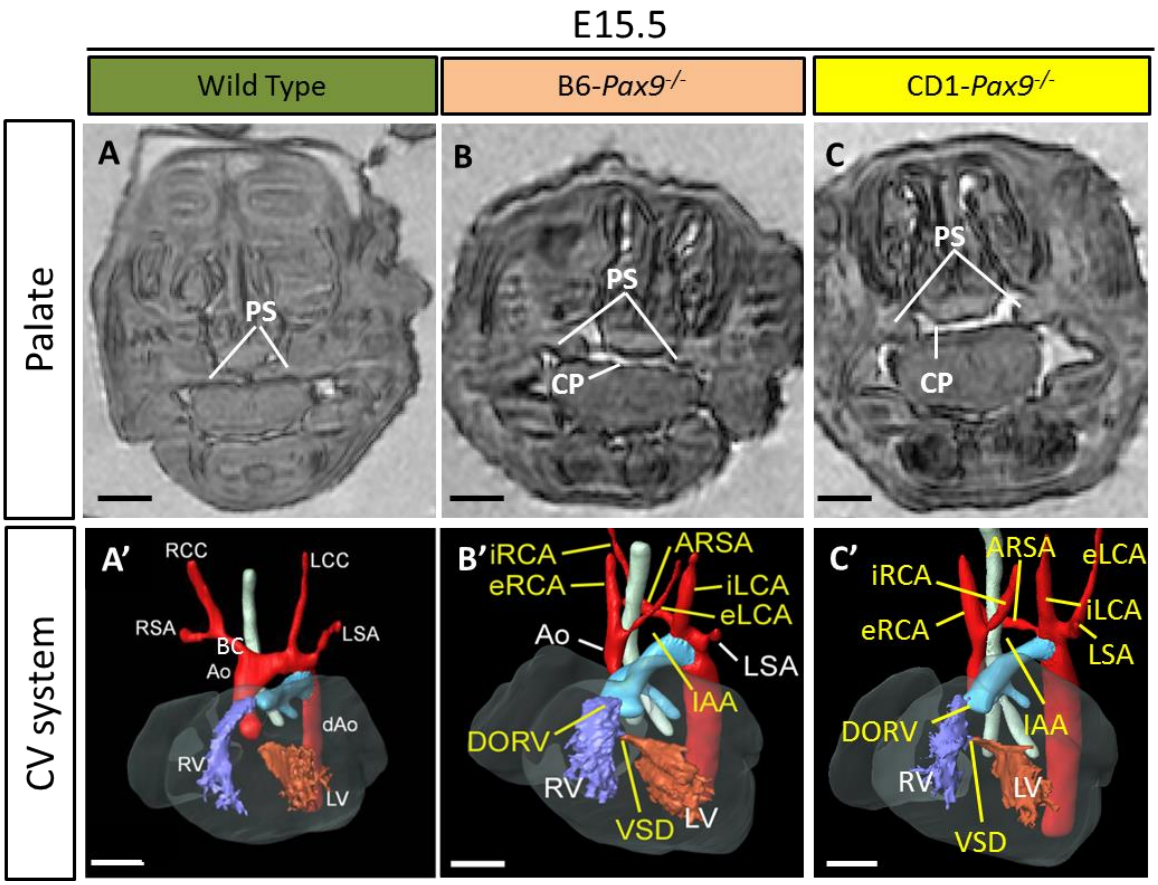

Figure 3-2 : Comparison of the *Pax9*-null phenotype on C57Bl6/J and CD1 genetic backgrounds at E15.5.

Embryos at 15.5 underwent MRI and the acquired data was analysed using Amira software.

(A – C) 2D images of the palate. **(A)** Wild type embryos show normal palate development with the palatal shelves (PS) fused. The PS have failed to fuse in *Pax9*$^{-/-}$ embryos on a B6 (**B**) and CD1 (**C**) genetic background leading to a cleft palate (CP).

(A' – C') 3D reconstructions of the cardiovascular system**. (A')** Wild-type embryos showed normal branching of the great arteries where the aorta (Ao) arose from the left ventricle (LV) forming the aortic arch to connect with the descending aorta (dAo). The brachiocephalic artery (BC) is the first vessel to branch off the arch and divides into the right subclavian artery (RSA) and the right common carotid artery (RCC). The left common carotid (LCC) and the left subclavian artery (LSA) are the second and third vessels respectively to branch off the aortic arch. **(B')** A *Pax9*$^{-/-}$ embryo on a C57Bl/6 (B6) genetic background presented with cardiovascular defects, including ventricular septal defect (VSD), double-outlet right ventricle (DORV), aberrant (retro-esophageal) right subclavian artery (ARSA) and interruption of the aortic arch type B (IAA). Both common carotid arteries were absent, consequently causing the internal and external carotids to arise directly from the aortae. **(C')** A *Pax9*$^{-/-}$ embryo on a CD1 genetic background presented with similar arch artery defects to those identified in *Pax9*$^{-/-}$-B6 embryos including IAA, ARSA and absent carotid arteries. This embryo also had a VSD.

Abbreviations: eLCA, external left carotid artery; eRCA, external right carotid artery; iLCA, internal left carotid artery; iRCA, internal right carotid artery; LV, left ventricle; RV, right ventricle. Scale bar, 500µm.

(B6-*Pax9*$^{-/-}$ images provided by Dr. Simon Bamforth).

Table 3-1: Comparison of the *Pax9*-null phenotype on C57Bl6/J and CD1 genetic backgrounds at E15.5.

	Phenotypes								
	Pre-axial digit duplication	Cleft palate	Absent thymus	Isolated VSD	DORV+IVC	Hypoplastic aorta	IAA	ARSA	Abnormal carotid arteries
B6-*Pax9*$^{-/-}$	19	19	19	3	15	17	17	14	15
N=19	100%	100%	100%	15,8%	79%	89%	89%	74%	79%
CD1-*Pax9*$^{-/-}$	13	13	13	2	3 (↓*)	1 (↓*)	10	13	10
N=13	100%	100%	100%	15%	23%	8%	77%	100%	77%

Statistically significant differences in the presentation of a phenotype, are indicated: *p<0.05 (Pearson Chi-Square).

Abbreviations: ARSA, aberrant right subclavian artery; DORV, double outlet right ventricle; IAA, interrupted aortic arch; IVC, interventricular communication; VSD, ventricular septal defect.

Analysis by MRI revealed that *Pax9*-null embryos on a CD1 genetic background displayed similar arch artery phenotypes to those on a C57Bl/6J background, although fewer outflow tract defects were observed. The embryos imaged by MRI were recovered from the MRI tube and processed for histological analysis to allow for higher resolution images to be analysed to confirm the defects observed using Amira software. This technique would also allow the identification of any subtle defects, which could not be identified by MRI (Figure 3-3). Analysis by histology confirmed all the arch artery and outflow tract defects identified by MRI. However, the diameter of the ascending aorta could be assessed more accurately by histology. This demonstrated that the majority of CD1-*Pax9*$^{-/-}$ embryos presented with a diameter of the aorta (12/13) comparable to the wild type embryos, with only one out of thirteen embryos having a hypoplastic ascending aorta. In comparison, 79% (15/19) of B6-*Pax9*$^{-/-}$ embryos suffered from a hypoplastic aorta (Figure 3-3, Table 3-1).

Histological analysis confirmed all the phenotypes identified by MRI demonstrating that MRI is a robust and reliable technique to non-destructively analyse mutant embryos at E15.5. However, more subtle defects that rely on accurate measurements to confirm a phenotype, such as the hypoplastic aorta, require histology to provide a definitive result.

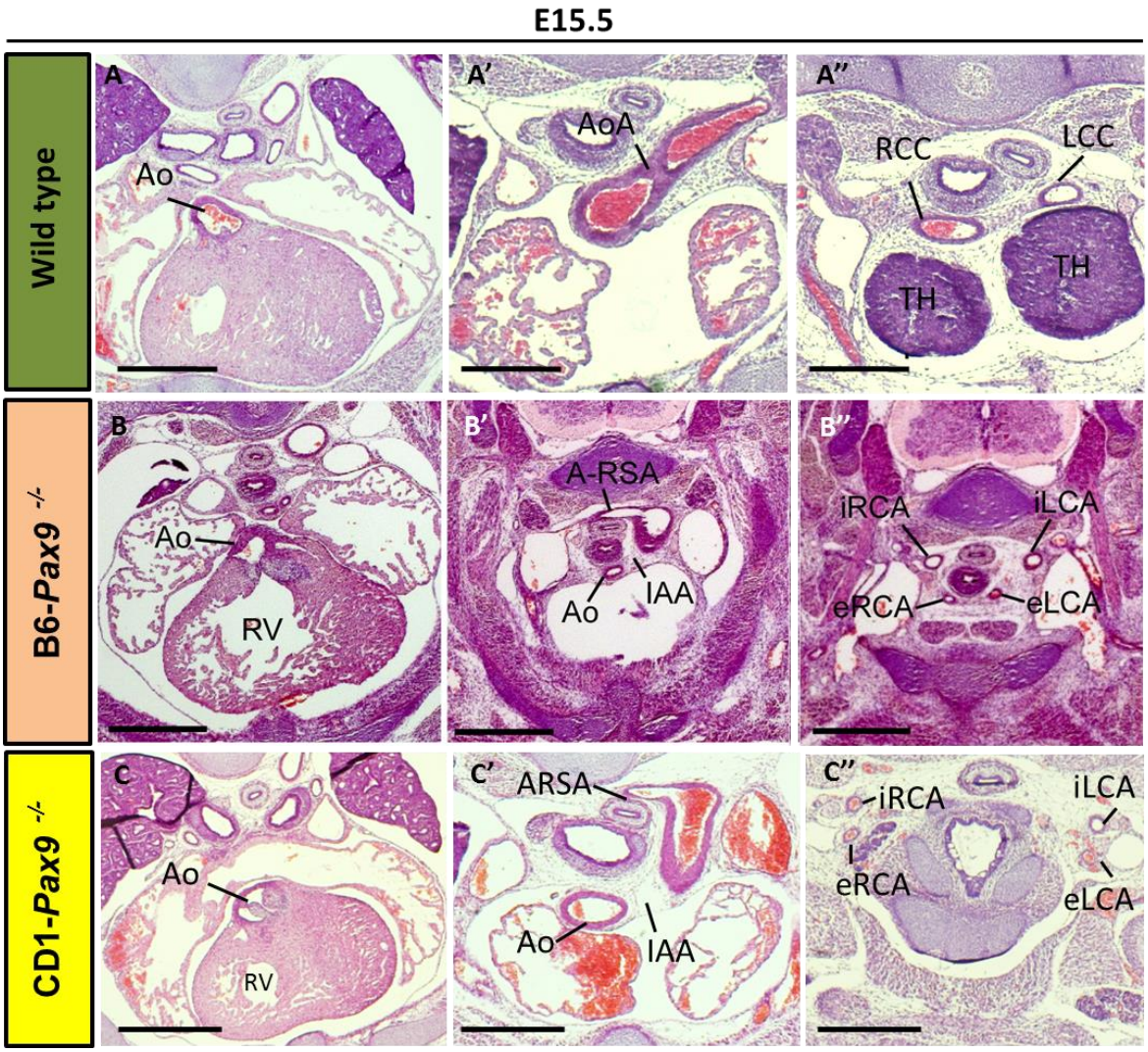

Figure 3-3: Histological analysis of E15.5 *Pax9*-null embryos on B6 and CD1 genetic backgrounds.

Transverse sections were cut and stained with haematoxylin and eosin. (**A**) Wild type embryo heart showing normal development of the cardiovascular system, where the aorta arises from the left ventricle (**A**), and the arch of aorta (AOA) is formed connecting the ascending aorta with the descending aorta (**A'**). Anteriorly the left and right common carotid arteries (LCC, RCC) can be identified, as well as the thymus (TH) (**A''**). (**B**) In the *Pax9*-null embryos on a C57Bl/6J (B6) background the aorta (Ao) arises from the right ventricle (RV), known as double outlet right ventricle. (**B'**) A hypoplastic Ao, interrupted aortic arch (IAA) and aberrant right subclavian artery (ARSA) are also seen. (**B''**) The common carotid arteries are absent causing the internal and external right and left carotid arteries to arise directly from the arch arteries. The thymus is also absent. (**C**) In the *Pax9*-null embryo on a CD1 background the aorta (Ao) arises correctly from the left ventricle. (**C'**) The Ao is of a normal size, but IAA and ARSA are present. (**C''**) The common carotid arteries, and the thymus, are absent.

Abbreviations: eLCA, external left carotid artery; eRCA, external right carotid artery; iLCA, internal left carotid artery; iRCA, internal right carotid artery. Scale bar, 100μm.

(B6-*Pax9*$^{-/-}$ images provided by Dr. Simon Bamforth).

The aortic arch arteries are derived from the pharyngeal arch arteries (PAA), which are symmetrical at E10.5 and yet to undergo the remodeling process to transform them into the asymmetrical aortic arch arteries. To assess the developmental patterning of the PAA, and to compare the effect of genetic background on the *Pax9*-null cardiovascular phenotype, intracardiac ink injection was performed at E10.5 on CD1-*Pax9*$^{-/-}$ and B6-*Pax9*$^{-/-}$ embryos (Figure 3-4, Table 3-2). The wildtype embryos displayed normal PAA development on both B6 (10/10) and CD1 (16/16) backgrounds. The 1st and 2nd PAA had regressed, and the 3rd, 4th and 6th PAA were fully formed and of approximately equal sizes (Figure 3-4). *Pax9*-null embryos on a C57Bl/6J background presented with defects affecting the 1st, 2nd, 3rd and 4th PAA as revealed by ink injection (Figure 3-4, Table 3-2). These defects included abnormal persistence of the 1st and 2nd PAA, absence or hypoplasia of the 3rd PAA, and absence of the 4th PAA. The 6th PAA was unaffected. The *Pax9*-null embryos on a CD1 background presented with a similar phenotype (Figure 3-4, Table 3-2), with defects affecting the 1st, 2nd, 3rd and 4th PAA not being significantly different from the defects observed on the C57Bl/6J background. However, a significant ($p<0.005$) increase in the penetrance of persistence of the 2nd PAA was seen in *Pax9*$^{-/-}$ embryos on the CD1 background (8/9) compared to the C57Bl/6J background (2/10).

This data therefore suggests that the genetic background affects the *Pax9*$^{-/-}$ cardiovascular phenotype, with the outflow tract defects being far less penetrant on the CD1 background compared to C57Bl/6J. However, the defects affecting the aortic arch arteries appear to be equally penetrant across both genetic backgrounds.

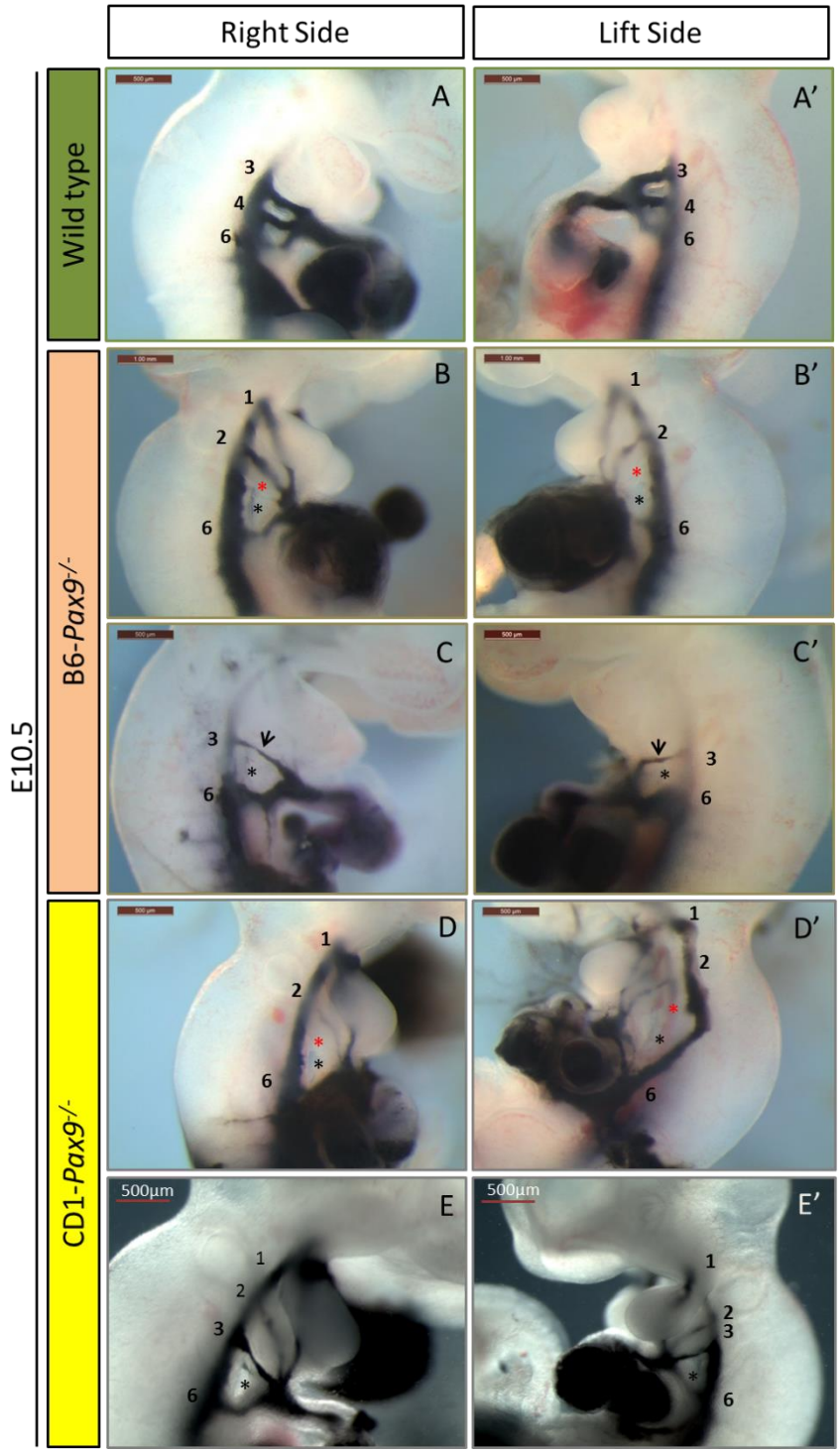

Figure 3-4: Pharyngeal arch artery defects of E10.5 *Pax9*-null embryos on C57Bl6/J and CD1 backgrounds.
Patterning of the pharyngeal arch arteries (PAA) at E10.5 was visualised by intracardiac injection of India ink. (**A**) Wild-type embryos presented with normal patterning of the 3rd, 4th and 6th PAAs on both sides. (**B, C)** *Pax9*$^{-/-}$ embryos on a C57Bl/6J (B6) background displayed patent 1st and 2nd PAA, absent (*red asterisk*) or thin (*arrow*) 3rd PAA, and absent 4th PAA (*black asterisk*). (**D-E**) *Pax9*$^{-/-}$ embryos on a CD1 background had a similar phenotype to embryos on a B6 background. The 1st and 2nd PAAs were patent, the 3rd PAA either missing (*red asterisk*) or thin, and the 4th PAA was absent (*black asterisk*). Scale bar, 500µm.
(B6-*Pax9*$^{-/-}$ images provided by Dr. Alberto Briones Leon).

Table 3-2: Pharyngeal arch artery defects of E10.5 *Pax9*-null embryos on C57Bl6/J and CD1 backgrounds.

						Bilateral defects			
Genetic background	**N**	**PAA #**	**Abnormal (%)**	**Unilateral defect**	**Bilateral defect**	**P/P**	**Th-P/Th-P**	**Th-P/NP**	**NP/NP**
B6-*Pax9*$^{-/-}$	10	1	5 (50%)	1	4	4	-	-	-
		2	2 (20%)	1	1	1	-	-	-
		3	6 (60%)	2	4	-	3	1	-
		4	10 (100%)	1	9	-	-	3	6
CD1-*Pax9*$^{-/-}$	9	1	7 (78%)	1	6	6	-	-	-
		2	8 (89%) **(↑*)**	1	7	7	-	-	-
		3	8 (89%)	0	8	-	2	1	5
		4	9 (100%)	0	9	-	-	-	9

Intra-cardiac injection of India ink into E10.5 embryos on C57Bl/6 and CD1 genetic backgrounds was used to evaluate the patency of the pharyngeal arch arteries (PAA). Each PAA (1 – 4) was scored if it was patent to ink (P), if it was patent yet thinner than normal (Th-P) or not patent to ink (NP). Whether the defect was unilateral or bilateral was also recorded. Wild type data were normal on bothB6 (N=10) and CD1 (N=12) backgrounds. Data not shown. (B6-*Pax9*$^{-/-}$ data provided by Dr. Alberto Briones Leon).

Statistically significant differences in the presentation of a phenotype, are indicated: *p<0.05 (Pearson Chi-Square).

3.4 DISCUSSION

The genetic background of a mouse model can be highly influential in any phenotype resulting from genetic modification. The data in this chapter shows there is a 100% penetrance of the PAA malformation in *Pax9*-null embryos on both B6 and CD1 genetic backgrounds as each embryo presented with at least one PAA malformation. However, the dramatic decrease in penetrance of intracardiac (VSD) and outflow tract defects (DORV and hypoplastic ascending aorta) on the CD1 background compared with C57Bl/6J is likely due to the change in genetic background, which indicates that the genetic background is an important factor in the penetrance of the cardiac phenotype in *Pax9*-null embryos.

The ink injection interestingly showed a persistence of the 2nd PAA in *Pax9*-null embryos on both backgrounds. Statistical analysis showed that persistence of the 2nd PAA was significantly higher in *Pax9*-null embryos on the CD1 background compared to the B6 background. It is not clear as to whether the 2nd PAA will persist during the entire development of the embryo and then participate in the formation of a mature blood vessel, or whether it will instead regress later in embryogenesis.

Padge (1948) reported that, in human embryology, the ventral pharyngeal artery is formed from the proximal portions of the 1st and 2nd PAA. It then combines with branches of the stapedial artery to form the external carotid artery (Chen *et al*., 2007; Padge, 1948). Hiruma *et al.* (2002) showed a slight difference between mouse and human regarding the development of the external carotid artery, whereby the ventral aorta is present in the mouse embryo and a primitive external carotid artery arises from it (Hiruma *et al.*, 2002).

It is possible that, in *Pax9*-null embryos, persistence of the 2nd PAA in combination with a failure of the 3rd PAA to be maintained which will result in the absence of the common carotid arteries, the ventral portion of the 2nd PAA may contribute to the development of the external carotid artery, in addition to the stapedial artery. Despite the differences between mouse and man as described above, this phenotype has been described in a patient. A 21 year old female patient with absent common carotid arteries was reported in 1978, the patient seen in the emergency room with left hemiplegia. The fluoroscopic scan was not identified a common carotid artery on

either side from the base of the skull to the aortic. The aortogram imaging was performed and showed that the first branch of the aorta gave rise to the right subclavian and right internal carotid arteries. The right external carotid, left external carotid, left internal carotid, and left subclavian arteries arose individually from the arch (Roberts and Gerald, 1978).

In patients, genetic background plays a major role in the variation of a phenotype within the same disease between different individuals. For example studying 18 individuals with Joubert syndrome from 14 families suffering from biallelic truncating mutations in CSPP1 showed that none of these individuals had a correlation in phenotype and the site of truncation with each other (Tuz *et al.*, 2014). A transgenic mouse model, *Cep290*^{LacZ}, was used to study mutations in the centrosomal-cilia protein *CEP290*. A high mortality level was observed in *Cep290*^{LacZ} mutant mice on a C57BL/6 background (Rachel *et al*., 2015; Ramsbottom *et al.*, 2015). These mice also had a low fertility level in which the breeding line did not pass the third generation. Importantly, mice with the *Cep290*^{LacZ} mutation on a 129/Ola background were viable for more than 12 months and were fertile (Rachel *et al*., 2015).

Other causes of differences in the phenotype that arise due to genetic background have been previously published. For example, *Tbx1* heterozygous mice show highly variable penetrance of 4th PAA defects depending on their genetic background (Calmont *et al*., 2009; Lindsay *et al*., 2001; Vitelli *et al.*, 2002). Likewise, the OFT tract phenotype caused by the deletion of *Pax9* appears to be affected by the genetic background. All of this indicates that genetic modifiers specific to each strain of mice can adversely affect the way in which disease presents.

Modifier genes can affect transcription and alter the immediate gene transcript expression, or they can alter phenotypes (Nadeau, 2001).

The most common effects of modifier genes can be described as additive or multiplicative (Gabriel *et al*., 2002). Modifying genes may also cause epistasis, in which an allele from one gene will mask the phenotype caused by a mutation or sequence alteration in another gene (Nadeau, 2001). Another effect of a modifier gene is to reduce the penetrance or the expression of a phenotype (Nadeau, 2001).

Genetic background effects in mice can be analysed and controlled by using specific targeting and breeding strategies. Detecting a modifier requires crossing the mutant allele with different strains to allow for random segregation of mutant and modifying alleles. There is no clear-cut strategy as to which outcross strain to use, but strains that provide a higher degree of genetic diversity, such as wild-derived strains or strains from a different genealogical subgroup, have been used successfully (Ikeda *et al.,* 1999). Initially microsatellite markers can be used across the genome to each of the genetic backgrounds that need to test (Miller *et al*., 2014). Heterozygous mutants on two different backgrounds will cross together. The mice that will generate from the first crossing will backcrossed to the mutant parental strain, in which a modifier affects the mutant allele only when in a homozygous state (Darvasi, 1998). Mutant progeny from backcrosses must be examin carefully for variation in phenotype. Finally RNA sequencing can be perform to identify a potential candidate modifier genes (Miller *et al.*, 2014).

It is important to accurately report the genetic background so that others can interpret the role of the genetic background in their research more accurately.

In this chapter, it has been demonstrated the *Pax9*-null outflow tract phenotype is sensitive to genetic background. However, the arch artery phenotype is equally penetrant on B6 and CD1 backgrounds. As the rest of this thesis will focus on PAA formation and development, all further studies were conducted on the congenic CD1 genetic background.

4 INVESTIGATING A *Pax9;Msx1* GENETIC INTERACTION IN CARDIOVASCULAR DEVELOPMENT

4.1 INTRODUCTION

The majority of DiGeorge Syndrome (DGS) patients suffer from a chromosomal deletion on chromosome 22q11.2 and studies using mouse models has identified that *TBX1*, a member of the T-box transcription factor family, is most likely responsible for the cardiovascular phenotype in these patients (Lindsay et al., 1999; Lindsay et al., 2001; Merscher et al., 2001; Prescott et al., 2005). Most DGS patients have a 3Mb deletion, but about 15% have smaller nested 1.5Mb deletion. Both deletions, however, remove *TBX1* transcription factor, which is located in the 22q11 region.

The patients exhibit a variation in the clinical presentation of their phenotype even among identical twins or family members with just a single *TBX1* point mutation (Vaz *et al.*, 2015). The clinical features of 22q11 deletion syndrome (DS) presented in individuals varies, ranging from normality to isolated heart defects, to multiple defects that include, dysmorphic facial features, cardiac outflow abnormalities, absence or hypoplasia of the thymus and parathyroid gland, mental retardation, psychiatric problems and velopharyngeal insufficiency (Davidson, 1995). The severity of the cardiac phenotype varies substantially between individuals (Davidson, 1995).

The variations in the clinical phenotypes may be due to a modifier that affects the representation of the phenotype. This modifier could be stochastic, environmental, or even genetic (Aggarwal and Morrow, 2008). For example, not all DGS patients live in the same environment and each patient is presenting with different social and genetic backgrounds from other patients.

There is some evidence that the phenotype observed in 22q11DS patients may be influenced by genetic modifiers that lie within or outside of the region of the deletion. In mouse models, mutations in *Crkl*, which lies within 22q11.2, and in *Fgf8*, which is lies outside this region, have both been shown to modulate the developmental phenotype by enhancing the effects of a *Tbx1*-null mutation (DeRuiter *et al*., 1993; Di

Nunno *et al*., 2004). Moreover, there is published evidence that *Tbx1* genetically interacts with other genes such as *Wnt5a* (Chen *et al.*, 2012) and *Gbx2* (Calmont *et al.*, 2009; Caprio and Baldini, 2014)

Microarray analyses of mouse embryos lacking *Tbx1* have been performed (Aggarwal and Morrow, 2008; Ivins *et al.*, 2005). Both of these studies identified a large number of genes that could be considered as acting as a modifier for 22q11DS that could affect the phenotype presentation. Among these genes, the transcription factor *Pax9* was found to be down regulated in $Tbx1^{-/-}$ embryos (Aggarwal and Morrow, 2008; Ivins *et al*., 2005).

Data from our lab showed that *Tbx1* and *Pax9* are both expressed and co-localised within the pharyngeal endoderm, and that they are both required for the normal development of the PAA. *Tbx1;Pax9* double heterozygous mice present with interruption of the aortic arch, caused by a failure in the formation of the 4th PAA.

Pax9-null embryos were generated in our lab by intercrossing $Pax9^{+/-}$ mice. $Pax9^{-/-}$ embryos present with severe cardiovascular defects, as shown in the introduction and chapter 3 of this thesis. In humans there are records of several patients that are diagnosed with 14q chromosomal deletions that include *PAX9* and suffer from cardiovascular defects (Buckingham *et al.*, 2005; Burton *et al*., 2004; Santen *et al.,* 2012) (section 1.6.3). This raises the question as to whether there is a reason that there are only apparently rare cases of cardiovascular defects associated with *PAX9* haploinsufficiency in humans. This question leads us to look for other modifier genes that may interact with *PAX9* during cardiovascular development.

Pax9 and *Msx1* transcription factors are known to be co-expressed in the dental mesenchyme (Nakatomi *et al.*, 2010; Ogawa *et al.*, 2006). In double heterozygous mouse mutants ($Pax9^{+/-}$; $Msx1^{+/-}$), the lower incisors are consistently missing (Nakatomi *et al.,* 2010; Paixao-Cortes *et al.*, 2011a) but mutants are alive and fertile. Assays have demonstrated that protein–protein interactions between Pax9 and Msx1 can occur (Ogawa *et al.*, 2005).

Published data indicates that loss of *Msx1* in mice does not result in cardiovascular defects (Boogerd *et al.*, 2010; Chen *et al.*, 2007). *Msx1/Msx2* double homozygous mutants, die *in utero* at ~E16, with cardiovascular defects including VSD, DORV,

TOF, and common arterial trunk (Chen *et al.*, 2007). This suggests that *Msx1* is potentially important during cardiovascular development, although, it may have a redundant role that is compensated by *Msx2*. To date, however, it is unclear if *Pax9* and *Msx1* interact genetically *in vivo* during cardiovascular development

4.2 AIMS OF CHAPTER

The main aim of this chapter is to investigate whether *Pax9* and *Msx1* genetically interact in the development of the mouse cardiovascular system.

4.3 RESULTS

4.3.1 CARDIOVASCULAR PHENOTYPE IN *Pax9;Msx1* NEONATES

The mouse lines used in this study have been described previously in section 2.2.1. *Pax9* and *Msx1* mutant mice were maintained on a congenic CD1 background. *Pax9;Msx1* double heterozygous mice were generated by crossing $Pax9^{+/-}$ with $Msx1^{+/-}$ mice. These doubly heterozygous mice (i.e. $Pax9^{+/-};Msx1^{+/-}$) are viable and fertile, although they lack the lower teeth (Nakatomi *et al*., 2010).

Initially, the effect of *Pax9;Msx1* complex genotypes on cardiovascular development was explored. Double heterozygous mice were intercrossed to produce mice with complex genotypes (Figure 4-1). All pups from the $Pax9^{+/-};Msx1^{+/-}$ intercross were born alive. However, a few dead pups were found in the breeding cage within hours after birth with a bloated abdomen, reminiscent of the *Pax9*-null phenotype (Figure 4-4).

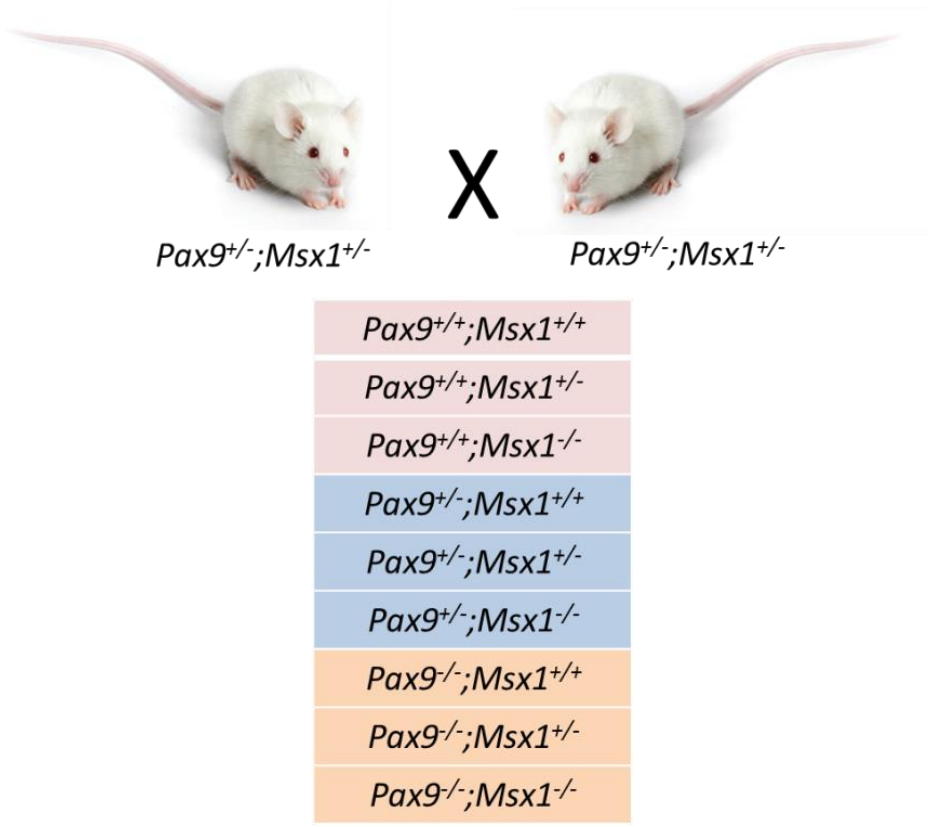

Figure 4-1: Schematic presentation of the possible genotypes from intercrossing *Pax9*$^{+/-}$ *;Msx1*$^{+/-}$ mice.
Nine possible genotypes are produced from intercrossing *Pax9*$^{+/-}$*;Msx1*$^{+/-}$ mice.

Dead pups were collected from the breeding cage as soon as they were found, which was usually on the day of birth, and genotyped by PCR (Table 4-1). A post mortem dissection was conducted on the dead pups, with particular attention paid to the palate, the thymus and the cardiovascular system. The advantage of using this method of analysis is that the adult females were preserved, allowing them to be re-used for further breeding and to collect new *Pax9;Msx1* double heterozygous mice for breeding experiments. In addition, the neonates had fully developed aortic arch arteries so the phenotype could be easily and accurately determined upon dissection.

All the dead pups were found to be either *Pax9*$^{-/-}$ and/or *Msx1*$^{-/-}$ with the rest of the pups surviving. To allow the collection of appropriate controls, some litters were euthanised using 200mg/ml of euthatal after the dead neonates were collected. On closer examination, it was found that all the dead pups had a cleft palate (Figure 4-2).

Cleft palate is assumed to cause respiratory insufficiency that may lead to the bloated abdomen in these neonates (Peters *et al.*, 1998).

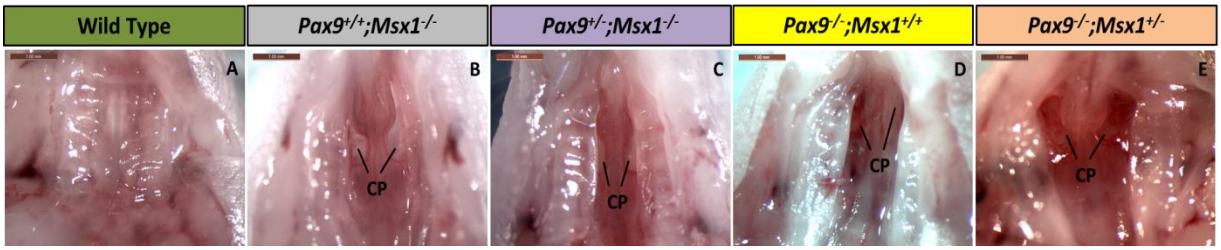

Figure 4-2: Identifying cleft palate in *Msx1*$^{-/-}$ or *Pax9*$^{-/-}$ neonates at P0.
The palate of each neonate was examined. (**A**) Normal fusion of the palate in a wild type neonate. (**B-E**) The mutant embryos that were either *Msx1*$^{-/-}$ or *Pax9*$^{-/-}$ in their genotype had a cleft palate (CP).

Of the dead neonates collected from the breeding cages, six were of the genotype *Pax9*$^{+/+}$*;Msx1*$^{-/-}$ and eight were *Pax9*$^{+/-}$*;Msx1*$^{-/-}$ (Table 4-1). Externally they were indistinguishable from the wild type embryos with normal digits. Dissecting these embryos revealed a normal sized thymus located at the midline of the neck similar to that found in wild type neonates. Following removal of the thymus a normal cardiovascular system was found, with the aortic arch having three great vessels arising from it (Figure 4-3).

Pax9$^{-/-}$ neonates were also found dead in the breeding cages on the day of birth. These neonates had a cleft palate and a bloated abdomen. Externally, *Pax9*$^{-/-}$ neonates presented with a pre-axial digit duplication as previously described (Peters *et al.*, 1998) (Figure 4-4). Upon dissection, it was noted they had no thymus, again as described (Peters *et al*., 1998). The cardiovascular system of the neonates was examined by direct visualisation using a dissecting microscope. All *Pax9*-null embryos displayed cardiovascular defects as expected (n = 22), including IAA, ARSA, and absence of one or both common carotid arteries (Figure 4-5, Table 4-1 A).

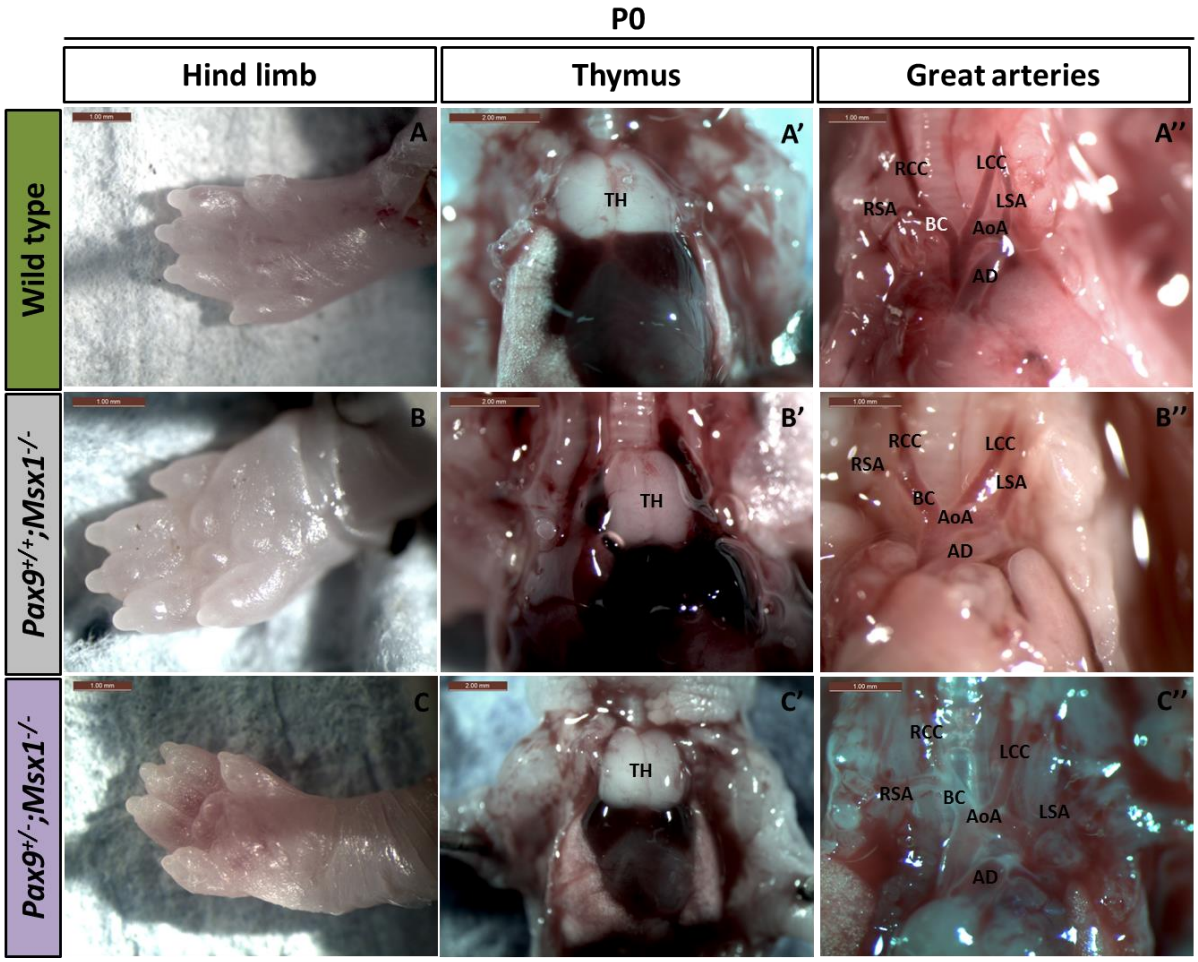

Figure 4-3: The phenotype of *Pax9*$^{+/+}$*;Msx1*$^{-/-}$ and *Pax9*$^{+/-}$*;Msx1*$^{-/-}$ mutant neonates.
The phenotype of wild type, *Pax9*$^{+/+}$*;Msx1*$^{-/-}$ and *Pax9*$^{+/-}$*;Msx1*$^{-/-}$ mutant neonates was compared. (**A**) Wild type neonates presented with a normal hindlimb, a normal thymus (TH) (**A'**) and a normal cardiovascular system (**A"**). (**B, C**) *Pax9*$^{+/+}$*;Msx1*$^{-/-}$ and *Pax9*$^{+/-}$*;Msx1*$^{-/-}$ mutant neonates are externally indistinguishable from wild type neonates. They had normal hindlimbs (**B, C**), a normal thymus (**B', C'**) and a normal cardiovascular system (**B'', C''**). In all cases, the aortic arch (AoA) gives rise to three great vessels: the brachiocephalic artery (BC), the left common carotid artery (LCC) and the left subclavian artery (LSA). Scale bars are indicated on each panel.

Since it is difficult to detect outflow tract defects by direct visualization, twelve hearts from the dead neonates were dissected free and processed for histological analysis. The histological analysis of the processed hearts showed that some *Pax9*-null embryos had isolated ventricular septal defect (3/12) and double-outlet right ventricle with interventricular communication (2/12) (Figure 4-6, Table 4-2).

Dead neonates with the genotype *Pax9*$^{-/-}$*;Msx1*$^{+/-}$ were also found in the breeding cages. They were externally similar to *Pax9*-null neonates, presenting with a pre-axial digit duplication and a bloated abdomen, presumably as a result of the gasping respiration from the cleft palate phenotype, also these neonates had a missing thymus (Figure 4-4). Unexpectedly, however, the *Pax9*$^{-/-}$*;Msx1*$^{+/-}$ mice showed a significant decrease (P=0.001) in the incidence of IAA which was seen in only 30% (6/20) of neonates, compared with an incidence of 100% in *Pax9*-null neonates (22/22) (Table 4-1). Interestingly, the aortic arch in the majority of the *Pax9*$^{-/-}$*;Msx1*$^{+/-}$ neonates was either normal (6/20; 30%) or a cervical aortic arch was present (8/20; 40%). This cervical aortic arch appeared capable of supporting the systemic circulation (Figure 4-5 C-C') as blood could clearly be seen within the vessel and it connected the ascending aorta with the descending aorta (Figure 4-5 B). The incidence of ARSA, however, was not significantly different between the two genotypes (91% in *Pax9*-null and 60% in *Pax9*$^{-/-}$*;Msx1*$^{+/-}$ neonates; P=0.352), and neither was the absence of one or both common carotid arteries (50% in *Pax9*-null and 30% in *Pax9*$^{-/-}$*;Msx1*$^{+/-}$ neonates; P=0.2051).

Eleven hearts from the dead neonates were processed for histological analysis (Table 4-2). The results indicated that only one out of the 11 *Pax9*$^{-/-}$*;Msx1*$^{+/-}$ neonatal hearts examined had a VSD. No outflow tract defects were observed in these neonates (Figure 4-6).

Only one double homozygous null (i.e. *Pax9*$^{-/-}$*;Msx1*$^{-/-}$) neonate was found during the collecting process. This neonate had a normal hind limb similar to wild type and no pre-axial digit duplication. However, the thymus was absent and palate cleft (Figure 4-4). The heart and great arteries of this neonate were normal (Figure 4-5, Figure 4-6).

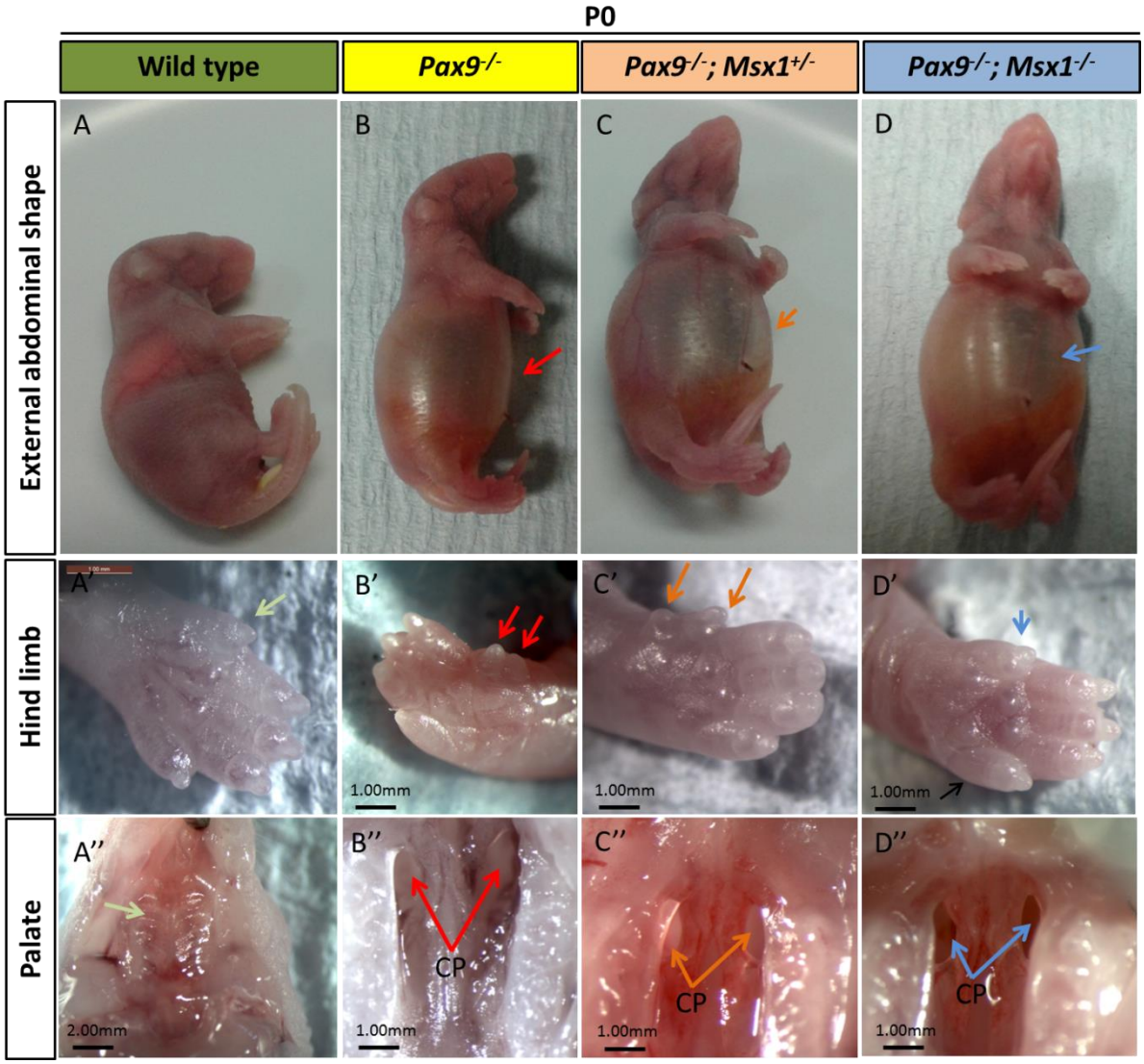

Figure 4-4: External and palate phenotypes in wild type and *Pax9;Msx1* mutant neonates. Neonates were collected on the day of birth and the external appearance as well as the condition of the palate was assessed. (**A**) Wild type neonates presented with a normal abdomen, normal hind limb (**A'**), and an intact palate (**A''**). **(B – D)** All *Pax9*$^{-/-}$ neonates, irrespective of *Msx1* genotype (i.e. *Pax9*$^{-/-}$*;Msx1*$^{+/+}$ (**B**), *Pax9*$^{-/-}$*;Msx1*$^{+/-}$ (**C**), *Pax9*$^{-/-}$*;Msx1*$^{-/-}$ (**D**), presented with a bloated abdomen (*arrow*; **B – D**) and cleft palate (CP; **B'' – D''**). Pre-axial digit duplication was found in *Pax9*$^{-/-}$ and *Pax9*$^{-/-}$*;Msx1*$^{+/-}$ neonates (*two arrows*; **B' – D**). A *Pax9*$^{-/-}$*;Msx1*$^{-/-}$ neonate presented a normal digits (*one arrow*; **D'**) similar to the wildtype neonate. Scale bars are indicated on each panel.

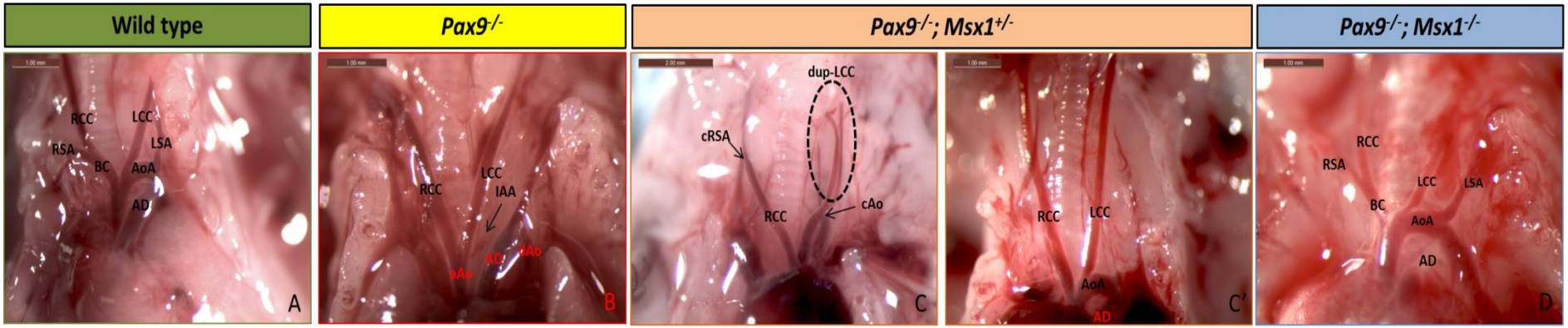

Figure 4-5: Cardiovascular phenotype of wild type and *Pax9;Msx1* mutant neonates.
Neonates were collected on the day of birth and dissected to assess the cardiovascular system. (**A**) Wild-type embryos displayed normal branching of the aortic arch (AoA) and its associated arteries. The aortic arch gives rise to the brachiocephalic artery (BC), which divides into the right subclavian artery (RSA) and right common carotid artery (RCC), the left common carotid artery (LCC) and the left subclavian artery (LSA). (**B**) A *Pax9*$^{-/-}$ neonate with abnormal aortic arch arteries. An interruption of the aortic arch (IAA) is seen, as is a presumed aberrant right subclavian artery due to the absence of the brachiocephalic artery. (**C - C'**) Two examples of the cardiovascular system in *Pax9*$^{-/-}$*;Msx1*$^{+/-}$ neonates. (**C**) A cervical aortic arch (cAo) with duplication of the left common carotid (dup-LCC) and a cervical right subclavian artery (cRSA) are seen. The cAO connects the ascending and the descending aorta and is filled with blood. (**C'**) An intact aortic arch is seen with the left and right common carotid arteries (LCC; RCC) present. No brachiocephalic artery is seen, implying that the right subclavian artery is aberrant. (**D**) A *Pax9*$^{-/-}$*;Msx1*$^{-/-}$ neonate with a normal cardiovascular system, in which it had an intact arch of aorta similar to the wild type neonate, the three major blood vessels then arose from the aortic arch: namely the left subclavian artery (LSA), the left common carotid and the brachiocephalic artery (BC). Scale bars are indicated on each panel.

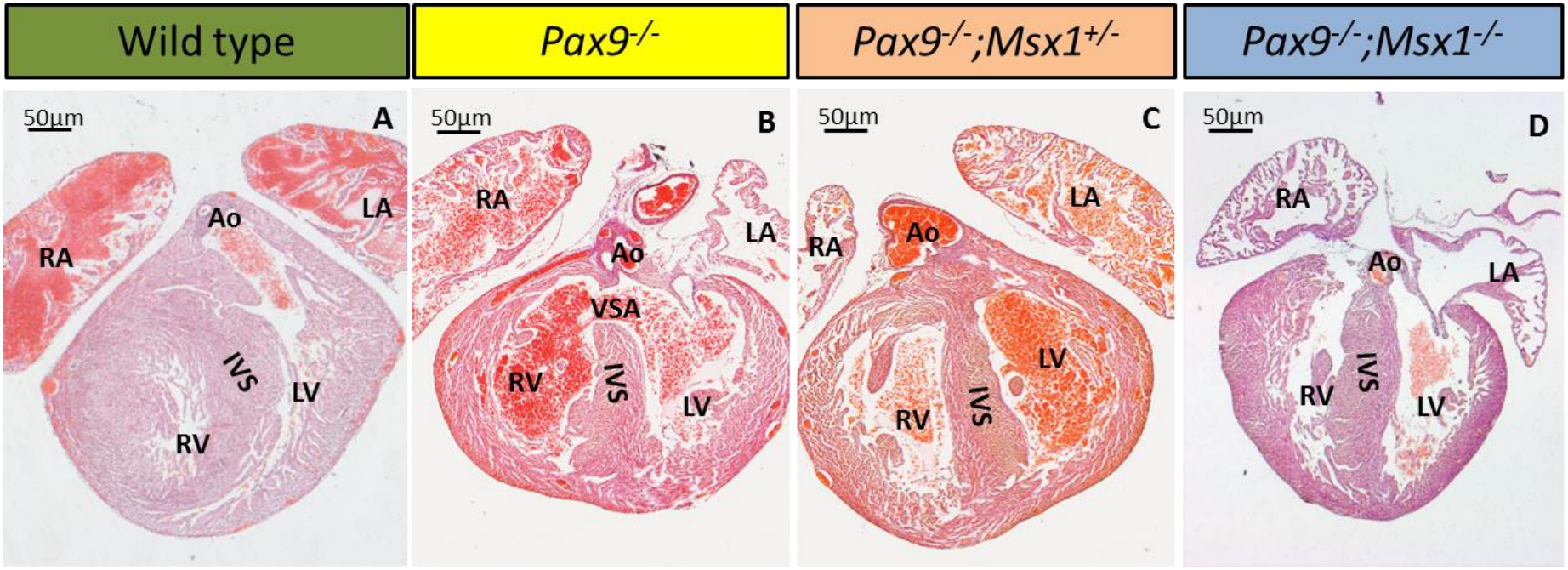

Figure 4-6: Histological analysis of *Pax9;Msx1* mutant hearts.
P0 neonatal hearts were processed for histological analysis using haematoxylin and eosin staining. (**A**) A wild type heart with a fully formed interventricular septum (IVS), and the aorta arising from the left ventricle (LV). (**B**) A *Pax9*$^{-/-}$ neonatal heart showing a ventricular septal defect (VSD). **(C)** A *Pax9*$^{-/-}$;*Msx1*$^{+/-}$ heart with normal IVS and outflow tract. **(D)** A *Pax9*$^{-/-}$;*Msx1*$^{-/-}$ heart also with normal structure. Scale bars are indicated on each panel.

Table 4-1: *Pax9;Msx1* mutant neonate phenotypes.

	Phenotype								
	Pre-axial digit duplication	**Absent thymus**	**Cleft palate**	**IAA**	**cAo**	**Normal Ao**	**ARSA**	**cRSA**	**Abnormal carotids arteries**
Wild type	0	0	0	0	0	5	0	0	0
5	0%	0%	0%	0%	0%	100%	0%	0%	0%
***Pax9*$^{+/+}$*;Msx1*$^{-/-}$**	0	0	6	0	0	6	0	0	0
6	0%	0%	100%	0%	0%	100%	0%	0%	0%
***Pax9*$^{+/-}$*;Msx1*$^{-/-}$**	0	0	8	0	0	8	0	0	0
8	6%	0%	100%	0%	0%	100%	0%	0%	0%
***Pax9*$^{-/-}$**	22	22	22	22	0	0	20	3	11
22	100%	100%	100%	100%	0%	0%	91%	14%	50%
***Pax9*$^{-/-}$*;Msx1*$^{+/-}$**	20	20	20	6 (↓*)	8	6	12	7	6
20	100%	100%	100%	30%	40%	30%	60%	35%	30%
***Pax9*$^{-/-}$*;Msx1*$^{-/-}$**	0	1	1	0	0	1	0	0	0
1	0%	100%	100%	0%	0%	100%	0%	0%	0%

Statistically significant differences in the presentation of a phenotype, from that seen in *Pax9*$^{-/-}$ mice are indicated: *p<0.05, (Pearson Chi-Square).

Abbreviations: ARSA, aberrant right subclavian artery; Ao, aorta; cAo, cervical aorta; cRSA, cervical right subclavian artery; IAA, interruption of the aortic arch.

Table 4-2: Outflow tract phenotype of *Pax9*;*Msx1* hearts examined by histology.

	Phenotype	
	Outflow tract defects	
	VSD	DORV+IVC
***Pax9*$^{-/-}$**	**3**	**2**
N=12	**25%**	**9%**
***Pax9*$^{-/-}$*;Msx1*$^{+/-}$**	**1**	**0**
N=11	**9%**	**0%**
***Pax9*$^{-/-}$ *Msx1*$^{+/-}$**	**0**	**0**
N=1	**0%**	**0%**

This table is a sub-table from Table 4-1 showing the heart and the outflow tract defects in those hearts that were selected for histology.
Abbreviations: DORV, double outlet right ventricle; IVC, interventricular communication; VSD, ventricular septal defect.

4.3.2 CARDIOVASCULAR PHENOTYPE OF *Pax9;Msx1* EMBRYOS AT E15.5.

Embryos from *Pax9;Msx1* double heterozygous intercrosses were collected at E15.5, a stage where cardiovascular development is complete and sent for either micro CT (µCT) or magnetic resonance (MRI) imaging.

In total 32 embryos were collected for µCT (n=8) and MRI (n=24) scanning, including 3 wild type, 6 $Pax9^{+/-};Msx1^{-/-}$, 8 $Pax9^{-/-}$, 13 $Pax9^{-/-};Msx1^{+/-}$ and 2 $Pax9^{-/-};Msx1^{-/-}$ embryos (Table 4-4).

Imaging using these two techniques essentially generates datasets that can be segmented using Amira software to create three-dimensional images of complex structures such as the cardiovascular system. There are advantages and disadvantages to each method in comparison to each other and histology. Both methods allow any section of the embryo to be viewed regardless of the angle in which it was embedded, in contrast to standard histology. MRI produces images with a resolution of 25µm, which is the equivalent of a very thick section when compared to histology, but the embryos can be recovered after imaging and then processed for standard histology (Bamforth *et al.*, 2012). Embryos younger than E15.5, however, do not produce very good images due to the poor contrast achieved from softer tissues. This can be overcome with µCT imaging (Wong *et al.*, 2012), as younger embryos can be stained with Lugol solution, which is basically an iodine, to achieve soft tissue contrast and give a better resolution than MRI of 5µm. Because of the iodine treatment, however, the embryos cannot be successfully recovered and processed for histology.

Following imaging, either by µCT or MRI, the data was analysed using Amira software and 3D models constructed to more easily assess the cardiovascular phenotype. All results were combined irrespective of the imaging system used.

Externally, $Pax9^{-/-}$ and $Pax9^{-/-};Msx1^{+/-}$ embryos at E15.5 were indistinguishable from each other. They both presented with a pre-axial digit duplication as already described. *Pax9;Msx1* double heterozygous (i.e. $Pax9^{+/-};Msx1^{+/-}$) and *Pax9;Msx1* double homozygous (i.e. $Pax9^{-/-};Msx1^{-/-}$) embryos are externally similar to wild-type embryos as they presented with a normal hind limb with five toes and no extra digit present (Figure 4-7).

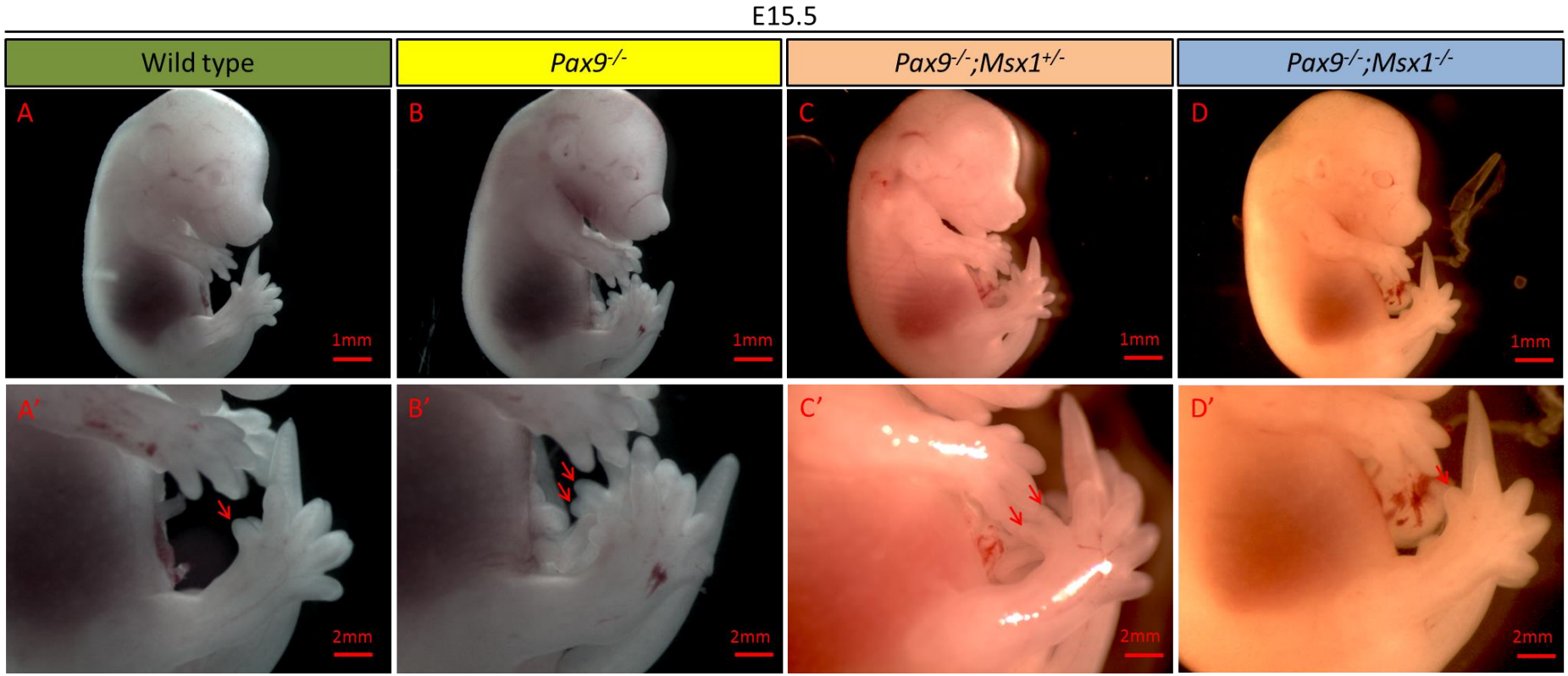

Figure 4-7: External phenotype of E15.5 wild type and *Pax9;Msx1* mutants.
Embryos at E15.5 were collected and examined for external defects. (**A**) Wild type embryo with a normal external appearance. (**B**) *Pax9*$^{-/-}$ and (**C**) *Pax9*$^{-/-}$*;Msx1*$^{+/-}$ embryos are indistinguishable from each other as both genotypes display a pre-axial digit duplication (*two arrows;* **B', C'**). (**D**) Externally the *Pax9*$^{-/-}$*;Msx1*$^{-/-}$ embryo is similar to the wild type embryo with a normal hind limb (*arrow;* **D'**). Scale bars are indicated on each panel.

Analysis of the data from both scanning methods showed that the wild type embryos (n = 3) all had a normal cardiovascular system, with a normal heart and an aortic arch arising from the left ventricle. Three major vessels arose from the aortic arch, with the brachiocephalic artery (BC) as the first branch and the left common carotid (LCC) and left subclavian (LSA) arteries as the 2nd and 3rd branch, respectively.

Of the 6 *Pax9*$^{+/-}$*;Msx1*$^{-/-}$ embryos scanned. All had a cleft palate (Table 4-3). However, no cardiovascular defects were seen (Table 4-3).

The *Pax9*$^{-/-}$ embryos (n = 8) all displayed a range of cardiovascular phenotypes (Figure 4-9, Table 4-3). Only one embryo presented with DORV and an associated interventricular communication (13%). Isolated VSD was found in 50% (4/8) of the dataset. Five out of eight (63%) embryos displayed IAA and ARSA. Although these phenotypes overlapped in most cases (5/8), two *Pax9*$^{-/-}$ mutants had cervical aortic arch (25%) and one embryo (13%) presented with abnormal carotid arteries. One embryo (13%) presented with a normal aortic arch.

Of the 13 *Pax9*$^{-/-}$*;Msx1*$^{+/-}$ embryos analysed, seven (54%) presented with isolated VSD but none of the embryos displayed DORV. Only three (23%) embryos had an IAA and nine (70%) embryos had a normal aortic arch. The statistical analysis showed that this decrease in the incidence of IAA in *Pax9*$^{-/-}$*;Msx1*$^{+/-}$ embryos compared with *Pax9*$^{-/-}$ embryos was significant (p=0.00172). One embryo (8%) presented with a cervical aortic arch. Five embryos (38%) had an ARSA and only one embryo showed an abnormal carotid artery (Figure 4-9, Table 4-3).

The scanning data was also used to check the penetrance of the cleft palate and absent thymus phenotypes. All *Pax9*$^{-/-}$ and *Pax9*$^{-/-}$*;Max1*$^{+/-}$ embryos had these phenotypes, showing 100% penetrance at E15.5 on both genotypes.

Only two *Pax9*$^{-/-}$*; Msx1*$^{-/-}$ embryos were collected at E15.5 (Table 4-3). One embryo had a normal cardiovascular system but one presented with IAA and ARSA, as well as DORV with interventricular communication (Figure 4-8).

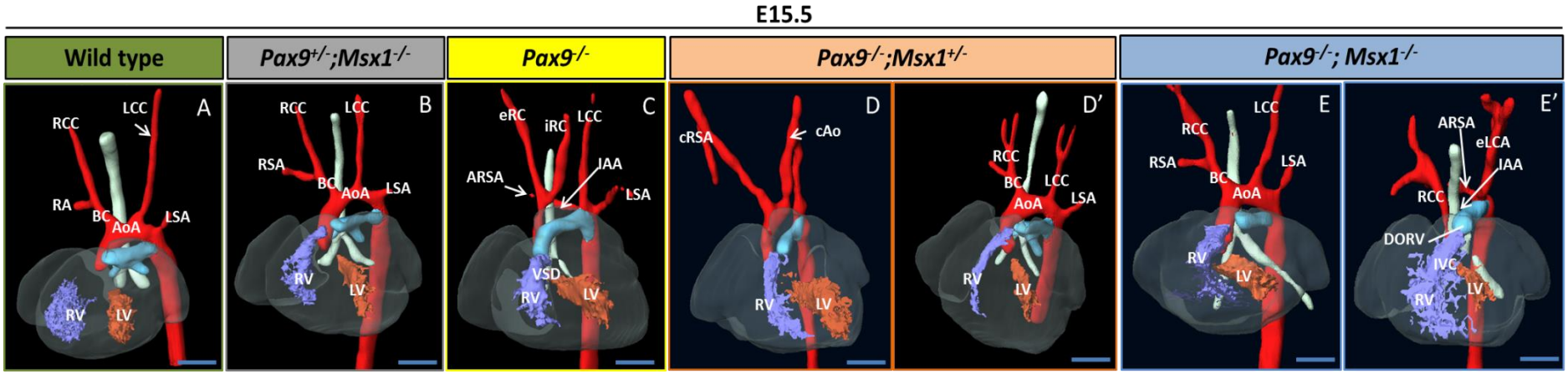

Figure 4-8: Cardiovascular phenotype of E15.5 *Pax9;Msx1* mutant embryos.
Embryos were collected and processed for µCT and MRI analysis and 3D reconstructions were made from the acquired datasets. (**A**) Wild type embryo with normal branching of the great arteries, in which the brachiocephalic artery (BC), the left common carotid artery and left subclavian artery emerge directly from the aortic arch. (**B**) A *Pax9*$^{+/-}$*;Msx1*$^{-/-}$ embryo with a normal cardiovascular system. (**C**) *Pax9*$^{-/-}$ embryo with cardiovascular defects including interruption of the aortic arch (IAA), aberrant right subclavian artery (ARSA) and ventricular septal defect (VSD). The internal carotid artery rises anomalously from the persisting dorsal aorta. (**D, D'**) *Pax9*$^{-/-}$*;Msx1*$^{+/-}$ embryos. (**D**) This embryo showed has a cervical aortic arch (cAo) and a cervical right subclavian artery (cRSA). (**D'**) *Pax9*$^{-/-}$*;Msx1*$^{+/-}$ embryo with a normal cardiovascular system. (**E-E'**) Two *Pax9*$^{-/-}$*;Msx1*$^{-/-}$ mutant embryos were collected, one with a normal cardiovascular system (**E**), and one with VSD, IAA, ARSA, DORV associated with interventricular communication (IVC) , moreover the left common carotid appear to be missing and the external left carotid artery (eLCA) can be identify in this embryo(**E'**).
Abbreviations: Ao, aorta; RV, right ventricle; LV, left ventricle; RSA, right subclavian artery; RCC, right common carotid artery; LSA, left subclavian artery; LCC, left common carotid artery. Scale bar, 500µm.

Table 4-3: E15.5 *Pax9;Msx1* mutant phenotypes.

	Phenotype										
				Cardiovascular defects							
	Pre-axial digit duplication	**Absent thymus**	**Cleft palate**	**VSD**	**DORV + IVC**	**IAA**	**cAo**	**Normal Ao**	**ARSA**	**cRSA**	**Abnormal carotid arteries**
Wild type	0	0	0	0	0	0	0	3	0	0	0
3	0%	0%	0%	0%	0%	0%	0%	100%	0%	0%	0%
***Pax9*$^{+/-}$*;Msx1*$^{-/-}$**	0	0	0	0	0	0	0	6	0	0	0
6	0%	0%	0%	0%	0%	0%	0%	100%	0%	0%	0%
***Pax9*$^{-/-}$**	8	8	8	4	1	5	2	1	5	2	1
8	100%	100%	100%	50%	13%	63%	25%	13%	63%	25%	13%
***Pax9*$^{-/-}$*;Msx1*$^{+/-}$**	13	13	13	7	0	**3 (↓*)**	1	**9(↑*)**	5	2	1
13	100%	100%	100%	54%	0%	23%	8%	69%	38%	15%	8%
***Pax9*$^{-/-}$*;Msx1*$^{-/-}$**	0	2	2	0	1	1	0	**1(↑*)**	1	1	0
2	0%	100%	100%	0%	50%	50%	0%	50%	50%	50%	0%

Statistically significant differences in the presentation of a phenotype, and whether up or down, from that seen in *Pax9*$^{-/-}$ mice are indicated: *p<0.05, **p≤0.001 (Pearson Chi-Square). Any phenotype with a value of zero was excluded from statistical analysis.

Abbreviations: ARSA, aberrant right subclavian artery; cAo, cervical aorta; cRSA, cervical right subclavian artery; DORV, double outlet right ventricle; IVC, interventricular communication; VSD, ventricular septal defect.

To confirm the phenotypes observed by MRI analysis at a higher resolution, and to potentially identify more subtle defects, the embryos were recovered and processed for standard histology and haematoxylin and eosin staining (Figure 4-9). In addition to the embryos analysed by MRI, twelve more E15.5 embryos were collected and processed for histology (four *Pax9*$^{-/-}$, five *Pax9*$^{-/-}$*;Msx1*$^{+/-}$ embryos and three *Pax9*$^{-/-}$*;Msx1*$^{-/-}$). Externally these embryos displayed the expected phenotypes such as a duplicated pre-axial digit, except in the *Pax9*$^{-/-}$*;Msx1*$^{-/-}$ embryos which all had normal limbs, and cleft palate (Table 4-4).

From the histological analysis of the additional embryos collected (n = 12), all the embryos homozygous null for *Pax9* lacked a thymus. A VSD was found in one *Pax9*$^{-/-}$ embryo and one *Pax9*$^{-/-}$*;Msx1*$^{+/-}$ embryo. No other outflow defects were observed in these embryos (Figure 4-9, Table 4-4). All four of the *Pax9*$^{-/-}$ embryos displayed an IAA and ARSA and two had abnormal carotid arteries. In the *Pax9*$^{-/-}$*;Msx1*$^{+/-}$ embryos (n = 5), two presented with IAA and ARSA (40%) but the remaining three embryos had an intact aortic arch (60%). One embryo had a cervical right subclavian artery, and two embryos had abnormal carotid arteries.

Of the three *Pax9*$^{-/-}$*;Msx1*$^{-/-}$ embryos collected and analyzed in this dataset all had a normal cardiovascular system, but presented with a cleft palate and absent thymus.

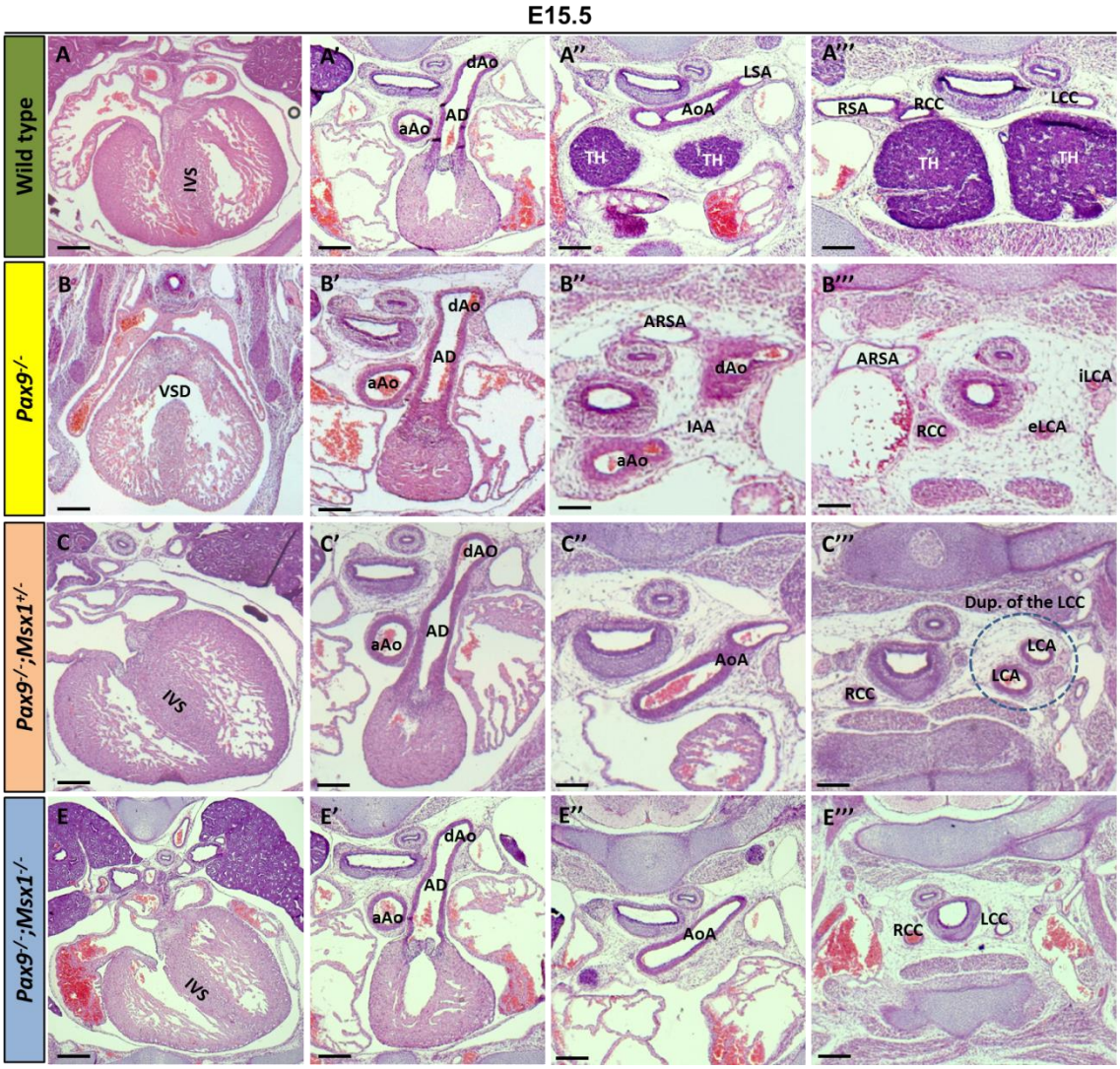

Figure 4-9: Histological analysis of *Pax9$^{-/-}$;Msx1$^{+/-}$* embryos.
Embryos at E15.5 were collected and analysed by histology using haematoxylin and eosin staining. (**A**) Wild-type embryo with an intact interventricular septum, normal outflow tract (**A'**), aortic arch (**A''**) and right subclavian artery, common carotid arteries and the thymus is present (**A'''**). (**B**) *Pax9$^{-/-}$* embryo displaying VSD, a normal outflow tract (**B'**), interrupted aortic arch (IAA) and aberrant right subclavian artery (ARSA; **B''**) and abnormal carotid arteries (**B'''**). The thymus is absent. (**C**) *Pax9$^{-/-}$;Msx1$^{+/-}$* embryo with an intact septum, and normal outflow tract (**C'**) as well as an intact aortic arch (**C''**). This embryo has a duplicated left carotid artery (dup-LCC) and the thymus is absent (**C'''**). (**E**) A *Pax9$^{-/-}$;Msx1$^{-/-}$* embryo with a normal interventricular septum, normal outflow tract (**E'**), an intact aortic arch (**E''**), and normal carotid arteries (**E'''**). The thymus is absent.
Ao, aorta; AD, arterial duct; dAo, dorsal aorta; LCC, left common carotid artery; LSA, left subclavian artery; LV, left ventricle; RCC, right common carotid artery; RSA, right subclavian artery; RV, right ventricle. Scale, 500μm.

Analysis of the cardiovascular defects in mutant *Pax9;Msx1* mice was carried out over different stages of development (i.e. E15.5 and neonatal stages) using a range of imaging techniques (direct observation, MRI, μCT and histology). Both stages and the techniques used, however, allow the cardiovascular defects to be recorded and grouped together as cardiovascular patterning is complete by E15.5. This means that if an embryo were to develop IAA, it would have done so before the E15.5 stage is reached. Because of this, all of the collected data (via the various techniques and at the different stages) on the *Pax9;Msx1* mutant phenotypes was pooled together for a final analysis. A total of 34 *Pax9*$^{-/-}$, 40 *Pax9*$^{-/-}$*;Msx1*$^{+/-}$ and six *Pax9*$^{-/-}$*;Msx1*$^{-/-}$ embryos at E15.5 and neonates were analysed for statistically significant differences in the cardiovascular defects observed (Table 4-5).

The majority of the *Pax9*$^{-/-}$ neonates and embryos analysed in this study presented with IAA (31/34; 91%) and ARSA (29/34; 85%). However, the incidence of these phenotypes were significantly reduced in the *Pax9*$^{-/-}$*;Msx1*$^{+/-}$ neonates and embryos, which displayed only 11 out of 40 instances of IAA (28%; $p<0.001$) and 18 out of 40 cases of ARSA (45%; $p=0.01$). Moreover, the presence of a normal aortic arch was significantly increased in the *Pax9*$^{-/-}$*;Msx1*$^{+/-}$ mice compared to *Pax9*$^{-/-}$ (50% compared to 3% respectively; $p<0.001$), and the occurrence of a cervical aortic arch was also increased (23% versus 6%; $p<0.05$). There was no significant difference in the presence of cervical right subclavian artery or abnormal carotid arteries between the two genotypes.

Comparing the *Pax9*$^{-/-}$ phenotypes to the *Pax9*$^{-/-}$*;Msx1*$^{-/-}$ neonates and embryos revealed that the presence of IAA (91% compared to 17% respectively; $p<0.001$) and ARSA (85% versus 17%; $p<0.001$) were also significantly reduced. A normal aortic arch occurred in 83% of *Pax9*$^{-/-}$*;Msx1*$^{-/-}$ mice, significantly more than in the *Pax9*$^{-/-}$ mice (3%; $p<0.001$). The cervical aortic arch and cervical right subclavian artery phenotypes could not be statistically assessed for the *Pax9*$^{-/-}$*;Msx1*$^{-/-}$ genotype as neither of these defects was observed.

There were no statistically significant differences in the presentation of phenotypes between the *Pax9*$^{-/-}$;*Msx1*$^{+/-}$ and *Pax9*$^{-/-}$;*Msx1*$^{-/-}$ neonates and embryos. Therefore, it cannot be stated that the effect of losing both alleles of *Msx1* in the context of the *Pax9*-null cardiovascular phenotype further reduces the severity of the defects. However, none of *Pax9*$^{-/-}$;*Msx1*$^{-/-}$ embryos displayed any defect of the carotid arteries.

Table 4-4: Phenotype of E15.5 *Pax9;Msx1* mutant embryos examined by histology only.

	Phenotype											
	Pre-axial digit duplication	Absent thymus	Cleft palate	Carotid deformities								
				VSD	DORV + IVC	IAA	cAo	Normal Ao	ARSA	cRSA	Abnormal carotid arteries
***Pax9*$^{-/-}$**	4	4	4	1	0	4	0	0	4	0	2
4	100%	100%	100%	25%	0%	100%	0%	0%	100%	0%	50%
***Pax9*$^{-/-}$*;Msx1*$^{+/-}$**	5	5	5	1	0	**2 (↓*)**	0	**3(↑*)**	2	1	2
5	100%	100%	100%	20%	0%	40%	0%	60%	40%	20%	40%
***Pax9*$^{-/-}$*;Msx1*$^{-/-}$**	0	3	3	0	0	**0**	0	**3(↑**)**	0	0	0
3	0%	100%	100%	0%	0%	0%	0%	100%	0%	0%	0

Statistically significant differences in the presentation of a phenotype, and whether up or down, from that seen in *Pax9*$^{-/-}$ mice are indicated: *p<0.05, **p≤0.001 (Pearson Chi-Square). Any phenotype with a value of zero was excluded from statistical analysis.

Abbreviations: ARSA, anomalies right subclavian artery; AO, aorta; cAo, cervical aorta; cRSA, cervical right subclavian artery; IAA, interruption of the aortic arch; DORV, double outlet right ventricle; IVC, interventricular communication; VSD, ventricular septal defect

Table 4-5: Phenotypes found in all *Pax9;Msx1* mutant pups and neonates were collated for analysis.

	Phenotype								
	Pre-axial digit duplication	Absent thymus	Cleft palate	Cardiovascular defects					
				IAA	cAo	Normal Ao	ARSA	cRSA	Abnormal carotid arteries
***Pax9*$^{-/-}$**	34	34	34	31	2	1	29	5	14
34	100%	100%	100%	91%	6%	3%	85%	15%	41%
***Pax9*$^{-/-}$*;Msx1*$^{+/-}$**	40	40	40	**11(↓**)**	**9(↑*)**	**20(↑**)**	**18(↓**)**	10	9
40	100%	100%	100%	28%	23%	50%	45%	25%	23%
***Pax9*$^{-/-}$*;Msx1*$^{-/-}$**	0	6	6	**1(↓**)**	0	**5(↑**)**	**1(↓**)**	1	0
6	0%	100%	100%	17%	0%	83%	17%	17%	0%

Statistically significant differences in the presentation of a phenotype, and whether up or down, from that seen in *Pax9*$^{-/-}$ mice are indicated: *$p<0.05$, **$p\leq0.001$ (Pearson Chi-Square). Any phenotype with a value of zero was excluded from statistical analysis.

Abbreviations: ARSA, aberrant right subclavian artery; Ao, aorta; cAo, cervical aorta; cRSA, cervical right subclavian artery; IAA, interruption of the aortic arch.

4.3.2.1 Analysis of the observed Pax9/Msx1 genotypes

From all the *Pax9*$^{+/-}$;*Msx1*$^{+/-}$ intercrosses performed, a total of 136 embryos at E15.5 were collected for MRI and histological analysis. The number of each genotype collected was recorded (Table 4-6) and checked for any deviation from the expected Mendelian ratio using the Chi-Square test. This analysis confirmed that there was no statistically significant deviation from the expected number for each genotype compared to those observed.

Table 4-6: The observed and expected Mendelian ratio of E15.5 embryos acquired from *Pax9*$^{+/-}$*;Msx1*$^{+/-}$ intercrosses.

Genotype	Observed	Expected
Wild type	10	8.375
***Pax9*$^{+/+}$*;Msx1*$^{+/-}$**	20	16.75
***Pax9*$^{+/+}$*;Msx1*$^{-/-}$**	6	8.375
***Pax9*$^{+/-}$*;Msx1*$^{+/+}$**	18	16.75
***Pax9*$^{+/-}$*;Msx1*$^{+/-}$**	40	33.5
***Pax9*$^{+/-}$*;Msx1*$^{-/-}$**	10	16.75
***Pax9*$^{-/-}$*;Msx1*$^{+/+}$**	13	8.375
***Pax9*$^{-/-}$*;Msx1*$^{+/-}$**	13	16.75
***Pax9*$^{-/-}$*;Msx1*$^{-/-}$**	6	8.375
Total	136	

4.3.3 PHARYNGEAL ARCH ARTERY FORMATION AND REMODELLING

As described in the introduction (section 1.3.3), the great arteries develop from six pairs of PAA that run through the pharyngeal arches. Before E10.5 the 1st and 2nd PAA have almost completely regressed except for the maxillary artery and the stapedial artery respectively. The 3rd, 4th, and 6th PAA remodel into asymmetrical great arteries. The left and right common carotid arteries are derived from the left and right 3rd PAA. The arch of aorta is derived from the left 4th PAA, and the left 6th PAA gives rise to the arterial duct. The 5th PAA completely regresses before it is fully developed.

4.3.3.1 Pharyngeal arch artery formation

To explore the development of the PAA, India ink was used to visualize the blood vessels and see if they were capable of carrying blood. India ink was injected into the left ventricle of the beating hearts of control and mutant embryos at E10.5, where it was pumped into the PAA.

Double heterozygous mice were intercrossed to generate embryos for analysis. However, to generate sufficient embryos for these studies, it became necessary to also use female mice with single heterozygous genotypes (i.e. *Pax9*$^{+/-}$) crossed with *Pax9*$^{+/-}$;*Msx1*$^{+/-}$ males. This produced embryos with the *Pax9*$^{-/-}$;*Msx1*$^{+/-}$ genotype, but not double homozygous mutant embryos.

A total of 103 embryos were collected and subjected to intra-cardiac ink injection. All of the wild type embryos (n = 16) presented with normal cardiovascular patterning where the 1st and 2nd PAA were fully regressed and no longer visible. The 3rd, 4th and 6th PAA were fully developed on both the left and right sides of all the wild type embryos, and were of approximately equal size (Figure 4-10). The following genotypes also had normal PAA development (not shown): *Msx1*$^{+/-}$ (n = 11), *Msx1*$^{-/-}$ (n = 6), *Pax9*$^{+/-}$ (n = 14), *Pax9*$^{+/-}$;*Msx1*$^{+/-}$ (n = 19), and *Pax9*$^{+/-}$;*Msx1*$^{-/-}$ (n = 7).

Nine *Pax9*$^{-/-}$ embryos were analysed, and they displayed abnormal bilateral persistence of the 1st (7/9; 85%) and 2nd (8/9; 89%) PAA, which is a sign of their late remodeling. The 3rd PAA was bilaterally affected in seven embryos (78%) with five embryos having this vessel non-patent to ink (5/9; 56%). Only one embryo showed a normal 3rd PAA on both sides (11%). All *Pax9*$^{-/-}$ embryos (9/9, 100%) presented with a bilaterally non-patent 4th PAA (Figure 4-10, Table 4-7).

The majority of *Pax9*$^{-/-}$*;Msx1*$^{+/-}$ embryos also showed a delayed regression of the 1st (8/16, 50%) and 2nd (8/16, 50%) PAA similar to *Pax9*$^{-/-}$ embryos, as visualised by the India ink injection. However, the penetrance of bilateral 3rd PAA defects at E10.5 (4/16; 25%), was significantly decreased in *Pax9*$^{-/-}$*;Msx1*$^{+/-}$ embryos compared with *Pax9*$^{-/-}$ embryos (Table 4-7) ($p = 0.02$). The remaining 12 unaffected *Pax9*$^{-/-}$*;Msx1*$^{+/-}$ embryos had normally sized 3rd PAA in comparison to wild type embryos.

The majority of *Pax9*$^{-/-}$*;Msx1*$^{+/-}$ embryos (10/16, 69%), however, displayed bilaterally non-patent 4th PAA, and six embryos showed a bilateral or unilateral hypoplastic 4th PAA (38%) (Figure 4-10, Table 4-7).

These results indicated a less severe phenotype of the PAA in *Pax9*$^{-/-}$*;Msx1*$^{+/-}$ embryos compared with *Pax9*$^{-/-}$ embryos at E10.5. This suggested that loss of one *Msx1* allele is somehow rescuing the 3rd PAA phenotype that occurs in the *Pax9*$^{-/-}$ embryos. Moreover, four *Pax9*$^{-/-}$*;Msx1*$^{+/-}$ embryos had a hypoplastic 4th PAA which was not seen in *Pax9*$^{-/-}$ embryos. This also resembles a less severe PAA phenotype than observed in *Pax9*$^{-/-}$ embryos.

Only one *Pax9*$^{-/-}$*;Msx1*$^{-/-}$ embryo was generated in this experiment. This embryo showed a unilaterally patent 1st and a bilateral patent 2nd PAA similar to *Pax9*$^{-/-}$ and *Pax9*$^{-/-}$*;Msx1*$^{+/-}$ embryos. It also presented with normal 3rd PAA, and a hypoplatic 4th PAA on both sides (Figure 4-10, Table 4-7).

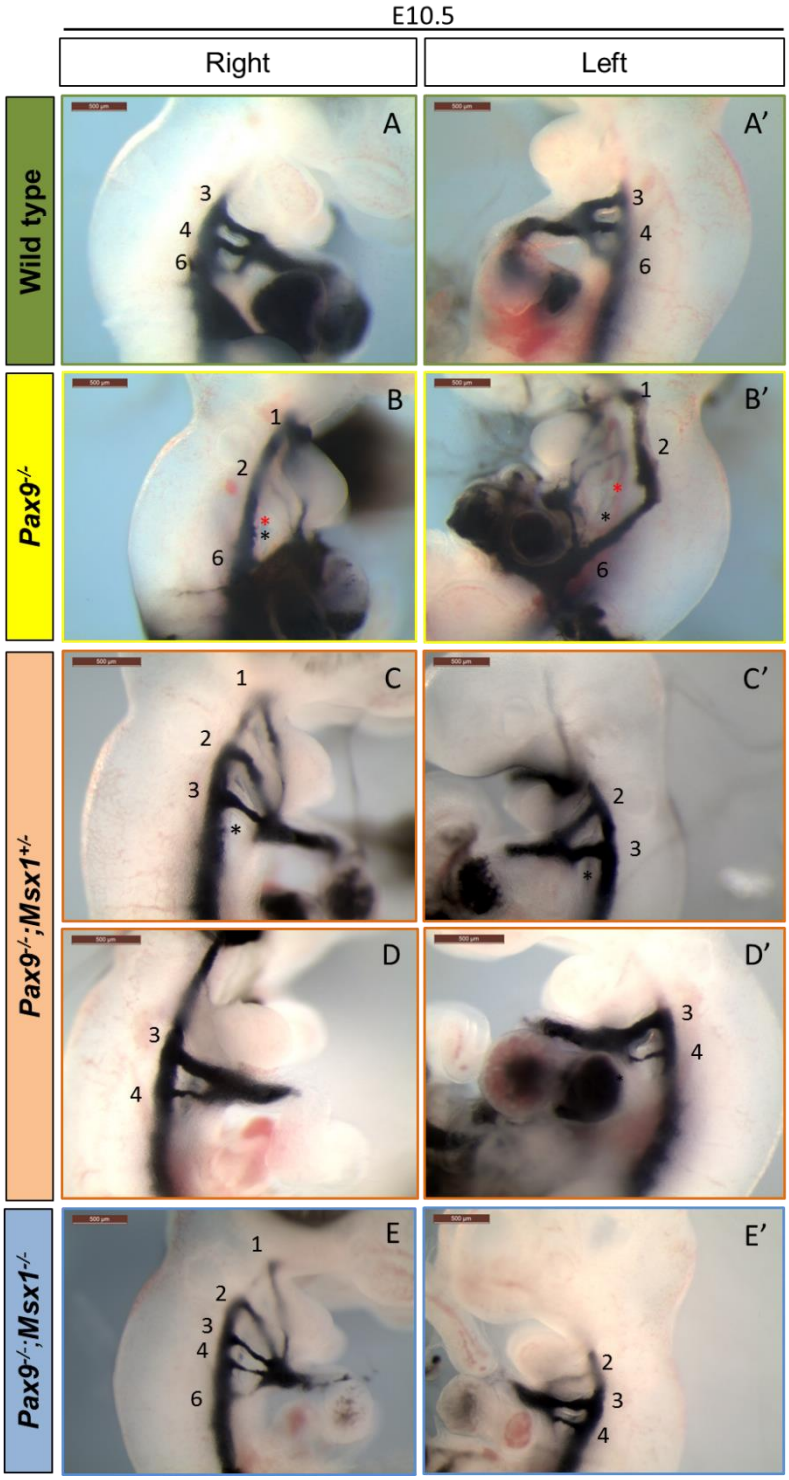

Figure 4-10: Pharyngeal arch artery patterning defects in *Pax9;Msx1* mutant embryos.
India ink was injected into the heart of E10.5 embryos to visualize the developing pharyngeal arch arteries (PAA). (**A**) Wild type embryo with normal development of the 3rd, 4th and 6th PAA. The 1st and 2nd PAA have regressed by this stage. (**B**) *Pax9*$^{-/-}$ embryo with abnormal persistence of the 1st and 2nd PAA. The 3rd (*red asterisk*) and 4th (*black asterisk*) PAA are bilaterally absent in this embryo. (**C, D**) *Pax9*$^{-/-}$*;Msx1*$^{+/-}$ embryos displayed persistent 1st and 2nd PAA (**C**) or these had regressed (**D**). The 3rd PAA was frequently of normal size and patent to ink, but the 4th PAA may be absent (*black asterisk*; **C**) or hypoplastic (**D**). **(E-E')** *Pax9*$^{-/-}$*;Msx1*$^{-/-}$ embryo with a patent 1st PAA on the right side only, while the second PAA was patent on both sides. The embryo presented a normal 3rd PAA and a hypoplastic 4th PAA similar to *Pax9*$^{-/-}$*;Msx1*$^{+/-}$ embryos. Scale, 500 µm.

Table 4-7: Patency of pharyngeal arch arteries in *Pax9;Msx1* mutants using ink at E10.5.

						Bilateral defects		
	N	PAA #	Abnormal (%)	Unilateral defect	Bilateral defect	P/P	Th-P/Th-P	Th-P/NP	NP/NP
***Pax9*$^{-/-}$**	9	**1**	7(85%)	1	6	6	-	-	
		2	8(89%)	1	7	7	-	-	
		3	8(89%)	1	7	-	1	1	5
		4	9(100%)	0	9	-	-	-	9
***Pax9*$^{-/-}$*;Msx1*$^{+/-}$**	16	**1**	8(50%)	0	8	8	-	-	-
		2	8(50%)	0	8	8	-	-	-
		3	4(25%)	0	4	-	-	3	1
		4	16(100%)	0	16	-	4	2	10
***Pax9*$^{-/-}$*;Msx1*$^{-/-}$**	1	**1**	1(100%)	1	0	-	-	-	-
		2	1 (100%)	0	1	1	-	-	-
		3	0 (0%)	0	-	-	-	-	-
		4	1(100%)	0	1	-	1	-	-

Following intracardiac ink injection, each pharyngeal arch artery (PAA) was recorded as having a unilateral or bilateral defect, and whether the PAA was patent to ink (P), thin (Th) or not patent (NP). Only the genotypes that presented with defects are shown. All other genotypes showed normal PAA patency to ink.

4.3.3.2 Pharyngeal arch artery remodeling

Ink injection into E10.5 embryos is an excellent way to visualise the recently formed and symmetrical PAA. However, this technique becomes difficult to utilise at later stages as the external epithelium of the embryo begins to thicken and the heart is no longer accessible for ink injection. Therefore, to analyse embryos at a later stage for the remodelling of the PAA embryos at E12.5 were collected and sent for µCT scanning (performed by Dr Jürgen Schneider, University of Oxford). At this stage of embryonic development, the portion of the paired dorsal aorta between the 3rd and 4th PAA, the carotid duct, has totally regressed, which allows the 3rd PAA to continue cranially from the dorsal aorta as the internal carotid artery.

Twelve embryos at E12.5 in total were collected and sent for µCT: two wild type, four *Pax9*$^{-/-}$, and six *Pax9*$^{-/-}$*;Msx1*$^{+/-}$. The aligned .tiff stacks generated by this method were analysed with Amira software and 3-dimensional models of the observed cardiovascular phenotypes were created (Figure 4-11).

Both of the wild type embryos imaged displayed normal cardiovascular development for this stage. The right dorsal aorta was in the process of regressing and the right 6th PAA was fully regressed, whereas the left 6th PAA had formed the arterial duct. The left and right 4th PAA had become the aortic arch and the proximal part of the right subclavian artery, respectively. Following the involution of the carotid ducts, the 3rd PAA had formed the common carotid arteries. (Figure 4-11 A-A'').

All *Pax9*$^{-/-}$ embryos (n = 4, Table 4-8) presented with complex cardiovascular development defects. Three had a persistence of the 2nd PAA and bilaterally absent 3rd PAA (Figure 4-11 B-C''), while the fourth embryo had a hypoplastic left 3rd PAA and an absent right 3rd PAA. None of these embryos had a 4th PAA.

Six *Pax9*$^{-/-}$*;Msx1*$^{+/-}$ mutant embryos were examined at E12.5 using µCT scanning (Table 4-8). None of these embryos showed a delay in the regression of the 1st and 2nd PAA (100%). The majority of the embryos had a normal 3rd PAA similar to that seen in the wild type embryos (5/6) (Figure 4-11 D-E''). One embryo, however, lacked the left 3rd PAA but the right 3rd PAA was present. Interestingly, two out of the six *Pax9*$^{-/-}$*;Msx1*$^{+/-}$ embryos had a normal PAA system similar to the wild type embryos (Figure 4-11 D-D''). Moreover, five embryos had the left 4th PAA, which was

of a normal size in the majority (4/6) of them, but was hypoplastic in one embryo (1/6). Only two embryos showed a right 4th PAA.

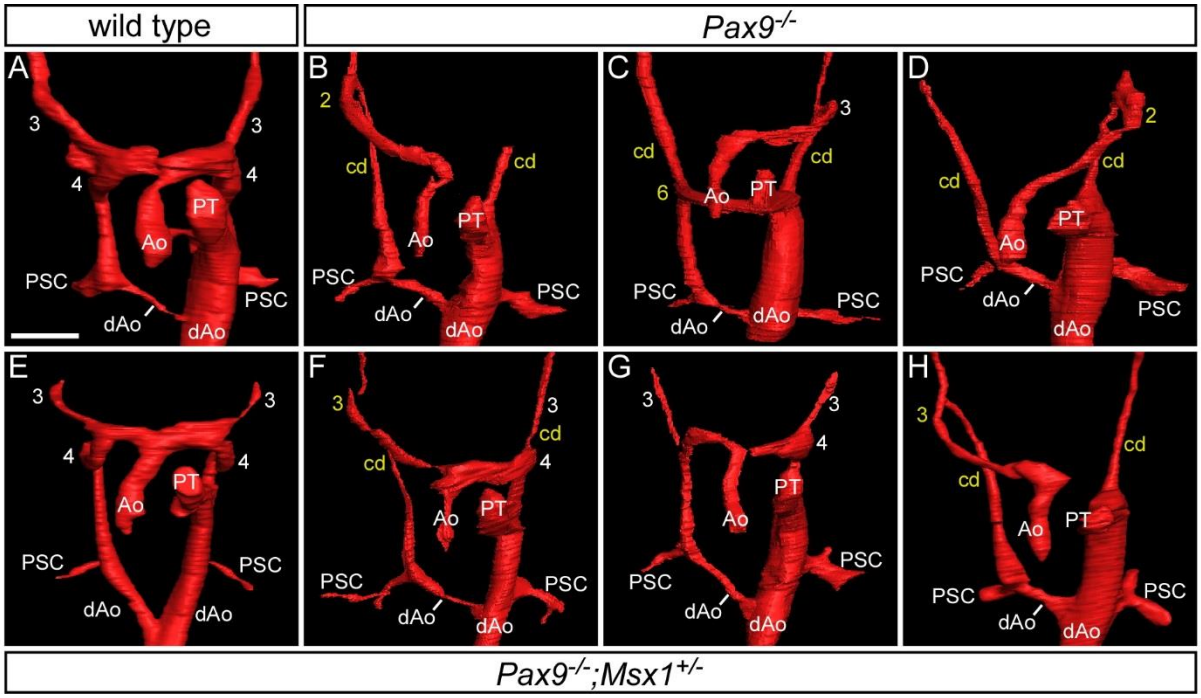

Figure 4-11: Pharyngeal arch artery remodeling defects in *Pax9;Msx1* mutant embryos. Embryos at E12,5 were imaged by µCT and 3D reconstructions were made using Amira software. (**A**) A wild type embryo with normal remodeling of the arteries. The aorta (Ao) and pulmonary trunk (PT) have septated into separate vessels leaving the heart. The right dorsal aorta (dAo) is regressing while on the left it is enlarging. The 3rd PAA have formed the common carotid arteries. The 4th PAA has formed the aortic arch on the left, while on the right the 4th will form the right subclavian artery in conjunction with the primitive subclavian (PSC). (**B - D**) *Pax9*$^{-/-}$ embryos present with complex PAA defects including absent 3rd and 4th PAA, and persistence of the 2nd PAA (**B, D**). (**E – H**) *Pax9*$^{-/-}$*;Msx1*$^{+/-}$ embryos had less severe cardiovascular defects than the *Pax9*$^{-/-}$ embryos, being either normal (**E**) or having an intact aortic arch and 3rd PAA (**F, G**). Some *Pax9*$^{-/-}$*;Msx1*$^{+/-}$ embryos were occasionally found with more severe defects (**H**). Scale bar, 500 µm.

Table 4-8: Cardiovascular defects in *Pax9;Msx1* mutant embryos at E12.5

Genotype	N	PAA defects			Persistent carotid duct
		Normal	left 3rd	left 4th	
wild type	2	2	0/2	0/2	0/2
***Pax9*$^{-/-}$**	4	0	4/4	4/4	4/4
***Pax9*$^{-/-}$*;Msx1*$^{+/-}$**	6	2	1/6(↓**)	2/6	4/6

Statistically significant differences in the presentation of a phenotype, from that seen in *Pax9*$^{-/-}$ mice are indicated**p≤0.001 (Pearson Chi-Square).

E12.5 embryos were imaged by μCT and the cardiovascular defects affecting the development of the 3rd and 4th PAA recorded. For each embryo, the right and left vessels were counted independently (Table 4-8). There is a statistically significant decrease in the number of absent 3rd PAA in the *Pax9*$^{-/-}$*;Msx1*$^{+/-}$ embryos compared to the *Pax9*-nulls (*p = 0.017, Pearson Chi-Squared test). This test could not be applied for the absent 4th or persistent carotid duct phenotypes as the number of normal vessels was zero in the *Pax9*-nulls. These values are invisible to statistical procedures which require positively weighted cases.

4.3.4 STUDY OF Pax9–Msx1 PROTEIN INTERACTION

Pax9 and *Msx1* encode transcription factors with different DNA binding motifs, a paired domain and a homeodomain, respectively, and are co-expressed during mouse craniofacial and tooth development (Conley *et al.*, 1979; Mackenzie *et al*., 1991b).

Msx1 and *Pax9* were previously shown to interact during development of the maxillofacial region and dentition (Nakatomi *et al.*, 2010). Whereas the dentition is normal in single heterozygous *Pax9*$^{+/-}$ or *Msx1*$^{+/-}$ mice, all adult *Pax9*$^{+/-}$*;Msx1*$^{+/-}$ mice lack lower incisors (Nakatomi *et al.*, 2010).

It has been shown that *Pax9* and *Msx1* could interact at the protein level (Ogawa *et al.*, 2005). Although this study claims to show an interaction *in vivo*, this was in fact two plasmid constructs co-transfected into cells followed by a co-immunoprecipitation and Western blotting. This should really be considered as an *in vitro* assay as it does not involve examining endogenous protein interactions in living cells.

To confirm this published evidence for a Pax9-Msx1 interaction *in vitro*, an alternative approach was taken, using the Bimolecular Fluorescence Complementation (BiFCo) assay (Kerppola, 2008). BiFCo analysis enables the direct visualisation of protein interactions in living cells. This assay is based on the formation of a yellow fluorescent protein (YFP) brought about through the association between two non-fluorescent fragments the Venus C terminal (VEC) and Venus N terminal (VEN) of a fluorescent protein. When the fragments are brought into close proximity by an interaction between proteins fused to the fragments, YFP is formed. VEN and VEC do not interact on their own so BiFCo enables direct visualisation of protein interactions and does not rely on their secondary effects. These interactions can be visualised in living cells, eliminating the potential artifacts associated with cell lysis or fixation.

Plasmids containing VEC, VEN, VEN-GALA4 and VEC-GALA 4 were generously provided to us by Dr. José Braganća (University of Algarve, Portugal). To perform BiFCo, *Pax9* and *Msx1* were fused to the N- and C-terminal halves of the enhanced VENUS variant of the yellow fluorescent protein to form VEC-*Pax9* and VEN-*Msx1* (Figure 4-12).

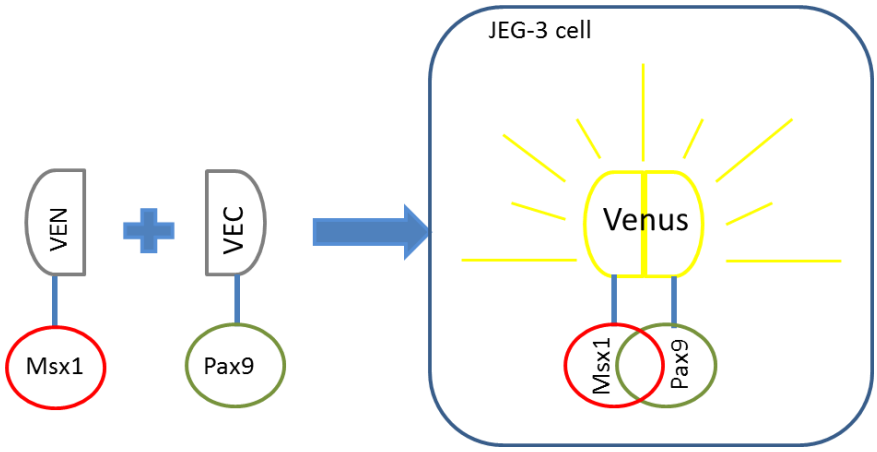

Figure 4-12: Schematic of the BiFCo assay using Pax9 and Msx1.
The Pax9 cDNA was cloned in frame with the N-terminal fragment of Venus/YFP (VEN), and the Msx1 cDNA was cloned in frame with the C-terminal fragment of Venus/YFP (VEC). The VEC-Pax9 and VEN-Msx1 constructs were co-transfected into JEG-3 cells.

After transient co-transfection of the VEC-*Pax9* and VEN-*Msx1* constructs into JEG3 cells. JEG3 cells are used routinely in the Bamforth Lab for Tbx1 luciferase assays and they are able to be transfected with high efficiency. It has also been shown that Tbx1 and Pax9 proteins are expressed in these cells when transfected with expression plasmids (Alberto Briones-Leon, pers. comm.) . YFP fluorescence was observed (Figure 4-13). This indicates that the co-expression of Pax9 and Msx1 produced a direct physical interaction between the two proteins. At the same time, the control wells did not show any fluorescence expression.

To verify expression of Pax9 and Msx1 proteins, transfected JEG3 cells were stained using immunohistochemistry and antibodies raised against Pax9 and Msx1. Images were taken using a fluorescence microscope (Figure 4-14).

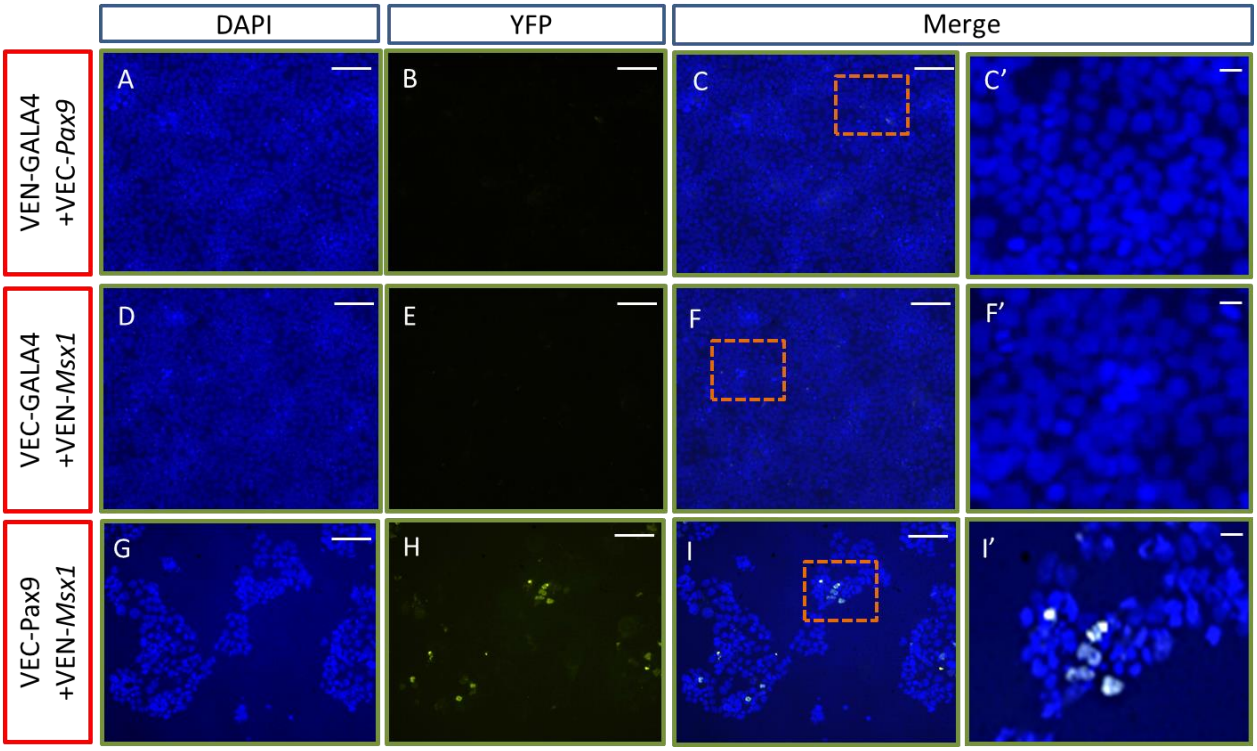

Figure 4-13: Pax9 and Msx1 proteins interact with each other.
Bimolecular fluorescence complementation was used to analyse the protein-protein interaction of Pax9 and Msx1. (**A, D, G**) DAPI fluorescence representing nuclei of the JEG3 cells in control transfected cells (VEN-GAL4 + VEC-Pax9, **A**; VEC-GAL4 + VEN-Msx1, **D**) and VEC-Pax9 + VEN-Msx1 (**G**). (**H, I**) Restored Venus fluorescence resulting from the interaction of Pax9 and Msx1. No fluorescence was observed from the control transfections (**B, C, E, F**). **(C', F', I')** Higher magnification images of **(C, F, I).** Scale bar, 50 μm.

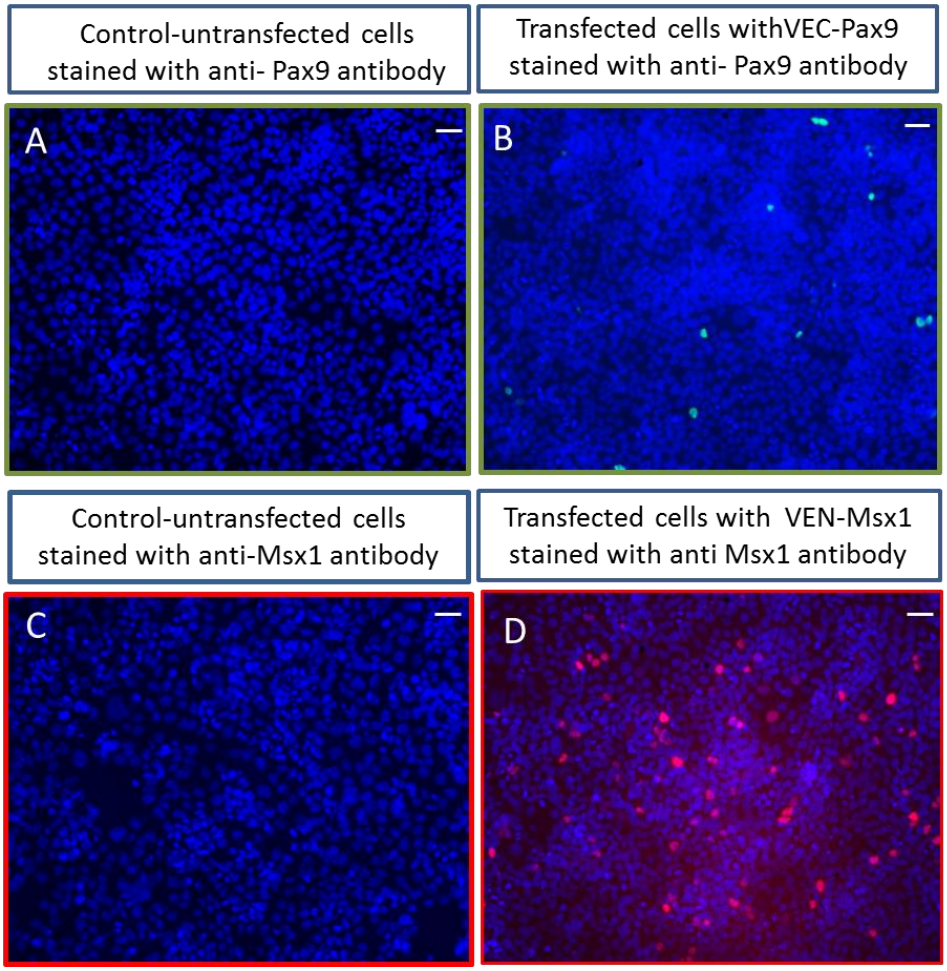

Figure 4-14: Pax9 and Msx1 immunostaining in transfected cells.
JEG-3 cells were transfected with the VEC-*Pax9* (B) and VEN-*Msx1* (C) plasmids and subsequently immunostained for Pax9 and Msx1. (**A**) Untransfected control cells showed no immunostaining after they stained with anti Pax9 antibody. Positive immunostaining was identified for Pax9 (**B**). **(C)** untransfected cells that did not showed any sign of fluorescent staining after they attained with anti Msx1 antibody. **(D)** A positive fluorescent signal was detected for the cells that transfected with Msx1 and stained with anti-Msx1 antibody. Scale bar, 50 μm.

Western blotting was also used to confirm protein expression in the transfected cells. Cells transfected with the VEC-Pax9 plasmid were lysed and run on a polyacrylamide gel. Following transfer to a membrane, immunoblotting for Pax9 was carried out. No endogenous Pax9 was detected in untransfected cells, but a band between 30 and 40 kilo Dalton (kDa) was visualised in the transfected cell lysate, corresponding to the predicted molecular weight for Pax9 of 38 kDa (Figure 4-15). This procedure was also carried out for cells transfected with VEN-Msx1, but unfortunately, the *Msx1* antibody did not detect any band, even after attempts to

optimise the method, suggesting that this antibody is not suitable for Western blotting.

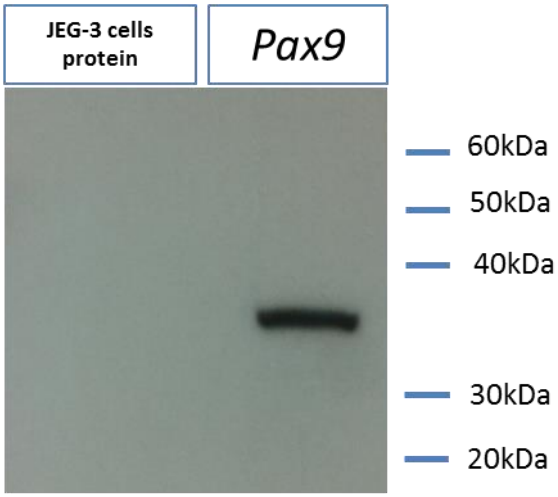

Figure 4-15: Western blot for Pax9.
Western blot analysis was performed using lysed protein from JEG3 cells transfected with VEC-Pax9 and an anti-Pax9 antibody. A specific band of the predicted molecular weight for Pax9 (38kDa) was observed. No Pax9 protein was seen in non-transfected JEG-3 cells.

4.3.5 INVESTIGATING *Pax9* GENE EXPRESSION *IN VIVO*.

As illustrated above, Pax9 and Msx1 proteins are able to physically interact with each other *in vitro*, and this is also likely to be true *in vivo* as *Pax9;Msx1* double heterozygous mice have a craniofacial phenotype. However, it is not known whether these two proteins are co-expressed in the pharyngeal region to be critical for PAA development.

During normal development *Pax9* is expressed at mid gestation (E9.0) exclusively in the pharyngeal endoderm, which generates the thymus, parathyroid glands, ultimobrachial bodies and eustachian tube(Peters *et al*., 1998). To investigate the expression of *Pax9* during normal mouse development and to simultaneously validate a novel *Pax9cre* allele which will be used for subsequent experiments (see chapter 5), X-gal staining of whole mount embryos was performed. For the whole mount staining a *Pax9cre* male mouse was crossed with *Rosa26R-lacZ* reporter female mice carrying the bacterial β-galactosidase gene (Soriano, 1999). When subjected to *Cre*-mediated recombination the stop sequence is removed allowing for

expression of β-galactosidase activity in cells that express Pax9. Embryos were collected at E9.5 and X-gal staining was performed, as reported in section 2.7.2, then subsequently sectioned and counter stained using eosin.

The staining revealed that *Pax9* expression was restricted to the pharyngeal endoderm as expected (Peters *et al*., 1998). Histological sections showed expression of *Pax9* in the pharyngeal endoderm and the gut endoderm of these embryos (Figure 4-16).

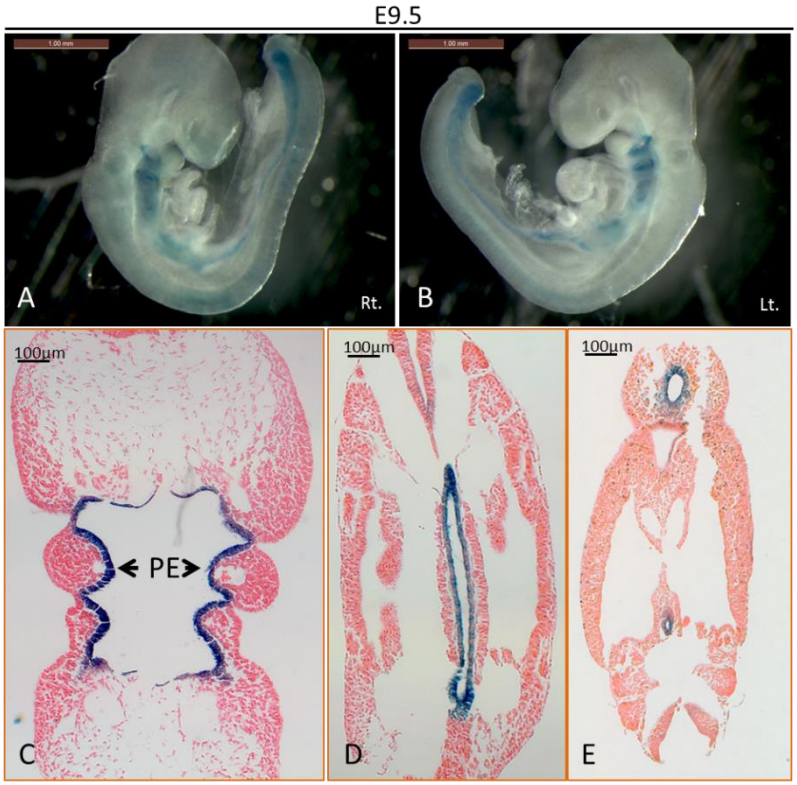

Figure 4-16: Pax9 expression in *Pax9cre;Rosa26R* embryos.
Pax9cre;Rosa26R embryos at E9.5 were whole mount stained with X-gal and subsequently sectioned. (**A, B**) Left and right views of the embryo showing B-galactosidase activity in the pharyngeal region and gut. (**C – E**) Coronal sections of the embryo in **A** and **B**, showing specific activity in the pharyngeal endoderm (**C**) and gut (**D, E**). Scale bars are indicated on each panel.

4.3.6 INVESTIGATING *Msx1* GENE EXPRESSION *IN VIVO*

To investigate whether there is an overlap between *Pax9* and *Msx1* expression during development, *in situ* hybridization was performed on E9.5 and E10.5 wild type embryos. Unfortunately, the results were inconclusive and the localisation of *Msx1* expression could not be confirmed. As an alternative approach, transgenic embryos were acquired from Dr. Stephane Zaffran (Pasteur Institute, Paris, France) which had been lineage traced using a novel *Msx1* reporter allele (Papoutsi *et al.*, 2015). $Msx1^{+/Cre}$ transgenic mice, which have the *Cre* gene inserted into the *Msx1* locus (Figure 4-17), were crossed with *Rosa26R-lacZ* reporter mice and the *Msx1cre* allele activated with administration of tamoxifen. Embryos were collected at E9.5 and E10.5 and stained with X-Gal to visualize the *lacZ* gene product. The stained embryos were shipped to the IGM for analysis. Images of the whole embryos were taken before they were processed and sectioned for histological investigation.

Wholemount X-gal staining revealed the presence of *Msx1* expression in presumed NCC during migration (Figure 4-18). The histological sections revealed that no *lacZ* positive cells were present in the pharyngeal endoderm at E9.5 or E10.5 which indicated that *Pax9* and *Msx1* expression does not overlap in the endoderm at mid-embryogenesis (Figure 4-19).

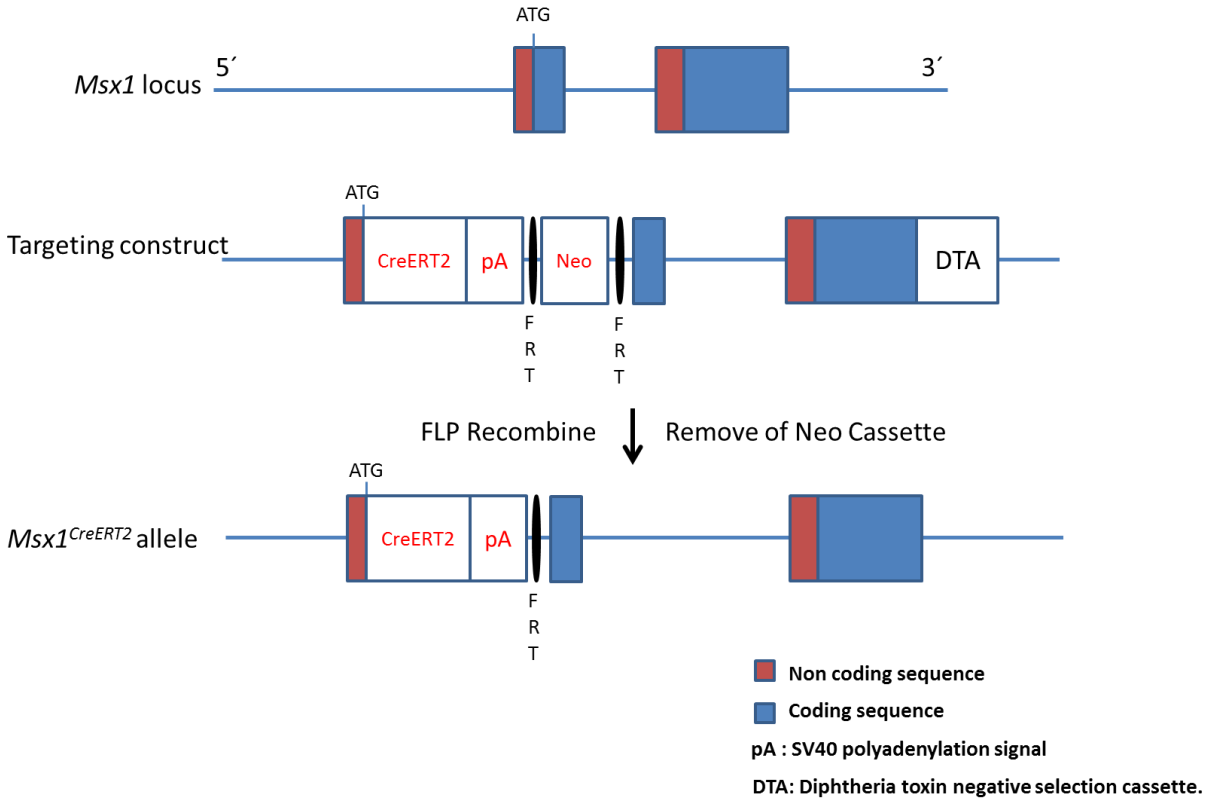

Figure 4-17: Cartoon of the *Msx1creERT2* allele.
A CreERT2 cassette was inserted into the first exon of the *Msx1* coding sequence in frame with the endogenous ATG initiation codon. The insertion resulted in the deletion of 218 bp in the coding sequence of *Msx1*. The *Msx1creERT2* allele allows the production of the tamoxifen which can activate CreERT2 recombinase in cells normally expressing *Msx1* (adapted from Papoutsi, *et al*, 2015).

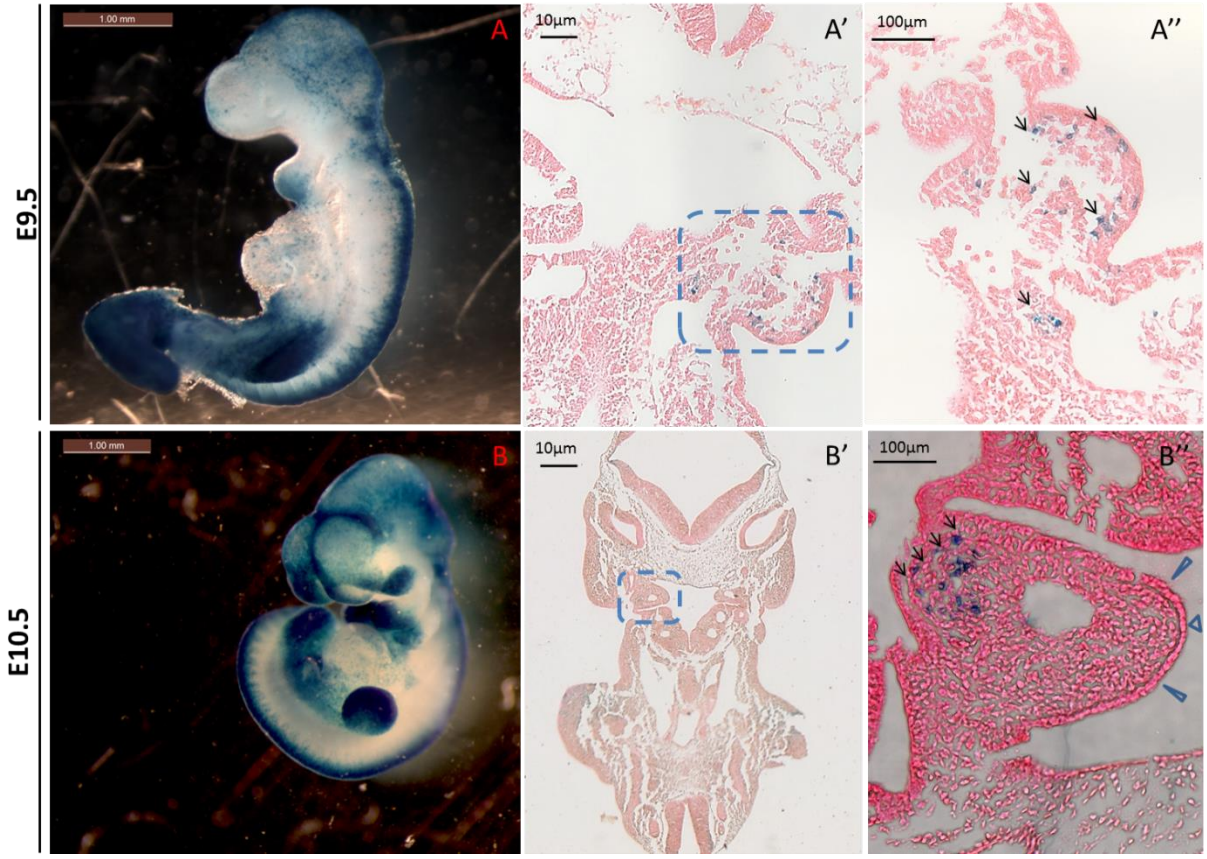

Figure 4-18: *Msx1* expression in wild type embryos using X-gal staining.
(**A, B**) X-gal staining was performed on a *Msx1*$^{+/Cre}$*;Rosa26R-Lacz* embryos at E9.5 and E10.5. At E9.5 *Msx1* was expressed in presumed neural crest cells during migration (*black arrows*, **A'**). At E10.5 there was no expression for *Msx1* in the pharyngeal endoderm (*arrowheads*) and the expression was restricted to the neural crest cells (*black arrows*, **B'-B''**). Scale bars are indicated on each panel.

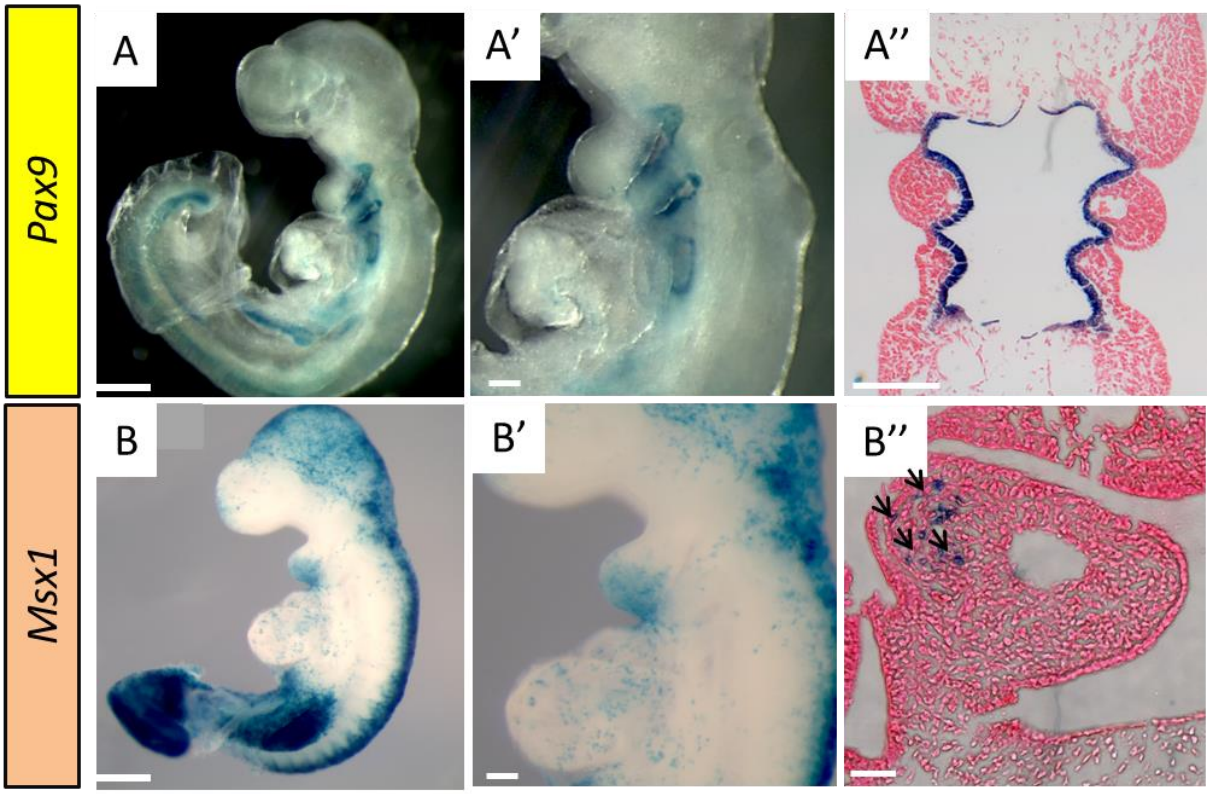

Figure 4-19: Comparison of *Pax9* and *Msx1* expression at E9.5 using whole mount X-gal staining.
(A) At E9.5, *Pax9* expression was restricted to the pharyngeal endoderm. (**B**) At the same stage *Msx1* was expressed in presumed neural crest cells, with no evidence of staining in the pharyngeal endoderm. Scale bars are indicated on each panel.

4.4 DISCUSSION

This chapter aimed to investigate possible genetic interaction between *Pax9* and *Msx1* in the development of the mouse cardiovascular system. In order to do so, all the possible genotypes that can derive from *Pax9;Msx1* double heterozygous mice crossing were studied. *Pax9*$^{+/+}$*;Msx1*$^{+/-}$, *Pax9*$^{+/+}$*;Msx1*$^{-/-}$, *Pax9*$^{+/-}$*;Msx1*$^{+/-}$, and *Pax9*$^{+/-}$*;Msx1*$^{-/-}$ embryos and neonates had a normal cardiovascular systems similar to the wild type. Which suggest that suppress *Msx1* by itself does not cause cardiovascular defects.

Pax9-null embryos show cardiovascular defects (as shown in chapter 3). However heterozygosity for *Msx1* seems to rescue in part these defects, since the majority of *Pax9*$^{-/-}$*;Msx1*$^{+/-}$ embryos and neonates showed either a normal or a modified aortic arch that was not observed in *Pax9*$^{-/-}$ embryos and neonates. Moreover, a more detailed analysis of the data collected from E15.5 embryos and P0 neonates reveals that *Pax9;Msx1* double mutant embryos show an even milder phenotype compared to the other genotypes, including *Pax9*$^{-/-}$*;Msx1*$^{+/-}$; this observation suggests that the total suppression of *Msx1* increases the chance of rescuing *Pax9*$^{-/-}$ cardiovascular phenotype. However, unfortunately, the possibility of getting *Pax9*$^{-/-}$*;Msx1*$^{-/-}$ embryos is very low (1 out of 16), and in fact in this work only 6 embryos out of a total of 136 embryos collected were *Pax9*$^{-/-}$*;Msx1*$^{-/-}$. On the other hand, the possibility of getting *Pax9*$^{-/-}$*;Msx1*$^{+/-}$ embryos is higher (1 out of 8); in this study 10 embryos out of 136 collected were *Pax9*$^{-/-}$*;Msx1*$^{+/-}$. Based on this observations, the study concentrated on *Pax9*$^{-/-}$*;Msx1*$^{+/-}$ embryos and neonates.

In contrast to *Pax9*$^{-/-}$ embryos and neonates, the majority of *Pax9*$^{-/-}$*;Msx1*$^{+/-}$ embryos and neonates at E10.5 presented with a well formed 3rd PAA; additionally, in some cases, they presented with a hypoplastic 4th PAA. At E12.5 the majority of *Pax9*$^{-/-}$*;Msx1*$^{+/-}$ embryos presented with a normal 3rd PAA and in many causes a normal left 4th PAA. Altogether, this suggests that some form of recovery is occurring during the development and remodelling of the PAA.

The 3rd PAA is required for the formation of the left and right common carotid arteries, and, in the absence of the 4th PAA, the 3rd PAA may participate in the formation of a modified aortic arch, namely the so-called “cervical aortic arch”. The cervical aortic

arch is thought to be compatible with life. Evidence exists that human patients can survive for many years despite being affected by cervical aortic arch. For example, the case of a six year old boy with interruption of the aortic arch type B, and presentation of arterial duct was recently reported (Suntratonpipat *et al.*, 2015). These researchers assumed that this case was a rare case of presentation of carotid duct or maybe cervical aortic arch, but the patient did not have any clinical feature such as pulsatile mass in the neck (Suntratonpipat *et al.*, 2015). Also, recently the case of 6 year old boy with a right sided cervical aortic arch has been published (Rajbanshi *et al.*, 2016). A possible explanation as to why these two patients survived for such a long time is that collateral vessels may compensate for the absence of the aortic arch.

Moreover, the data in this chapter could indicate a possibility of recovery of the hypoplastic 4th PAA observed in *Pax9*$^{-/-}$*;Msx1*$^{+/-}$ embryos at E10.5. It is well recognised that the frequency of a hypoplastic or even absent 4th PAA (seen around mid-embryogenesis E10.5) in *Tbx1*$^{+/-}$ embryos is much higher compared to the incidence of 4th PAA-derived defects in older embryos (Calmont *et al*., 2009; Vitelli *et al*., 2002). This indicates that some form of recovery is occurring during the development and remodelling of the PAA in the later stages (the mechanism for 4th PAA recovery in *Tbx1*$^{+/-}$ embryos will be described later in section 6.4)(Lindsay and Baldini, 2001). This suggests the possibility that the hypoplastic 4th PAA seen in *Pax9*$^{-/-}$*;Msx1*$^{+/-}$ embryos at E10.5 may recover to form a normal aortic arch.

There is published evidence to show that genes do not produce any clear role in a defect except in the presence of another modifier. For example, mice, which are, double heterozygous for a hypomorphic allele of *Notch2* and a null allele of *Jag1* show features of Alagille syndrome. These mice show several phenotypes including growth retardation, defects in the development of the intrahepatic bile ducts, heart, eyes and kidney; however importantly these phenotypes are not found in *Jag1* heterozygotes or homozygotes (McCright *et al.*, 2002), suggesting that Jag1 and Notch2 have a role together in several developmental events. Similarly, for many human diseases and syndromes no clear relationship between the genotype and the phenotype was uncovered. However, recent studies had implicated that syndromes can result from disorders attributable to high penetrance of a single gene.

Nevertheless, for some phenotypes, it is clear that mutations in a single gene can be insufficient to cause the phenotype itself without sequence alterations in another gene. Gene modifiers have become increasingly recognized as an important source of phenotypic variation that may explain the relationship between phenotype to genotype (Dipple and McCabe, 2000; Ming and Muenke, 2002; Nadeau, 2001). This is similar to the effect of *Msx1* in conjunction with *Pax9* observed in this study, although here *Msx1* is modifying the *Pax9*-null phenotype, making it apparently less severe. Therefore, these results indicate that *Msx1* acts somehow as a repressor for the *Pax9*- null phenotype.

Importantly, despite *Msx1*$^{-/-}$;*Msx2*$^{-/-}$ mice having heart defects (Boogerd *et al.*, 2010), knocking out *Msx1* by itself does not cause any cardiovascular defects, although, mutant pups did not survive to term due to cleft palate. Moreover, knocking out *Msx2* by itself produce a mouse raised to adulthood without any apparent cardiac manifestation (Chen *et al.*, 2007). These data indicate that a single allele of either *Msx1* or *Msx2* is sufficient to support normal cardiogenesis. Msx1 and Msx2 proteins factors share 55% overall amino acid identity, with 58/60 identical residues within the homeodomains which mean that thus are genuinely different genes (Khadka *et al.*, 2006). On the other hand, previous studies have demonstrated that regions of *Msx1* and *Msx2* expression within the embryo are often adjacent or overlapping, and that such regions are often associated with epithelial-mesenchymal cell interactions (Coelho *et al.*, 1991; Monaghan *et al.*, 1991; Takahashi *et al.*, 1991).

Msx1 haploinsufficiency only affects the formation of the aortic arch but it does not modify any other part of the phenotype within the pharyngeal arches. Also, *Pax9* transcription factor is required for development of some pharyngeal arch-derived tissues including the thymus (Peters *et al*., 1998), *Pax9*$^{-/-}$;*Msx1*$^{+/-}$ embryos and neonates lacked the thymus, parathyroid and ultimobranchial bodies similar to *Pax9*$^{-/-}$ embryos and neonates, suggesting that *Msx1* haploinsufficiency is not affecting the tissue that is derived from the pharyngeal endoderm. The data also show *Pax9;Msx1* double mutant embryos and neonates having a the digit phenotype rescued; these neonates and embryos do not have pre-axial digit duplication as seen in *Pax9*$^{-/-}$ and *Pax9*$^{-/-}$;*Msx1*$^{+/-}$ embryos and neonates, suggesting that the absence of *Msx1* can rescue this pre-axial digit duplication and the cardiovascular defect. However,

despite the presence of 50% of *Msx1* can rescue the cardiovascular phenotype in *Pax9*$^{-/-}$ embryos and neonates, it does not affect the pre-axial digit duplication, possibly indicating that the rescue of the *Pax9*-null phenotype by *Msx1* is dosage-dependent.

Due to the limitations associated with the work of Ogawa *et al.* (2005) mentioned in section 4.3.4, a Bimolecular Fluorescence Complementation (BiFCO) assay was performed to overcome the lack of an *in vivo* assay. The results show a direct interaction between *Pax9* and *Msx1* transcription factors at the protein level in living cells. However, this does not mean that they do interact under normal circumstances because they are not expressed in the same domain within the pharyngeal arches; *Pax9* is expressed in the pharyngeal endoderm while *Msx1* is expressed in the NCC (Chen *et al*., 2007; Ishii *et al.*, 2005).

All these data together led to the suggestion of two possible theories: *Pax9* and *Msx1* transcription factors could work through a common target present in the pharyngeal arches or even in neural crest cells, which will lead to a non-cell autonomous interaction between these two genes. Alternatively, *Pax9* and *Msx1* transcription factors could work independently and the overall result affects the formation of the aortic arch. Before testing either of these theories, the modified aortic arch was dissected and analysed in detail, to check if it has the ability to work as efficiently as the normal aortic arch.

5 IDENTIFYING THE CAUSE OF DEATH IN *Pax9*$^{-/-}$;*Msx1*$^{+/-}$ NEONATES

5.1 INTRODUCTION

Pax9$^{-/-}$;*Msx1*$^{+/-}$ neonates die shortly after birth despite approximately 75% having what appears to be an intact systemic circulation provided by either a cervical origin of the aortic arch coupled with the persisting carotid duct or normal aortic arch similar to the wildtype neonates. However, these mutants are born with an absent thymus or a very small thymus misplaced high in the pharynx. Since they are born in individually ventilated cages which give the mice a high degree of protection from allergens, these mice can theoretically live 3-5 days past the neonatal period without a thymus. Indeed, the athymic nude mouse that used as a model to study immunity and the pharmacological treatment of human tumours, is unable to produce T cells, and is therefore immunodeficient. However, this mouse can live from six months up to one year without problems in a pathogen free environment (McDermott-Lancaster *et al*., 1987; Pelleitier and Montplaisir, 1975). This could suggest that athymic *Pax9*$^{-/-}$;*Msx1*$^{+/-}$ neonates with an intact circulatory system could in theory survive for a few days after birth in our close cage system.

Pax9$^{-/-}$;*Msx1*$^{+/-}$ mice, however, are born with a cleft palate which could be the cause of death as this has been implicated in the failure of *Pax9*-null pups to survive the post-natal period (Peters *et al.*, 1998). The cleft palate leads to respiratory insufficiency resulting in a bloated abdomen and air bubbles are seen in the gut (Peters *et al*., 1998). Figure 5-1 summarises the phenotypes of *Pax9*$^{-/-}$;*Msx1*$^{+/-}$ neonates at P0.

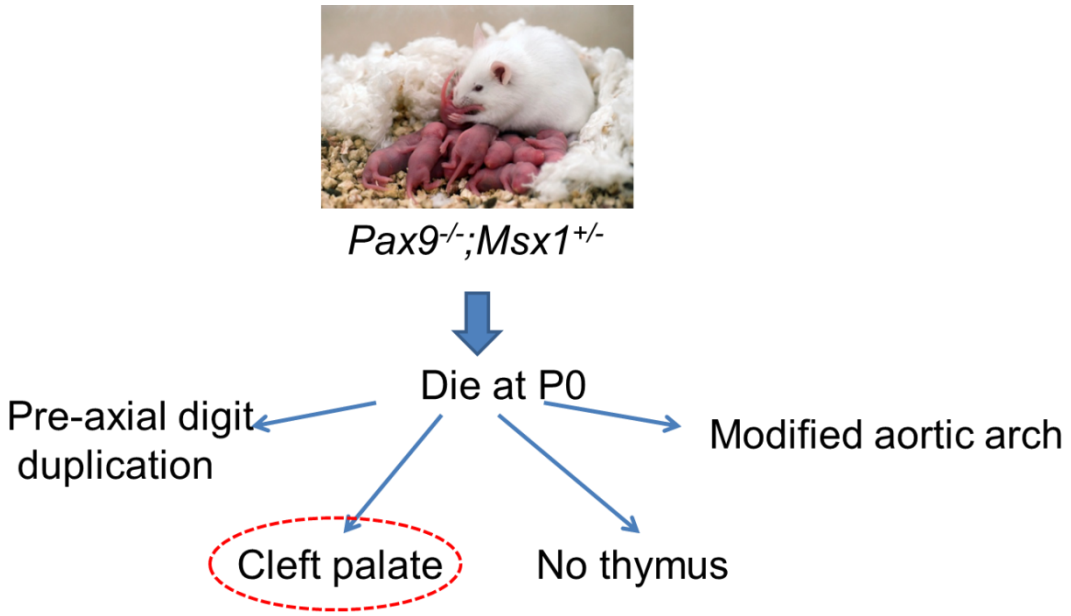

Figure 5-1: The main phenotypes for *Pax9*$^{-/-}$;*Msx1*$^{+/-}$ neonates at P0.
Pax9$^{-/-}$;*Msx1*$^{+/-}$ neonates are born with pre-axial digit duplication which is a characteristic phenotype for *Pax9*-null embryos, but this phenotype is compatible with life. At the same time, these neonates suffer from a cleft palate, which causes respiratory insufficiency and is not compatible with life. *Pax9*$^{-/-}$;*Msx1*$^{+/-}$ neonates also suffer from thymus defects but this can be tolerated for several days in ventilated cages. Finally *Pax9*$^{-/-}$;*Msx1*$^{+/-}$ neonates are born with a modified aortic arch that appears to be compatible with life as it is expected to provide an intact systemic circulation.

During mid-embryogenesis, *Pax9* expression is restricted to the pharyngeal endoderm, but it is later expressed in the neural crest derived mesenchyme mainly in the craniofacial region (Peters *et al.*, 1998). In an attempt to prevent the *Pax9* phenotype including the cleft palate, a conditional deletion approach was adopted to selectively delete *Pax9* from the pharyngeal endoderm, but leave expression in the neural crest derived mesenchyme intact.

5.2 AIMS OF CHAPTER

In this chapter, we aimed to delete *Pax9* from the pharyngeal endoderm, but retain expression within the neural crest derived mesenchyme to allow the palate to form normally and to also replicate the *Pax9*-null cardiovascular phenotype. This would therefore allow analysis of whether the observed modified aortic arch phenotype was capable of supporting life in *Pax9*$^{-/-}$;*Msx1*$^{+/-}$ mice. In order to do this, *Isl1cre* transgenic mice were employed (Yang *et al*., 2006). *Isl1* expressing progenitors contribute to the outflow tract, right ventricle and the right atria as well as a small

proportion of cells within the left ventricle and atria, and this domain of expression is referred to as the second heart field (Cai *et al*., 2003; Kelly and Buckingham, 2002). Importantly, however, *Isl1cre* is also active in the pharyngeal endoderm at E9.5, the same time as *Pax9* as expressed (Figure 5-2). This means that *Isl1cre* mice can be used to conditionally delete *Pax9* from the pharyngeal endoderm.

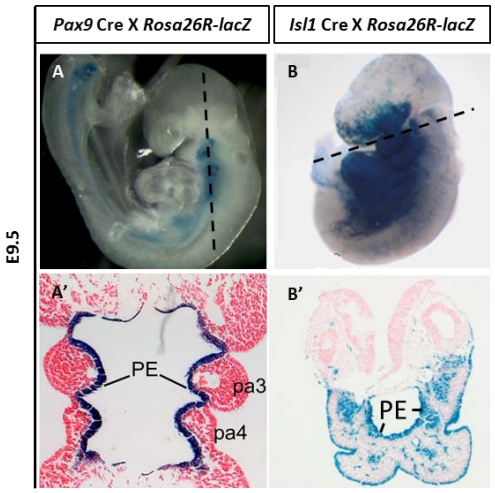

Figure 5-2: Overlapping expression of *Pax9cre* and *Isl1cre* activity.
Pax9cre and *Islcre* mice were crossed to *Rosa26r-LacZ* reporter mice and E9.5 embryos stained with X-Gal and then sectioned. (**A**) X-gal staining of *LacZ* expression in a *Pax9cre;R26R-lacZ* embryo. (**B**) X-gal staining of *LacZ* expression in an *Isl1cre;R26R-lacZ* embryo. The pharyngeal endoderm in both embryos shows lacZ activity indicating that each gene is expressed in this tissue.

5.3 RESULTS

5.3.1 CONDITIONAL DELETION OF *Pax9* FROM THE PHARYNGEAL ENDODERM USING *Isl1cre*

Isl1cre was used to delete *Pax9* from the pharyngeal endoderm without affecting the expression in the neural crest derived mesenchyme. The *Isl1cre* transgenic mouse was generated by knocking the *Cre* gene into the endogenous *Isl1* ATG after the Isl1 promoter (Yang *et al.*, 2006). The *Isl1cre* mouse was used in conjunction with a floxed allele of *Pax9*. The *Pax9*^{flox} allele mouse (generously provided by Dr. Heiko Peters) was generated by removing the neo cassette from the *Pax9*^{neo} mouse using FLP- mediated recombination, leaving behind two loxP sites flanking exon 1 and exon 2 (Kist *et al.*, 2007) (Figure 3-5).

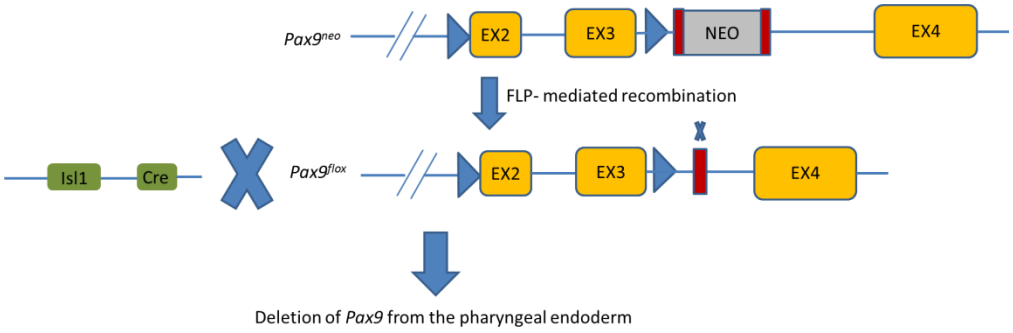

Figure 5-3: Schematic of the *Pax9*^{flox} allele.
The Neo cassette of the *Pax9*^{neo} mouse was removed by FLP-mediated recombination resulting in a *Pax9*^{flox} mouse. A *Pax9*^{flox} mouse was crossed with an *Isl1cre* mouse to delete *Pax9* from the pharyngeal endoderm.

Isl1cre is active in the pharyngeal endoderm (Cai *et al.*, 2003) and was therefore used to delete *Pax9* specifically from this tissue without affecting expression in the neural crest derived mesenchyme (Figure 5-3). *Isl1cre* and *Pax9*$^{+/-}$ mice were intercrossed to generate *Pax9*$^{+/-}$;*Is1cre* stud males, and *Pax9*$^{+/flox}$ (hereafter referred to as *Pax9*$^{+/f}$) mice were intercrossed to produce *Pax9*$^{f/f}$ females (Figure 5-4). Finally, *Pax9*$^{f/f}$ females were crossed to *Pax9*$^{+/-}$;*Isl1cre* males to generate *Pax9*$^{+/f}$;*Isl1cre* (control) or *Pax9*$^{f/f}$;*Isl1cre* (*Pax9* deleted from the pharyngeal endoderm; *Pax9*$^{\Delta PE}$) embryos.

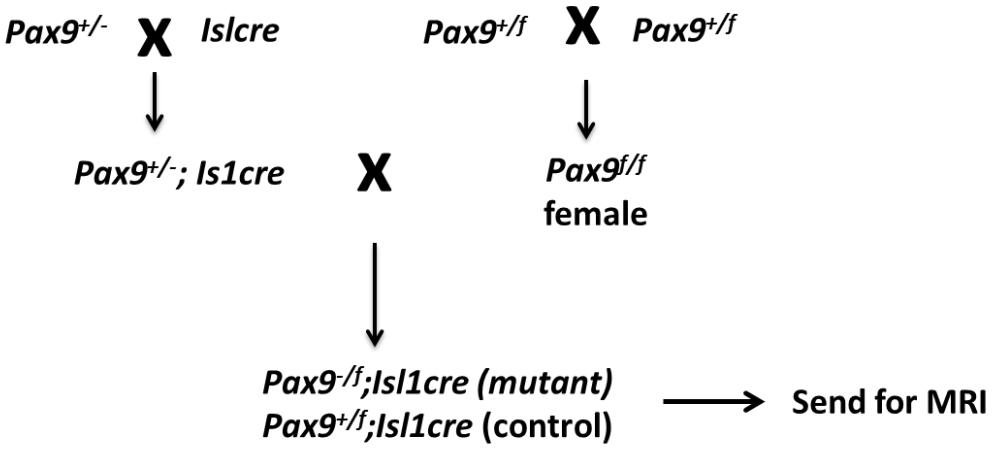

Figure 5-4: Breeding strategy for generating *Pax9*$^{+/f}$;*Isl1cre* and *Pax9*$^{-/f}$;*Isl1cre* embryos for analysis.
Pax9$^{+/-}$ mice were crossed to *Isl1cre* mice to produce *Pax9*$^{+/-}$;*Is1cre* stud males. *Pax9*$^{+/f}$ mice were intercrossed to produce *Pax9*$^{f/f}$ females. *Pax9*$^{+/f}$;*Isl1cre* and *Pax9*$^{f/f}$ mice were crossed to generate *Pax9*$^{-/f}$;*Isl1cre* embryos for analysis along with *Pax9*$^{+/f}$;*Isl1cre* controls.

Nine *Pax9*$^{\Delta PE}$ mutant embryos were collected at E15.5 for MRI analysis, and 3D models of the heart and great arteries were built from the MRI data sets using Amira software. Analysis showed that 100% (9/9) of *Pax9*$^{\Delta PE}$ embryos had cardiovascular defects indicating that the conditional deletion of *Pax9* from the pharyngeal endoderm recapitulated the global *Pax9*-null cardiovascular phenotype (Figure 5-5, Table 5-1).

Importantly, MRI analysis also revealed that 100% (9/9) of *Pax9*$^{\Delta PE}$ embryos had a fully formed palate identical to that seen in controls (Figure 5-6). The MRI embryos were then processed for histological analysis which was used to validate the MRI results. These data confirmed that deletion of *Pax9* from the pharyngeal endoderm using *Is1cre* recapitulates the *Pax9*$^{-/-}$ cardiovascular phenotype but does not impair palate formation.

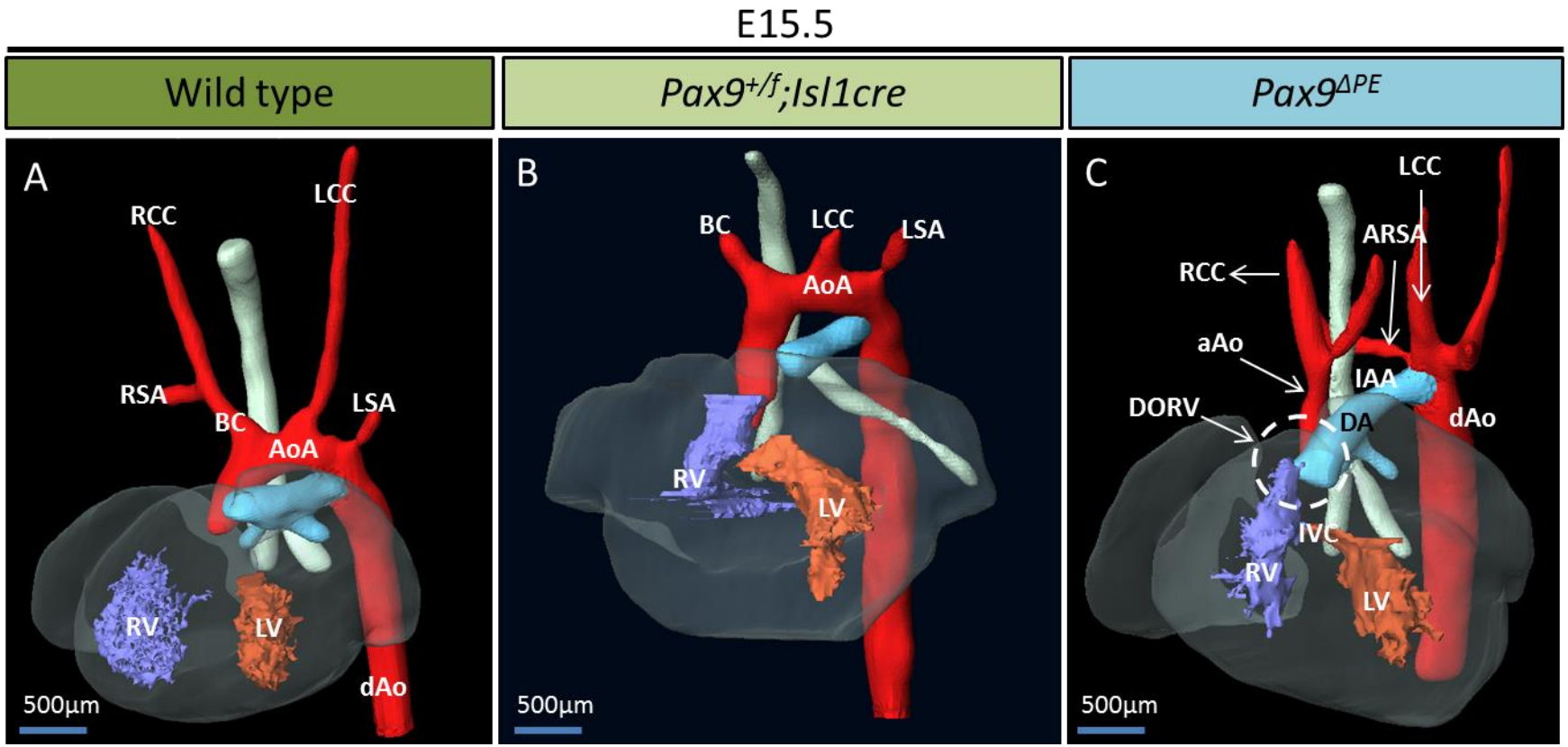

Figure 5-5: Cardiovascular phenotypes of E15.5 *Pax9*$^{-/f}$*;Isl1cre* embryos.
(A-B) Control wild type and *Pax9*$^{+/f}$*;Isl1cre* embryos presented with normal cardiovascular anatomy, whereas *Pax9*$^{-/f}$*;Isl1cre* embryos (**C)** presented with cardiovascular defects including interrupted aortic arch (IAA), aberrant right subclavian artery (ARSA), and double-outlet right ventricle (DORV) interventricular communication (IVC). This showed that deletion of *Pax9* from the pharyngeal endoderm recapitulated the cardiovascular defects of the *Pax9*$^{-/-}$ embryos. Ao, aorta; dAo, dorsal aorta; RV, right ventricle; LV, left ventricle; RSA, right subclavian artery; RCC, right common carotid artery; LSA, left subclavian artery; LCC, left common carotid artery. Scale, 500µm.

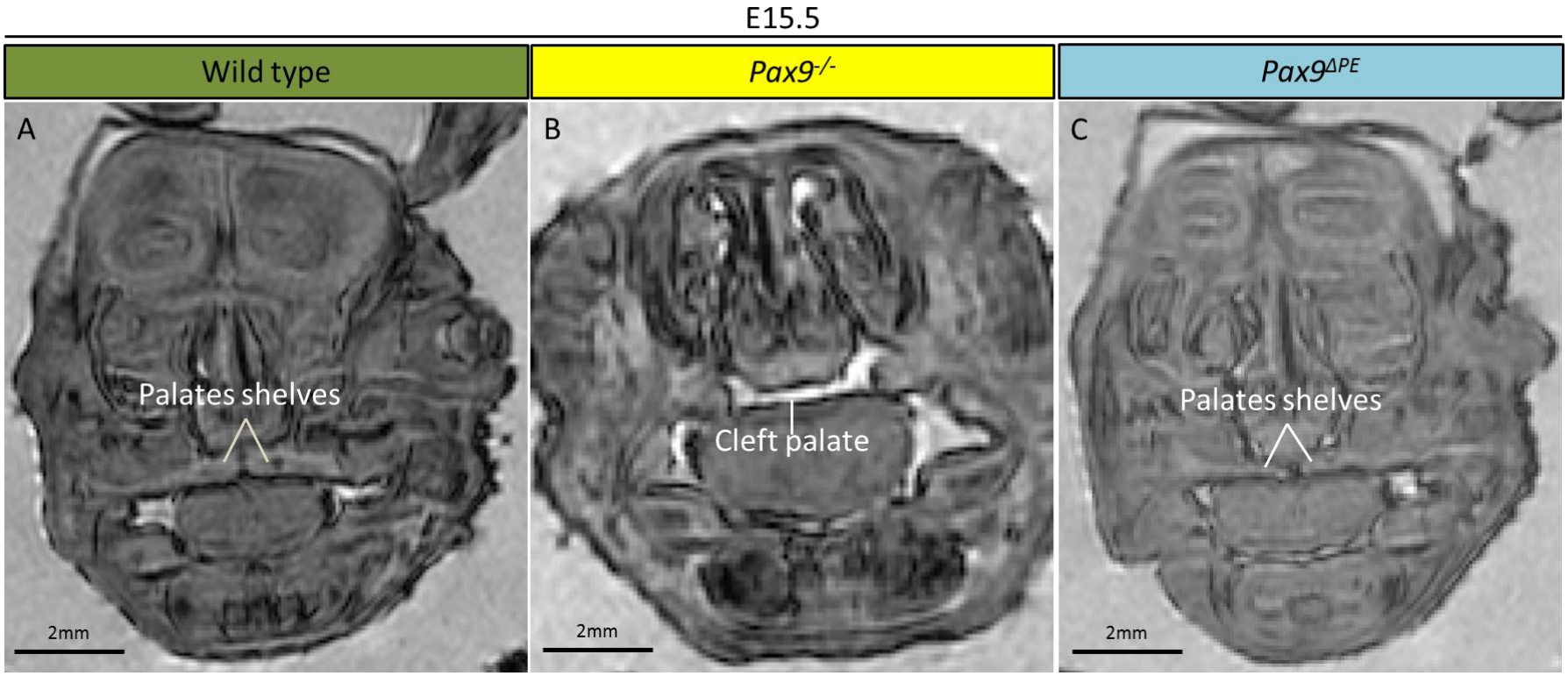

Figure 5-6: Cleft palate formation in *Pax9*$^{-/f}$;*Isl1cre* embryos.
(**A**) Normal fusion of the palatal shelves was observed in all wild type embryos. (**B**) A cleft palate was clearly seen in *Pax9*$^{-/-}$ embryos. (**C**) *Pax9*$^{-/f}$;*Isl1cre* mutant embryos had an intact palate.

Table 5-1: Phenotype of *Pax9*$^{-/f;}$*Isl1cre* mutants at E15.5.

	Phenotypes							
	Pre-axial digit duplication	**Cleft palate**	**Absent thymus**	**VSD**	**DORV+ IVC**	**IAA**	**ARSA**	**Abnormal carotids**
Pax9*$^{+/f}$;*Isl1cre	0	0	0	0	0	0	0	0
N=3	0%	0%	0%	0%	0%	0%	0%	0%
Pax9*$^{-/f}$;*Isl1cre	9	0	9	1	6	9	7	5
N=9	100%	0%	100%	11%	67%	100%	78%	56%

IAA, interruption of the aortic arch; DORV, double outlet right ventricle; IVC, interventricular communication; VSD, ventricular septum defect.

5.3.2 CONDITIONAL DELETION OF *Pax9* FROM THE PHARYNGEAL ENDODERM OF *Pax9*$^{-/-}$;*Msx1*$^{+/-}$ EMBRYOS USING *Isl1cre.*

Having confirmed that *Isl1cre* mediated deletion of *Pax9* recapitulates the *Pax9*-null cardiovascular defects and maintains palate formation, the *Msx1*-null allele was then crossed in to create *Pax9*$^{-/f}$;*Msx1*$^{+/-}$ females, which were toothless. These females were crossed with *Pax9*$^{+/f}$;*Isl1cre* males to generate embryos for analysis. However, due to an unexpected recombination event, the floxed allele in these *Pax9* males was recombined and transferred through the germ line. This resulted in stud males with the genotype *Pax9*$^{rec/f}$;*Isl1cre* (Figure 5-8) where "rec" denotes the recombined allele (Figure 5-7).

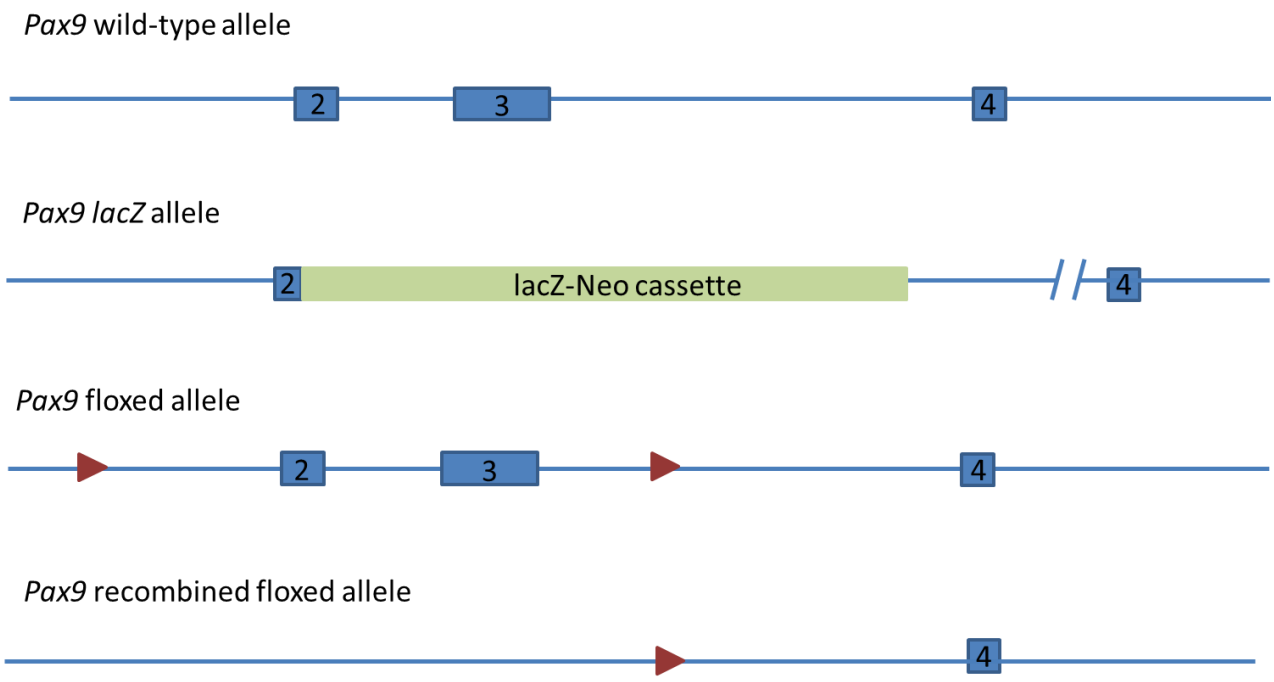

Figure 5-7: Schematic of the *Pax9* alleles in this part of the study
The figure shows the *Pax9* wildtype allele, the *Pax9 lacZ* allele, the *Pax9* floxed allele and the recombined *Pax9* floxed allele, which served as a null allele as two essential coding exons had been removed.

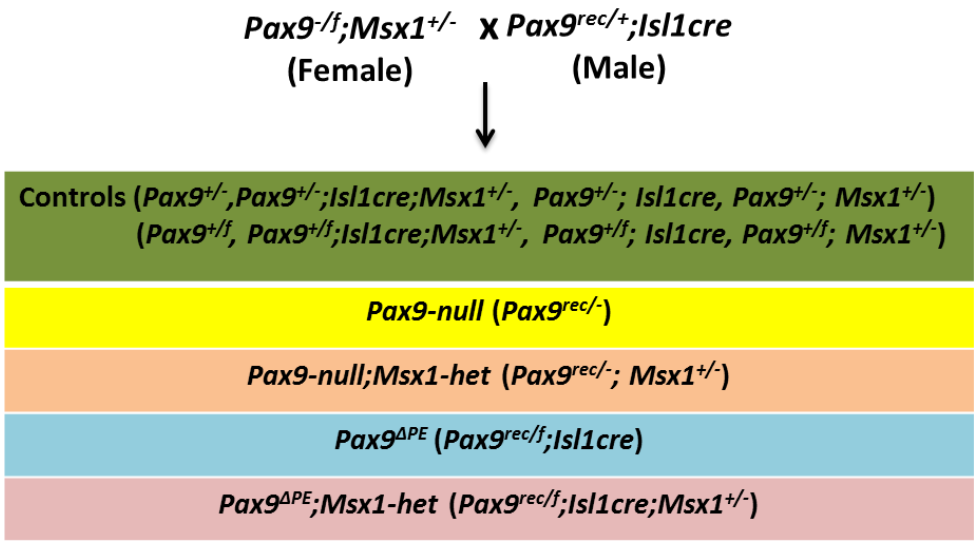

Figure 5-8: Breeding strategy for generating *Pax9*$^{\Delta PE}$; *Msx1*$^{+/-}$ mutant neonates.
A *Pax9*$^{rec/f;}$*Isl1cre* male mouse which had a *Pax9* recombined floxed allele was crossed to a *Pax9*$^{-/f}$;*Msx1*+/- female to generate *Pax9*$^{\Delta PE}$;*Msx1*$^{+/-}$ mutant neonates with *Pax9* deleted from the pharyngeal endoderm. All possible genotypes are shown.

Neonates were observed from the day of birth. All dead neonates were collected and examined by direct visualisation using a dissection microscope (Table 5-2).

The control neonates (n = 5) had a normal palate that separated the oral cavity from the nasal cavity, and they also had no cardiovascular malformations (Figure 5-9 A-A''). *Pax9*$^{-/-}$ neonates (n = 5), however, displayed a cleft palate and several abnormalities with the great arteries (Figure 5-9 B-B''). Analysing *Pax9*$^{-/-}$;*Msx1*$^{+/-}$ (n = 2) at P0 indicated that these neonates had a cleft palate, but had either a normal or cervical aortic arch accompanied with either normal or cervical RSA, which was expected (Figure 5-9 C-C'').

Pax9$^{\Delta PE}$ (n = 1), showed correct fusion of the palatal shelves similar to the wildtype neonates. At the same time, they displayed typical *Pax9*$^{-/-}$ cardiovascular defects including IAA, ARSA, and carotid defects (Figure 5-9 D-D''). Despite only one *Pax9*$^{\Delta PE}$ embryo identified from this breeding, the phenotype was consistent with the previous nine *Pax9*$^{\Delta PE}$ embryos examined by MRI at E15.5.

Pax9$^{f/f}$;*Isl1cre*;*Msx1*$^{+/-}$ (*Pax9*$^{\Delta PE}$;*Msx1*$^{+/-}$) neonates (n = 8) presented with a complete fusion of the palatal shelves. They also displayed a normal or cervical aortic arch suggestive of an intact and potentially functional systemic circulation (Figure 5-9 E-E'').

Both *Pax9*$^{\Delta PE}$ and *Pax9*$^{\Delta PE}$;*Msx1*$^{+/-}$ neonates also presented with a pre-axial digit duplication. Lineage studies have revealed that *Isl1* progenitors contribute to a majority of hind limb cells (Yang *et al*., 2006), which means that *Isl1* is required for hind limb development. Using *Isl1cre* to delete *Pax9* will therefore not only delete *Pax9* from the pharyngeal endoderm, but also from the hind limb, which explains why *Pax9*$^{\Delta PE}$ neonates presented with pre-axial digit duplication.

Despite having an apparently intact circulatory system, *Pax9*$^{\Delta PE}$;*Msx1*$^{+/-}$ neonates, however, were all found dead on the day of birth. It was predicted that a normal or cervical aortic arch coupled with a normal palate would be sufficient for the neonates to survive the neonatal period and closure of the arterial duct. Based on this assumption, it was expected that these pups would live to at least 3 to 5 days.

Both the normal and the cervical aortic arches appeared to be supporting the systemic circulation since they were always full of blood (Figure 5-9). The hearts of *Pax9*$^{\Delta PE}$;*Msx1*$^{+/-}$ pups were collected, sectioned and stained using H & E to check their morphology. The histological sections showed no structural defects in the interventricular septum or outflow tract (8/8). Also these neonates presented with a normal outflow tract valve with three leaflets which indicated that these mutants had normal intra-cardiac development and therefore the cause of death of these neonates was not thought to be due to cardiac anomalies (Figure 5-10). In contrast, one *Pax9*$^{-/-}$ neonate suffered from isolated VSD (1/5) and two neonates had VSD associated with overriding aorta (2/5). However, all *Pax9*$^{-/-}$ (5/5) neonates had normal aortic valve leaflets and none of them suffered from bicuspid aortic valve.

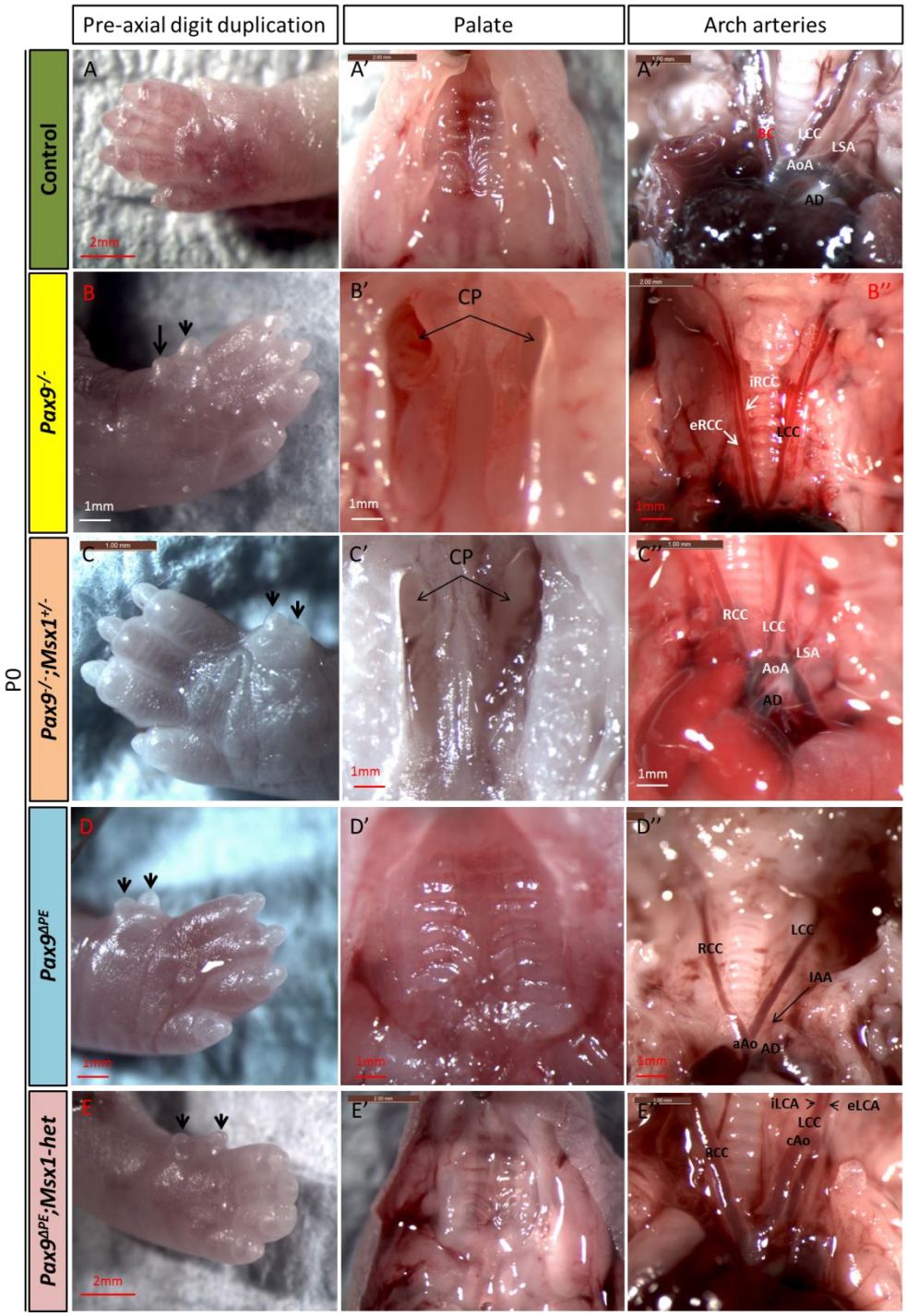

Figure 5-9: Phenotypes observed in *Pax9;Is1cre;Msx1* mutant and control mice.
Neonates at P0 were examined for limb, palate and cardiovascular phenotypes. (**A**) control neonate with a normal HL digit, a normal palate (**A'**) and a normal cardiovascular system (**A''**). (**B**) *Pax9*$^{-/-}$ neonate with a pre-axial digit duplication (*two arrows*), cleft palate (CP; **B'**), and abnormal arch arteries (**B''**). (**C**) *Pax9*$^{-/-}$;*Msx1*$^{+/-}$ neonate with a pre-axial digit duplication (*two arrows*), cleft palate (CP; **C'**), and normal arch arteries (**C''**). (**D**) Neonate with *Pax9* conditionally deleted from the pharyngeal endoderm with *Isl1cre* had a pre-axial digit duplication (*two arrows*), a normal palate (**D'**), but abnormal arch arteries (**D''**). (**E**) *Pax9*$^{\Delta PE}$;*Msx1*$^{+/-}$ neonates showed a pre-axial digit duplication (*two arrows*), a normal palate (**E'**), and a presumptive functional systemic circulation (**E''**).
Ao, aorta; dAo, dorsal aorta; cAo, cervical aorta; IAA, interruption of aortic arch; AD: arterial duct; RSA, right subclavian artery; RCC, right common carotid artery; LSA, left subclavian artery; LCC, left common carotid artery; eLCA, external left carotid artery ; iLCA; internal left carotid artery. Scale bars are indicated on each panel.

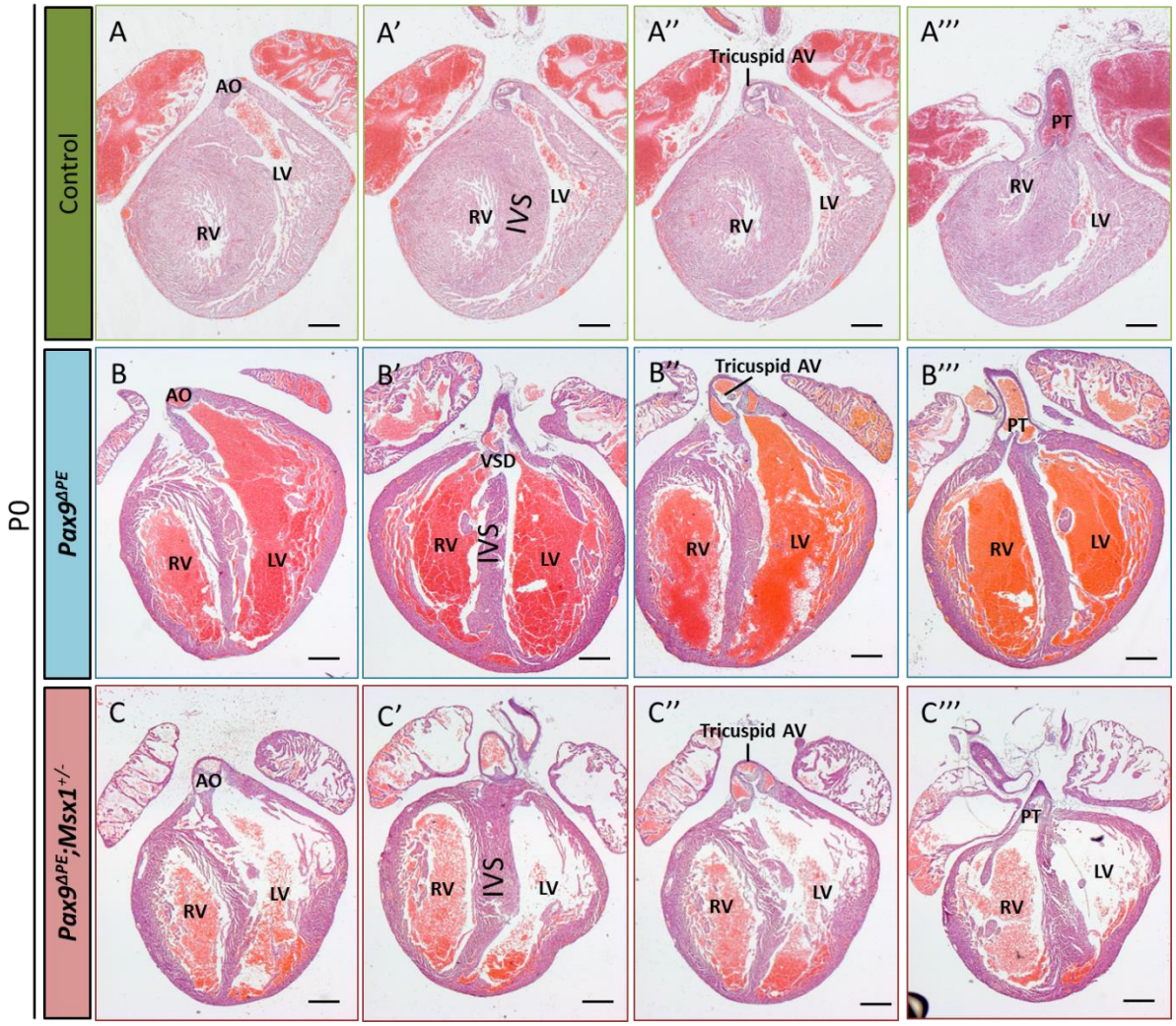

Figure 5-10: Histological analysis of *Pax9*$^{\Delta PE}$ and *Pax9*$^{\Delta PE}$;*Msx1*$^{+/-}$ neonatal hearts at P0.
A series of sections of the four-chambered view of the heart are shown, stained with H&E. (**A**) control heart with normal interventricular septum (IVS), tricuspid aortic valve (AV). The aorta (AO) comes off the left ventricle (LV), while the pulmonary trunk (PT) arises from the right ventricle (RV). (**B**) *Pax9*$^{\Delta PE}$ neonate with a ventricular septal defect (VSD), and an overriding aorta. None of the *Pax9* mutants had a bicuspid aortic valve. (**C**) *Pax9*$^{\Delta PE}$;*Msx1*$^{+/-}$ neonate heart with a normal phenotype. Scale, 50μm.

Table 5-2: Phenotype of *Pax9*$^{\Delta PE}$; *Msx1*$^{+/-}$ mutants and control at P0.

Genotype	N	Palate	Aorta	RSA
control	5	Normal palate	Normal	Normal
Pax9-null	5	Cleft palate	IAA	ARSA
Pax9-null;Msx1-het	2	Cleft palate	Normal/cAo	Normal/cRSA
***Pax9*$^{\Delta PE}$**	1	Normal palate	IAA	ARSA
Pax9*$^{\Delta PE}$*;Msx1-het	8	Normal palate	Normal/cAo	Normal/cRSA

It was predicted that loss of *Pax9* from the pharyngeal endoderm only, concomitant with haploinsufficiency of *Msx1*, would be sufficient to allow mutant pups to survive the neonatal period. However, they all died following birth despite having an apparently intact systemic circulation and a normal palate. As has already been published, loss of *Pax9* causes bone deformities, such as the pre-axial digit duplication and cleft palate. In addition to these previously reported defects, the absence of *Pax9* also causes malformation of the lesser and greater horns of the hyoid bone (Peters *et al.*, 1998). Therefore, the skeletal system in these neonates was investigated in detail using bone and cartilage staining to see if any phenotype here could explain the neonatal death.

5.3.3 INVESTIGATING THE SKELETON OF *Pax9*$^{-/-}$;*Msx1*$^{+/-}$ NEONATES

The study by Peters *et al.* (1998) demonstrated that *Pax9* deletion results in craniofacial and skeletal defects, including defects in the hyoid bone. Peters *et al.* (1998) reported a malformation in the greater and lesser horn of the hyoid bone, as well as a malformation in the thyroidal cartilage, in which the inferior horn that is attached to the cricoid cartilage is missing (Peters *et al.*, 1998). To investigate the hyoid bone in *Pax9*$^{\Delta PE}$;*Msx1*$^{+/-}$ mutants, neonates were collected at P0 and processed for bone and cartilage staining.

Alcian blue and alizarin red staining of the whole mouse neonate was employed. This method produces a red staining of the bone and blue staining of the cartilage, so that anomalies of both the cartilaginous and the bony skeleton can be examined.

Bone staining of *Pax9*$^{\Delta PE}$;*Msx1*$^{+/-}$ neonates revealed the presence of the extra fore limb digit, which was not obvious from gross inspection, unlike the extra hind limb digit. Instead of having one metacarpal bone to form the first digit, the mutant neonates appeared to have two separate bones, one that articulated to the styloid process of the radius bone while the second bone articulated normally to the trapezium bone. Each one of these two metacarpals continued to articulate to its own proximal phalanges bone, which joined at the distal phalanges region and formed what appeared to be a single digit of the forelimb (Figure 5-11, Figure 5-13 C'). In the hind limb there are two bones that form the first digit and, unlike the forelimb, these bones remain separated; one bone appeared to articulate to the medial malleolus while the second metatarsal bone appeared to articulate normally to the medial cuneiform bone (Figure 5-12,Figure 5-13 C''). These two bones remained separated to form a pre-axial digit in the hind limb of the mutant neonate. All of these phenotypes were also found in the *Pax9*$^{-/-}$ neonates (Figure 5-13 B-B''). Previous studies have shown that *Pax9*-null embryos form an additional mesenchyme in the anterior limb region, which later differentiates into a supernumerary digit (Peters *et al.*, 1998).

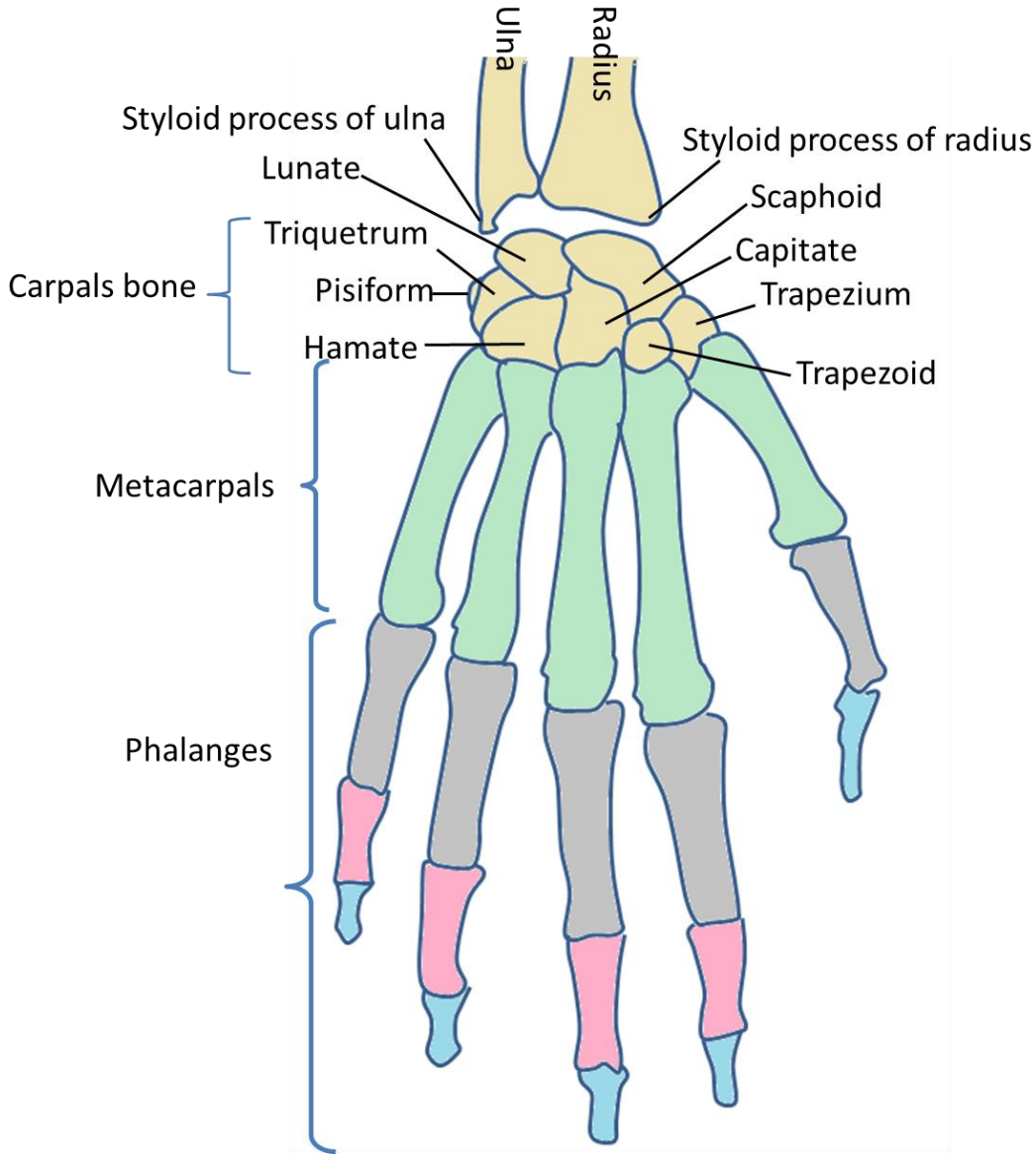

Figure 5-11: Schematic representation of the hand and the lower part of the arm.
The forearm contains two bones, the radius and the ulna, which extend in parallel from the elbow where they articulate with the humerus to the wrist where they articulate with the carpals. The radius is located laterally, nearer the thumb, and the ulna medially, nearer the little finger. The radius and the ulna have a styloid process at the distal end and are attachment sites for many muscles. The wrist consists eight small carpal bones that are firmly bound in two rows of four bones each. Proximally, the scaphoid and lunate articulate with the radius and ulna to form the wrist joint. In the distal row, all of the carpal bones articulate with the metacarpals.

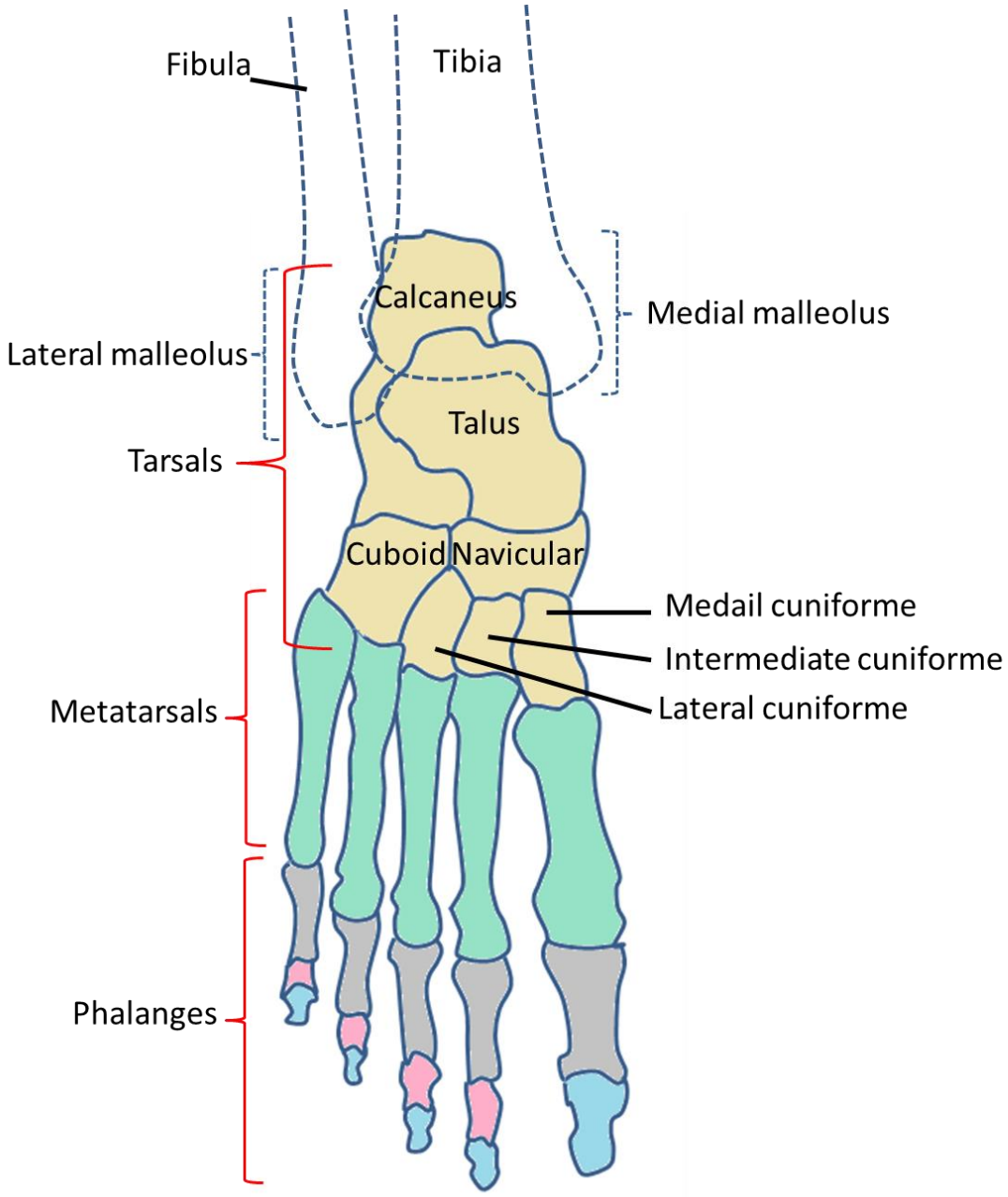

Figure 5-12: Schematic representation of the foot and the lower part of the leg.
The lower leg contains two bones. The tibia which is parallels and articulates with the tibia. The tarsals are the seven bones of the ankle, which transmits the weight of the body from the tibia and the fibula to the foot. The metatarsals are the five bones of the foot, while the phalanges are the 14 bones of the toes.

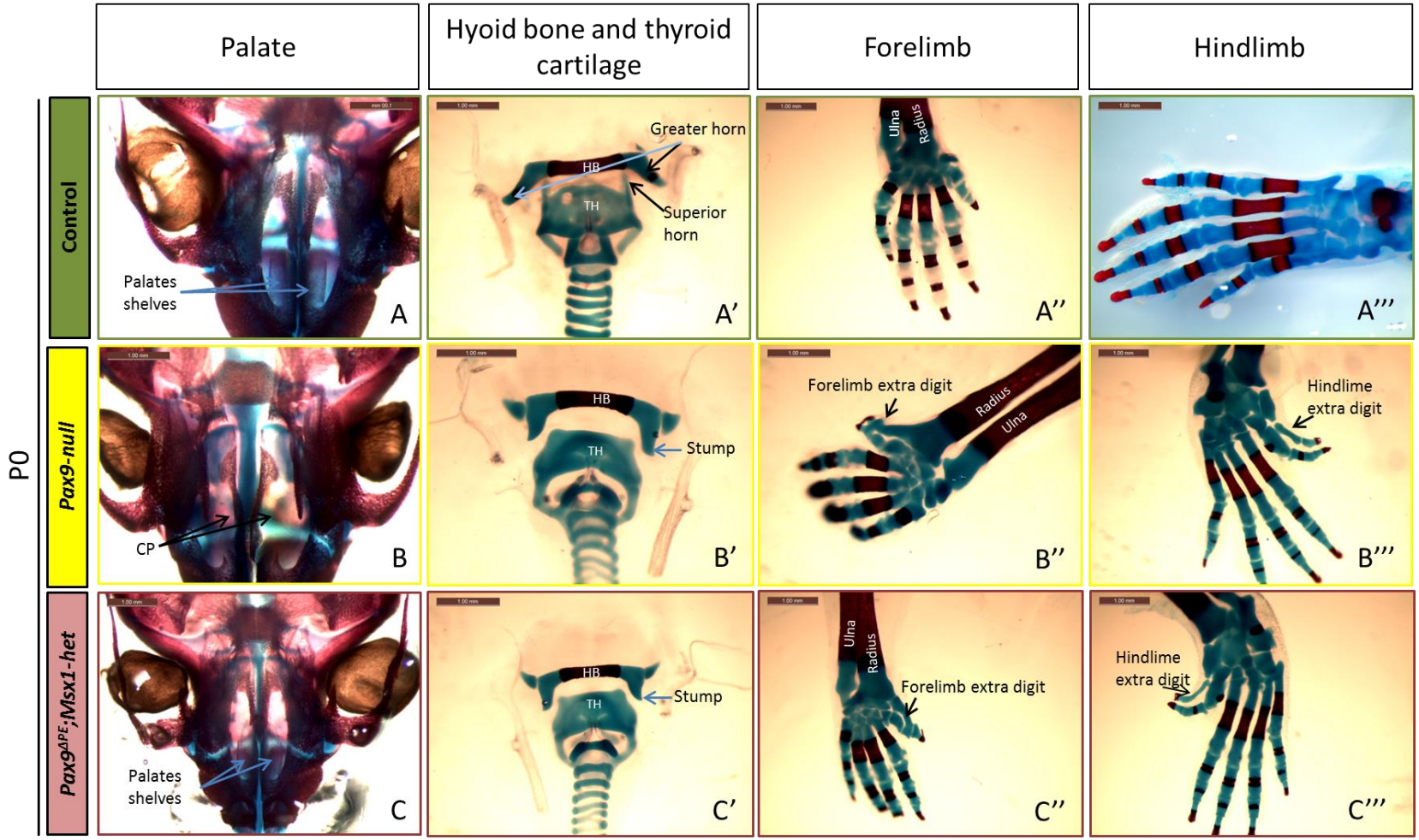

Figure 5-13: Bone deformities in *Pax9* mutant neonates.
Neonates at P0 were collected and processed for bone and cartilage staining. (**A**) Control neonate with normal palatal shelves, fore limb (**A''**) and hind limb (**A'''**). (**B**) *Pax9*$^{-/-}$ neonate with cleft palate (CP) and pre-axial digit duplications in the fore (**B''**) and hind limbs (**B'''**). (**C**) *Pax9*$^{\Delta PE}$;*Msx1*$^{+/-}$ neonate with a normal palate and pre-axial digit duplications in the fore (**C''**) and hind limbs (**C'''**).

Skeletal analysis revealed a striking shortening of the hyoid bone in the mutant neonates. The normal hyoid bone in the wildtype neonates had a horseshoe-shape, with an elongated and flat body, and two pairs of horn: the greater horn and the lesser horn. The greater horns projected backward from the outer borders of the body and connected the hyoid bone to the lateral thyrohyoid ligament (Figure 5-14). In addition, it provided a place of attachment for many muscles associated with the mouth's floor, as well as the larynx, pharynx, and epiglottis.

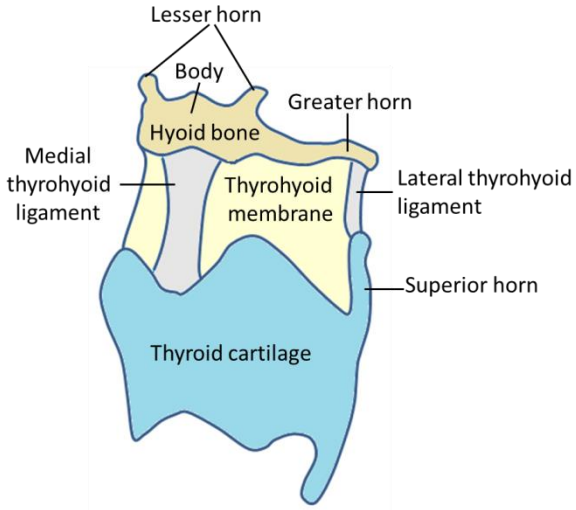

Figure 5-14: Schematic representation of the hyoid bone.
The hyoid is the only human bone that is attached to only muscles, not to another bone. Anatomically, the hyoid bone has three major parts, which are the body, and the greater and lesser horns. The greater horn of the hyoid bone attaches to the superior horn of the thyroid cartilage through the lateral thyrohyoid ligament.

In contrast, the hyoid bone of the mutant (both *Pax9*$^{-/-}$ and *Pax9*$^{\Delta PE}$;*Msx1*$^{+/-}$) neonates presented with deformities. The body of the hyoid bone was shorter compared to controls, and instead of the great horn a stump is present (Figure 5-16).

In order to normalise the measurements of the hyoid bone, and to allow direct comparisons between the control and mutant genotypes, the ulna bone was selected. The length of the ulna bone was measured in the wildtype, *Pax9*$^{-/-}$ and *Pax9*$^{\Delta PE}$;*Msx1*$^{+/-}$ neonates and was found to be not significantly different in length between the genotypes (Figure 5-15). All measurements were therefore divided by the length of the ulna to normalise data and to prevent any differences in neonate size from affecting the results.

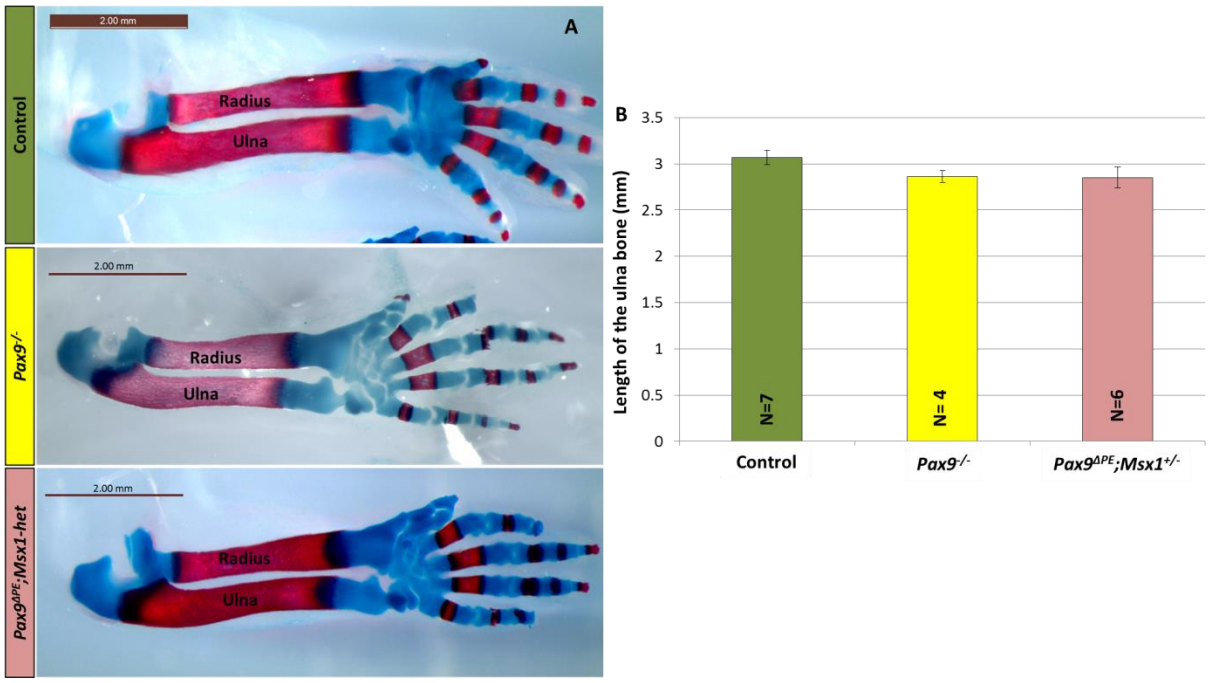

Figure 5-15: Direct measurement of the ulna bone in control and *Pax9;Msx1* mutants.
The stained skeletons of neonates at P0 were disarticulated. (**A**) Fore limbs of control (**top panel**), *Pax9*$^{-/-}$ (**middle**) and *Pax9*$^{\Delta PE}$;*Msx1*$^{+/-}$ (**bottom**) neonates. Scale, 2mm. (**B**) The length of the ulna was measured for each genotype. There is no significant difference in the length of the ulna bone between the wild type (WT) and the mutant neonates.

Statistical analysis revealed a significant decrease in the length of the body of the hyoid bone between the control neonates and *Pax9*$^{-/-}$ neonates (P=0.0260). There was also a significant decrease (P=0.00133) in the length of the hyoid bone between the control neonates and *Pax9*$^{\Delta PE}$;*Msx1*$^{+/-}$ neonates at P0. There was no significant difference (P=0.371) in the length of the body of the hyoid bone between *Pax9*$^{-/-}$ and *Pax9*$^{\Delta PE}$;*Msx1*$^{+/-}$ neonates (Figure 5-16 C).

The angle between the lesser horn of the hyoid bone and the body was measured, and analysis showed that the angle was significantly decreased (P<0.05) in the mutant (*Pax9*$^{-/-}$ and *Pax9*$^{\Delta PE}$;*Msx1*$^{+/-}$) neonates compared with the control neonates on both left and right sides. There was no significant difference in the angle between *Pax9*$^{-/-}$ and *Pax9*$^{\Delta PE}$;*Msx1*$^{+/-}$ neonates in either the left or the right side at P0 (Figure 5-17).

The hyoid bone has a unique embryonic origin from cranial neural crest unlike the more posterior axial and appendicular skeletons which are derived from mesoderm (Santagati and Rijli, 2003). Since *Isl1cre* was used to delete *Pax9* from the

pharyngeal endoderm without affecting the expression in the neural crest derived mesenchyme, we investigated the expression area of *Isl1cre* to check if it is expressed in the hyoid bone or not. In order to do this, *Isl1cre* male mice were crossed with eYFP females, the embryos where collected at E15.5 and processed for histology. Wax sections were immunostained using a GFP antibody which also cross-reacts with eYFP protein.

GFP immunofluorescent staining at E15.5 showed that *Isl1cre* is expressed in the hyoid bone but there was no expression in the hard palate (Figure 5-18). This result suggests that *Isl1cre* mice caused a conditional loss of *Pax9* from the hyoid bone and that the deformities in this bone might be a consequence of *Pax9* deletion. The lack of *Isl1cre* expression in the hard palate means that *Pax9* was not deleted from the neural crest derived mesenchyme.

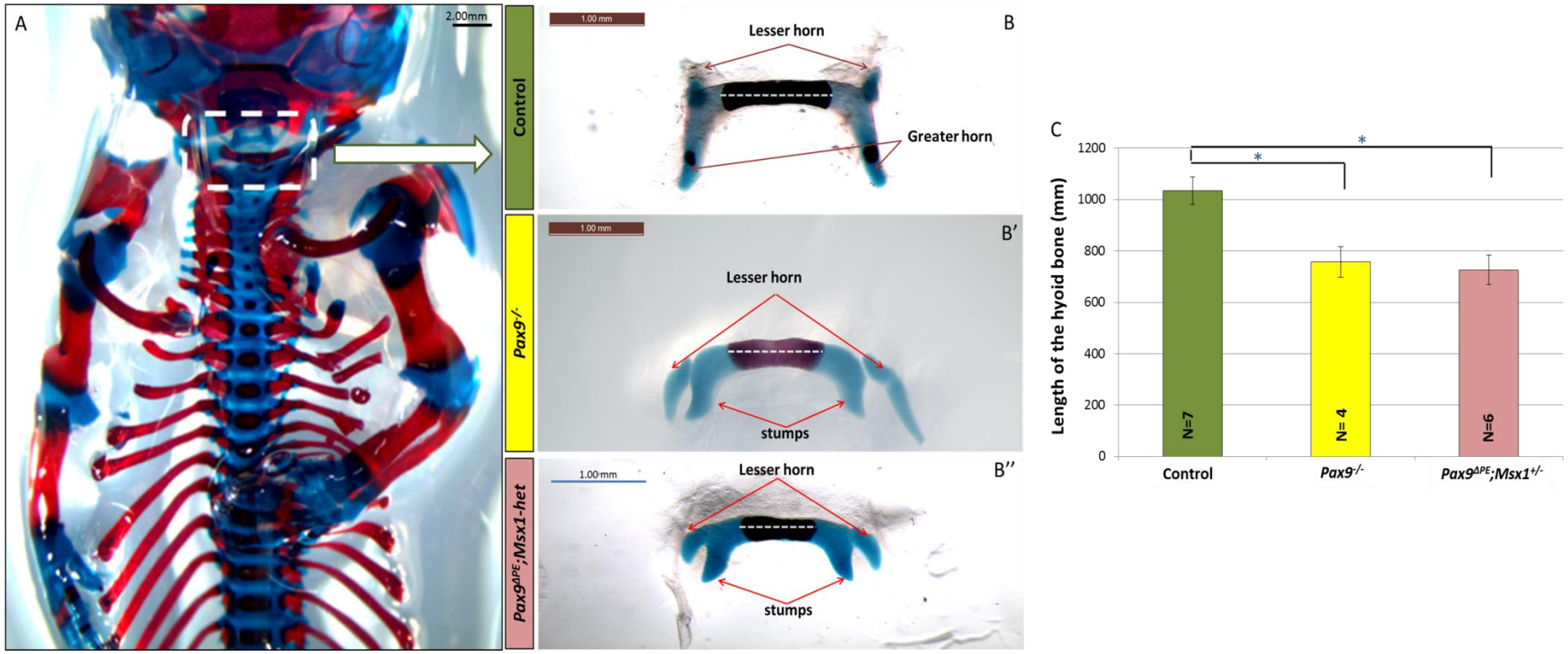

Figure 5-16: Analysis of the hyoid bone in control and *Pax9*$^{\Delta PE}$;*Msx1*$^{+/-}$ neonates.
(**A**) The skeletons of wild type and mutant neonates at P0 were stained with alizarin red (bone) and alcian blue (cartilage). The dashed box indicates the position of the hyoid bone just under the mandible in the neck area. Scale, 2mm. The skeletons were disarticulated to examine the hyoid bone in wild type (**B**), *Pax9*$^{-/-}$ (**B'**) and *Pax9*$^{\Delta PE}$;*Msx1*$^{+/-}$ (**B"**) neonates. In the wild type the hyoid bone has the lesser horn extending anteriorly and greater horn extending posteriorly. In *Pax9*$^{-/-}$ and *Pax9*$^{\Delta PE}$;*Msx1*$^{+/-}$ neonates, however, the hyoid bone appeared smaller, the lesser horn extended laterally and the greater horn was reduced in length. The white dashed line shows the length of the hyoid bone measured in both the control and the mutant neonates. Scale, 1mm. (**C**) There was a significant decrease in the length of the hyoid bone between the control and the mutant (*Pax9*$^{-/-}$ *and Pax9*$^{\Delta PE}$;*Msx1*$^{+/-}$) neonates. However, there is no difference in the length of the hyoid bone between *Pax9*$^{-/-}$ and *Pax9*$^{\Delta PE}$;*Msx1*$^{+/-}$ neonates. *t*-test; *p < 0.05.

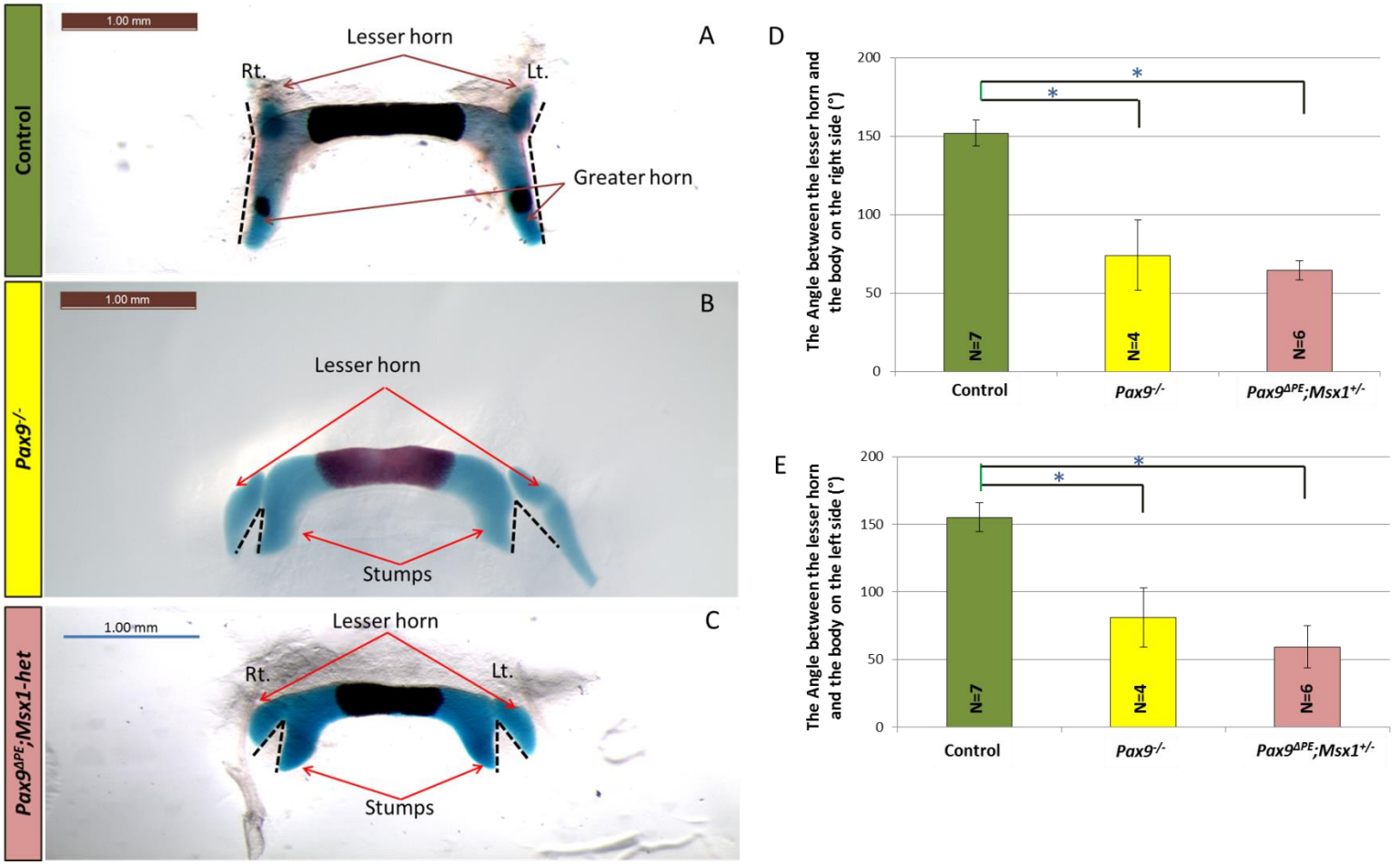

Figure 5-17: Further analysis of the hyoid bone in control and *Pax9*$^{\Delta PE}$;*Msx1*$^{+/-}$ neonates.
(**A-C**) Images of the disarticulated hyoid bones as seen in Figure 5-16. The black dashed line indicates the angle measured between the lesser and greater horn of the hyoid bone or the stumps that replaced the greater horn. Scale, 1mm. (**D, E**) Graphical representation of the measured angles on the right and left side respectively. There is a significant decrease in the angle between the body and the lesser horn of the hyoid bone between the control and the mutant (*Pax9*$^{-/-}$ *and Pax9*$^{\Delta PE}$;*Msx1*$^{+/-}$) neonates. There is no difference in this angle between *Pax9*$^{-/-}$ and *Pax9*$^{\Delta PE}$;*Msx1*$^{+/-}$ neonates. *t*-test; *p < 0.05.

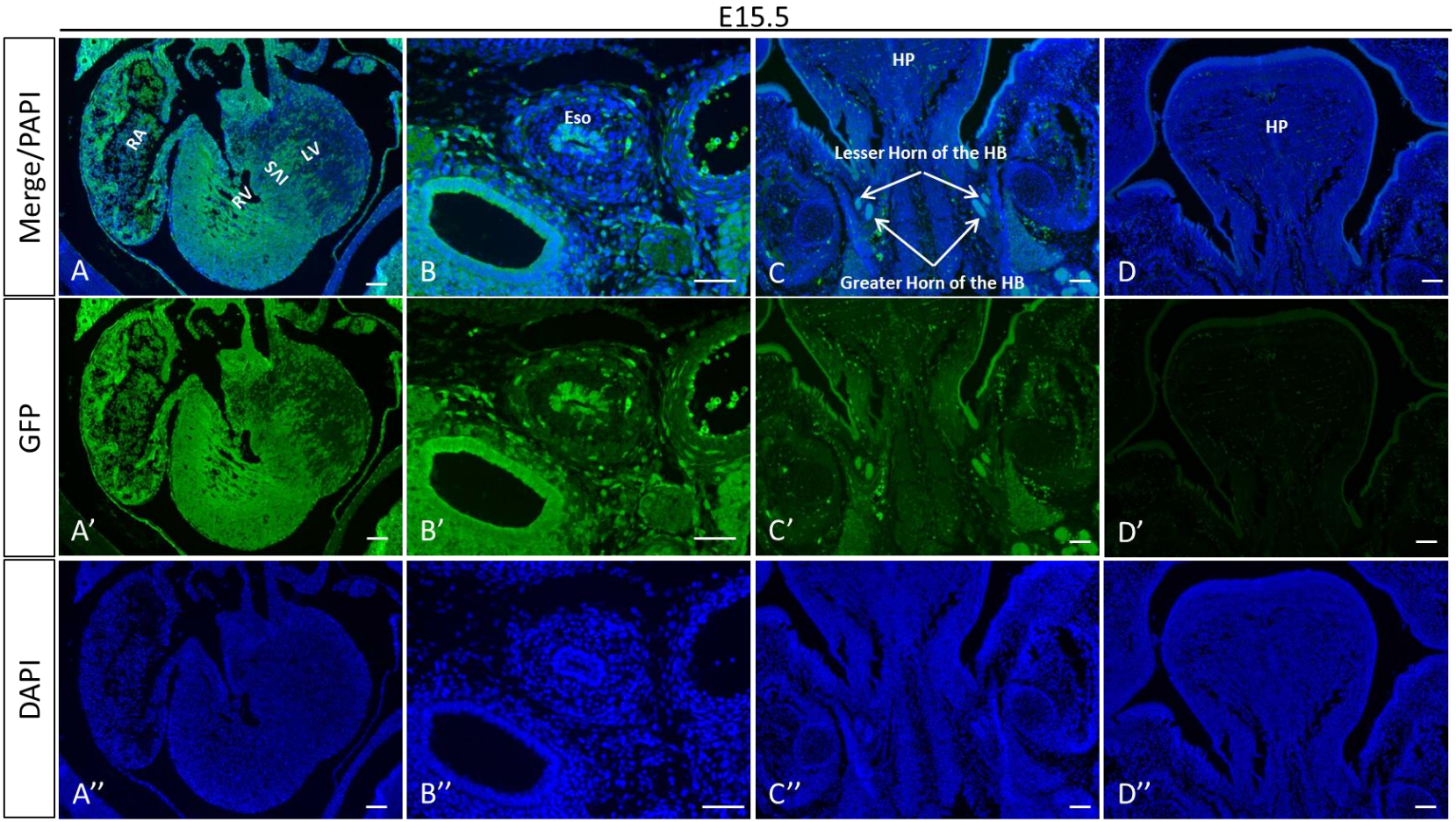

Figure 5-18: GFP immunostaining for *Isl1cre* expression.
Isl1cre mice were crossed with *R26R-eYFP* reporter mice and E15.5 embryos processed and sectioned for immunostaining with an antibody raised against GFP. The results demonstrate that *Isl1Cre* is expressed in the right ventricle (RV) (**A**). In addition, *Isl1cre* is expressed in the oesophagus (Eso; **B**) and in the hyoid bone (HB; **C**). There is no activity of *Isl1cre* in the hard palate (HP; **D**).
RA; right atria, IVS; interventricular septum. Scale, 50μm.

The hyoid bone appears to lack the greater horns. The greater horns of the hyoid bone bind to the thyroid cartilage through the lateral thyrohyoid ligament (Figure 5-14). Loss of *Pax9* causes thyroidal cartilage deformities, where the thyroid cartilage is broader and lacks the lateral processes normally connecting the thyroid and cricoid cartilages (Peters *et al*., 1998). Because of this reported phenotype, the thyroid cartilage in the *Pax9*$^{\Delta PE}$;*Msx1*$^{+/-}$ neonates was investigated.

The wild type neonates showed a normal thyroidal cartilage with two laminae that fused together anteriorly. The posterior border of each lamina was free and created projections called the superior and inferior horns (Figure 5-19 and shown in Figure 5-20).

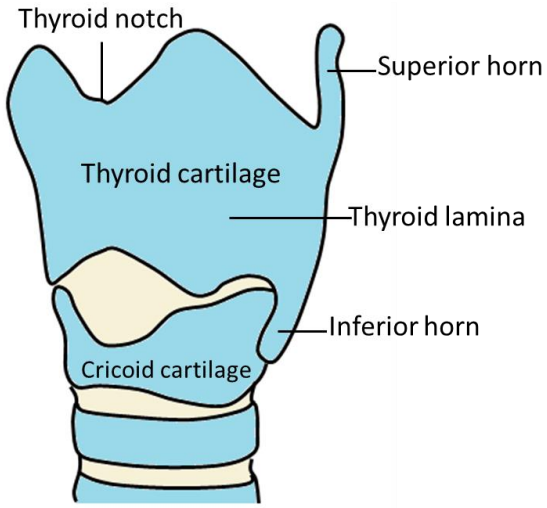

Figure 5-19: Schematic representation of the thyroid cartilage.
The thyroid cartilage is the largest of the laryngeal cartilages. It consists of two plates called laminae, which fuse anteriorly in their inferior two thirds, but are separated superiorly by the deep thyroid notch. The superior horn attaches with the hyoid bone through the lateral thyrohyoid ligament. The inferior horns of the thyroid cartilage articulate with the sides of the cricoid cartilage.

The thyroid cartilage appeared to be smaller in *Pax9*$^{-/-}$ and *Pax9*$^{\Delta PE}$;*Msx1*$^{+/-}$ neonates when compared to the control neonates, and they also lacked the superior horn (Figure 5-20). The inferior cornu of the thyroid cartilage was present and still connected the thyroid to the cricoid cartilage forming the cricothyroid joint; however, they appeared slightly shorter in the mutant neonates compared with the control. The length of the inferior horn of the thyroid cartilage was measured, and revealed a statistically significant decrease in the length between the control and the mutant (*Pax9*$^{-/-}$ and *Pax9*$^{\Delta PE}$;*Msx1*$^{+/-}$) neonates (Figure 5-20). There was no significant difference between the *Pax9*$^{-/-}$ and *Pax9*$^{\Delta PE}$;*Msx1*$^{+/-}$ neonates at P0 (Figure 5-20 E).

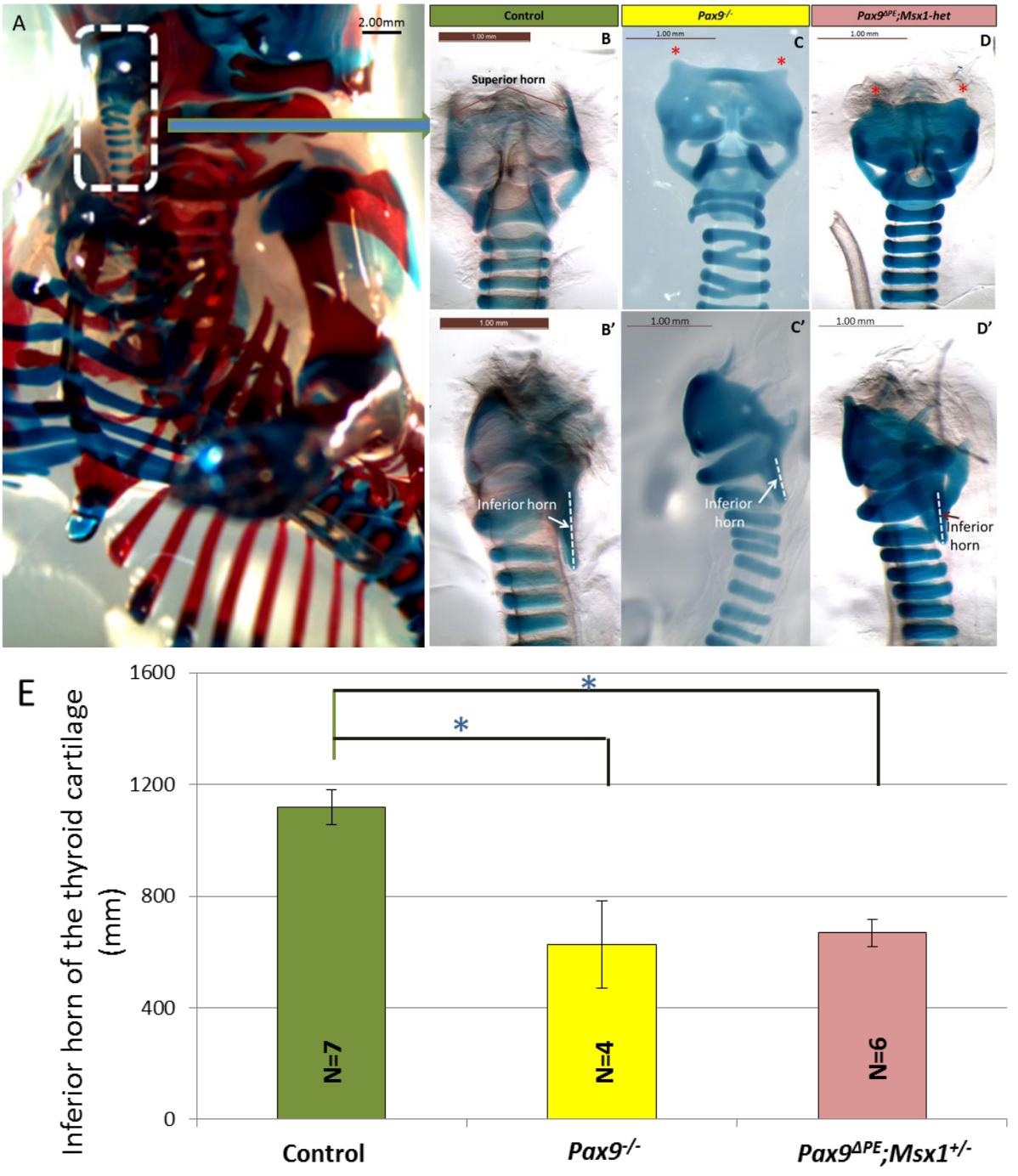

Figure 5-20: Analysis of the thyroid cartilage in control and *Pax9;Msx1* mutant neonates.

(**A**) The skeletons of control and mutant neonates at P0 were stained with alizarin red (bone) and alcian blue (cartilage). The dashed box indicates the position of the thyroid cartilage just under the hyoid bone within the anterior aspect of the neck. Scale, 2mm. The skeletons were disarticulated to examine the cartilage in control (**B**), *Pax9*$^{-/-}$ (**C**) and *Pax9*$^{\Delta PE}$;*Msx1*$^{+/-}$ (**D**) neonates. Scale, 1mm. The superior horn of the wild type thyroid cartilage pointed upward and inferior horn pointed downward. In *Pax9*$^{-/-}$ and *Pax9*$^{\Delta PE}$;*Msx1*$^{+/-}$ neonates the thyroid cartilage appears smaller and missed the superior horn (*red asterisks*). (**B' - D'**) The white dotted line indicates the length of the inferior horn of the thyroid cartilage which is presented graphically (**E**). There is a significant decrease in the length of the inferior horn between the control and the mutant (*Pax9*$^{-/-}$ and *Pax9*$^{\Delta PE}$;*Msx1*$^{+/-}$) neonates. There is no different in this length between *Pax9*$^{-/-}$ and *Pax9*$^{\Delta PE}$;*Msx1*$^{+/-}$ neonates. *t*-test; *p < 0.05.

5.4 DISCUSSION

This chapter aimed to investigate if the modified aortic arch found in *Pax9*$^{-/-}$;*Msx1*$^{+/-}$ mice is functional and can support life. The primary data collected suggested that this aortic arch which had a comparable size to the normal aortic arch should have the ability to transfer blood from the ascending aorta to the descending aorta since it is full of blood during the dissection.

Peters *et al.* (1998) suggested that the main cause of death for *Pax9*-null neonates was the cleft palate, which is an opening at the roof of the oral cavity that leads to a communication between the oral cavity and the respiratory cavity. In our study, *Isl1cre* was used to delete *Pax9* from the pharyngeal endoderm, which gave us a mouse that had all the *Pax9*-null cardiovascular phenotypes but without a cleft palate. At the same time *Msx1* heterozygosity gave these mice a modified aortic arch and prevented the IAA caused by loss of *Pax9*.

Pax9 $^{\Delta PE}$;*Msx1*$^{+/-}$ neonates had a normal palate and a modified aortic arch but were found dead immediately after birth which was not predicted by our hypothesis. Alizarin Red and Alcian Blue staining was used to stain the bone and the cartilage respectively and this revealed there was a severe deformity in the hyoid bone and the thyroid cartilage.

The hyoid bone provides protection for the fragile tissues of the larynx and pharynx. The greater horn of the hyoid bone attaches with the lateral thyrohyoid ligament which is a round elastic cord that passes between the tip of the superior horn of the thyroid cartilage and the extremity of the greater horn of the hyoid bone. The hyoid bone can be fractured if exposed to excessive force. Typically, a broken hyoid results from forced strangulation (Fineron *et al.*, 1995). Fracture of the hyoid bone can occur in the area between the greater horn and the body, which will result in the greater horn becoming loose. If this occurs then the hyoid bone would move backwards towards the trachea and the oesophagus which could cause strangulation (Fineron *et al.,* 1995).

Loss of the greater horn of the hyoid bone in *Pax9*$^{\Delta PE}$;*Msx1*$^{+/-}$ mice and at the same time a lack of the superior horn of the thyroid cartilage may mean that the lateral thyrohyoid ligament has nowhere to attach. The results shown in this chapter, with

the neonates lacking the greater horn of the hyoid may be similar to the case of having a fracture. If this is the case then neonates may undergo strangulation in the same way as a broken hyoid bone would.

A deformity in the hyoid bone suggests the existence of embryological malformations (Shimizu *et al*., 2005). Some previously described cases in humans associated with embryological malformation of the hyoid bone, though rare, include bilateral absence of the lesser cornua, abnormal unilateral bone attachments to the corpus, thyroglossal cysts trapped within the hyoid bone, and abnormal ossifications of the greater and lesser horns with components of the hyoid bone and surrounding structures (Di Nunno *et al*., 2004; Gok *et al.*, 2012). On the other hand, there is no record for a case with an absent greater horn of the hyoid bone.

These observations suggest that the hyoid phenotype may be the cause of death in *Pax9*$^{\Delta PE}$;*Msx1*$^{+/-}$ neonates with a normal or cervical aortic arch. There is no evidence that the pups feed after birth as there was a lack of milk in the stomach, which was confirmed in *Pax9*$^{\Delta PE}$;*Msx1*$^{+/-}$ neonates. In addition, none of these neonates presented with a bloated abdomen as a sign of gasping in breathing, which may also support that these neonates suffocated to death. This may explain why *Pax9*$^{\Delta PE}$;*Msx1*$^{+/-}$ neonates are dying at birth even with an apparently functional systemic circulation.

In this context, cleft palate is a relatively common, non-life-threatening abnormality in humans. There is a case report of a male patient that was born with a cleft palate and did not have an operation to repair this until the age of 35 (Fukunaga *et al.*, 2014). This supports the idea that cleft palate is not be the main cause of death for *Pax9*$^{-/-}$ and *Pax9*$^{-/-}$;*Msx1*$^{+/-}$ neonates.

Moreover, Beavan and Fatti published the first clinical reported case of a cervical aortic arch in 1947. Interestingly, the patient died following ligation of a cervical aorta that had been mistaken for an aneurysm of the right innominate artery (Beavan and Fatti, 1947). One of the more recent reported cases of a cervical aortic arch was in an 8 year old boy with a pulsatile swelling in the right carotid triangle present since birth (Guha *et al.*, 2016). A computer tomography scan revealed a right sided cervical aortic arch with left common carotid artery arising from the ascending aorta

and the right external and internal carotid arteries originating separately from the cervical arch (Guha *et al.,* 2016). This strongly suggests that a cervical aortic arch can support life in humans and therefore may also be true for mice.

Msx1 heterozygosity is therefore affecting and somehow compensating for the IAA phenotype, but it is not correcting the bone deformity that is associated with *Pax9* mutation. This could mean that *Pax9* and *Msx1* somehow compensate each other during the formation of the pharyngeal arch arteries.

6 CELL FATE IN THE *Pax9;Msx1* MUTANT PHARYNGEAL ARCHES

6.1 INTRODUCTION

During pharyngeal arch artery (PAA) development, the 1st PAA are remodeled to form the maxillary artery and the external carotid artery, while the 2nd PAA are remodeled into the stapedial and hyoid arteries by E10.5. At this stage, the 3rd, 4th and 6th PAA are bilaterally symmetrical and of similar size; it is these vessels that will be remodeled to form the mature vasculature of the great arteries.

The 3rd PAA forms the right and left common carotid arteries. The right 4th artery remodels and becomes part of the right subclavian artery, whereas the left 4th artery enlarges and forms the segment of the aortic arch that connects the aortic sac to the descending aorta. Moreover, the left 6th PAA becomes the arterial duct, while most of right 6th PAA regress and the remaining part contributes to the basal pulmonary artery.

Pax9$^{-/-}$ embryos lack the 4th PAA, which causes IAA, and most of them show a hypoplastic 3rd PAA which eventually regresses resulting in absence of one or both of the common carotid arteries. This, coupled with a failure of the carotid duct to involute, results in the internal and external carotid arteries rising directly from the ascending aorta and the descending aorta.

The pharyngeal arches consist of an internal endodermal pouch, a mesenchymal core, and external ectodermal cleft (Graham, 2001). Each arch mesenchymal core contains the mesoderm and a ring of neural crest cells (Graham, 2001).

The neural crest cells (NCC) are a migratory population of cells that originate from the dorsal aspect of the neural tube (Kirby *et al.*, 1985). A specific crest cell population, called the cardiac neural crest (cNCC), is an important type of crest-derived ectomesenchyme in cardiovascular development, and it is also responsible for morphogenesis of the outflow region of the developing heart (Kirby *et al.*, 1985).

The cNCC are not required for aortic arch artery formation, but are required for their repatterning (Bockman *et al.*, 1987) and outflow tract septation. The PAA arise as endothelial tubes. The endothelial cells of the arteries are derived from pharyngeal

mesoderm, whereas their smooth muscle is derived from neural crest (Bergwerff *et al.*, 1998). So during the remodelling of the PAA the contribution of the cNCC is the major determinant of whether a particular arch artery will persist or will regress (Bockman *et al.,* 1989).

The NCC migrate ventrally into the 3rd, 4th and then 6th pharyngeal arch as each arch forms sequentially. The cells migrate between the pharyngeal ectoderm and endoderm. They then proliferate and surround the PAA and differentiate into the smooth muscle tunica media of the arteries (Bergwerff *et al*., 1998). The smooth muscle cells (SMC) support the vessels as they are remodeled, helping to stabilize the vessels as the haemodynamic pressure increases (Maarten Bergwerff *et al.*, 1998).

The importance of the cNCC population for normal heart development was confirmed in studies of chick embryos in which this population was surgically removed. These embryos displayed cardiovascular malformations, such as persistent of the common arterial trunk, VSD, inflow anomalies, and interruption or persistence of the aortic arch arteries (Bockman *et al.,* 1989; Kirby and Waldo, 1990). Transgenic mouse models with mutations in genes necessary for NCC function also have PAA development defects reminiscent of those seen in the chick embryos. For example, the splotch mouse, which contains a naturally occurring mutation in the *Pax3* gene, it has a NCC deficiency that develops a spectrum of cardiac outflow tract malformations including common arterial trunk, DORV, VSD and pharyngeal arch artery patterning defects (Bradshaw *et al*., 2009; Conway *et al.*, 1997; Franz, 1989). Also, if the NCC are ablated genetically using diphtheria toxin, similar outflow tract and PAA development defects occur including common arterial trunk and abnormal persistence or regression of the PAA (Olaopa *et al*., 2011).

In addition to the NCC, several mechanisms have been postulated to play a role in the remodelling process, such as apoptosis, proliferation and differentiation factors such as haemodynamic factors, especially the rate of blood flow through the arteries, have also been suggested to contribute to the remodelling process (Le Lievre and Le Douarin, 1975; Meeson *et al*., 1996).

Apoptosis is an important process in forming the asymmetric structure of the aortic arch. Apoptosis begins in the mesenchyme surrounding the right dorsal aorta and right 6th PAA immediately before the vessels regress. Apoptosis within the media of the vessel becomes more prominent as the vessel thins into a strand of SMC before completely regressing. In addition, work in a rat model has also indicated an increased level of apoptosis surrounding the carotid ducts before they begin to regress (Molin *et al*., 2002). Aberrant patterns of apoptosis within the vessel walls may lead to abnormal regression or persistence of specific segments of the aortic arch.

In addition to the cNCC and the apoptosis contribution to the PAA remodelling, proliferation play an important role in maintaining the cells viability as they arrive collectively to participate in the morphological process. For example, in the *Hoxa3*-null mutants, the neural crest cells were able to migrate normally into the 3rd pharyngeal arch, but their proliferation in the pharyngeal region markedly diminished, which led to a delay in the fusion of the 3rd PAA with the 4th and 2nd arch arteries at E12.0. Also, the 3rd PAA was hypoplastic and still can be seen at E12.5 (Chisaka and Kameda, 2005)

6.2 AIMS OF CHAPTER

The aim of this chapter was to look at the cellular events occurring within the pharyngeal arches and to compare and contrast any differences between wild type, *Pax9*$^{-/-}$ and *Pax9*$^{-/-}$*;Msx1*$^{+/-}$ mutant embryos. This was achieved by:

- The Examining rates of apoptosis and proliferation pathway was explored within the 3rd and 4th pharyngeal arches at E9.5 and E10.5 in both *Pax9*$^{-/-}$ and *Pax9*$^{-/-}$*;Msx1*$^{+/-}$ embryos.

- Investigating Additionally, NCC migration into the pharyngeal arches was investigated at E9.5 and E10.5, with and the differentiation into smooth muscle cells supporting the PAA during remodelling at E11.5.

- Examining endothelial cell arrangement around the 3rd PAA was investigated at E11.5.

- Moreover, the mechanism that allows two genes not expressed with the same domain to affect each other was explored by immunostaining

6.3 RESULTS

6.3.1 APOPTOSIS AND PROLIFERATION

Apoptosis and proliferation are cellular processes that are important for the development of the pharyngeal arches. In order to determine whether abnormal development of the PAA in *Pax9*$^{-/-}$ and *Pax9*$^{-/-}$;*Msx1*$^{+/-}$ mutant embryos is a consequence of abnormal cell death or cell division, the apoptosis and proliferation rate was calculated in the 3rd and 4th pharyngeal arches. Embryos were collected at E9.5 and E10.5, as these are stages critical for the formation of the PAA. For example, the 3rd pharyngeal arch is formed at E9.5, while the 4th pharyngeal arch begins to form at mid E9.5 and develops further during E10.5 (Savolainen *et al.*, 2009). Coronal sections were prepared and immunostained. Phospho-histone H3 (PH3) antibody was used as a proliferation marker and an antibody to Caspase-3 was used to detect apoptotic cells. Proliferating and apoptotic cells in the 3rd and 4th pharyngeal arches manually counted using Image J software and statistical analysis was performed on the collected data.

6.3.1.1 Proliferation

In order to compare the level of proliferation between control and mutant (*Pax9*$^{-/-}$ and *Pax9*$^{-/-}$;*Msx1*$^{+/-}$) embryos (n = 3 of each; 3 sections per embryo, every 3rd section was counted), an anti-PH3 antibody was used to label cells in all phases of mitosis (Li *et al*., 2005).

At E9.5, proliferation was detected in the 3rd pharyngeal arch in the mutant and control embryos (Figure 6-1 A). At this stage the 4th pharyngeal arch was not developed in all embryos, therefore a proliferation index for the 4th arch was not performed at E9.5.

The positively stained proliferating cells as well as all DAPI stained cells were counted to calculate a proliferation index. In wild type embryos a mean of 401.16 ± 8.19 cells were counted giving a proliferation index of 0.088 ± 0.002 (Figure 6-1 B). In the mutant embryos, the mean cell count in the 3rd pharyngeal arch in *Pax9*$^{-/-}$ and

Pax9$^{-/-}$;*Msx1*$^{+/-}$ was 227.7 ± 13.2 and 232.5 ± 7.79 respectively. The proliferation rate for *Pax9*$^{-/-}$ was 0.079 ± 0.003 and for *Pax9*$^{-/-}$;*Msx1*$^{+/-}$ it was 0.091 ± 0.0029 (Figure 6-1 B).

There was no statistically significant difference in the proliferation rate between the wild type and mutant (*Pax9*$^{-/-}$ and *Pax9*$^{-/-}$;*Msx1*$^{+/-}$) embryos (Figure 6-1 C). Moreover, the analysis did not show any significant difference between *Pax9*$^{-/-}$ and *Pax9*$^{-/-}$;*Msx1*$^{+/-}$mutant embryos.

The proliferation index of the ectoderm, endoderm and mesenchyme were also separately calculated, but the results also showed no significant difference in proliferation between the control and the mutant (*Pax9*$^{-/-}$ and *Pax9*$^{-/-}$;*Msx1*$^{+/-}$) 3rd pharyngeal arch, or between the *Pax9*$^{-/-}$ and *Pax9*$^{-/-}$;*Msx1*$^{+/-}$ embryos (Figure 6-1 D).

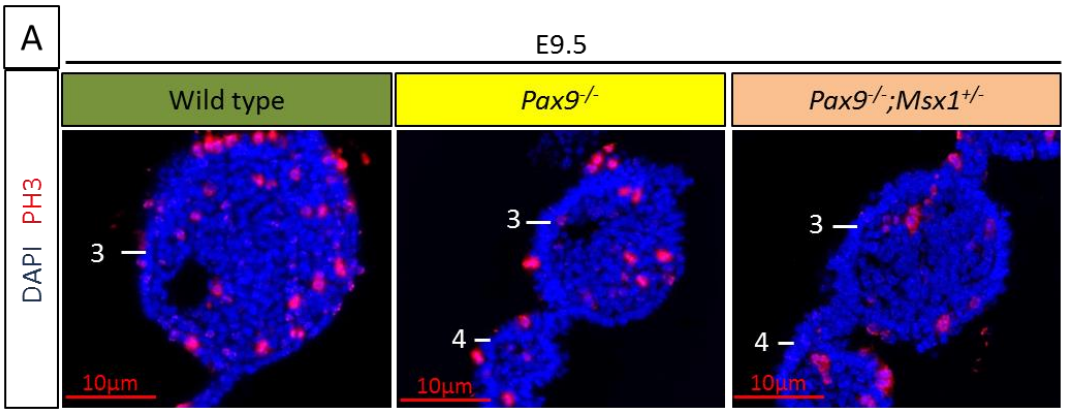

B		Wild type	*Pax9*$^{-/-}$	*Pax9*$^{-/-}$;*Msx1*$^{+/-}$
3rd PA	Mean of cell counting	401.16 ± 8.192	227.77 ± 13.29	232.5 ± 7.79
	Mean of proliferated cells	33 ± 2.91	19.27 ± 5.524	19.05 ± 2.59
	Proliferation rate	0.088 ± 0.00205	0.0798 ± 0.00358	0.0918 ± 0.00294

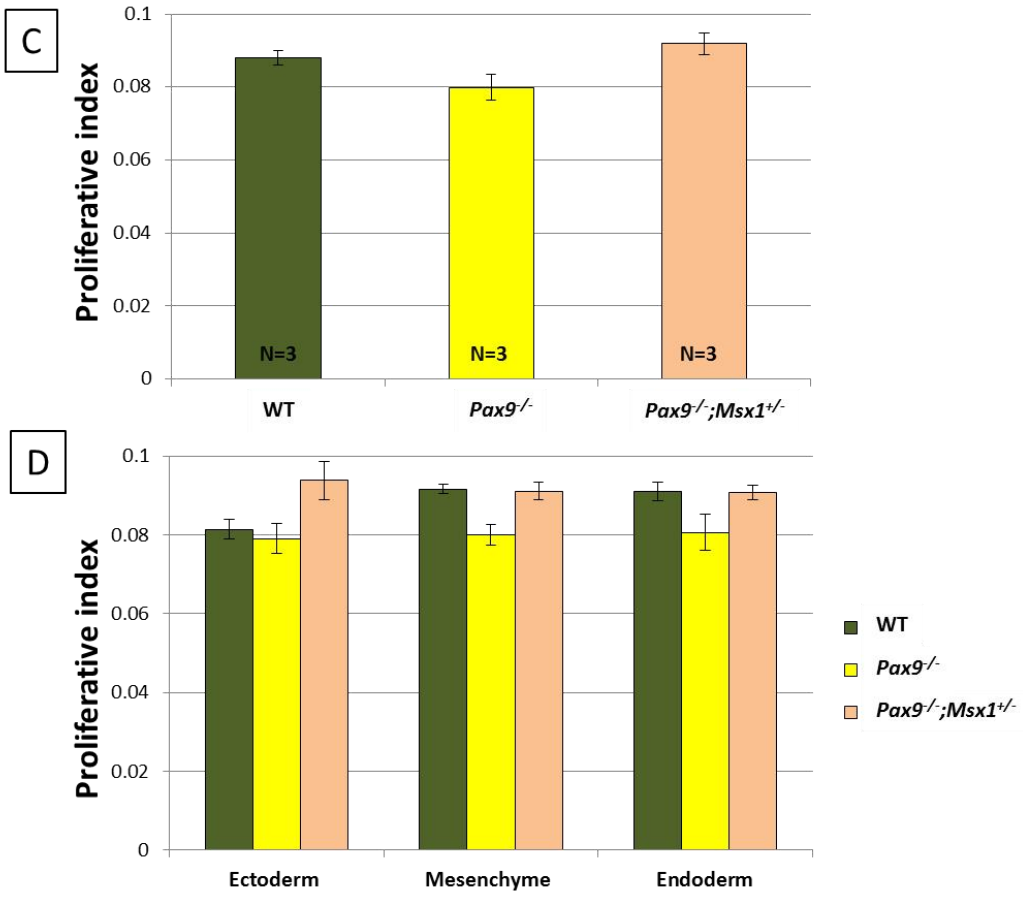

Figure 6-1: Proliferation in the pharyngeal arch of control and mutant embryos at E9.5.
(A) Coronal sections of wild type, *Pax9*$^{-/-}$ and *Pax9*$^{-/-}$;*Msx1*$^{+/-}$ embryos immunostained with PH3 antibody. **(B)** Table shows the mean count for each genotype, with the number of proliferating cells and the proliferation rate. **(C)** Graphical presentation of the proliferation index. There is no significant difference in the proliferation index within the 3rd pharyngeal arches between the wild type, *Pax9*$^{-/-}$ and *Pax9*$^{-/-}$;*Msx1*$^{+/-}$ embryos. **(D)** Proliferation index within the individual tissues of the 3rd pharyngeal arch.

Cellular proliferation levels were next calculated for the 3rd and 4th pharyngeal arch at E10.5 (Figure 6-2 A). The 3rd pharyngeal arch of wild type embryos contained a mean of 910.4 ± 33.1 cells and the proliferation index was 0.071 ± 0.0029. The number of cells within the 3rd pharyngeal arch of mutant *Pax9*$^{-/-}$ and *Pax9*$^{-/-}$*;Msx1*$^{+/-}$ embryos was reduced in comparison to the wild type, although this reduction did not achieve significance (p = 0.132, p = 0.166 respectively). There was a mean of 528.8 ± 18.4 cells in *Pax9*$^{-/-}$ and 707.6 ± 23.8 cells in *Pax9*$^{-/-}$*;Msx1*$^{+/-}$ embryos (P=0.511). There was no significant change in proliferation between wild type and mutant embryos which had proliferation indices of 0.062 ± 0.003 for *Pax9*$^{-/-}$ and 0.064 ± 0.003 for *Pax9*$^{-/-}$*;Msx1*$^{+/-}$ (Figure 6-2 B). There was no significant difference in the proliferation index between *Pax9*$^{-/-}$ and *Pax9*$^{-/-}$*;Msx1*$^{+/-}$ embryos (P=0.901).

To examine this further, the levels of proliferation within each tissue of the 3rd pharyngeal arch (ectoderm, endoderm and mesoderm) was quantified. No significant difference in the proliferation indices in each tissue across the genotypes analysed was found (Figure 6-2 E).

Next, the rates of cellular proliferation within the 4th pharyngeal arch was assessed. In the wild type 4th pharyngeal arch a mean of 384.1 ± 9.08 cells was counted with a proliferation index of 0.062 ± 0.003. Fewer cells were counted within the hypoplastic 4th pharyngeal arch of the mutant embryos, as expected, with a mean of 96.05 ± 8.7 cells in *Pax9*$^{-/-}$ embryos and a mean of 163.6 ± 8.3 cells in *Pax9*$^{-/-}$*; Msx1*$^{+/-}$ embryos. The proliferation indices for each of the mutants at 0.056 ± 0.0045 and 0.0511 ± 0.003 respectively were not significantly different from wild type (Figure 6-4 B-D). To further dissect the levels of proliferation within the 4th pharyngeal arch, the level of proliferation within the different tissues was examined. No significant differences were found (Figure 6-2 F).

Overall these results demonstrate that there is no significant difference in the proliferation rate between the wild type and mutant embryos (*Pax9*$^{-/-}$ and *Pax9*$^{-/-}$*;Msx1*$^{+/-}$*)* within the 3rd pharyngeal arch at E9.5, or within the 3rd and 4th pharyngeal arch at E10.5.

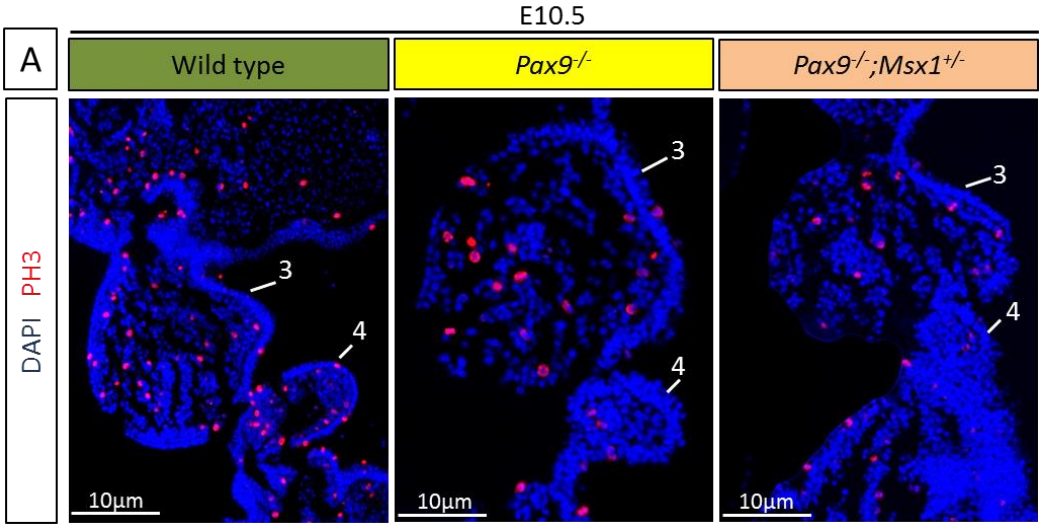

B		Wild type	*Pax9*$^{-/-}$	*Pax9*$^{-/-}$;*Msx1*$^{+/-}$
3rd PA	Mean of cell counting	910.41 ± 33.18	528.77 ± 18.47	707.61 ± 23.82
	Mean of proliferated cells	70.61 ± 9.85	36.88 ± 8.94	46.83 ± 7.72
	Proliferation rate	0.0715 ± 0.0029	0.0624 ± 0.00301	0.0641 ± 0.0032
4th PA	Mean of cell counting	384.125 ± 9.08	96.05 ± 8.7	163.61 ± 8.3
	Mean of proliferated cells	24.05 ± 4.97	7.83 ± 1.824	11.16 ± 2.41
	Proliferation rate	0.0619 ± 0.00314	0.0561 ± 0.00456	0.0511 ± 0.00347

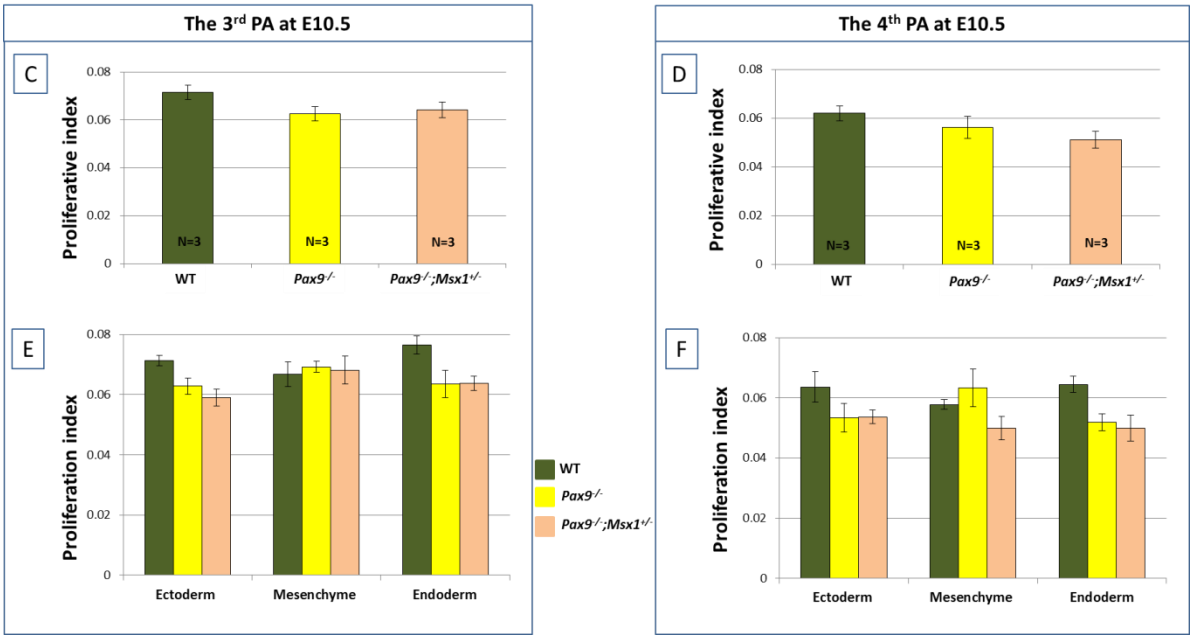

Figure 6-2: Proliferation in the pharyngeal arch of control and mutant embryos at E10.5.
(A) Coronal sections of wild type, *Pax9*$^{-/-}$ and *Pax9*$^{-/-}$;*Msx1*$^{+/-}$ E10.5 embryos immunostained with PH3 antibody. **(B)** Table shows the mean count for each genotype, with the number of proliferating cells and the proliferation index. **(C, D)** The proliferation index within the 3rd pharyngeal arch (**C**) or 4th pharyngeal arch (**D**) showed no significant difference between the wild type and *Pax9*$^{-/-}$ or *Pax9*$^{-/-}$;*Msx1*$^{+/-}$ embryos.**(E; F)** There was no significant difference between the levels of proliferation within the individual tissues of the 3rd **(E)** and 4th **(F)** pharyngeal arch.

6.3.1.2 Apoptosis

To compare the rate of apoptosis in wild type and mutant (*Pax9*$^{-/-}$ and *Pax9*$^{-/-}$;*Msx1*$^{+/-}$) embryos (n = 3 of each; 3 sections per embryo, every 3rd section was counted), coronal sections were prepared from E9.5 and E10.5 embryos and immunostained with an antibody raised against cleaved caspase 3.

Overall, very little apoptosis was observed throughout the pharyngeal arches irrespective of genotype. At E9.5 the 3rd pharyngeal arch was examined, the cells were counted and expressed as an apoptotic index from the total number of cells within each pharyngeal arch (Figure 6-3 A).

No significant increase in the mean apoptotic index between control (0.0181 ± 0.00144), *Pax9*$^{-/-}$ (0.02396 ± 0.00152) and *Pax9*$^{-/-}$;*Msx1*$^{+/-}$ (0.0209 ± 0.00168) embryos was observed within the 3rd pharyngeal arch at E9.5 (Figure 6-3 B).

Analysing the apoptotic index of individual tissues of the pharyngeal arch (i.e. endoderm, mesenchyme and ectoderm) also did not yield any significant difference between them (Figure 6-3 D).

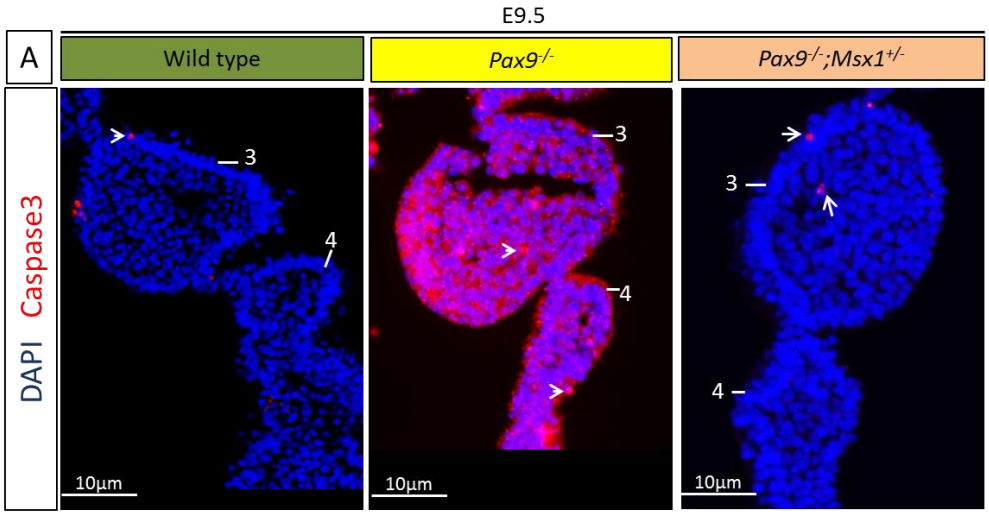

B		Wild type	*Pax9*$^{-/-}$	*Pax9*$^{-/-}$;*Msx1*$^{+/-}$
3rd PA	Mean of cell counting	401.16 ± 8.192	227.77 ± 13.29	232.5 ± 7.79
	Mean of apoptotic cells	5.38 ± 0.79	5.55 ± 0.92	4.72 ± 0.611
	apoptosis rate	0.0181 ± 0.00144	0.0239 ± 0.00152	0.0209 ± 0.00168

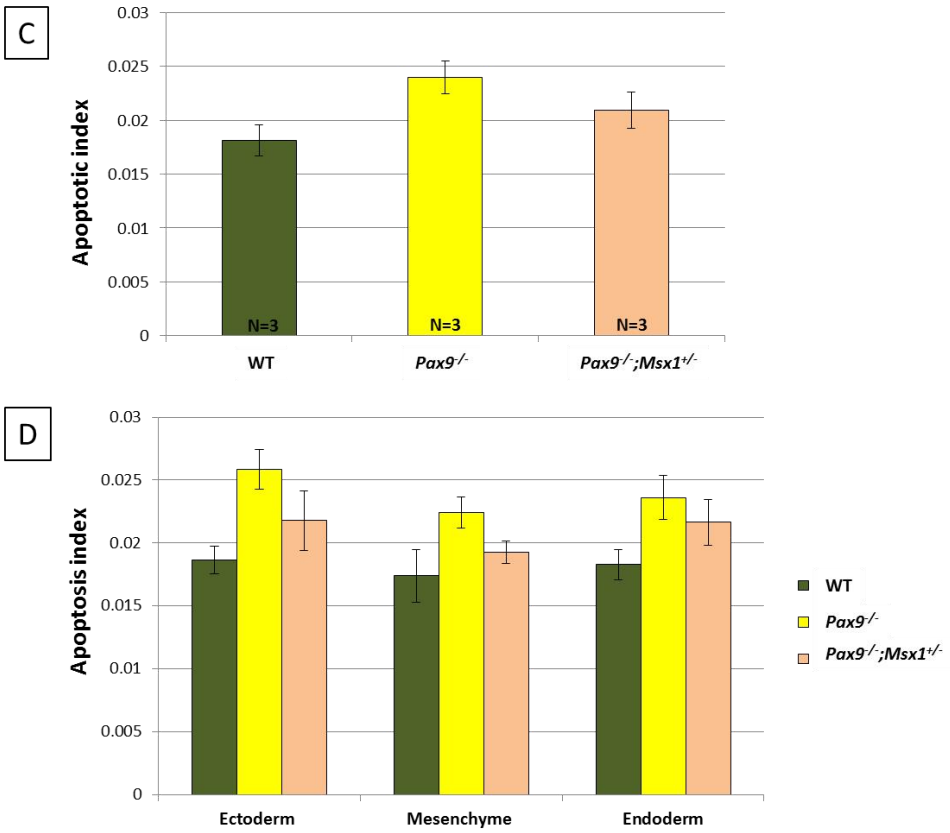

Figure 6-3: Apoptosis in the 3rd pharyngeal arch of control and mutant embryos at E9.5.
(A) Coronal sections of wild type and mutant (*Pax9*$^{-/-}$ *and Pax9*$^{-/-}$;*Msx1*$^{+/-}$) embryos immunostained with anti-caspase3 antibody. Very low levels of apoptosis was seen. **(B-C)** Quantification of apoptosis within the 3rd pharyngeal arch did not show any significant change in the apoptosis index between the wild type and *Pax9*$^{-/-}$ or *Pax9*$^{-/-}$;*Msx1*$^{+/-}$ embryos. Moreover, there was no significant difference between *Pax9*$^{-/-}$ and *Pax9*$^{-/-}$;*Msx1*$^{+/-}$ embryos. **(D)** There were no differences between the levels of apoptosis within the individual tissues of the 3rd pharyngeal arch.

As no change in the apoptotic index was found at E9.5, embryos at E10.5 were next examined to see if apoptosis could be occurring at a stage when the 3rd, 4th and 6th pharyngeal arch had already formed, but before they had begun to remodel. Any change in the rate of apoptosis in the mutant embryos could be related to the hypoplasia of the 3rd and 4th pharyngeal arches.

Apoptotic cells were detected in the 3rd and 4th pharyngeal arch of all embryos examined at E10.5. These cells were counted and expressed as an apoptotic index from the total number of cells within each pharyngeal arch. There was no significant difference between the wild type (0.01379 ± 0.00101), *Pax9*$^{-/-}$ (0.01459 ± 0.005) or *Pax9*$^{-/-}$*;Msx1*$^{+/-}$ (0.01361 ± 0.00173) embryos, or between the mutant embryos themselves (Figure 6-4 B).

To investigate this farther, the apoptotic index within the different tissues of the pharyngeal arch (ectoderm, endoderm and mesenchyme) in the 3rd pharyngeal arch was analysed, but no significant changes between the control and the mutant (*Pax9*$^{-/-}$ and *Pax9*$^{-/-}$*;Msx1*$^{+/-}$) embryos at E10.5 or between the mutant embryos themselves was identified (Figure 6-4 C).

Similarly, when the number of apoptotic cells was compared within the 4th pharyngeal arch, no significant change in the levels of apoptosis in controls and mutant (*Pax9*$^{-/-}$ and *Pax9*$^{-/-}$*;Msx1*$^{+/-}$) embryos was seen (Figure 6-5 B-C). Moreover, comparing the level of apoptosis within the different tissues of the pharyngeal arch showed no significant change between the control and the mutant embryos and between the mutant embryos themselves (Figure 6-5 D).

Overall, the analysis of apoptosis within the pharyngeal arch of E9.5 and E10.5 mutant embryos showed there was no significant difference in this compared with wild type embryos.

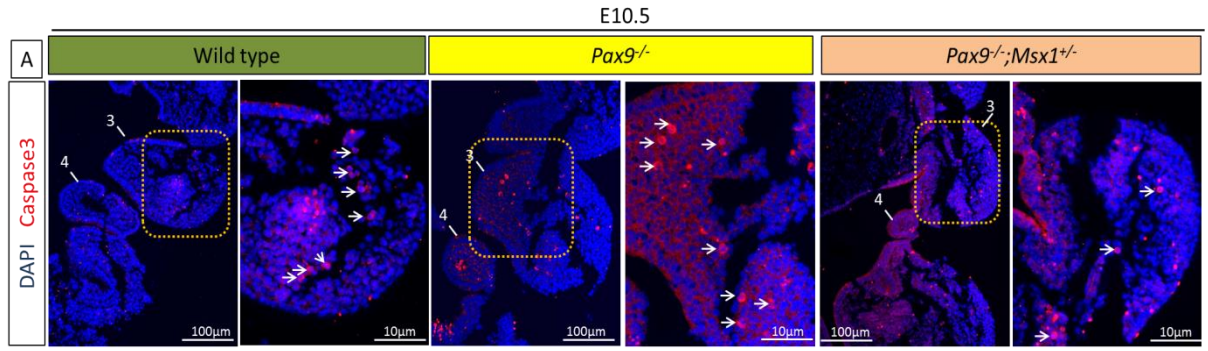

B		Wild type	*Pax9*$^{-/-}$	*Pax9*$^{-/-}$;*Msx1*$^{+/-}$
3rd PA	Mean of cell counting	910.41 ± 33.18	528.77 ± 18.47	707.61 ± 23.82
	Mean of apoptotic cells	13.5 ± 3.014	8.33 ± 1.31	10.2 ± 2.59
	Apoptosis rate	0.0137 ± 0.00101	0.0145 ± 0.00576	0.0136 ± 0.00173

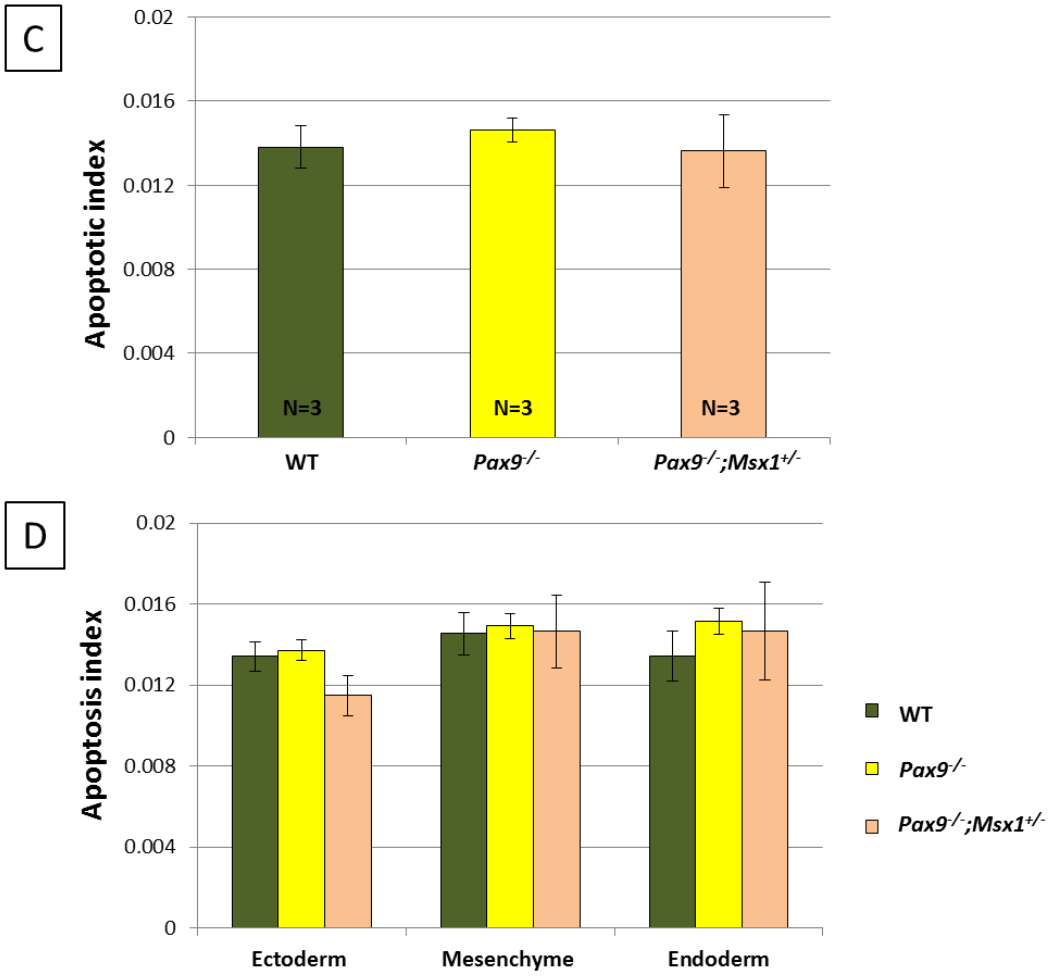

Figure 6-4: Apoptosis within the 3rd pharyngeal arch of control and *Pax9;Msx1* mutant embryos at E10.5.
(A) Coronal sections of wild type and mutant (*Pax9*$^{-/-}$ *and Pax9*$^{-/-}$;*Msx1*$^{+/-}$) embryos immunostained with anti-caspase3 antibody. **(B-C)** Quantification of apoptosis within the 3rd pharyngeal arch did not show any significant change in the level of apoptosis between wild type and mutant embryos (*Pax9*$^{-/-}$ or *Pax9*$^{-/-}$;*Msx1*$^{+/-}$). No difference was found in the apoptotic index between the mutant embryos. **(D)** Levels of apoptosis within the individual tissues of the 3rd pharyngeal arches did not reveal any significant difference in the apoptotic index.

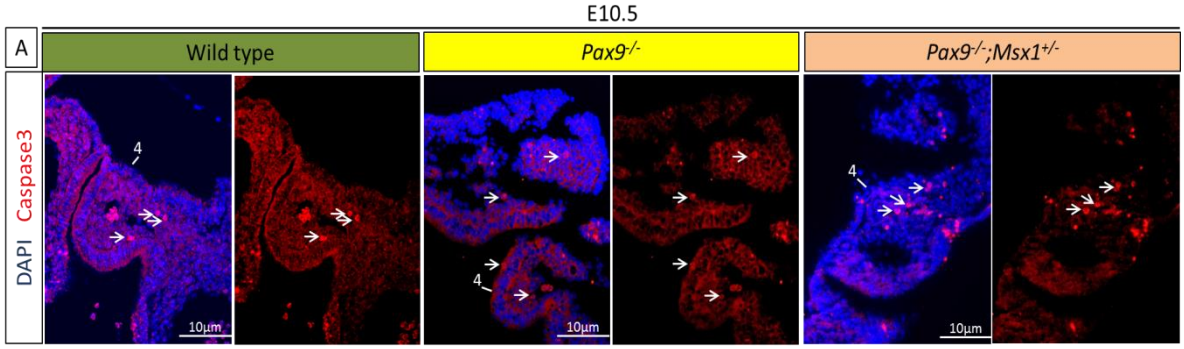

B		Wild type	*Pax9*$^{-/-}$	*Pax9*$^{-/-}$;*Msx1*$^{+/-}$
4th PA	Mean of cell counting	384.125 ± 9.08	96.05 ± 8.7	163.61
	Mean of apoptotic cells	8.00 ± 2.01	1.94 ± 0.91	2.88 ± 0.795
	Apoptosis rate	0.00.0151 ± 0.00137	0.017 ± 0.00214	0.0193 ± 0.00191

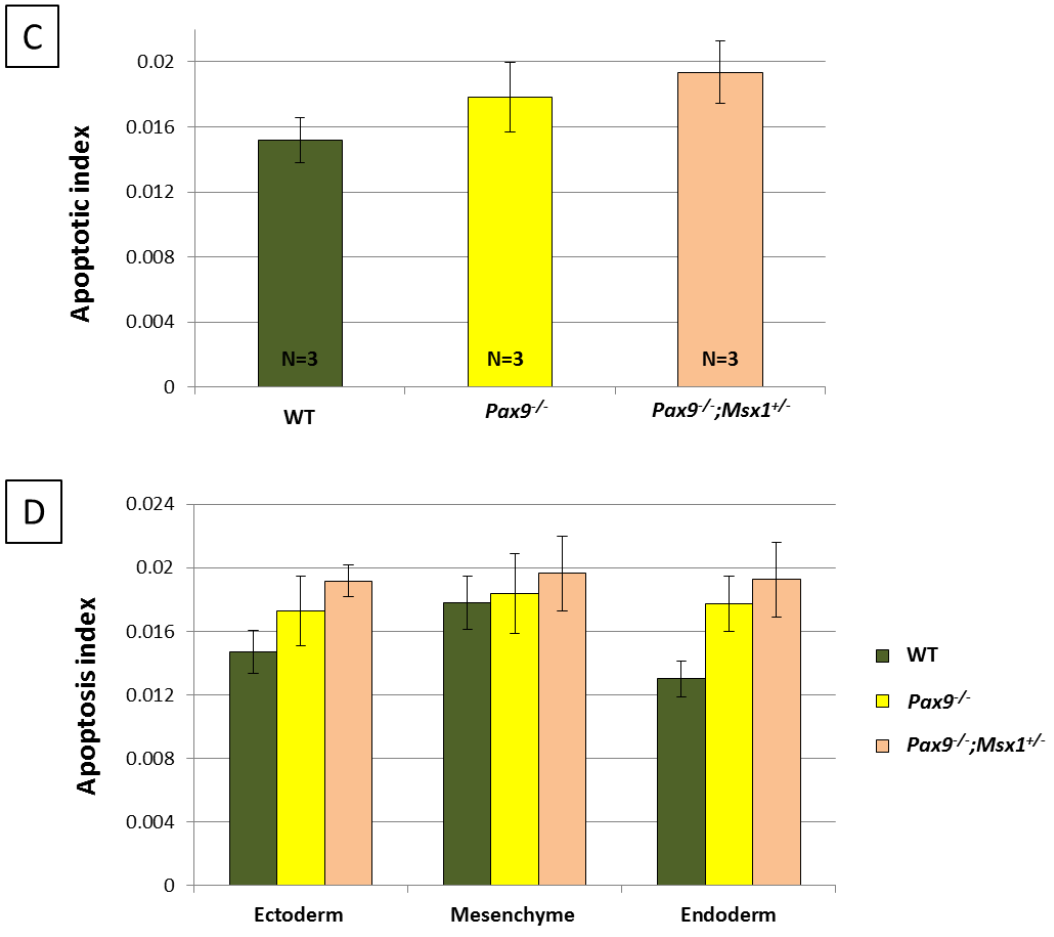

Figure 6-5: Apoptosis within the 4th pharyngeal arch of control and *Pax9;Msx1* mutant embryos at E10.5.

(A) Coronal sections of wild type and mutant (*Pax9*$^{-/-}$ *and Pax9*$^{-/-}$;*Msx1*$^{+/-}$) embryos stained with anti-caspase3 antibody. Examination of the mutant embryos (*Pax9*$^{-/-}$ and *Pax9*$^{-/-}$;*Msx1*$^{+/-}$) revealed a low level of apoptosis within the hypoplastic 4th pharyngeal arches at E10.5. (**B, C**) Quantification of apoptosis within the 4th pharyngeal arches did not show any significant change between the wild type and the mutant embryos (*Pax9*$^{-/-}$ or *Pax9*$^{-/-}$;*Msx1*$^{+/-}$). There was no significant difference in the apoptosis index between *Pax9*$^{-/-}$ and *Pax9*$^{-/-}$;*Msx1*$^{+/-}$ embryos either. (**D**) Levels of apoptosis within the individual tissues of the 4th pharyngeal arch did not reveal any significant difference in the apoptotic index.

6.3.2 NEURAL CREST CELL MIGRATION INTO THE PHARYNGEAL ARCHES

6.3.2.1 Immunofluorescent staining for NCC

The cNCC play a major role in cardiovascular patterning by participation in the remodelling of the PAA and their derivatives. The cNCC migrate from the neural tube into the caudal pharyngeal arches 3, 4 and 6. Within the pharyngeal arches, they surround the PAA and differentiate into the smooth muscle lining of the vessel. The smooth muscle cells support the vessels as they remodel and stabilise the vessels as the haemodynamic pressures increase (Fulcoli *et al*., 2009; Kirby *et al*., 1983).

To assess NCC within the pharyngeal arches, control and mutant (*Pax9*$^{-/-}$ and *Pax9*$^{-/-}$*;Msx1*$^{+/-}$) embryos were collected at E10.5 and processed for histology. Coronal sections were cut and immunostained with an antibody to AP2α, which marks NCC as well as the pharyngeal surface ectoderm (Garcia-Martinez and Schoenwolf, 1993).

NCC were observed within the 3rd and 4th pharyngeal arch in both control and mutant (*Pax9*$^{-/-}$ and *Pax9*$^{-/-}$*;Msx1*$^{+/-}$) embryos (Figure 6-6). To quantify the number of NCC within the 3rd pharyngeal arch at E10.5 three sections each from wild type (n=3), *Pax9*$^{-/-}$ (n=3) and *Pax9*$^{-/-}$*;Msx1*$^{+/-}$ (n=3) embryos were analysed. Images were acquired at 20X objective magnification and Image J was used to count the NCC.

Analysis showed a statistically significant decrease (67%, P=0.000527) in the number of NCC present in the 3rd pharyngeal arch of *Pax9*$^{-/-}$ embryos (44.2 ± 6.03 cells) compared to wild type embryos (200.5 ± 14.99 cells). In *Pax9*$^{-/-}$*;Msx1*$^{+/-}$ embryos, however, there was only a 14% decrease in the number of NCC (140.6 ± 16.1 cells) compared to wild type and this was not a statistically significant difference. Moreover, *Pax9*$^{-/-}$*;Msx1*$^{+/-}$ embryos presented a significant increase (P=0.0051) in the number of NCC compared with *Pax9*$^{-/-}$ embryos (Figure 6-6 B).

The number of the NCC within the 4th pharyngeal arch was also investigated in wild-type, *Pax9*$^{-/-}$ and *Pax9*$^{-/-}$*;Msx1*$^{+/-}$ embryos. The number of NCC within the 4th pharyngeal arch of both mutant genotypes was significantly reduced compared to wild type, although there was no significant difference between *Pax9*$^{-/-}$ and *Pax9*$^{-/-}$*;Msx1*$^{+/-}$ embryos (Figure 6-6 C). This suggests that the effect of the *Msx1* genotype on the number of NCC is restricted to the 3rd pharyngeal arch.

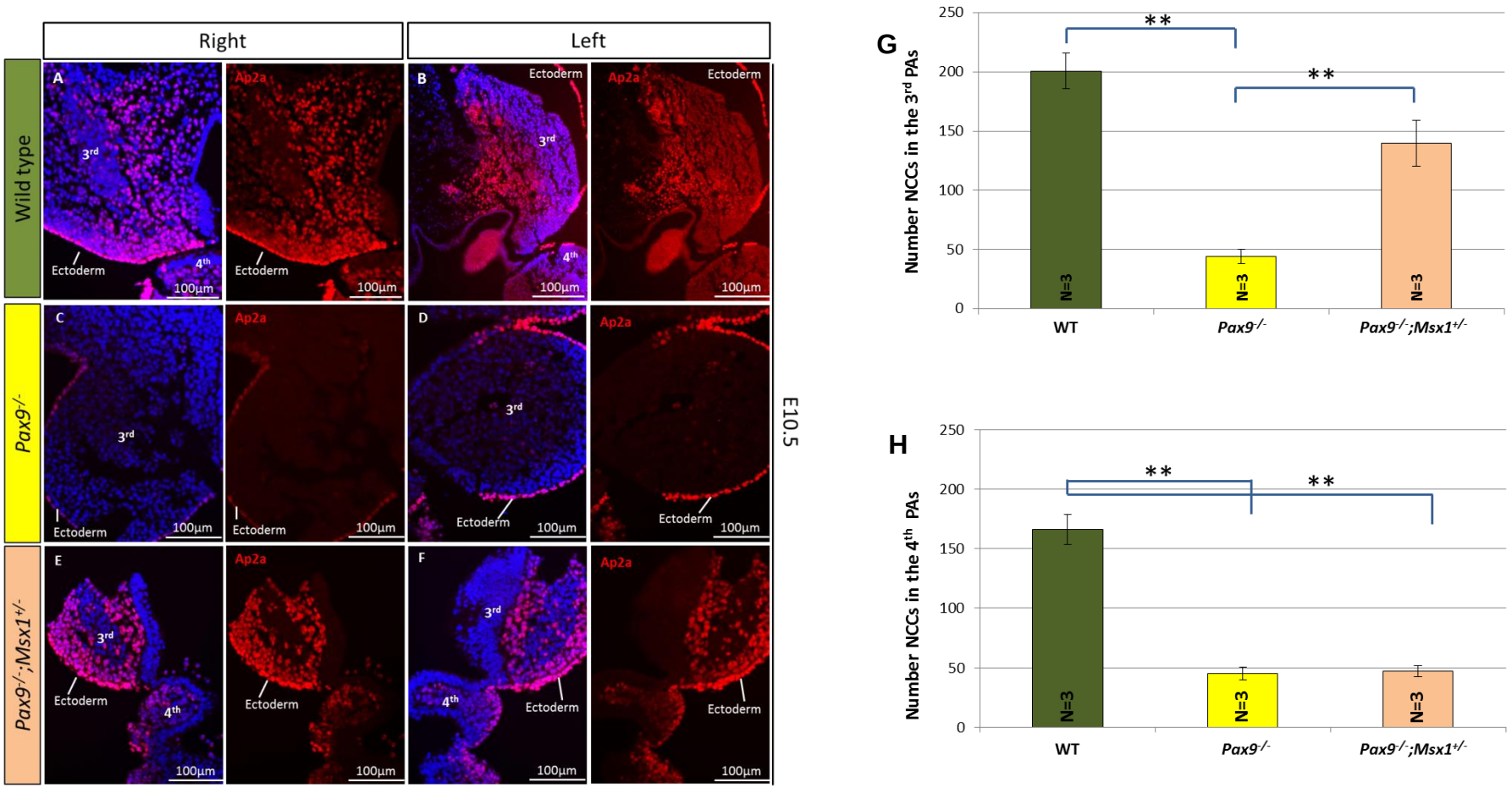

Figure 6-6 : Distribution of neural crest cells (NCC) in the 3rd and 4th in control and mutants (*Pax9*$^{-/-}$ and *Pax9*$^{-/-}$;*Msx1* $^{+/-}$) embryos at E10.5. Coronal cross sections of the pharyngeal arches from E10.5 wild type **(A, B)** and mutant (*Pax9*$^{-/-}$; **C, D** and *Pax9*$^{-/-}$;*Msx1*$^{+/-}$; **E, F**) embryos were immunostained with an antibody to AP-2α to label NCC (red). The NCC were counted and the data analysed (**G, H**). (**G**) NCC numbers were significantly reduced in the 3rd pharyngeal arch of *Pax9*$^{-/-}$ embryos compared to wild type, but not in *Pax9*$^{-/-}$;*Msx1*$^{+/-}$ embryos. The number of NCC in *Pax9*$^{-/-}$;*Msx1*$^{+/-}$ embryos was significantly higher than in *Pax9*$^{-/-}$ embryos. (**H**) NCC numbers were significantly reduced in the 4th pharyngeal arch of *Pax9*$^{-/-}$ and *Pax9*$^{-/-}$;*Msx1*$^{+/-}$ embryos compared to wild type. *t*-test; **p≤0.001.

6.3.2.2 Total cell counts within the 3rd pharyngeal arch

Counting of cNCC within the pharyngeal arches using immunostaining revealed that the low number seen in the 3rd arch in *Pax9*$^{-/-}$ embryos appeared to be partially rescued in *Pax9*$^{-/-}$*;Msx1*$^{+/-}$ embryos. To investigate whether there were any differences in cell number within the other tissues that comprise the pharyngeal arches, all cells within the ectoderm, mesenchyme and the endoderm of the 3rd pharyngeal arch of all genotypes were counted from coronal sections ((n = 3 of each; 3 sections per embryo, every 3rd section was counted) at E10.5.

The overall counts revealed that the total number of cells in the 3rd pharyngeal arch was significantly decreased in *Pax9*$^{-/-}$ (p=0.000394) and *Pax9*$^{-/-}$*;Msx1*$^{+/-}$ (p=0.0097) embryos compared to wild type. However, there was a significant increase in the number of cells in the 3rd pharyngeal arch of *Pax9*$^{-/-}$*;Msx1*$^{+/-}$ embryos when compared to *Pax9*$^{-/-}$ embryos (p=0.052) (Figure 6-7 B).

In wild type embryos there was a total of 910.42 ± 33.18 cells in the 3rd pharyngeal arch: 140 ± 23.70 cells in the ectoderm, 685.25 ± 22.18 cells in the mesenchyme and 84.70 ± 4.921 cells in the endoderm (Figure 6-7 A).

The number of endoderm cells were not significantly different between the wild type and mutant (*Pax9*$^{-/-}$ and *Pax9*$^{-/-}$*;Msx1*$^{+/-}$) embryos (Figure 6-7 C). However, the number of ectoderm cells in *Pax9*$^{-/-}$ and *Pax9*$^{-/-}$*;Msx1*$^{+/-}$ embryos was significantly decreased when compared to wild type: 89.22 ± 20 cells in *Pax9*$^{-/-}$ (p=0.01) and 102.77 ± 22.4 cells in *Pax9*$^{-/-}$*;Msx1*$^{+/-}$ (p=0.0344). There was no statistical difference in the number of ectoderm cells between *Pax9*$^{-/-}$ and *Pax9*$^{-/-}$*;Msx1*$^{+/-}$ embryos (p=0.221) (Figure 6-7 C).

In agreement with the immunostained cNCC counts, the number of mesenchymal cells were significantly decreased to 366.11 ± 18.73 cells in *Pax9*$^{-/-}$ embryos (p=0.000524). The number of mesenchymal cells in the *Pax9*$^{-/-}$*;Msx1*$^{+/-}$ embryos (524.55 ± 40.96) was not significantly different from wild type (p=0.215), although the difference between *Pax9*$^{-/-}$ embryos and *Pax9*$^{-/-}$*;Msx1*$^{+/-}$ embryos was significant (p=0.00538) (Figure 6-7 C).

A	Wild type	*Pax9*$^{-/-}$	*Pax9*$^{-/-}$;*Msx1*$^{+/-}$
Total number of cells	910.42±33.18	528.78±18.47	707.61±23.82
Number of cells in the ectoderm	140.45 ± 23.70	89.22 ± 20.09	102.77 ± 22.42
Number of cells in the mesenchyme	685.25 ± 22.18	366.11 ± 18.37	524.96 ± 40.96
Number of cells in the endoderm	84.70 ± 4.921	71.78 ± 9.22	79.22 ± 15.508

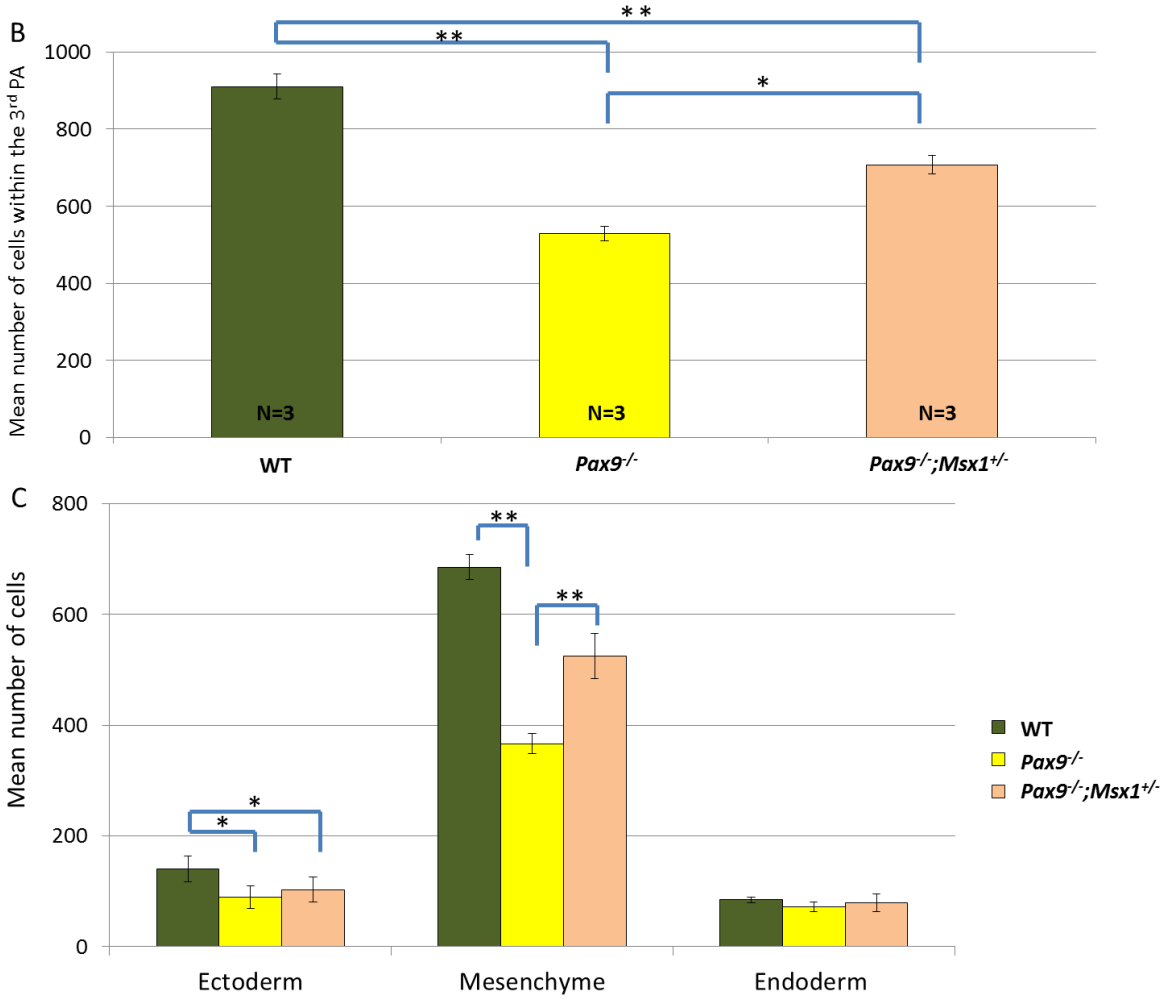

Figure 6-7: Cell counts within the 3rd pharyngeal arch of control and *Pax9;Msx1* mutant embryos at E10.5.
(A) The number of cells within the 3rd pharyngeal arch of control and mutant embryos was calculated for the different layers of the 3rd arch. **(B)** Total cell counts for each genotype. There is a significant decrease in the number of cells between the control and the mutant (*Pax9*$^{-/-}$ and *Pax9*$^{-/-}$;*Msx1*$^{+/-}$) embryos, but there are significantly more cells present in the *Pax9*$^{-/-}$;*Msx1*$^{+/-}$ embryos compared to *Pax9*$^{-/-}$ embryos. **(C)** Separate cell counts from ectoderm, mesenchyme and endoderm of the 3rd pharyngeal arch. In the ectoderm there is a significant decrease in the number of cells in the mutant genotypes compared to the wild type. For the mesenchyme counts, there are significantly fewer cells in the *Pax9*$^{-/-}$ embryos, but not in the *Pax9*$^{-/-}$;*Msx1*$^{+/-}$ embryos when compared to wild type. No change in cell counts was seen in the endoderm between the genotypes. *t*-test; $p<0.05$, $^{**}p\leq0.001$.

6.3.3 ENDOTHELIAL AND SMOOTH MUSCLE CELL CONTRIBUTION TO THE FORMATION OF THE 3rd PAA

As demonstrated above, there is a significant increase in the number of NCC in the 3rd pharyngeal arch in *Pax9*$^{-/-}$*;Msx1*$^{+/-}$ embryos compared with *Pax9*$^{-/-}$ embryos at E10.5. Also, and importantly, this number was not significantly different from the number of NCC observed in wild type embryos. As NCC are expected to differentiate into smooth muscle cells to support the PAA, it is possible that in the *Pax9*$^{-/-}$*;Msx1*$^{+/-}$ genotype more NCC are present within the 3rd pharyngeal arch to be able to fulfil this role. To investigate whether more smooth muscle cells are present around the 3rd PAA of *Pax9*$^{-/-}$*;Msx1*$^{+/-}$ embryos compared to *Pax9*$^{-/-}$ embryos, immunostaining was performed at E11.5. This stage was selected as before this time the differentiation of NCC into smooth muscle cells investing round the 3rd PAA has not occurred, or only occurred partially around the 3rd PAA (Kochilas *et al.*, 2002).

To investigate the recruitment of smooth muscle cells around the 3rd PAA, a total of six embryos each of the control and mutant genotypes were collected at E11.5, and immunohistochemistry performed on coronal sections using an alpha-smooth muscle actin (α-SMA) antibody and an antibody raised against ERG as a marker for endothelial cells.

ERG is an ETS family transcription factor, that is known to be expressed in the nucleus of endothelial cells (Sharrocks, 2001).

In wild type embryos, α-SMA immunostaining showed a smooth muscle layer around the 3rd, 4th and the 6th PAA (Figure 6-8, Figure 6-9). These PAA were also fully lumenised with a layer of endothelial cells labelled with the ERG antibody. In *Pax9*$^{-/-}$ embryos, however, there was a reduction in α-SMA staining around the 3rd PAA although staining was maintained around the dorsal aorta and the 6th PAA (Figure 6-8, Figure 6-9). ERG staining to mark the endothelium, showed a hypoplastic 3rd PAA in three out of six *Pax9*$^{-/-}$ embryos (unilateral or bilateral). One embryo had a disrupted irregular layer of endothelial cells, and in two embryos the ERG staining was not detected, which indicated that the 3rd PAA was absent (Figure 6-9).

Comparing the smooth muscle cell and endothelial immunostaining in the wild type and *Pax9*$^{-/-}$ embryos set a baseline for the experiment, since they both act as essential controls to compare with *Pax9*$^{-/-}$*;Msx1*$^{+/-}$ embryos. The wild type showed a well formed circular layer of smooth muscle around the 3rd PAA, and this layer is important to support this vessel during remodeling. In *Pax9*$^{-/-}$ embryos, the smooth muscle either not exist or was formed as a thin layer around one side of the 3rd PAA but not a full circle around the vessel.

Immunostaining for α-SMA in *Pax9*$^{-/-}$*;Msx1*$^{+/-}$ embryos revealed that the 3rd PAA was surrounded by smooth muscle cells in all cases (n = 6). The 3rd PAA also showed positive staining for a ring of endothelial cells indicating that this vessel was fully lumenised. In some cases, a hypoplastic 4th PAA was detected (2/6), which was either partly surrounded with a layer of smooth muscle cells or none were detected. However, a layer of endothelial cells was present.

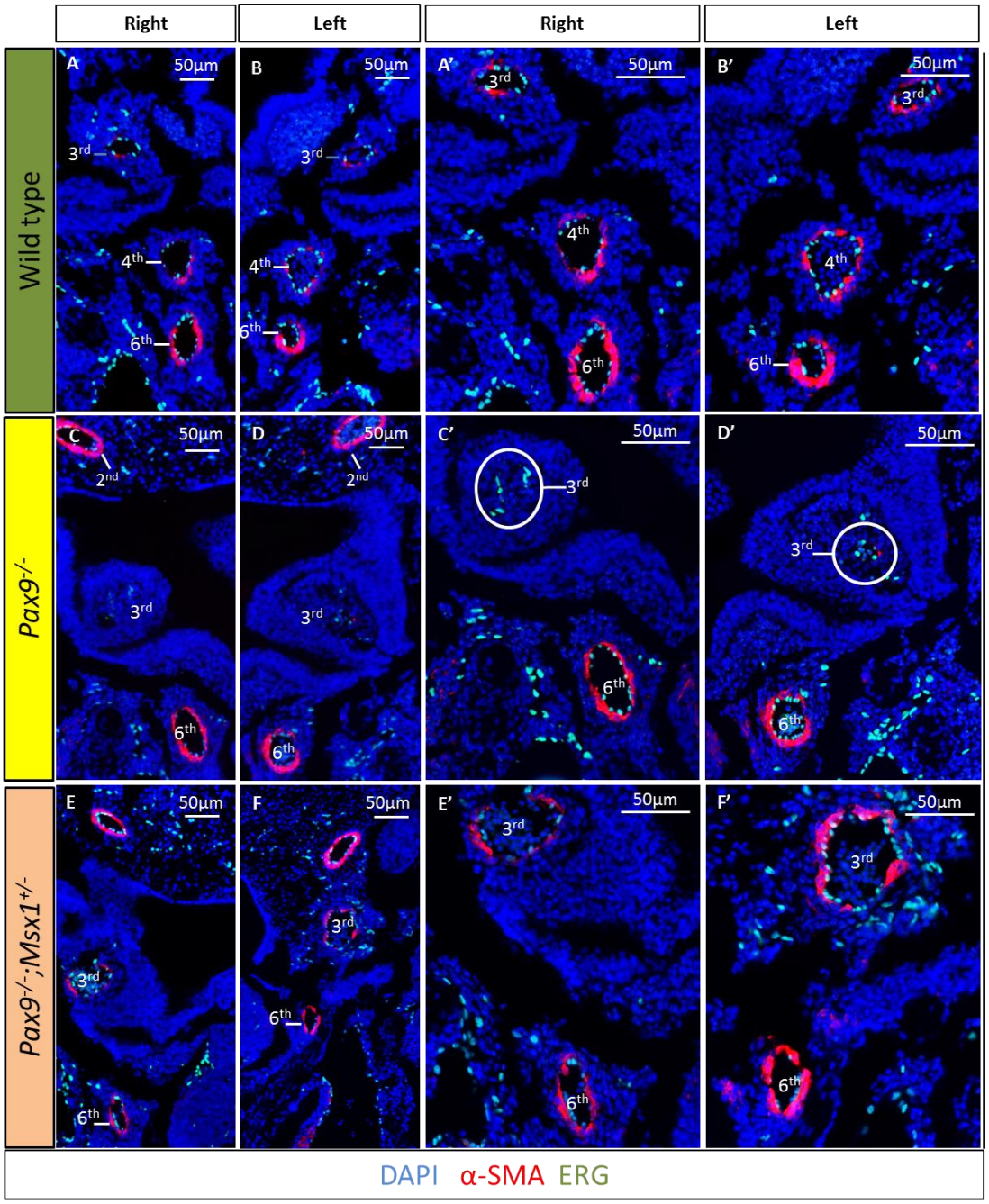

Figure 6-8: Dual immunofluorescence staining for smooth muscle actin and endothelium in control and *Pax9;Msx1* mutant embryos.
Coronal sections of E11.5 wild-type, *Pax9*$^{-/-}$ and *Pax9*$^{-/-}$;*Msx1*$^{+/-}$ embryos immunostained using αSMA and ERG antibodies. (**A, B**) Wild type embryo showing a well formed layer of smooth muscle cells (red) around the 3rd, 4th, and the 6th PAA bilaterally. A layer of endothelial cells can also be seen for each PAA (green). (**C, D**) *Pax9*$^{-/-}$ embryo with robust aSMA staining around the abnormally persisting 2nd and normal 6th PAA., Minimal (**C'**) or absent (**D'**) staining for aSMA can be seen in the 3rd pharyngeal arch. ERG staining indicates a disrupted layer of endothelial cells around the 3rd PAA. (**E, F**) *Pax9*$^{-/-}$;*Msx1*$^{+/-}$ embryo with robust bilateral α-SMA staining around the 3rd PAA. ERG staining indicates a layer of endothelial cells around the 3rd PAA.

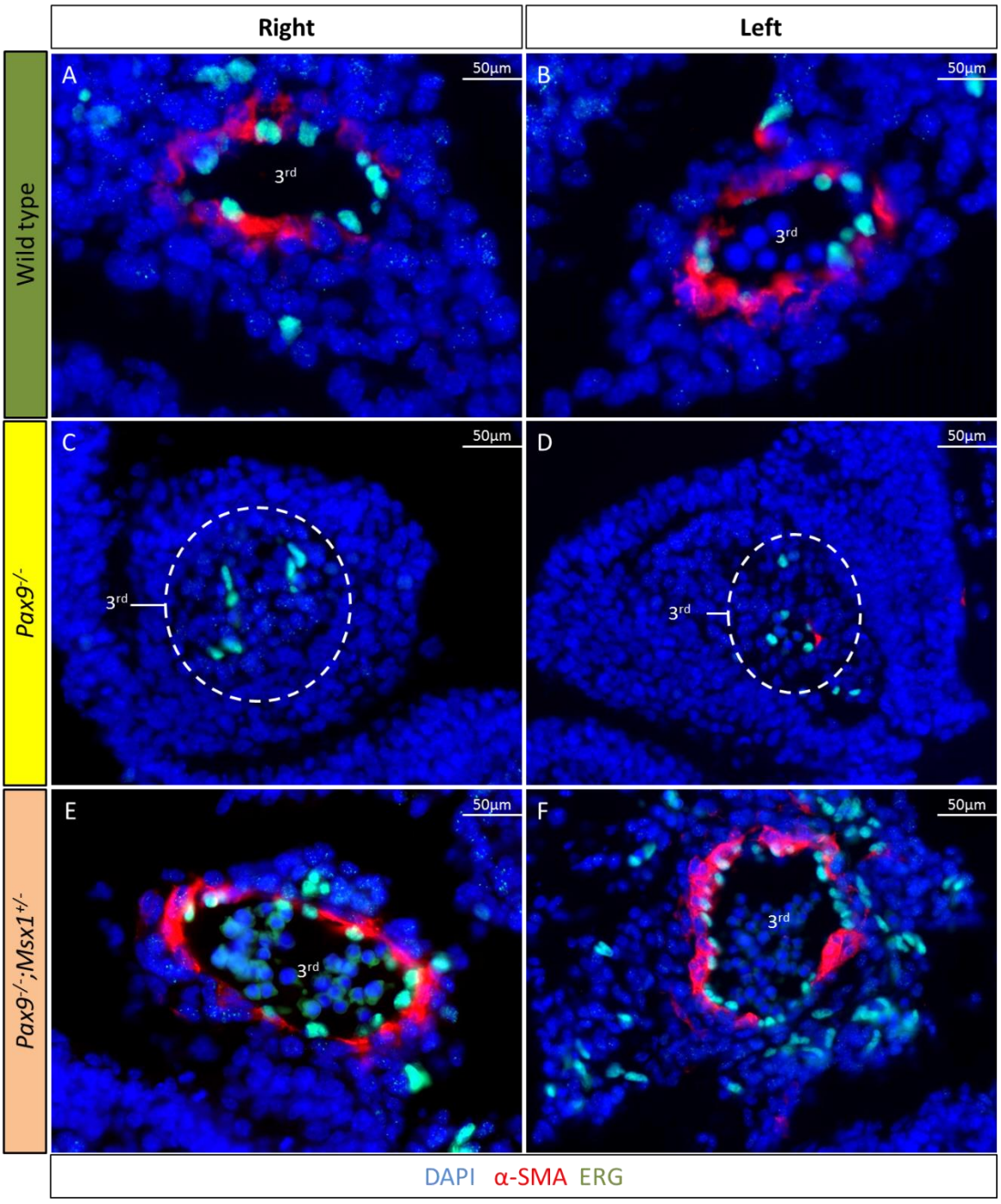

Figure 6-9: Dual immunofluorescence staining for smooth muscle actin and endothelium in control and *Pax9;Msx1* mutant embryos at a higher magnification.
Higher magnification of the images shown in
Figure **6-8**. **(A, B)** Wild type embryo showing a layer of smooth muscle (red) surrounding a single layer of endothelial cells (green) in the 3rd pharyngeal arch. **(C, D)** *Pax9*$^{-/-}$ embryo with no smooth muscle cell staining around the 3rd PAA, and disorganized endothelial cells. **(E, F)** *Pax9*$^{-/-}$*;Msx1*$^{+/-}$ embryo with a well formed layer of smooth muscle cells surrounding an organized single layer of endothelial cells.

6.3.4 EXPLORING A CELLULAR MECHANISM ALLOWING LOSS OF *Msx1* TO MODULATE THE *Pax9*-NULL CARDIOVASCULAR PHENOTYPE

In the pharyngeal arches at mid-embryogenesis, *Pax9* is specifically expressed in the pharyngeal endoderm, whereas *Msx1* is expressed in the neural crest cells (section 4.3.5 and section 4.3.6). The data presented in this thesis has shown that the *Pax9*-null cardiovascular phenotype is modulated by *Msx1* heterozygosity to such a degree that a physiologically intact systemic circulation is restored. As each gene is expressed in a discrete compartment within the pharyngeal arches, it raised the question as to how these two genes could be interacting or communicating with each other in normal cardiovascular development.

To investigate this immunostaining was performed to identify how close the different tissue within the pharyngeal arches are associated with each other, which could imply communication between cell types.

To mark *Pax9* in the pharyngeal endoderm, fate mapping of *Pax9*-expressing cells was carried out using a novel *Pax9cre* transgenic mouse (Heiko Peters, unpublished) (section for the lacz staining 5.2), in which the *Cre* recombinase gene is expressed under the control of the endogenous *Pax9* promoter. Male *Pax9cre* mice were crossed with homozygous *eYFP* females (Srinivas *et al*., 2001) which express an enhanced yellow fluorescent protein (eYFP) under control of the ubiquitously expressed *Rosa* locus following *Cre* mediated recombination (Srinivas *et al.*, 2001). E9.5 embryos were collected and processed for immunostaining with antibodies raised against GFP (for the Cre activated eYFP expression) and ERG (for endothelium) (Figure 6-10).

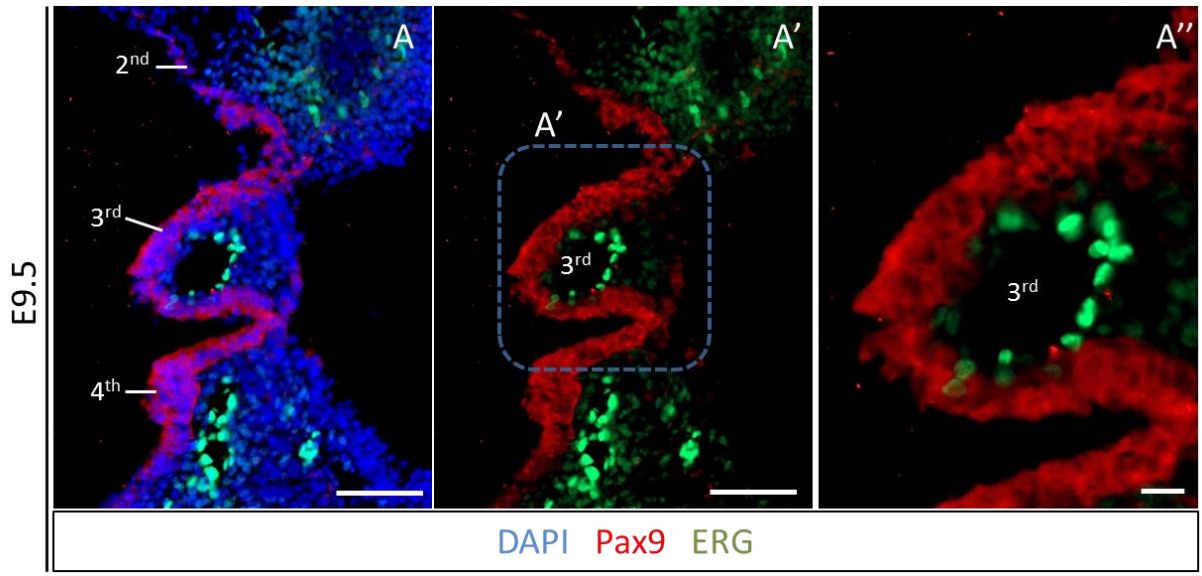

Figure 6-10: Dual immunostaining for *Pax9* expression and endothelium.
(**A-A'**) A coronal section of a *Pax9cre;eYFP* embryo at E9.5, immunostained with antibodies for GFP (red) and ERG (green) to mark the pharyngeal endoderm and PAA endothelium respectively of the 3rd pharyngeal arch. The endothelial layer of the 3rd PAA appears to be in close apposition with the pharyngeal endoderm (**A''**). Scale bar indicate 10 µm.

The immunostaining showed the luminal surface of the 3rd PAA was a single layer of endothelial cells. Moreover, the endothelial layer appeared to be in close apposition with the endoderm. However, either a single, or more, layers of cells appeared to separate the endothelium from the endoderm. To identify the identity of these layers, an antibody to AP2α, which is a marker for NCC and the most likely candidate for a cell in this location, was used. The immunostaining revealed a layer of AP2α positive cells between the endoderm and the endothelium, indicating that a layer of NCC is separating the endoderm from the endothelium (Figure 6-11).

This data suggested a possibility for communication between the endoderm, the vascular endothelium and the NCC since all the layers are in contact with each other and this could make it possible for *Pax9* and *Msx1* to interact with each other through a non-cell autonomous interaction with neighboring cells.

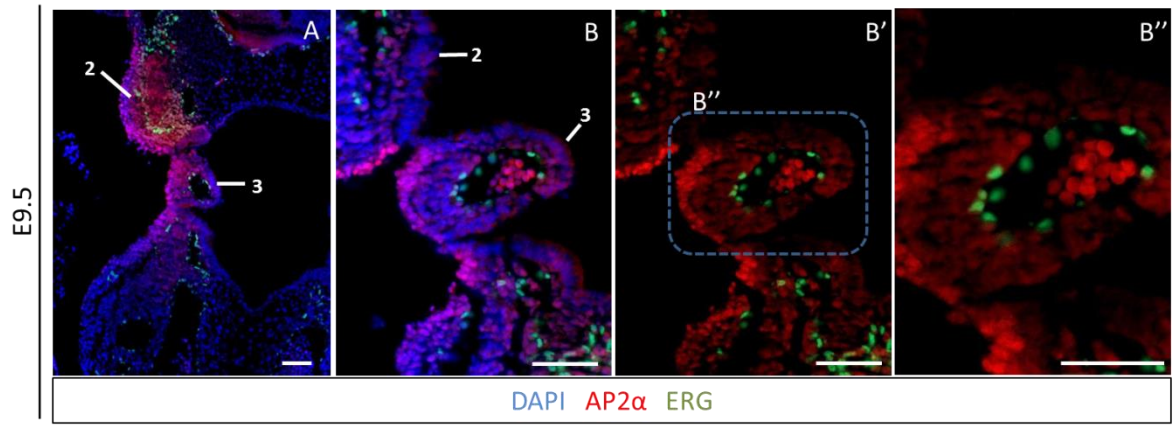

Figure 6-11: Dual immunostaining for NCC and endothelial cells.
Immunostaining was performed with antibodies raised against AP2α (NCC; red) and ERG (endothelium; green) on a coronal section from an E9.5 embryo. **(A)** Low power image to demonstrate specificity of AP2α staining in NCC and surface ectoderm **(B-B')** Immunostaining shows that NCC are in direct contact with the endothelium. **(B'')** Higher magnification image of **B'**. Scale bar indicate 10 µm.

A RNAseq analysis was performed to compare the transcriptome of wild type and *Pax9*$^{-/-}$ embryos at E9.5. The preliminary analysis of the data indicates that there is a reduced expression of many Notch pathway related genes (Appendix A). Therefore, in an attempt to identify whether Notch signaling between cell types was affected in *Pax9;Msx1* mutant embryos, Notch1 activity was investigated within the pharyngeal arches.

An antibody raised against the active form of Notch1 (the intercellular domain; ICD) was used as a marker to investigate Notch signalling within the 3rd pharyngeal arch in E9.5 embryos. In the control embryos a specific Notch1 signal was found to be expressed in cells forming a continuous ring surrounding the 3rd PAA (n=3) (Figure 6-12, Figure 6-13).

Double immunostaining with the Notch ICD antibody and PECAM1 antibody in control E9.5 embryo sections revealed these to be endothelial cells (Figure 6-12). In the 3rd pharyngeal arch of *Pax9*$^{-/-}$ embryos fewer Notch1 positively stained cells were present and these formed a disrupted ring around the 3rd PAA (Figure 6-13). In *Pax9*$^{-/-}$*;Msx1*$^{+/-}$ embryos, however, a continuous ring of Notch1 positively stained cells was observed around the 3rd PAA, similar to that seen in the wild type (Figure 6-13).

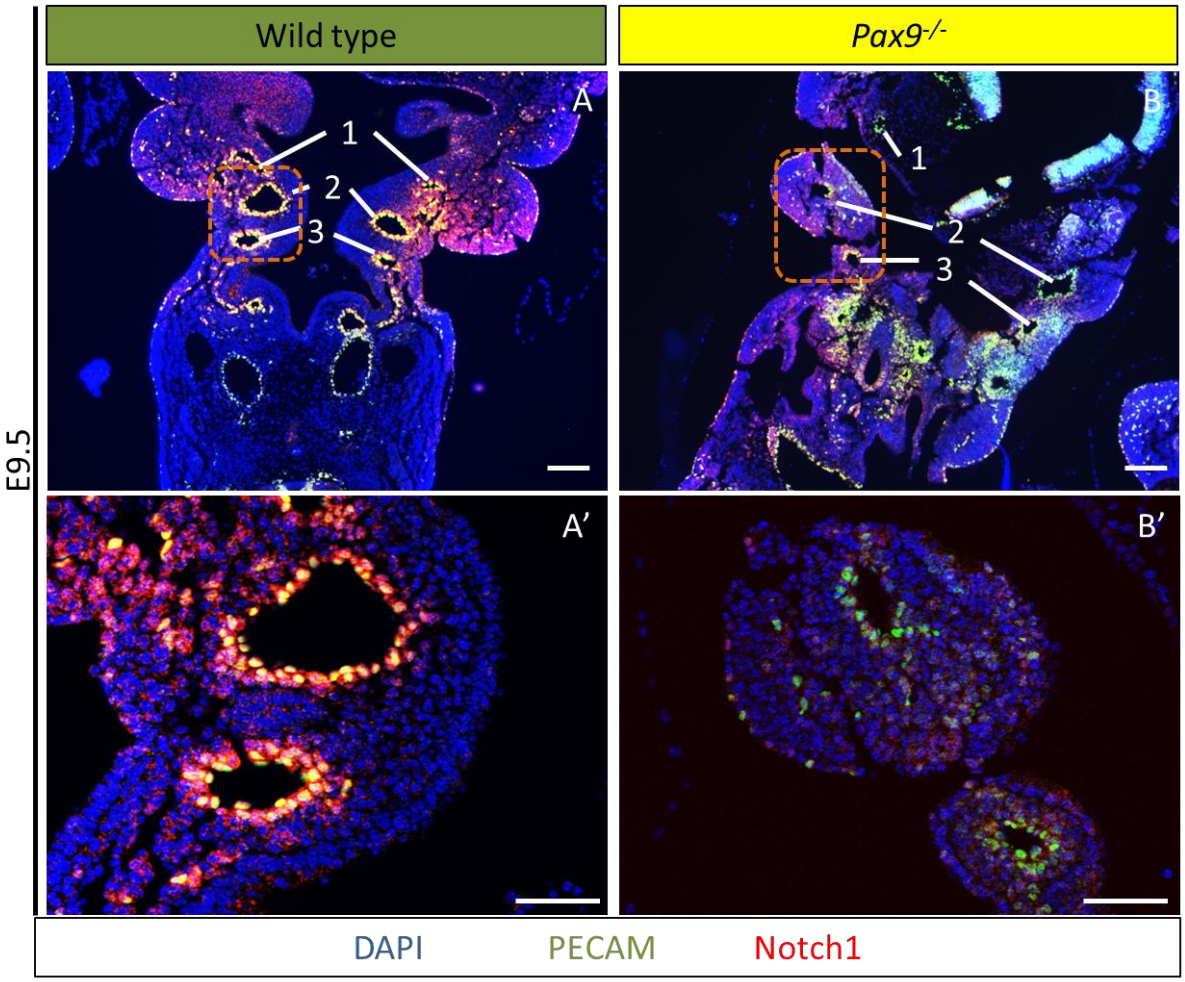

Figure 6-12: Dual immunostaining for Notch1 signaling and endothelial cells within the 3rd pharyngeal arch of E9.5 embryos.
Immunostaining was performed with antibodies raised against antibody raised against the cleaved intracellular domain of Notch1 (red), representing the active form of the protein and PECAM1 (endothelium; green) on a coronal section from an E9.5 embryo. (**A, A'**) Wild type embryo showing Notch1 and PECAM1 overlapping expression in the cells surrounding the 3rd PAA. (**B, B'**) A *Pax9*$^{-/-}$ embryo with reduced Notch1 activity around the 3rd PAA but the PECAM1 staining still strongly expressed (Zainab Akhter). Scale bar indicate 10µm.

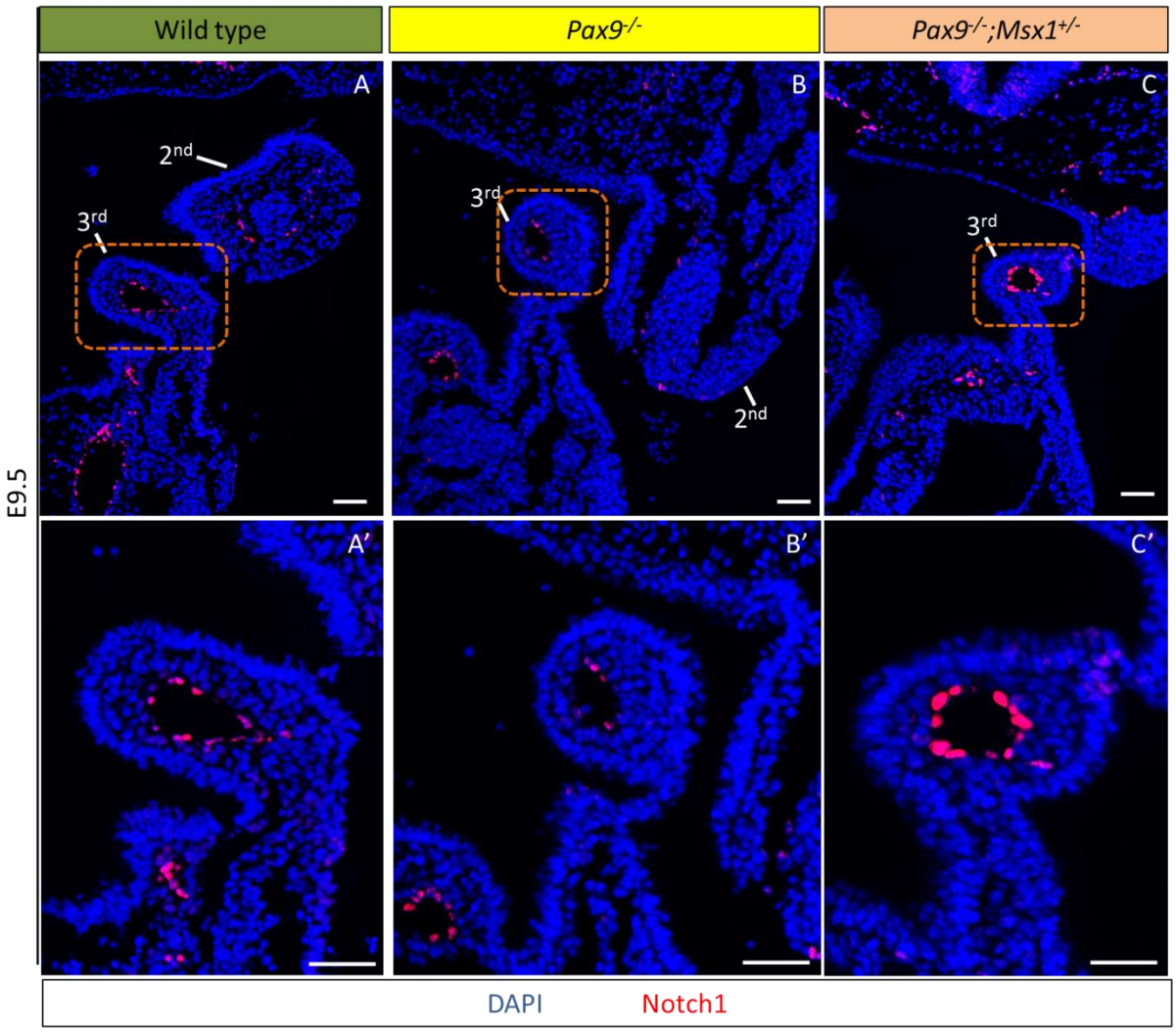

Figure 6-13: Notch1 activity within the 3rd pharyngeal arch of E9.5 embryos.
Coronal sections of E9.5 embryos were immunostained with an antibody raised against the cleaved intracellular domain of Notch1, representing the active form of the protein. (**A, A'**) Wild type embryo showing Notch1 expression in the cells surrounding the 3rd PAA. (**B, B'**) A *Pax9*$^{-/-}$ embryo with reduced Notch1 activity. (**C, C'**) *Pax9*$^{-/-}$;*Msx1*$^{+/-}$ embryo showing a continuous ring of cells with positive Notch1 staining around the 3rd PAA similar to the wild type embryo.
Scale bar indicate 10 µm.

6.4 DISCUSSION

In this chapter, the fate of the cells that comprise the pharyngeal arches was investigated, to see whether any explanation as to how *Msx1* could be modifying the *Pax9*-null cardiovascular phenotype could be found.

Cell proliferation and apoptosis were investigated within the 3rd pharyngeal arch at E9.5 and within the 3rd and 4th pharyngeal arch at E10.5. The results, however, revealed that there was no statistically significant change in either the apoptosis or the proliferation pathway within *Pax9*$^{-/-}$ or *Pax9*$^{-/-}$*;Msx1*$^{+/-}$ embryos compared to wild type, or between *Pax9*$^{-/-}$ and *Pax9*$^{-/-}$*;Msx1*$^{+/-}$ embryos.

The NCC that migrate into the 3rd pharyngeal arches at E10.5 were counted by immunostaining following labelling with an antibody against AP2α, and also by manual counting of all cells between the endoderm and ectoderm. Although this counting method will also include mesoderm-derived cells, the majority of cells will be cNCC (Waldo *et al*., 1996). The data showed that the number of NCC in *Pax9*$^{-/-}$*;Msx1*$^{+/-}$ embryos was not significantly lower than in the controls. Moreover, the number of NCC in *Pax9*$^{-/-}$*;Msx1*$^{+/-}$ embryos was significantly higher than in *Pax9*$^{-/-}$ embryos. This strongly suggests that the heterozygous expression of *Msx1* is allowing more NCC to migrate into the 3rd pharyngeal arch compared to *Pax9*$^{-/-}$ embryos.

Vascular SMC (vSMC) are reported to originate from either the splanchnic mesoderm (Hungerford *et al*., 1996; Saint-Jeannet *et al*., 1992) or NCC (Le Lievre and Le Douarin, 1975). The smooth muscle around the PAA was shown to consist almost exclusively of cNCC derivatives (Le Lievre and Le Douarin, 1975; Waldo and Kirby, 1993). As a result, the smooth muscle around the 3rd PAAs was investigated in E11.5 embryos using immunofluorescence staining. *Pax9*$^{-/-}$ embryos showed little or no recruitment of smooth muscle around the 3rd PAA; only in a few cases a thin disrupted layer of smooth muscle at the side of the 3rd PAA was observed, but no continuous ring around the artery was ever seen. It therefore appears that the reduction in NCC numbers migrating into the 3rd pharyngeal arch directly leads to the lack of smooth muscle cells investing around the 3rd arch artery.

Without the support of the smooth muscle layer around the vessels, the PAA may collapse and/or regress and not participate in the formation of the great vessels (Waldo *et al.*, 1996). In contrast, the 3rd PAA appeared to be well supported with smooth muscle in *Pax9*$^{-/-}$*;Msx1*$^{+/-}$ embryos. This support is likely sufficient to protect the artery from collapsing during remodeling as is likely to be the case in the *Pax9*-null embryos. As Consequently, the 3rd PAA will remain intact and participate in the formation of the cAo observed in *Pax9*$^{-/-}$*;Msx1*$^{+/-}$ embryos and neonates. Calmont *et al* (2009) suggest a similar mechanism to recover the hypoplastic 4th PAA observed in *Tbx1*$^{+/-}$ embryos. *Tbx1* triggers essential directional signals from the pharyngeal endoderm to the adjacent cNCC en-route to the caudal PAA; the NCC differentiate into the smooth muscle supporting the 4th PAA during remodelling and prevent it from collapsing (Calmont *et al.*, 2009). It remains to be seen if the loss of *Msx1* can provide an analogous mechanism of 3rd arch artery maintenance.

This study revealed a possible communication between the pharyngeal endoderm, the endothelium layer of the 3rd PAA and the NCC, since these cells are close to each other and in-touch to each other, which may be an indication of a non-autonomous cell communication between these cells.

As previously mentioned, the results in this chapter also show a significant increase in the number of NCC in *Pax9*$^{-/-}$*;Msx1*$^{+/-}$ embryos compared with *Pax9*$^{-/-}$ embryos. Altogether, these data could suggest that in the reducing the NCC in *Pax9*$^{-/-}$ embryos, the link between the pharyngeal endoderm and the endothelium is disrupted and therefore there is no more communication between these two layers. Conversely, in *Pax9*$^{-/-}$*;Msx1*$^{+/-}$ embryos enough NCC are maintained to keep the communication between the pharyngeal endoderm and the endothelium; these NCC eventually participate in the survival of the 3rd PAA by differentiating into smooth muscle cells that support the remodelling of the 3rd PAA and formation of the modulated aortic arch observed in *Pax9*$^{-/-}$*;Msx1*$^{+/-}$ embryos and neonates. In addition, this may explain how *Pax9*, which is a gene expressed in the pharyngeal endoderm, can communicate with *Msx1*, which is a gene expressed in the NCC.

These data also suggest that *Msx1* could be helping the NCC to remain functionally active in *Pax9*$^{-/-}$*;Msx1*$^{+/-}$ embryos. Consistently, *Msx1* is strongly expressed in migrating NCC, and its expression continues during NCC colonization in the facial

prominences and branchial arches (Catron *et al*., 1996; Hill *et al.*, 1989; MacKenzie *et al*., 1991a). In the pharyngeal arches, the cNCC maintain their positional identity until they receive signals that influence them to achieve their differentiation. For example, *Msx1* is influencing the NCC in the 2nd pharyngeal arch to participate in the formation of the maxillary and the mandibular region (Minoux and Rijli, 2010). In mouse, *Msx1* loss of its function results in multiple craniofacial abnormalities (Satokata and Maas, 1994).

Moreover, *Msx1* inhibits cellular differentiation (Hu *et al.*, 2001). *Msx1* transcription factor regulates the fate of cranial NCC during tooth morphogenesis, it is critical for proliferation of NCC in the dental mesenchyme. Specifically, *Msx1* inhibits the expression of the CDK (*p19^{INK4d}*) inhibitor, thus facilitating cell cycle progression. *Msx1* inhibits *p19^{INK4d}* expression during tooth formation. In *Msx1*-null mutants, elevated *p19^{INK4d}* activity significantly inhibits the phosphorylation of retinoblastoma proteins in the cranial NCC dental mesenchyme. Hypophosphorylation of retinoblastoma proteins prevents the activation of the cell cycle gene and the G_1-to-S phase transition, thus inhibiting cell proliferation in the cranial NCC dental mesenchyme of *Msx1*-null mutants (Han *et al.*, 2003). Additionally, *Msx1* deficiency has been shown to lead to mis-differentiation of the NCC derived dental mesenchyme.

The data in this chapter also shows an apparent rescue for the Notch signaling pathway around the 3rd PAA in *Pax9$^{-/-}$; Msx1$^{+/-}$* embryos compared to *Pax9$^{-/-}$* embryos. In the pharyngeal arches, Notch signaling from the PAA endothelium mediates differentiation of the adjacent NCC layers into vSMC, and the region of active Notch around the PAA endothelium corresponds to the area within which NCC undergo vSMC differentiation (High *et al.*, 2007; Manderfield *et al.*, 2012). Moreover, Notch also plays a critical, cell-autonomous role in the differentiation of cNCC into smooth muscle cells both *in vitro* and *in vivo* (High *et al*., 2007).

7 FINAL DISCUSSION

Pax9 plays an important role in cardiovascular development, particularly for the correct development of the PAA. By reducing *Msx1* levels in *Pax9*-null embryos the PAA-associated cardiovascular defects were found to be altered with a modified or even normal aortic arch often observed.

7.1 *Pax9*-NULL PHARYNGEAL ARCH ARTERY PHENOTYPES

Pax9 clearly has an important role in cardiovascular development, as absence of this gene results in severe cardiovascular defects. Embryos lacking *Pax9* have developmental malformations of the 3rd and 4th PAA but the etiology of the defects affecting each PAA appears to be very different. The 3rd PAA carries blood for a while, but then becomes hypoplastic and collapses. This results in absent common carotid arteries and the internal and external carotids arising directly from the main arch arteries. In contrast, the 4th PAA never forms. The lack of formation of the 4th PAA on the left side leads to IAA, whereas the absent right 4th PAA results in ARSA. However, the mechanisms by which these cardiovascular developmental mutations occur in *Pax9*$^{-/-}$ embryos had not yet been elucidated.

There are two possible explanations as to why the PAA could fail to form correctly in mutant mice. The first way is failure of the PAA to form or remodel properly within a normal arch, which may be due to abnormal signalling events, for example in recruiting NCC. For example, in *Gbx2*-null embryos the 3rd pharyngeal arch forms normally, but the 4th pharyngeal arch appears either hypoplastic or absent, yet this occurs with proper segmentation of the pharyngeal arches (Byrd and Meyers, 2005; Calmont *et al.*, 2009). *Gbx2* mutant embryos also present with defects in the remodelling of the PAA (Byrd and Meyers, 2005). In *Tbx1* heterozygous embryos, the 4th PAA is frequently hypoplastic or absent but segmentation of the pharyngeal arches is normal (Zhang *et al*., 2005). In both of these models migration of NCC has been shown to be perturbed, and this results in the concomitant PAA defects observed (Calmont *et al.*, 2009). Calmont *et al.* (2009) demonstrated that the 4th PAA phenotype originates from a cNCC deficiency at the level of the 4th pharyngeal arch

in both *Gbx2*$^{-/-}$ and *Tbx1*$^{+/-}$ mutants, highlighting a central function for the cNCC in PAA prior to their differentiation into smooth muscle cells.

The second reason that could lead to failure in the proper formation of the PAA is that the pharyngeal arches do not form or segment properly. For example, *Tbx1*-null embryos present with severe defects in the formation and remodelling of the PAA, which are thought to result directly from a lack of distinct segmentation of the caudal pharyngeal arches (Zhang *et al.*, 2006). It appears that the pharyngeal arches caudal to the second arch do not segment resulting in a common arterial trunk formed from the 2nd PAA (S. Bamforth, unpublished observations).

Another example of a gene that leads to cardiovascular malformation because the pharyngeal arches fail to segment properly is *Ripply3*, which is strongly expressed in the pharyngeal ectoderm and the endoderm, in a pattern that partially overlaps with *Tbx1* (Okubo *et al.*, 2011). *Ripply3* homozygous mutant embryos exhibit abnormal development of the caudal pharyngeal arches, in which the 3rd and 4th pharyngeal arches are severely hypoplastic and thin, and as a result, the 3rd and 4th PAA are absent. *Ripply3*-null embryos present with VSD, hypoplastic aorta, IAA and ARSA. Moreover, *Ripply3*$^{-/-}$ embryos have thymus and parathyroid gland abnormalities (Okubo *et al.*, 2011).

In contrast to the above-mentioned mutants, the pharyngeal arches do form in *Pax9*$^{-/-}$ embryos although the 3rd and 4th pharyngeal arches are hypoplastic compared to controls as shown in chapters 4 and 6. This indicates that it is not the actual structure of the arches that is causing the phenotype, but something within the arches that has gone wrong. As *Pax9* is expressed specifically within the pharyngeal endoderm at mid-embryogenesis (section 1.6.1 and section 4.3.5), a time that is critical for PAA morphogenesis, this indicates that the phenotype could be derived directly by a problem with the endoderm.

Previous studies have looked at the role of the pharyngeal endoderm during embryonic development using Cre-LoxP mediated conditional knockout mice. These studies show that the pharyngeal endoderm plays an important role in directing pharyngeal arch development. For example, endodermal deletion of *Tbx1* resulted in embryos failing to form the caudal pharyngeal pouches (Jackson *et al*., 2014), and

resulted in defects of the thymus and the outflow tract (Arnold *et al*., 2006; Xu *et al*., 2005). The pharyngeal ectoderm, however, does not appear to be required for pouch morphogenesis and pharyngeal segmentation (Calmont *et al*., 2009; Zhang *et al*., 2005). Also, *Tbx1* deletion from the pharyngeal mesoderm was sufficient to cause caudal pharyngeal segmentation defects and thymus aplasia (Zhang *et al.*, 2006). All this indicates that *Tbx1* is important in the pharyngeal endoderm more than the mesoderm and the ectoderm.

Fgf8$^{neo/-}$ mice (a hypomorphic mutant) also present with abnormal cardiovascular patterning, including outflow tract, arch artery and intracardiac defects (Abu-Issa *et al*., 2002), *Fgf8* is expressed in the pharyngeal ectoderm and endoderm. Ablating *Fgf8* from the pharyngeal arch endoderm causes failure of formation of the 4th PAA resulting in aortic arch and subclavian artery malformation including DORV, IAA and ARSA. Surprisingly, however, no cardiac, outflow tract or glandular defects were found in ectodermal-domain mutants (Macatee *et al.*, 2003).

These studies and the data shown in this thesis strongly suggest that the pharyngeal endoderm maybe a key player in organizing the PAA, and could be important for the development and remodelling of the PAA.

This thesis has demonstrated that *Pax9*$^{-/-}$ embryos have a significant reduction in the number of NCC within the 3rd and 4th pharyngeal arches. Loss of *Tbx1* or *Gbx2* from the pharyngeal ectoderm results in 4th PAA abnormalities associated with cNCC deficiency in the 4th pharyngeal arch. This is thought to be a result of a non-cell-autonomous function for *Tbx1* or *Gbx2* in cNCC migration and correlates the 4th PAA deficiency with cNCC migration defects (Calmont *et al.*, 2009). Because if this, it was speculated that a similar non-cell autonomous function for *Pax9* expression within the pharyngeal endoderm and its effect on NCC, since loss of *Pax9* from the pharyngeal endoderm is associated with reduction in NCC numbers within the 3rd pharyngeal arch similar to *Tbx1* and *Gbx2* mutant embryos. The NCC within the pharyngeal arches will differentiate to smooth muscle surrounding the PAA, which is necessary for persistence of the PAA during remodelling.

7.2 LOSS of *Msx1* MODULATES THE *Pax9*-NULL PHENOTYPE

The data presented in this thesis strongly demonstrates that *Msx1* heterozygosity modifies the *Pax9*-null phenotype: the cardiovascular defects are less severe and the pre-axial limb duplication does not occur. Although *Msx1* deletion alone does not cause any cardiovascular defects (Chen *et al.*, 2007) this does not exclude the possibility that this gene is important during cardiovascular development. Several studies indicate that *Msx1* and *Msx2* double mutants mice have cardiovascular defects affecting the heart outflow tract and reduced endocardial cushion formation (Chen *et al*., 2008; Satokata and Maas, 1994), which suggests that there may be some complementary roles for *Msx1* and *Msx2* transcription factors in heart development, or that an element of redundancy occurs.

Msx1 and *Msx2* have 98% homology with each other (Khadka *et al.*, 2006). They exhibit dynamic and partially overlapping patterns of expression during organogenesis (Coelho *et al.*, 1991; Davidson *et al.,* 1991; Robert *et al*., 1989). Both genes are expressed in the ectoderm and underlying mesenchyme of the developing limb, in mesenchyme derived from the cranial neural crest, in developing eye, ear, teeth, and heart and the migratory NCC to the OFT (Davidson *et al.*, 1991; Hill *et al.*, 1989).

Msx1 and *Msx2* could also be involved in epithelial-mesenchymal interactions that link growth of a tissue to its patterning (Muneoka and Sassoon, 1992). The functions of *Msx1* and *Msx2* in epithelial-mesenchymal interactions were investigated with chicken-mouse interspecies grafts (Davidson *et al*., 1991) and in chicken by removal of the apical ectodermal ridge (Ros *et al.*, 1992) and by analysis of *Msx1* expression in limbless mutants (Coelho *et al.*, 1991). Results of these studies suggest that *Msx1* expression in the progress zone may depend upon a signal provided by the apical ectodermal ridge, whereas *Msx2* could be involved in some aspect of apical ectodermal ridge function. *Msx1* may inhibit the proliferative and regulate undifferentiated, properties of cells of the progress zone, as suggested by the differentiation-defective phenotype of myogenic cells in which *Msx1* expression has been ectopically induced (Song *et al.*, 1992).

When *Msx1* levels are reduced in *Pax9*-null embryos, either by removing one allele of *Msx1* or both, the severity of the cardiovascular phenotype is reduced or may even be absent. In double mutant embryos (i.e. *Pax9*$^{-/-}$;*Msx1*$^{-/-}$) only one out of six had a cardiovascular phenotype (IAA) but all mutant embryos lacked the pre-axial digit duplication seen in *Pax9*$^{-/-}$ embryos. This suggests that a more profound rescue of the *Pax9*-null phenotype occurs with total loss of *Msx1*, although the cleft palate and absent thymus phenotypes were not rescued.

The literature contains many examples of complex genotypes in transgenic mouse models that can make the phenotype worse, but it is unusual to find an example of a rescue similar to that presented in this study. For example, the transcription factor, *Pbx1,* is implicated in the events underlying the patterning of the PAA and formation of the cardiac outflow tract as *Pbx1*-null embryos have a common arterial trunk associated with VSD, ARSA and absence of the arterial duct (Chang *et al.*, 2008). Surprisingly, the loss of one or both alleles of *Msx2*, modulated the *Pbx1*-null phenotype, making it less severe. *Pbx1*$^{-/-}$;*Msx2*$^{+/-}$ embryos had a reduce in the incidence of common arterial trunk, in which *Pbx1*$^{-/-}$;*Msx2*$^{+/-}$ embryos showed a significant decrease in the incidence of common arterial trunk, whereas *Pbx1*$^{-/-}$;*Msx2*$^{-/-}$ embryos had no common arterial trunk defects at all in which they show a separation of the distal part of the outflow tract. This indicates that removing *Msx2* in *Pbx1*$^{-/-}$ embryos leads to rescue of the outflow tract defect. However, *Pbx1*$^{-/-}$;*Msx2*$^{+/-}$ and *Pbx1*$^{-/-}$;*Msx2*$^{-/-}$ embryos still exhibit the same spectrum of great artery defects such as ARSA (Chang *et al.*, 2008). The main mechanism suggested for this rescue is that supressing *Msx2* leads to a potential recovery of the NCC, which contributed to outflow tract septation in *Pbx1*$^{-/-}$ embryos. This is analogous to the phenotypic rescue described in this thesis in *Pax9*$^{-/-}$;*Msx1*$^{+/-}$ and *Pax9*$^{-/-}$;*Msx1*$^{-/-}$ embryos, in which a reduction in *Msx1* rescue the *Pax9*$^{-/-}$ PAA defects.

7.3 EXPLORING A CELLULAR MECHANISM ALLOWING LOSS OF *Msx1* TO MODULATE THE *Pax9*-NULL CARDIOVASCULAR PHENOTYPE

Pax9 and Msx1 proteins are able to physically interact during craniofacial development (Nakatomi *et al.*, 2010) and *in vitro* (section 4.3.4). A direct interaction within the pharyngeal region, however, does not seem possible as *Pax9* and *Msx1* are expressed in separate and distinct domains at mid-embryogenesis: *Pax9* in the endoderm and *Msx1* in the NCC. It is possible that Pax9 and Msx1 are acting independently of each other, although they may be part of a gene regulatory network.

Expression of the *Msx1* gene is closely related to the development of NCC. The early expression of *Msx1* demarcates the area in which the NCC migrate (Waldo *et al.*, 1996). Immunofluorescent staining using Ap2α as a marker for the NCC showed a significant decrease in the number of NCC within the 3rd pharyngeal arch of $Pax9^{-/-}$ embryos at E10.5. In $Pax9^{-/-};Msx1^{+/-}$ embryos, however, the number of NCC were significantly increased compared with $Pax9^{-/-}$ embryos. Moreover, in $Pax9^{-/-};Msx1^{+/-}$ there was no significant difference observed in the number of NCC between $Pax9^{-/-};Msx1^{+/-}$ embryos and the wild type embryos at E10.5.

Msx1 has been shown to be an inhibitor of cellular differentiation (Hu *et al.*, 2001). For example, *Msx1* inhibits the expression of the CDK ($p19^{INK4d}$) inhibitor (see discussion of chapter 6). More evidence to support this comes from cell culture data, which have shown that forced expression of *Msx1* in myogenic precursors blocks their differentiation and represses expression of lineage specific genes, such as MyoD (Song *et al*., 1992; Woloshin *et al.*, 1995). Moreover, ectopic expression of *Msx1* during chicken embryogenesis inhibits development of the limb musculature and represses MyoD expression *in vivo* (Bendall *et al*., 1999). All this suggests that *Msx1* may inhibit differentiation of NCC to smooth muscle in the pharyngeal arches, while reduced expression of *Msx1* may leads to reinstated cNCC differentiation to smooth muscle around the 3rd PAA.

cNCC originate from the neural tube (Kirby *et al*., 1983). They migrate through the posterior pharyngeal arches to the cardiac outflow tract and the proximal great vessels (Kirby and Waldo, 1990). During remodelling of the PAA system, the contribution of NCC is thought to be the major determinant of whether a particular

vascular component persist or is reabsorbed (Bockman *et al.*, 1989) since they can contribute to the development of the vascular smooth muscle cell layer of the PAA (Bergwerff *et al.*, 1999; Byrd and Meyers, 2005).The smooth muscle formation is important because it supports the PAA during remodelling (Waldo *et al.*, 1996).

It is possible that the 3rd PAA fails to form in *Pax9*$^{-/-}$ embryos as a result of absence of smooth muscle cells that are supposed to envelop the 3rd PAA, as the smooth muscle cells are required to sustain the structure of the PAA, preventing them from collapsing. This does fit with the finding that *Pax9*$^{-/-}$ embryos have a significant reduction in the number of NCC where the 3rd PAA collapses, and in *Pax9*$^{-/-}$*;Msx1*$^{+/-}$ embryos with wild-type numbers of NCC where the 3rd PAA is maintained. As a result, the 3rd PAA may remain connected with the carotid duct, which will lead to the formation of the cervical aorta.

To address the potential communication between *Pax9* and *Msx1* expressing cells, a direct contact between the endothelial layer with both the endoderm layer and the NCC were investigated. The results show that these three layer are in close proximity to each other suggesting that a form of non-autonomous cell communication occurs between these three cell types within the pharyngeal arch. This would allow *Pax9* and *Msx1* expressing cells to communicate with each other. Notch signalling was investigated at E9.5 and this showed that an activated Notch signal is robustly expressed in the endothelial cells of the 3rd PAA in wildtype embryos. *Pax9*-null embryos showed a reduction in Notch signalling within the endothelial cells, despite the staining showing no reduction in the endothelial cell numbers. Finally, the results presented a normal Notch signal in *Pax9*$^{-/-}$*;Msx1*$^{+/-}$ embryos, similar to the wild type embryos.

The mechanism for how Notch participates in this communication is not clear, but we can hypothesise that perhaps Notch sets up another signalling event for the smooth muscle cells later and helps the NCC differentiate.

The Notch signalling pathway is involved in cell fate and differentiation throughout the embryo. Alagille syndrome is an autosomal dominant disorder characterized by defects involving the cardiac outflow tract, and this syndrome is caused by mutation in Jagged1, a ligand for the Notch receptor (Li *et al.*, 1997; Oda *et al.*, 1997).

The data of the present study are consistent with the concept that Notch induces an endothelial to mesenchymal communication as the Notch signalling pathway is activated in more endothelial cells of the 3rd PAA of *Pax9*$^{-/-}$;*Msx1*$^{+/-}$ embryos compared to *Pax9*$^{-/-}$ embryos. The underlying mechanism requires further elucidation. Notch activation may indirectly affect the transcription of genes found in NCC within the mesenchyme of the pharyngeal arches and facilitates the complex process of NCC differentiation to smooth muscle around the PAA. This supports the concept that cell-to-cell communication contributes to dictate cell fate (Trainor and Krumlauf, 2001). Obviously, the activation of Notch signaling is only one of multiple possible cell-to-cell communication pathways within the pharyngeal arches and other signalling pathways will need to be investigated to identify the exact communication mechanism between the pharyngeal endoderm, NCC and the endothelial of the PAA.

7.4 FUTURE WORK

The finding that *Pax9* and *Msx1* affect each other even though they are not expressed within the same cells in the pharyngeal arches during embryogenesis raises a question about how the endoderm affects the development of a blood vessel, and how genes not expressed within the same domain could affect each other. It is clear that there is contact between the endoderm, NCC and the endothelial layers in wild type embryos. This cell to cell communication will need to be studied in more detail, in wild type and in *Pax9*$^{-/-}$ embryos, to understand the signaling processes that occur. These can then be investigated in mutant embryos to see what is being affected that could cause a failure of the PAA to form correctly. *Msx1* mutation could also be included to determine if the presence of *Msx1* affects this communication.

The present work shows a decrease in Notch signalling in *Pax9*$^{-/-}$ embryos, while this same signalling appears to be restored to the normal levels in *Pax9*$^{-/-}$;*Msx1*$^{+/-}$ embryos. However, the exact mechanism for how Notch signalling plays in both *Pax9*$^{-/-}$ and *Pax9*$^{-/-}$;*Msx1*$^{+/-}$ embryos is still unclear, therefore further investigations will be required to uncover the role of Notch signalling within the endothelium of the pharyngeal arches in both *Pax9*$^{-/-}$ and *Pax9*$^{-/-}$;*Msx1*$^{+/-}$ embryos.

Furthermore, it would be interesting to generate *Pax9;Msx2* double heterozygous mice and *Pax9;Msx1;Msx2* triple heterozygotes, and use them to analyse the incidence of 3rd and 4th PAA defects.

Another question that needs to be addressed is PAA formation. In this work, we were looking at a snapshot during the formation of the PAA using immunostaining, ink injection and imaging techniques, but this could leave gaps in our understanding about how the PAA form. To solve this problem, *Pax9*$^{-/-}$ and *Pax9*$^{-/-}$*;Msx1*$^{+/-}$ embryos could be dissected and collected at E9.0. At this stage, the 3rd PAA start to form while the 4th PAA is not formed yet. These embryos could then be cultured in a defined medium in an atmosphere of 95% O2 / 5% CO2 in a rolling bottle culture apparatus at 37°C for 16-40 hours, and should exhibit morphological growth and development comparable to embryos developing *in utero*. Using a live-imaging camera, the formation processes of the 3rd and 4th PAA in a continuous video recording could be captured instead of just a snapshot. After that, the embryos that had been cultured could be processed for histological analysis.

7.5 CONCLUSIONS

The data presented in this thesis demonstrates that *Pax9* is required for correct development of the PAA. Moreover, a genetic reduction in *Msx1* levels modulates the aortic arch artery defects that are seen in *Pax9*$^{-/-}$ embryos and neonates.

Studying the genetic background shows that the genetic background affects the penetrance of the cardiac phenotype (VSD and DORV) in *Pax9*$^{-/-}$ mice, but it is not affecting the PAA abnormalities.

The results also demonstrate that *Msx1* plays a role in correcting *Pax9*$^{-/-}$-induced aortic arch defects. This indicates that *Msx1* is acting as a modifier gene that supresses the interrupted aortic arch phenotype in *Pax9*$^{-/-}$ embryos and neonates

Cleft palate is not the main cause of death for *Pax9*$^{-/-}$ embryos. The evidence presented in this thesis suggests that the deformities in the hyoid bone are the main cause of death for these mice.

Msx1 and *Pax9* have been shown to interact with each other at the protein level during tooth development, however, within the pharyngeal arches they cannot

directly interact since they are not expressed in the same area during embryogenesis.

The hypoplastic 4th PAA observed in *Pax9*$^{-/-}$*;Msx1*$^{-/-}$ embryos appears to be recovered later during development and participate in the formation of a normal arch of aorta, similarly to the wild type embryos.

Finally, the results presented in this thesis have led to the construction of the following model that may explain the interaction between *Pax9* and *Msx1* during the formation of the PAA (Figure 7-1). In wild type embryos, *Pax9* is possibly supressing, either directly or indirectly, *Msx1*, leading to increased NCC proliferation within the pharyngeal arches. NCC have a ligand for Notch and Notch activity is expressed in the endothelial cells of the 3rd PAA. It is proposed that Notch will activate genes in the endothelial cells which will subsequently lead to the differentiation of NCC to smooth muscle cells that will support the remodelling of the 3rd PAA (Figure 7-1 A).

In this model, with *Pax9*$^{-/-}$ embryos here is no *Pax9* to directly or indirectly supress *Msx1*, so *Msx1* will either reduce the proliferation or inhibit the differentiation of the NCC in the mesenchyme. As a result, there will be fewer NCC within the 3rd pharyngeal arch which means there are fewer Notch ligands. The amount of endothelial cells is similar to that in the wild type but Notch activity reduced, meaning there is not enough ligand to activate Notch within the endothelial cells. This then prevents NCC from differentiating into smooth muscle, by an unknown sequence of signalling events. As a result, there will be no smooth muscle to support the third PAA during remodelling and the vessel will collapse (Figure 7-1 B).

Pax9$^{-/-}$*;Msx1*$^{+/-}$ and *Pax9*$^{-/-}$*;Msx1*$^{-/-}$ embryos do not have *Pax9* but they have either half or no *Msx1*, which means that *Msx1* expression is naturally reduced in these embryos. As a result, the effect of *Msx1* on the NCC in the mesenchyme is reduced as well. The NCC will proliferate, at the same time, the endothelial cells in *Pax9*$^{-/-}$*;Msx1*$^{+/-}$ embryos appear to have Notch activity similar to the wild type embryos. The Notch ligand in the NCC will bind to the Notch receptors in the endothelium and this will lead to the differentiation of NCC to vSMC around the 3rd PAA which supports the remodelling of the vessel (Figure 7-1 C).

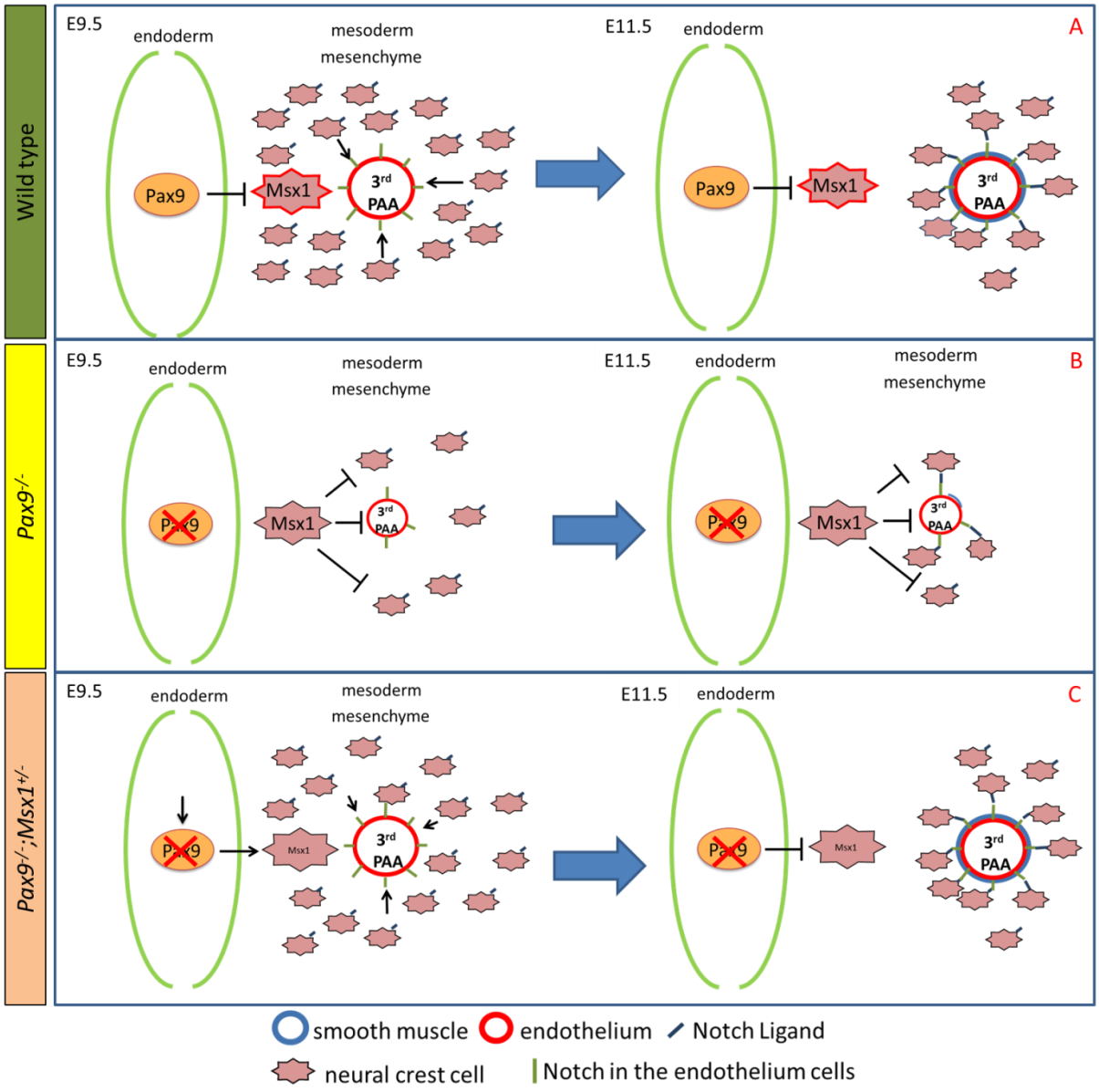

Figure 7-1: Proposed model to explain the interaction between *Pax9* and *Msx1* in the pharyngeal arches.
Based on the results from the dissertation this model was proposed. (**A**) In E9.5 wild type embryos, *Pax9* is suppressing *Msx1* in NCC. The NCC express a Notch ligand that leads to activated Notch signaling within the endothelial cells. By E11.5 a Notch dependent signaling event occurs allowing the NCC to differentiate into vSMC and support the 3rd PAA during remodeling. (**B**) In *Pax9*$^{-/-}$ embryo, there is no *Pax9* to suppress *Msx1*, NCC numbers are reduced. This results in a reduction in Notch signaling within the endothelial cells and a failure of NCC to differentiate into vSMC and the 3rd PAA collapses.. (**C**) In *Pax9*$^{-/-}$;*Msx1*$^{+/-}$ embryos there is no *Pax9* and *Msx1* is genetically reduced, allowing NCC to be present in the pharyngeal arch. This leads to restored Notch activity in the endothelial cells, which will lead to NCC differentiating into vSMC, which will support the 3rd PAA during remodeling.

Appendix A. Notch related genes significantly (p<0.05) differentially expressed in E9.5 *Pax9-null* embryos as identified by RNAseq analysis

Gene_symbol	Description	Component
Mib2	mindbomb homolog 2	Activation
Neurl4	neuralized homolog 4	?
Cntn2	contactin 2	Ligand
Dll3	delta-like 3	Ligand
Cntn1	contactin 1	ligand
Jag2	jagged 2	Ligand
Notch1	notch 1	Receptor
Notch2	notch 2	Receptor
Notch3	notch 3	Receptor
Adamts15	a disintegrin-like and metallopeptidase (reprolysin type) with thrombospondin type 1 motif, 15	S2 cleavage
Adam19	a disintegrin and metallopeptidase domain 19 (meltrin beta)	S2 cleavage
Adamts12	a disintegrin-like and metallopeptidase (reprolysin type) with thrombospondin type 1 motif, 12	S2 cleavage
Adamts7	a disintegrin-like and metallopeptidase (reprolysin type) with thrombospondin type 1 motif, 7	S2 cleavage
Adamts4	a disintegrin-like and metallopeptidase (reprolysin type) with thrombospondin type 1 motif, 4	S2 cleavage
Ncstn	nicastrin	S3 cleavage
Psen2	presenilin 2	S3 cleavage
Aph1a	anterior pharynx defective 1a homolog (C. elegans)	S3 cleavage
Psen1	presenilin 1	S3 cleavage
Maml1	mastermind like 1	Co-activator
Maml3	mastermind like 3	Co-activator
Hes1	hairy and enhancer of split 1	Tx repressor
Hey2	hairy/enhancer-of-split related with YRPW motif	Tx repressor
Hdac5	histone deacetylase 5	Hdac (TxF repression)
Hdac6	histone deacetylase 6	Hdac (TxF repression)
Hdac7	histone deacetylase 7	Hdac (TxF repression)
Hdac11	histone deacetylase 11	Hdac (TxF repression)
Furin	furin (paired basic amino acid cleaving enzyme)	S1 cleavage

References

Abu-Issa, R., Smyth, G., Smoak, I., Yamamura, K., Meyers, E.N., 2002. Fgf8 is required for pharyngeal arch and cardiovascular development in the mouse. Development 129, 4613-4625.

Aggarwal, V.S., Morrow, B.E., 2008. Genetic modifiers of the physical malformations in velo-cardio-facial syndrome/DiGeorge syndrome. Dev Disabil Res Rev 14, 19-25.

Almeida, C.V., Andrade, S.C., Saito, C.P., Ramenzoni, L.L., Line, S.R., 2010. Transcriptional analysis of the human PAX9 promoter. J Appl Oral Sci 18, 482-486.

Anderson, M.J., Pham, V.N., Vogel, A.M., Weinstein, B.M., Roman, B.L., 2008. Loss of unc45a precipitates arteriovenous shunting in the aortic arches. Dev Biol 318, 258-267.

Anderson, R.H., Chaudhry, B., Mohun, T.J., Bamforth, S.D., Hoyland, D., Phillips, H.M., Webb, S., Moorman, A.F., Brown, N.A., Henderson, D.J., 2012. Normal and abnormal development of the intrapericardial arterial trunks in humans and mice. Cardiovasc Res 95, 108-115.

Anderson, R.H., Webb, S., Brown, N.A., Lamers, W., Moorman, A., 2003. Development of the heart: (3) formation of the ventricular outflow tracts, arterial valves, and intrapericardial arterial trunks. Heart 89, 1110-1118.

Arnold, J.S., Werling, U., Braunstein, E.M., Liao, J., Nowotschin, S., Edelmann, W., Hebert, J.M., Morrow, B.E., 2006. Inactivation of Tbx1 in the pharyngeal endoderm results in 22q11DS malformations. Development 133, 977-987.

Bajolle, F., Zaffran, S., Kelly, R.G., Hadchouel, J., Bonnet, D., Brown, N.A., Buckingham, M.E., 2006. Rotation of the Myocardial Wall of the Outflow Tract Is Implicated in the Normal Positioning of the Great Arteries. Circ Res 98, 421-428.

Bamforth, S.D., Chaudhry, B., Bennett, M., Wilson, R., Mohun, T.J., Van Mierop, L.H., Henderson, D.J., Anderson, R.H., 2013. Clarification of the identity of the mammalian fifth pharyngeal arch artery. Clin Anat 26, 173-182.

Bamforth, S.D., Schneider, J.E., Bhattacharya, S., 2012. High-throughput analysis of mouse embryos by magnetic resonance imaging. Cold Spring Harb Protoc 2012, 93-101.

Batzoglou, S., Pachter, L., Mesirov, J.P., Berger, B., Lander, E.S., 2000. Human and mouse gene structure: comparative analysis and application to exon prediction. Genome Res 10, 950-958.

Beavan, T.E., Fatti, L., 1947. Ligature of aortic arch in the neck. Br J Surg 34, 414-416.

Bendall, A.J., Abate-Shen, C., 2000. Roles for Msx and Dlx homeoproteins in vertebrate development. Gene 247, 17-31.

Bendall, A.J., Ding, J., Hu, G., Shen, M.M., Abate-Shen, C., 1999. Msx1 antagonizes the myogenic activity of Pax3 in migrating limb muscle precursors. Development 126, 4965-4976.

Bergwerff, M., DeRuiter, M.C., Hall, S., Poelmann, R.E., Gittenberger-de Groot, A.C., 1999. Unique vascular morphology of the fourth aortic arches: possible implications for pathogenesis of type-B aortic arch interruption and anomalous right subclavian artery. Cardiovasc Res 44, 185-196.

Bergwerff, M., Verberne, M.E., DeRuiter, M.C., Poelmann, R.E., Gittenberger-de Groot, A.C., 1998. Neural Crest Cell Contribution to the Developing Circulatory System Implications for Vascular Morphology? Circ Res. 82, 221-231.

Bockman, D.E., Redmond, M.E., Kirby, M.L., 1989. Alteration of early vascular development after ablation of cranial neural crest. Anat Rec 225, 209-217.

Bockman, D.E., Redmond, M.E., Waldo, K., Davis, H., Kirby, M.L., 1987. Effect of neural crest ablation on development of the heart and arch arteries in the chick. Am J Anat 180, 332-341.

Boogerd, C.J., Moorman, A.F., Barnett, P., 2010. Expression of muscle segment homeobox genes in the developing myocardium. Anat Rec (Hoboken) 293, 998-1001.

Bradshaw, L., Chaudhry, B., Hildreth, V., Webb, S., Henderson, D.J., 2009. Dual role for neural crest cells during outflow tract septation in the neural crest-deficient mutant Splotch(2H). J Anat 214, 245-257.

Brun, T., He, K.H.H., Lupi, R., Boehm, B., Wojtusciszyn, A., Sauter, N., Donath, M., Marchetti, P., Maedler, K., Gauthier, B.R., 2008. The diabetes-linked transcription factor Pax4 is expressed in human pancreatic islets and is activated by mitogens and GLP-1. Human molecular genetics 17, 478-489.

Bruneau, B.G., 2008. The developmental genetics of congenital heart disease. Nature Publishing Group 451, 943-948.

Buckingham, M., Meilhac, S., Zaffran, S., 2005. Building the mammalian heart from two sources of myocardial cells. Nat Rev Genet 6, 826-835.

Burn, J., Goodship, J., 1996. Developmental genetics of the heart. Curr Opin Genet Dev 6, 322-325.

Burton, Q., Cole, L.K., Mulheisen, M., Chang, W., Wu, D.K., 2004. The role of Pax2 in mouse inner ear development. Dev Biol 272, 161-175.

Byrd, N.A., Meyers, E.N., 2005. Loss of Gbx2 results in neural crest cell patterning and pharyngeal arch artery defects in the mouse embryo. Dev Biol 284, 233-245.

Cai, C.L., Liang, X.Q., Shi, Y.Q., Chu, P.H., Pfaff, S.L., Chen, J., Evans, S., 2003. Isl1 identifies a cardiac progenitor population that proliferates prior to differentiation and contributes a majority of cells to the heart. Developmental Cell 5, 877-889.

Calmont, A., Ivins, S., Van Bueren, K.L., Papangeli, I., Kyriakopoulou, V., Andrews, W.D., Martin, J.F., Moon, A.M., Illingworth, E.A., Basson, M.A., Scambler, P.J., 2009. Tbx1 controls cardiac neural crest cell migration during arch artery development by regulating Gbx2 expression in the pharyngeal ectoderm. Development 136, 3173-3183.

Caprio, C., Baldini, A., 2014. p53 Suppression partially rescues the mutant phenotype in mouse models of DiGeorge syndrome. Proc Natl Acad Sci U S A 111, 13385-13390.

Catron, K.M., Wang, H., Hu, G., Shen, M.M., Abate-Shen, C., 1996. Comparison of MSX-1 and MSX-2 suggests a molecular basis for functional redundancy. Mech Dev 55, 185-199.

Catrona, K.M., Wanga, H., Hila, G., Shena, M.M., Abate-Shena, C., 1996. Comparison of MSX -1 and MSX -2 suggests a molecular basis for functional redundancy Mechanisms of Development 55, 185-199.

Cetta, F., Boston, U.S., Dearani, J.A., Hagler, D.J., 2005. Double outlet right ventricle: opinions regarding management. Curr Treat Options Cardiovasc Med. 5, 385-390.

Chakraborty, S., Combs, M.D., Yutzey, K.E., 2010. Transcriptional regulation of heart valve progenitor cells. Pediatr Cardiol 31, 414-421.

Chang, C.P., Stankunas, K., Shang, C., Kao, S.C., Twu, K.Y., Cleary, M.L., 2008. Pbx1 functions in distinct regulatory networks to pattern the great arteries and cardiac outflow tract. Development 135, 3577-3586.

Chapman, D.L., Garvey, N., Hancock, S., Alexiou, M., Agulnik, S.I., Gibson-Brown, J.J., Cebra-Thomas, J., Bollag, R.J., Silver, L.M., Papaioannou, V.E., 1996. Expression of the T-box family genes, Tbx1-Tbx5, during early mouse development. Developmental dynamics : an official publication of the American Association of Anatomists 206, 379-390.

Chen, L., Fulcoli, F.G., Ferrentino, R., Martucciello, S., Illingworth, E.A., Baldini, A., 2012. Transcriptional control in cardiac progenitors: Tbx1 interacts with the BAF chromatin remodeling complex and regulates Wnt5a. PLoS Genet 8, e1002571.

Chen, Y., Bei, M., Woo, I., Satokata, I., Maas, R., 1996. Msx1 controls inductive signaling in mammalian tooth morphogenesis. Development 122, 3035-3044.

Chen, Y.H., Ishii, M., Sucov, H.M., Maxson, R.E., Jr., 2008. Msx1 and Msx2 are required for endothelial-mesenchymal transformation of the atrioventricular cushions and patterning of the atrioventricular myocardium. BMC Dev Biol 8, 75.

Chen, Y.H., Ishii, M., Sun, J., Sucov, H.M., Maxson, R.E., Jr., 2007. Msx1 and Msx2 regulate survival of secondary heart field precursors and post-migratory proliferation of cardiac neural crest in the outflow tract. Dev Biol 308, 421-437.

Chisaka, O., Kameda, Y., 2005. Hoxa3 regulates the proliferation and differentiation of the third pharyngeal arch mesenchyme in mice. Cell Tissue Res 320, 77-89.

Chograni, M., Derouiche, K., Chaabouni, M., Lariani, I., Bouhamed, H.C., 2014. Molecular analysis of the PAX6 gene for aniridia and congenital cataracts in Tunisian families. Hum Genome Var 1, 14008.

Christoffels, V.M., Habets, P.E., Franco, D., Campione, M., de Jong, F., Lamers, W.H., Bao, Z.Z., Palmer, S., Biben, C., Harvey, R.P., Moorman, A.F., 2000. Chamber formation and morphogenesis in the developing mammalian heart. Dev Biol 223, 266-278.

Coceani, F., Baragatti, B., 2012. Mechanisms for ductus arteriosus closure. Semin Perinatol 36, 92-97.

Coelho, C.N., Krabbenhoft, K.M., Upholt, W.B., Fallon, J.F., Kosher, R.A., 1991. Altered expression of the chicken homeobox-containing genes GHox-7 and GHox-8 in the limb buds of limbless mutant chick embryos. Development 113, 1487-1493.

Conley, M.E., Beckwith, J.B., Mancer, J.F., Tenckhoff, L., 1979. The spectrum of the DiGeorge syndrome. J Pediatr 94, 883-890.

Conway, S.J., Henderson, D.J., Kirby, M.L., Anderson, R.H., Copp, A.J., 1997. Development of a lethal congenital heart defect in the splotch (Pax3) mutant mouse. Cardiovasc Res 36, 163-173.

Cordier, A.C., Haumont, S.M., 1980. Development of thymus, parathyroids, and ultimo-branchial bodies in NMRI and nude mice. Am J Anat 157, 227-263.

Crump, J.G., Swartz, M.E., Kimmel, C.B., 2004. An Integrin-Dependent Role of Pouch Endoderm in Hyoid Cartilage Development. PLOS Biology 2, 1432-1445.

Dahl, E., Koseki, H., Balling, R., 1997. Pax genes and organogenesis. Bioessays 19, 755-765.

Darvasi, A., 1998. Experimental strategies for the genetic dissection of complex traits in animal models. Nat Genet 18, 19-24.

Davidson, D., 1995. The function and evolution of Msx genes: pointers and paradoxes. Trends in genetics : TIG 11, 405-411.

Davidson, D.R., Crawley, A., Hill, R.E., Tickle, C., 1991. Position-dependent expression of two related homeobox genes in developing vertebrate limbs. Nature 352, 429-431.

De Coster, P.J., Marks, L.A., Martens, L.C., Huysseune, A., 2009. Dental agenesis: genetic and clinical perspectives. Journal of Oral Pathology & Medicine 38, 1-17.

DeRuiter, M.C., Groot, A.C.G.-d., Poelmann, R.E., VanIperen, L., Mentink, M.M., 1993. Development of the pharyngeal arch system related to the pulmonary and bronchial vessels in the avian embryo. With a concept on systemic-pulmonary collateral artery formation. Circulation 87, 1306-1319.

Di Nunno, N., Lombardo, S., Costantinides, F., Di Nunno, C., 2004. Anomalies and alterations of the hyoid-larynx complex in forensic radiographic studies. Am J Forensic Med Pathol 25, 14-19.

Dipple, K.M., McCabe, E.R., 2000. Phenotypes of patients with "simple" Mendelian disorders are complex traits: thresholds, modifiers, and systems dynamics. American journal of human genetics 66, 1729-1735.

Doevendans, P.A., Daemen, M.J., Muinck, E.D.d., Smits, J.F., 1998. Cardiovascular phenotyping in mice. Cardiovascular Research 39, 34-49.

Duncan, D., 1995. The function and evolution of Msx genes: pointers and paradoxes. Trends Genet. 10, 405-411.

Emes, R.D., Goodstadt, L., Winter, E.E., Ponting, C.P., 2003. Comparison of the genomes of human and mouse lays the foundation of genome zoology. Hum. Mol. Genet 12, 701–709.

Farrell, M.J., Stadt, H., Wallis, K.T., Scambler, P., Hixon, R.L., Wolfe, R., Leatherbury, L., Kirby, M.L., 1999. HIRA, a DiGeorge syndrome candidate gene, is required for cardiac outflow tract septation. Circulation Research 84, 127-135.

Festing, M.F.W., 2014. Evidence Should Trump Intuition by Preferring Inbred Strains to Outbred Stocks in Preclinical Research. Ilar Journal 55, 399-404.

Fineron, P.W., Turnbull, J.A., Busuttil, A., 1995. Fracture of the hyoid bone in survivors of attempted manual strangulation. J Clin Forensic Med 2, 195-197.

Francou, A., Saint-Michel, E., Mesbah, K., Theveniau-Ruissy, M., Rana, M.S., Christoffels, V.M., Kelly, R.G., 2013. Second heart field cardiac progenitor cells in the early mouse embryo. Biochim Biophys Acta 1833, 795-798.

Franz, T., 1989. Persistent truncus arteriosus in the Splotch mutant mouse. Anat Embryol (Berl) 180, 457-464.

Fukunaga, T., Honjo, T., Sakai, Y., Sasaki, K., Takano-Yamamoto, T., Yamashiro, T., 2014. A case report of multidisciplinary treatment of an adult patient with bilateral cleft lip and palate. Cleft Palate Craniofac J 51, 711-721.

Fulcoli, F.G., Huynh, T., Scambler, P.J., Baldini, A., 2009. Tbx1 Regulates the BMP-Smad1 Pathway in a Transcription Independent Manner. PLoS ONE 4, e6049.

Gabriel, S.B., Salomon, R., Pelet, A., Angrist, M., Amiel, J., Fornage, M., Attie-Bitach, T., Olson, J.M., Hofstra, R., Buys, C., Steffann, J., Munnich, A., Lyonnet, S., Chakravarti, A., 2002. Segregation at three loci explains familial and population risk in Hirschsprung disease. Nature Genetics 31, 89-93.

Garcia-Martinez, V., Schoenwolf, G.C., 1993. Primitive-streak origin of the cardiovascular system in avian embryos. Dev Biol 159, 706-719.

George, E.L., Georges-Labouesse, E.N., Patel-King, R.S., Rayburn, H., Hynes, R.O., 1993. Defects in mesoderm, neural tube and vascular development in mouse embryos lacking fibronectin. Development 119, 1079-1091.

Gok, E., Kafa, I.M., Fedakar, R., 2012. Unusual variation of the hyoid bone: bilateral absence of lesser cornua and abnormal bone attachment to the corpus. Surg Radiol Anat 34, 567-569.

Gordon, J.W., Scangost, G.A., Plotkin, D.J., Barbosaf, J.A., Ruddle, F.H., 1980. Genetic transformation of mouse embryos by microinjection of purified DNA. Proceedings of the National Academy of Sciences of the United States of America 77, 7380-7384.

Goulding, M.D., Chalepakis, G., Deutsch, U., Erselius, J.R., Gruss, P., 1991. Pax-3, a novel murine DNA binding protein expressed during early neurogenesis. EMBO J 10, 1135-1147.

Gournay, V., 2011. The ductus arteriosus: physiology, regulation, and functional and congenital anomalies. Arch Cardiovasc Dis 104, 578-585.

Graham, A., 2001. The development and evolution of the pharyngeal arches. J Anat 199, 133-141.

Graham, A., 2008. Deconstructing the pharyngeal metamere. J Exp Zool B Mol Dev Evol 310, 336-344.

Graham, A., Heyman, I., Lumsden, A., 1993. Even-numbered rhombomeres control the apoptotic elimination of neural crest cells from odd-numbered rhombomeres in the chick hindbrain. Development 119, 233-245.

Graham, A., Okabe, M., Quinlan, R., 2005. The role of the endoderm in the development and evolution of the pharyngeal arches. J Anat 207, 479-487.

Graham, A., Richardson, J., 2012. Developmental and evolutionary origins of the pharyngeal apparatus. Evodevo 3, 24.

Grevellec, A., Tucker, A.S., 2010. The pharyngeal pouches and clefts: Development, evolution, structure and derivatives. Seminars in Cell & Developmental Biology 21, 325-332.

Gridley, T., 2003. Notch signaling and inherited disease syndromes. Human molecular genetics 12 Spec No 1, R9-13.

Guha, S., Grover, V., Aiyer, P., Dhull, J., 2016. A unique case of right cervical aortic arch with anomalous left common carotid artery and absent right common carotid artery. Annals of Medicine and Surgery 9, 58-60.

Guris, D.L., Duester, G., Papaioannou, V.E., Imamoto, A., 2006. Dose-dependent interaction of Tbx1 and Crkl and locally aberrant RA signaling in a model of del22q11 syndrome. Dev Cell 10, 81-92.

Guris, D.L., Fantes, J., Tara, D., Druker, B.J., Imamoto, A., 2001. Mice lacking the homologue of the human 22q11.2 gene CRKL phenocopy neurocristopathies of DiGeorge syndrome. Nat Genet 27, 293-298.

Hamada, T., Yonetani, N., Ueda, C., Maesako, Y., Akasaka, H., Akasaka, T., Ohno, H., Kawakami, K., Amakawa, R., Okuma, M., 1998. Expression of the PAX5/BSAP transcription factor in haematological tumour cells and further molecular characterization of the t(9;14)(p13;q32) translocation in B-cell non-Hodgkin's lymphoma. British Journal of Haematology 102, 691-700.

Han, J., Ito, Y., Yeo, J., Sucov, H.M., Maas, R., Chai, Y., 2003. Cranial neural crest-derived mesenchymal proliferation is regulated by msx1-mediated p19ink4d expression during odontogenesis. Developmental Biology 261, 183-196.

Heltemes-Harris, L.M., Willette, M.J., Ramsey, L.B., Qiu, Y.H., Neeley, E.S., Zhang, N., Thomas, D.A., Koeuth, T., Baechler, E.C., Kornblau, S.M., Farrar, M.A., 2011. Ebf1 or Pax5 haploinsufficiency synergizes with STAT5 activation to initiate acute lymphoblastic leukemia. J Exp Med 208, 1135-1149.

Hewitt, J.E., Clark, L.N., Ivens, A., Williamson, R., 1991. Structure and sequence of the human homeobox gene HOX7. Genomics 11, 670-678.

High, F.A., Epstein, J.A., 2008. The multifaceted role of Notch in cardiac development and disease. Nat Rev Genet 9, 49-61.

High, F.A., Zhang, M., Proweller, A., Tu, L., Parmacek, M.S., Pear, W.S., Epstein, J.A., 2007. An essential role for Notch in neural crest during cardiovascular development and smooth muscle differentiation. The Journal of clinical investigation 117, 353-363.

Hilfer, S.R., Brown, J.W., 1984. The development of pharyngeal endocrine organs in mouse and chick embryos. Scan Electron Microsc 4, 2009-2022.

Hill, R.E., Jones, P.F., Rees, A.R., Sime, C.M., Justice, M.J., Copeland, N.G., Jenkins, N.A., Graham, E., Davidson, D.R., 1989. A new family of mouse homeo box-containing genes: molecular structure, chromosomal location, and developmental expression of Hox-7.1. Genes & development 3, 26-37.

Hiruma, T., Nakajima, Y., Nakamura, H., 2002. Development of pharyngeal arch arteries in early mouse embryo. J Anat 201, 15-29.

Hoang, T.T., Karkhoff-Schweizer, R.R., Kutchma, A.J., Schweizer, H.P., 1998. A broad-host-range Flp-FRT recombination system for site-specific excision of chromosomally-located DNA sequences: application for isolation of unmarked Pseudomonas aeruginosa mutants. Gene 212, 77-86.

Hu, G.Z., Lee, H., Price, S.M., Shen, M.M., Abate-Shen, C., 2001. Msx homeobox genes inhibit differentiation through upregulation of cyclin D1. Development 128, 2373-2384.

Hu, T., Yamagishi, H., Maeda, J., McAnally, J., Yamagishi, C., Srivastava, D., 2004. Tbx1 regulates fibroblast growth factors in the anterior heart field through a reinforcing autoregulatory loop involving forkhead transcription factors. Development 131, 5491-5502.

Hungerford, J.E., Owens, G.K., Argraves, W.S., Little, C.D., 1996. Development of the aortic vessel wall as defined by vascular smooth muscle and extracellular matrix markers. Dev Biol 178, 375-392.

Hurle, J.M., Colve~, E., Blanco, A.M., 1980. Development of Mouse Semilunar Valves. Anat. Embryol 160, 83-89.

Hutson, M.R., Kirby, M.L., 2003. Neural crest and cardiovascular development: a 20-year perspective. Birth defects research. Part C, Embryo today : reviews 69, 2-13.

Hutson, M.R., Kirby, M.L., 2007. Model systems for the study of heart development and disease. Cardiac neural crest and conotruncal malformations. Semin Cell Dev Biol 18, 101-110.

Ikeda, A., Zheng, Q.Y., Rosenstiel, P., Maddatu, T., Zuberi, A.R., Roopenian, D.C., North, M.A., Naggert, J.K., Johnson, K.R., Nishina, P.M., 1999. Genetic modification of heaving in tubby mice: evidence for the existence of a major gene (moth1) which protects tubby mice from hearing loss. Human molecular genetics 8, 1761-1767.

Ilagan, R., Abu-Issa, R., Brown, D., Yang, Y.P., Jiao, K., Schwartz, R.J., Klingensmith, J., Meyers, E.N., 2006. Fgf8 is required for anterior heart field development. Development 133, 2435-2445.

Ishii, M., Han, J., Yen, H.Y., Sucov, H.M., Chai, Y., Maxson, R.E., Jr., 2005. Combined deficiencies of Msx1 and Msx2 cause impaired patterning and survival of the cranial neural crest. Development 132, 4937-4950.

Ivins, S., Lammerts van Beuren, K., Roberts, C., James, C., Lindsay, E., Baldini, A., Ataliotis, P., Scambler, P.J., 2005. Microarray analysis detects differentially expressed genes in the pharyngeal region of mice lacking Tbx1. Dev Biol 285, 554-569.

Jackson, A., Kasah, S., Mansour, S.L., Morrow, B., Basson, M.A., 2014. Endoderm-specific deletion of Tbx1 reveals an FGF-independent role for Tbx1 in pharyngeal apparatus morphogenesis. Developmental dynamics : an official publication of the American Association of Anatomists 243, 1143-1151.

Jenkins, K.J., Correa, A., Feinstein, J.A., Botto, L., Britt, A.E., Daniels, S.R., Elixson, M., Warnes, C.A., Webb, C.L., 2007. Noninherited risk factors and congenital cardiovascular defects: current knowledge: a scientific statement from the American Heart Association Council on Cardiovascular Disease in the Young: endorsed by the American Academy of Pediatrics. Circulation. 115, 2995-3014.

Jerome, L.A., Papaioannou, V.E., 2001. DiGeorge syndrome phenotype in mice mutant for the T-box gene, Tbx1. Nat Genet 27, 286-291.

Kameda, Y., 2009. Hoxa3 and signaling molecules involved in aortic arch patterning and remodeling. Cell Tissue Res 336, 165-178.

Kelly, R.G., Brown, N.A., Buckingham, M.E., 2001. The arterial pole of the mouse heart forms from Fgf10-expressing cells in pharyngeal mesoderm. Dev Cell 1, 435-440.

Kelly, R.G., Buckingham, M.E., 2002. The anterior heart-forming field: voyage to the arterial pole of the heart. Trends in genetics : TIG 18, 210-216.

Kerppola, T.K., 2008. Bimolecular fluorescence complementation (BiFC) analysis as a probe of protein interactions in living cells. Annu Rev Biophys 37, 465-487.

Khadka, D., Luo, T., Sargent, T.D., 2006. Msx1 and Msx2 have shared essential functions in neural crest but may be dispensable in epidermis and axis formation in Xenopus. Int J Dev Biol 50, 499-503.

Kirby, M.L., 2002. Molecular embryogenesis of the heart. Pediatr Dev Pathol 5, 516-543.

Kirby, M.L., Bockman, D.E., 1984. Neural crest and normal development: a new perspective. The Anatomical Record 209, 1-6.

Kirby, M.L., Gale, T.F., Stewart, D.E., 1983. Neural crest cells contribute to normal aorticopulmonary septation. Science 220, 1059-1061.

Kirby, M.L., Turnage, K.L., 3rd, Hays, B.M., 1985. Characterization of conotruncal malformations following ablation of "cardiac" neural crest. Anat Rec 213, 87-93.

Kirby, M.L., Waldo, K.L., 1990. Role of neural crest in congenital heart disease. Circulation 82, 332-340.

Kist, R., Greally, E., Peters, H., 2007. Derivation of a mouse model for conditional inactivation of Pax9. Genesis 45, 460-464.

Knollmann, B.C., Schober, T., Petersen, A.O., Sirenko, S.G., Franz, M.R., 2007. Action potential characterization in intact mouse heart: steady-state cycle length dependence and electrical restitution. American journal of physiology. Heart and circulatory physiology 292, H614-621.

Kochilas, L., Merscher-Gomez, S., Lu, M.M., Potluri, V., Liao, J., Kucherlapati, R., Morrow, B., Epstein, J.A., 2002. The role of neural crest during cardiac development in a mouse model of DiGeorge syndrome. Dev Biol 251, 157-166.

Kramer, T.C., 1942. The partitioning of the truncus and conus and the formation of the membranous portion of the interventricular septum in the human heart. Am J Anat. 71, 343–370.

Kuratani, S., Kirby, M., 1992. Migration and distribution of circumpharyngeal crest cells in the chick embryo. Formation of the circumpharyngeal ridge and E/C8+ crest cells in the vertebrate head region. Anat Rec 234, 263-280.

Lai, H.C., Lin, Y.W., Huang, T.H., Yan, P., Huang, R.L., Wang, H.C., Liu, J., Chan, M.W., Chu, T.Y., Sun, C.A., Chang, C.C., Yu, M.H., 2008. Identification of novel DNA methylation markers in cervical cancer. Int J Cancer 123, 161-167.

Lawrence F. Levin, Pei Shu, Karen J. Moore, Breslow, J.L., Smith, J.D., Hayes M. Dansky, Sherri A. Charlton, John L. Sikes, Simon C. Heath, Ronit Simantov, 1999. Genetic Background Determines the Extent of Atherosclerosis in ApoE-Deficient Mice. American Heart Association 19, 1960-1968.

Lawson, A., Schoenwolf, G.C., 2003. Epiblast and primitive-streak origins of the endoderm in the gastrulating chick embryo. Development 130, 3491-3501.

Le Lievre, C.S., Le Douarin, N.M., 1975. Mesenchymal derivatives of the neural crest: analysis of chimaeric quail and chick embryos. J Embryol Exp Morphol 34, 125-154.

Lee, R.K., Stainier, D.Y., Weinstein, B.M., Fishman, M.C., 1994. Cardiovascular development in the zebrafish. II. Endocardial progenitors are sequestered within the heart field. Development 120, 3361-3366.

Li, D.W., Yang, Q., Chen, J.T., Zhou, H., Liu, R.M., Huang, X.T., 2005. Dynamic distribution of Ser-10 phosphorylated histone H3 in cytoplasm of MCF-7 and CHO cells during mitosis. Cell Res 15, 120-126.

Li, L.H., Krantz, I.D., Deng, Y., Genin, A., Banta, A.B., Collins, C.C., Qi, M., Trask, B.J., Kuo, W.L., Cochran, J., Costa, T., Pierpont, M.E.M., Rand, E.B., Piccoli, D.A.,

Hood, L., Spinner, N.B., 1997. Alagille syndrome is caused by mutations in human Jagged1, which encodes a ligand for Notch1. Nature Genetics 16, 243-251.

Li, P., Pashmforoush, M., Sucov, H.M., 2012. Mesodermal retinoic acid signaling regulates endothelial cell coalescence in caudal pharyngeal arch artery vasculogenesis. Dev Biol 361, 116-124.

Lidral, A.C., Romitti, P.A., Basart, A.M., Doetschman, T., Leysens, N.J., Daack-Hirsch, S., Semina, E.V., Johnson, L.R., Junichiro Machida, Burds, A., Parnell, T.J., Rubenstein, J.L.R., Murray, J.C., 1998. Association of MSX1 and TGFB3 with Nonsyndromic Clefting in Humans. Am. J. Hum. Genet 63, 557-568.

Lindsay, E.A., Baldini, A., 2001. Recovery from arterial growth delay reduces penetrance of cardiovascular defects in mice deleted for the DiGeorge syndrome region. Human molecular genetics 10, 997-1002.

Lindsay, E.A., Botta, A., Jurecic, V., Carattini-Rivera, S., Cheah, Y.C., Rosenblatt, H.M., Bradley, A., Baldini, A., 1999. Congenital heart disease in mice deficient for the DiGeorge syndrome region. Nature 401, 379-383.

Lindsay, E.A., Vitelli, F., Su, H., Morishima, M., Huynh, T., Pramparo, T., Jurecic, V., Ogunrinu, G., Sutherland, H.F., Scambler, P.J., Bradley, A., Baldini, A., 2001. Tbx1 haploinsufficiency in the DiGeorge syndrome region causes aortic arch defects in mice. Nature 410, 97-101.

Liu, J., Bressan, M., Hassel, D., Huisken, J., Staudt, D., Kikuchi, K., Poss, Kenneth D., Mikawa, T., Stainier, D.Y.R., 2010. A dual role for ErbB2 signaling in cardiac trabeculation. Development 137, 3867-3875.

Liu, Y.H., Kundu, R., Wu, L., Luo, W., Ignelzi, M.A., Jr., Snead, M.L., Maxson, R.E., Jr., 1995. Premature suture closure and ectopic cranial bone in mice expressing Msx2 transgenes in the developing skull. Proc Natl Acad Sci U S A 92, 6137-6141.

Lopez-Sanchez, C., Garcia-Martinez, V., 2011. Molecular determinants of cardiac specification. Cardiovasc Res 91, 185-195.

Maarten Bergwerff, Verberne, M.E., , M.C.D., Robert E. Poelmann, Groot, A.C.G.-d., 1998. Neural Crest Cell Contribution to the Developing Circulatory System Implications for Vascular Morphology? Circulation Research 82, 221-231.

Macatee, T.L., Hammond, B.P., Arenkiel, B.R., Francis, L., Frank, D.U., Moon, A.M., 2003. Ablation of specific expression domains reveals discrete functions of ectoderm- and endoderm-derived FGF8 during cardiovascular and pharyngeal development. Development 130, 6361-6374.

Macchia, P.E., Lapi, P., Krude, H., Pirro, M.T., Missero, C., Chiovato, L., Souabni, A., Baserga, M., Tassi, V., Pinchera, A., Fenzi, G., Gruters, A., Busslinger, M., Di Lauro, R., 1998. PAX8 mutations associated with congenital hypothyroidism caused by thyroid dysgenesis. Nat Genet 19, 83-86.

MacKenzie, A., Ferguson, M.W., Sharpe, P.T., 1991a. Hox-7 expression during murine craniofacial development. Development 113, 601-611.

Mackenzie, A., Leeming, G.L., Jowett, A.K., Ferguson, M.W., Sharpe, P.T., 1991b. The homeobox gene Hox 7.1 has specific regional and temporal expression patterns during early murine craniofacial embryogenesis, especially tooth development in vivo and in vitro. Development 111, 269-285.

Mallo, M., 2001. Formation of the middle ear: recent progress on the developmental and molecular mechanisms. Dev Biol 231, 410-419.

Manderfield, L.J., High, F.A., Engleka, K.A., Liu, F., Li, L., Rentschler, S., Epstein, J.A., 2012. Notch activation of Jagged1 contributes to the assembly of the arterial wall. Circulation 125, 314-323.

Männer, J., 2009. The Anatomy of Cardiac Looping: A Step Towards the Understanding of the Morphogenesis of Several Forms of Congenital Cardiac Malformations. Clinical Anatomy 22, 21-35.

McCright, B., Lozier, J., Gridley, T., 2002. A mouse model of Alagille syndrome: Notch2 as a genetic modifier of Jag1 haploinsufficiency. Development 129, 1075-1082.

McDermott-Lancaster, R.D., Ito, T., Kohsaka, K., Colston, M.J., 1987. The nude mouse--characteristics, breeding and husbandry. Int J Lepr Other Mycobact Dis. 55, 885-888.

McGaughran, J.M., Oates, A., Donnai, D., Read, A.P., Tassabehji, M., 2003. Mutations in PAX1 may be associated with Klippel-Feil syndrome. European Journal of Human Genetics 11, 468-474.

Mead, T.J., Yutzey, K.E., 2012. Notch pathway regulation of neural crest cell development in vivo. Developmental dynamics : an official publication of the American Association of Anatomists 241, 376-389.

Medio, M., Yeh, E., Popelut, A., Babajko, S., Berdal, A., Helms, J.A., 2012. Wnt/beta-catenin signaling and Msx1 promote outgrowth of the maxillary prominences. Front Physiol 3, 375.

Meeson, A., Palmer, M., Calfon, M., Lang, R., 1996. A relationship between apoptosis and flow during programmed capillary regression is revealed by vital analysis. Development 122, 3929-3938.

Meilhac, S.n.M., Esner, M., Kelly, R.G., Nicolas, J.-F.o., Buckingham, M.E., 2004. The Clonal Origin of Myocardial Cells in Different Regions of the Embryonic Mouse Heart. Developmental Cell 6, 685–698.

Merscher, S., Funke, B., Epstein, J.A., Heyer, J., Puech, A., Lu, M.M., Xavier, R.J., Demay, M.B., Russell, R.G., Factor, S., Tokooya, K., Jore, B.S., Lopez, M., Pandita, R.K., Lia, M., Carrion, D., Xu, H., Schorle, H., Kobler, J.B., Scambler, P., Wynshaw-Boris, A., Skoultchi, A.I., Morrow, B.E., Kucherlapati, R., 2001. TBX1 is responsible for cardiovascular defects in Velo-Cardio-Facial/DiGeorge syndrome. Cell 104, 619-629.

Miller, A.R., Hawkins, N.A., McCollom, C.E., Kearney, J.A., 2014. Mapping genetic modifiers of survival in a mouse model of Dravet syndrome. Genes Brain Behav 13, 163-172.

Ming, J.E., Muenke, M., 2002. Multiple hits during early embryonic development: digenic diseases and holoprosencephaly. American journal of human genetics 71, 1017-1032.

Minoux, M., Rijli, F.M., 2010. Molecular mechanisms of cranial neural crest cell migration and patterning in craniofacial development. Development 137, 2605-2621.

Mjaatvedt, C.H., Markwald, R.R., 1989. Induction of an epithelial-mesenchymal transition by an in vivo adheron-like complex. Dev Biol 136, 118-128.

Mjaatvedt, C.H., Nakaoka, T., Moreno-Rodriguez, R., Norris, R.A., Kern, M.J., Eisenberg, C.A., Turner, D., Markwald, R.R., 2001. The outflow tract of the heart is recruited from a novel heart-forming field. Dev Biol 238, 97-109.

Molin, D., Deruiter, M., Wisse, L., Azhar, M., Doetschman, T., Poelmann, R., Gittenbergerdegroot, A., 2002. Altered apoptosis pattern during pharyngeal arch artery remodelling is associated with aortic arch malformations in Tgfβ2 knock-out mice. Cardiovascular Research 56, 312-322.

Monaghan, A.P., Davidson, D.R., Sime, C., Graham, E., Baldock, R., Bhattacharya, S.S., Hill, R.E., 1991. The Msh-like homeobox genes define domains in the developing vertebrate eye. Development 112, 1053-1061.

Moretti, A., Caron, L., Nakano, A., Lam, J.T., Bernshausen, A., Chen, Y., Qyang, Y., Bu, L., Sasaki, M., Martin-Puig, i., Sun, Y., Evans, S.M., Laugwitz, K.-L., Chien, K.R., 2006. Multipotent Embryonic Isl1+ Progenitor Cells Lead to Cardiac, Smooth Muscle, and Endothelial Cell Diversification. cell 127, 1151–1165.

Morris, E.W., 1957. The interventricular septum. Thorax 12, 304-312.

Muller, T.S., Ebensperger, C., Neubuser, A., Koseki, H., Balling, R., Christ, B., Wilting, J., 1996. Expression of avian Pax1 and Pax9 is intrinsically regulated in the pharyngeal endoderm, but depends on environmental influences in the paraxial mesoderm. Dev Biol 178, 403-417.

Muneoka, K., Sassoon, D., 1992. Molecular aspects of regeneration in developing vertebrate limbs. Dev Biol 152, 37-49.

Muratovska, A., Zhou, C.M., He, S.J., Goodyer, P., Eccles, M.R., 2003. Paired-box genes are frequently expressed in cancer and often required for cancer cell survival. Oncogene 22, 7989-7997.

Nadeau, J.H., 2001. Modifier genes in mice and humans. Nat Rev Genet 2, 165-174.

Nagaraja, P., Singh, N.G., Simha, P.P., KR Davan, V.M., Jagadeesh, A., 2015. Role of perioperative transesophageal echocardiography in the management of adolescent truncus arteriosus: Rare case report. World J Pediatr Congenit Heart Surg. 18, 234-236.

Nagel, S., Ehrentraut, S., Meyer, C., Kaufmann, M., Drexler, H.G., MacLeod, R.A., 2014. Oncogenic deregulation of NKL homeobox gene MSX1 in mantle cell lymphoma. Leuk Lymphoma 55, 1893-1903.

Nakatomi, M., Wang, X.P., Key, D., Lund, J.J., Turbe-Doan, A., Kist, R., Aw, A., Chen, Y., Maas, R.L., Peters, H., 2010. Genetic interactions between Pax9 and Msx1 regulate lip development and several stages of tooth morphogenesis. Dev Biol 340, 438-449.

Newberry, E.P., Latifi, T., Battaile, J.T., Towler, D.A., 1997. Structure-function analysis of Msx2-mediated transcriptional suppression. Biochemistry 36, 10451-10462.

Nishibatake, M., Kirby, M.L., Mierop, L.H.S.V., 1987. Pathogenesis of persistent truncus arteriosus and dextroposed aorta in the chick embryo after neural crest ablation. Circulation 75, 255-264.

Nishimoto, K., Iijima, K., Shirakawa, T., Kitagawa, K., Satomura, K., Nakamura, H., Yoshikawa, N., 2001. PAX2 gene mutation in a family with isolated renal hypoplasia. J Am Soc Nephrol 12, 1769-1772.

Oda, T., Elkahloun, A.G., Pike, B.L., Okajima, K., Krantz, I.D., Genin, A., Piccoli, D.A., Meltzer, P.S., Spinner, N.B., Collins, F.S., Chandrasekharappa, S.C., 1997. Mutations in the human Jagged1 gene are responsible for Alagille syndrome. Nat Genet 16, 235-242.

Ogawa, T., Kapadia, H., Feng, J.Q., Raghow, R., Peters, H., D'Souza, R.N., 2006. Functional consequences of interactions between Pax9 and Msx1 genes in normal and abnormal tooth development. Journal of Biological Chemistry 281, 18363-18369.

Ogawa, T., Kapadia, H., Wang, B., D'Souza, R.N., 2005. Studies on Pax9-Msx1 protein interactions. Arch Oral Biol 50, 141-145.

Okubo, T., Kawamura, A., Takahashi, J., Yagi, H., Morishima, M., Matsuoka, R., Takada, S., 2011. Ripply3, a Tbx1 repressor, is required for development of the pharyngeal apparatus and its derivatives in mice. Development 138, 339-348.

Olaopa, M., Zhou, H.M., Snider, P., Wang, J., Schwartz, R.J., Moon, A.M., Conway, S.J., 2011. Pax3 is essential for normal cardiac neural crest morphogenesis but is not required during migration nor outflow tract septation. Dev Biol 356, 308-322.

Olson, E.N., Schneider, M.D., 2003. Sizing up the heart: development redux in disease. Genes & development 17, 1937-1956.

Olson, M.V., 1999. When less is more: Gene loss as an engine of evolutionary change. American journal of human genetics 64, 18-23.

Padge, D.H., 1948. The development of the cranial arteries in the human embryo, Washington.

Paixao-Cortes, V.R., Braga, T., Salzano, F.M., Mundstock, K., Mundstock, C.A., Bortolini, M.C., 2011a. PAX9 and MSX1 transcription factor genes in non-syndromic dental agenesis. Arch Oral Biol 56, 337-344.

Paixao-Cortes, V.R., Meyer, D., Pereira, T.V., Mazieres, S., Elion, J., Krishnamoorthy, R., Zago, M.A., Silva, W.A., Jr., Salzano, F.M., Bortolini, M.C., 2011b. Genetic variation among major human geographic groups supports a peculiar evolutionary trend in PAX9. PLoS One 6, e15656.

Papaioannou, V.E., Silver, L.M., 1998. The T-box gene family. Bioessays 20, 9-19.

Papoutsi, T., Odelin, G., Moore-Morris, T., Puceat, M., de la Pompa, J.L., Robert, B., Zaffran, S., 2015. Msx1CreERT2 knock-In allele: A useful tool to target embryonic and adult cardiac valves. Genesis 53, 337-345.

Paylor, R., Lindsay, E., 2006. Mouse models of 22q11 deletion syndrome. Biol Psychiatry 59, 1172-1179.

Pelleitier, M., Montplaisir, S., 1975. The nude mouse: a model of deficient T-cell function. Methods Achiev Exp Pathol 7, 149-166.

Pereira, T.V., Salzano, F.M., Mostowska, A., Trzeciak, W.H., Ruiz-Linares, A., Chies, J.A., Saavedra, C., Nagamachi, C., Hurtado, A.M., Hill, K., Castro-de-Guerra, D., Silva-Junior, W.A., Bortolini, M.C., 2006. Natural selection and molecular evolution in primate PAX9 gene, a major determinant of tooth development. Proc Natl Acad Sci U S A 103, 5676-5681.

Peters, H., Neubüser, A., Kratochwil, K., 1998. exhibit craniofacial and limb abnormalities Pax9-deficient mice lack pharyngeal pouch derivatives and teeth and. Genes Development 12, 2735-2747.

Prescott, K., Ivins, S., Hubank, M., Lindsay, E., Baldini, A., Scambler, P., 2005. Microarray analysis of the Df1 mouse model of the 22q11 deletion syndrome. Hum Genet 116, 486-496.

Psychoyos, D., Stern, C.D., 1996. Fates and migratory routes of primitive streak cells in the chick embryo. Development 122, 1523-1534.

Rachel, R.A., Yamamoto, E.A., Dewanjee, M.K., May-Simera, H.L., Sergeev, Y.V., Hackett, A.N., Pohida, K., Munasinghe, J., Gotoh, N., Wickstead, B., Fariss, R.N., Dong, L., Li, T., Swaroop, A., 2015. CEP290 alleles in mice disrupt tissue-specific cilia biogenesis and recapitulate features of syndromic ciliopathies. Human molecular genetics 24, 3775-3791.

Rajbanshi, B.G., Gautam, N.C., Pradhan, S., Sharma, A., Ghimire, R.K., Joyce, L.D., 2016. Complex Cervical Aortic Arch With Hypoplasia: A Simple Solution to a Complex Problem. Ann Thorac Surg 102, e27-29.

Ramsbottom, S., Miles, C., Sayer, J., 2015. Murine Cep290 phenotypes are modified by genetic backgrounds and provide an impetus for investigating disease modifier alleles. F1000Res 4, 590.

Reardon, M.J., Hallman, G.L., Cooley, D.A., 1984. Interrupted aortic arch: brief review and summary of an eighteen-year experience. Tex Heart Inst J 11, 250-259.

Robert, B., Sassoon, D., Jacq, B., Gehring, W., Buckingham, M., 1989. Hox-7, a mouse homeobox gene with a novel pattern of expression during embryogenesis. The EMBO Journal 8, 91-100.

Roberts, C., Sutherland, H.F., Farmer, H., Kimber, W., Halford, S., Carey, A., Brickman, J.M., Wynshaw-Boris, A., Scambler, P.J., 2002. Targeted mutagenesis of the Hira gene results in gastrulation defects and patterning abnormalities of mesoendodermal derivatives prior to early embryonic lethality. Mol Cell Biol 22, 2318-2328.

Roberts, L.K., Gerald, B., 1978. Absence of Both Common Carotid Arteries. American Journal of Roentgenology 130, 981-982.

Ros, M.A., Lyons, G., Kosher, R.A., Upholt, W.B., Coelho, C.N., Fallon, J.F., 1992. Apical ridge dependent and independent mesodermal domains of GHox-7 and GHox-8 expression in chick limb buds. Development 116, 811-818.

Saint-Jeannet, J.P., Levi, G., Girault, J.M., Koteliansky, V., Thiery, J.P., 1992. Ventrolateral regionalization of Xenopus laevis mesoderm is characterized by the expression of alpha-smooth muscle actin. Development 115, 1165-1173.

Saitta, S.C., McGrath, J.M., Mensch, H., Shaikh, T.H., Zackai, E.H., Emanuel, B.S., 1999. A 22q11.2 deletion that excludes UFD1L and CDC45L in a patient with conotruncal and craniofacial defects. American journal of human genetics 65, 562-566.

Santagati, F., Rijli, F.M., 2003. Cranial neural crest and the building of the vertebrate head. Nat Rev Neurosci 4, 806-818.

Santen, G.W.E., Sun, Y., Gijsbers, A.C.J., Carre, A., Holvoet, M., van Haeringen, A., Oberstein, S.A.J.L., Tomoda, A., Mabe, H., Polak, M., Devriendt, K., Ruivenkamp, C.A.L., Bijlsma, E.K., 2012. Further delineation of the phenotype of chromosome 14q13 deletions: (positional) involvement of FOXG1 appears the main determinant of

phenotype severity, with no evidence for a holoprosencephaly locus. Journal of Medical Genetics 49, 366-372.

Sato, T., Sasai, N., Sasai, Y., 2005. Neural crest determination by co-activation of Pax3 and Zic1 genes in Xenopus ectoderm. Development 132, 2355-2363.

Satoh, K., Ginsburg, E., Vonderhaar, B.K., 2004. Msx-1 and Msx-2 in mammary gland development. J Mammary Gland Biol Neoplasia 9, 195-205.

Satokata, I., Maas, R., 1994. Msx1 deficient mice exhibit cleft palate and abnormalities of craniofacial and tooth development. Nat Genet 6, 348-356.

Sauer, B., 1998. Inducible gene targeting in mice using the Cre/lox system. Methods 14, 381-392.

Savolainen, S.M., Foley, J.F., Elmore, S.A., 2009. Histology atlas of the developing mouse heart with emphasis on E11.5 to E18.5. Toxicol Pathol 37, 395-414.

Scambler, P.J., 2000. The 22q11 deletion syndromes. Human Molecular Genetics 9, 2421-2426.

Schneider, D.J., Moore, J.W., 2006. Patent ductus arteriosus. Circulation 114, 1873-1882.

Seale, P., Sabourin, L.A., Girgis-Gabardo, A., Mansouri, A., Gruss, P., Rudnicki, M.A., 2000. Pax7 is required for the specification of myogenic satellite cells. Cell 102, 777-786.

Sedmera, D., McQuinn, T., 2008. Embryogenesis of heart muscle. Heart Fail Clin 4, 235-245.

Sharrocks, A.D., 2001. The ETS-domain transcription factor family. Nat Rev Mol Cell Biol 2, 827-837.

Shimelda, S.M., McKayb, I.J., Sharpe, P.T., 1996. The murine homeobox gene Msx-3 shows highly restricted expression in the developing neural tube Mechanisms of Development 55, 201-210.

Shimizu, Y., Kanetaka, H., Kim, Y.H., Okayama, K., Kano, M., Kikuchi, M., 2005. Age-related morphological changes in the human hyoid bone. Cells Tissues Organs 180, 185-192.

Shuford, W.H., Sybers, R.G., Milledge, R.D., Brinsfield, D., 1972. The cervical aortic arch. Am J Roentgenol Radium Ther Nucl Med 116, 519-527.

Sigmund, C.D., 2000. Viewpoint: Are Studies in Genetically Altered Mice Out of Control? American Heart Association, 1425-1429.

Sivakamasundari, V., Kraus, P., Jie, S., Lufkin, T., 2013. Pax1(EGFP): new wildtype and mutant EGFP mouse lines for molecular and fate mapping studies. Genesis 51, 420-429.

Song, K., Wang, Y., Sassoon, D., 1992. Expression of Hox-7.1 in myoblasts inhibits terminal differentiation and induces cell transformation. Nature 360, 477-481.

Soriano, P., 1999. Generalized lacZ expression with the ROSA26 Cre reporter strain. Nat Genet 21, 70-71.

Srinivas, S., Watanabe, T., Lin, C., William, C.M., Tanabe, Y., Jessell, T.M., Costantini, F., 2001. Cre reporter strains produced by targeted insertion of EYFP and ECFP into the ROSA26 locus. BMC Developmental Biology 1, 4-4.

Stockton, D.W., Das, P., Goldenberg, M., D'Souza, R.N., Patel, P.I., 2000. Mutation of PAX9 is associated with oligodontia. Nature Genetics 24, 18-19.

Strachan, T., Read, A.P., 1994. PAX genes. Curr Opin Genet Dev 4, 427-438.

Stuart, E.T., Kioussi, C., Gruss, P., 1994. Mammalian Pax genes. Annu Rev Genet. 28, 219-236.

Sundaram, P.S., Sukulal, K., Bijulal, S., Tharakan, J.A., 2014. Cervical origin of left subclavian artery: A rare anomaly. Ann Pediatr Cardiol 7, 227-229.

Suntratonpipat, S., Bamforth, S.D., Johnson, A.L., Noga, M., Anderson, R.H., Smallhorn, J., Tham, E., 2015. Childhood presentation of interrupted aortic arch with persistent carotid ducts. World J Pediatr Congenit Heart Surg 6, 335-338.

Tadros, T.M., Klein, M.D., Shapira, O.M., 2009. Ascending Aortic Dilatation Associated With Bicuspid Aortic Valve. Cirulation 119.

Takahashi, Y., Bontoux, M., Le Douarin, N.M., 1991. Epithelio--mesenchymal interactions are critical for Quox 7 expression and membrane bone differentiation in the neural crest derived mandibular mesenchyme. EMBO J 10, 2387-2393.

Tassabehji, M., Read, A.P., Newton, V.E., Patton, M., Gruss, P., Harris, R., Strachan, T., 1993. Mutations in the PAX3 gene causing Waardenburg syndrome type 1 and type 2. Nat Genet 3, 26-30.

Tesfaye, D., Regassa, A., Rings, F., Ghanem, N., Phatsara, C., Tholen, E., Herwig, R., Un, C., Schellander, K., Hoelker, M., 2010. Suppression of the transcription factor MSX1 gene delays bovine preimplantation embryo development in vitro. Reproduction. 139, 857–870.

Thomas, K.F., Capecchi, M.R., 1987. Site-Directed Mutagenesis by Gene Targeting in Mouse Embryo-Derived Stem Cells cell 51, 503-512.

Tiraboschi, R., Crupi, G., Locatelli, G., Ho, S.Y., Parenzan, L., 1980. Cervical aortic arch with aortic obstruction: report of two cases. Thorax 35, 26-30.

Trainor, P.A., Krumlauf, R., 2001. Hox genes, neural crest cells and branchial arch patterning. Curr Opin Cell Biol 13, 698-705.

Turkvatan, A., Buyukbayraktar, F.G., Olcer, T., Cumhur, T., 2009. Congenital anomalies of the aortic arch: evaluation with the use of multidetector computed tomography. Korean J Radiol 10, 176-184.

Tuz, K., Bachmann-Gagescu, R., O'Day, D.R., Hua, K., Isabella, C.R., Phelps, I.G., Stolarski, A.E., O'Roak, B.J., Dempsey, J.C., Lourenco, C., Alswaid, A., Bonnemann, C.G., Medne, L., Nampoothiri, S., Stark, Z., Leventer, R.J., Topcu, M., Cansu, A., Jagadeesh, S., Done, S., Ishak, G.E., Glass, I.A., Shendure, J., Neuhauss, S.C., Haldeman-Englert, C.R., Doherty, D., Ferland, R.J., 2014. Mutations in CSPP1 cause primary cilia abnormalities and Joubert syndrome with or without Jeune asphyxiating thoracic dystrophy. American journal of human genetics 94, 62-72.

Umeda, T., Takashima, N., Nakagawa, R., Maekawa, M., Ikegami, S., Yoshikawa, T., Kobayashi, K., Okanoya, K., Inokuchi, K., Osumi, N., 2010. Evaluation of Pax6 mutant rat as a model for autism. PLoS One 5, e15500.

Vaickus, L.J., Bouchard, J., Kim, J., Natarajan, S., Remick, D.G., 2010. Inbred and Outbred Mice Have Equivalent Variability in a Cockroach Allergen-Induced Model of Asthma. Comparative Medicine 60, 420-426.

Van Heyningen, V., Williamson, K.A., 2002. PAX6 in sensory development. Human molecular genetics 11, 1161-1167.

Van Mierop, L.H., 1979. Embryology of the univentricular heart. Herz 4, 78-85.

Vaz, S.O., Pires, R., Pires, L.M., Carreira, I.M., Anjos, R., Maciel, P., Mota-Vieira, L., 2015. A unique phenotype in a patient with a rare triplication of the 22q11.2 region and new clinical insights of the 22q11.2 microduplication syndrome: a report of two cases. BMC Pediatr 15, 95.

Veitch, E., Begbie, J., Schilling, T.F., Smith, M.M., Graham, A., 1999. Pharyngeal arch patterning in the absence of neural crest. Curr Biol 9, 1481-1484.

Vitelli, F., Morishima, M., Taddei, I., Lindsay, E.A., Baldini, A., 2002. Tbx1 mutation causes multiple cardiovascular defects and disrupts neural crest and cranial nerve migratory pathways. Human molecular genetics 11, 915-922.

Wadey, R., McKie, J., Papapetrou, C., Sutherland, H., Lohman, F., Osinga, J., Frohn, I., Hofstra, R., Meijers, C., Amati, F., Conti, E., Pizzuti, A., Dallapiccola, B., Novelli, G., Scambler, P., 1999. Mutations of UFD1L are not responsible for the majority of cases of DiGeorge Syndrome/velocardiofacial syndrome without deletions within chromosome 22q11. American journal of human genetics 65, 247-249.

Waldo, K.L., Hutson, M.R., Stadt, H.A., Zdanowicz, M., Zdanowicz, J., Kirby, M.L., 2005. Cardiac neural crest is necessary for normal addition of the myocardium to the arterial pole from the secondary heart field. Dev Biol 281, 66-77.

Waldo, K.L., Kirby, M.L., 1993. Cardiac neural crest contribution to the pulmonary artery and sixth aortic arch artery complex in chick embryos aged 6 to 18 days. Anat Rec 237, 385-399.

Waldo, K.L., Kumiski, D., Kirby, M.L., 1996. Cardiac neural crest is essential for the persistence rather than the formation of an arch artery. Developmental Dynamics 205, 281-292.

Waldo, K.L., Kumiski, D.H., Wallis, K.T., Stadt, H.A., Hutson, M.R., Platt, D.H., Kirby, M.L., 2001. Conotruncal myocardium arises from a secondary heart field. Development 128, 3179-3188.

Wallin, J., Eibel, H., Neubuser, A., Wilting, J., Koseki, H., Balling, R., 1996. Pax1 is expressed during development of the thymus epithelium and is required for normal T-cell maturation. Development 122, 23-30.

Wallin, J., Mizutani, Y., Imai, K., Miyashita, N., Moriwaki, K., Taniguchi, M., Koseki, H., Bailing, R., 1993. A new Pax gene, Pax-9, maps to mouse Chromosome 12 Mammalian Genome 4, 354-358.

Walther, C., Guenet, J.L., Simon, D., Deutsch, U., Jostes, B., Goulding, M.D., Plachov, D., Balling, R., Gruss, P., 1991. Pax: a murine multigene family of paired box-containing genes. Genomics 11, 424-434.

Webb, S., Qayyum, S.R., Anderson, R.H., Lamers, W.H., Richardson, M.K., 2003. Septation and separation within the outflow tract of the developing heart. Journal of Anatomy 202, 327-342.

Wilkie, A.O., Tang, Z., Elanko, N., Walsh, S., Twigg, S.R., Hurst, J.A., Wall, S.A., Chrzanowska, K.H., Maxson, R.E., Jr., 2000. Functional haploinsufficiency of the human homeobox gene MSX2 causes defects in skull ossification. Nat Genet 24, 387-390.

Winyard, P.J., Risdon, R.A., Sams, V.R., Dressler, G.R., Woolf, A.S., 1996. The PAX2 tanscription factor is expressed in cystic and hyperproliferative dysplastic epithelia in human kidney malformations. The Journal of clinical investigation 98, 451-459.

Woloshin, P., Song, K., Degnin, C., Killary, A., Goldhamer, D.J., Sassoon, D., Thayer, M.J., 1995. MSX1 inhibits MyoD expression in fibroblast × 10T½ cell hybrids. Cell 82, 611-620.

Wong, M.D., Dorr, A.E., Walls, J.R., Lerch, J.P., Henkelman, R.M., 2012. A novel 3D mouse embryo atlas based on micro-CT. Development 139, 3248-3256.

Xu, H., Cerrato, F., Baldini, A., 2005. Timed mutation and cell-fate mapping reveal reiterated roles of Tbx1 during embryogenesis, and a crucial function during segmentation of the pharyngeal system via regulation of endoderm expansion. Development 132, 4387-4395.

Yamagishi, H., Maeda, J., Hu, T., McAnally, J., Conway, S.J., Kume, T., Meyers, E.N., Yamagishi, C., Srivastava, D., 2003. Tbx1 is regulated by tissue-specific forkhead proteins through a common Sonic hedgehog-responsive enhancer. Genes & development 17, 269-281.

Yang, L., Cai, C.L., Lin, L., Qyang, Y., Chung, C., Monteiro, R.M., Mummery, C.L., Fishman, G.I., Cogen, A., Evans, S., 2006. Isl1Cre reveals a common Bmp pathway in heart and limb development. Development 133, 1575-1585.

Yogarajah, M., Matarin, M., Vollmar, C., Thompson, P.J., Duncan, J.S., Symms, M., Moore, A.T., Liu, J., Thom, M., van Heyningen, V., Sisodiya, S.M., 2016. PAX6, brain structure and function in human adults: advanced MRI in aniridia. Ann Clin Transl Neurol 3, 314-330.

Zammit, P.S., Relaix, F., Nagata, Y., Ruiz, A.P., Collins, C.A., Partridge, T.A., Beauchamp, J.R., 2006. Pax7 and myogenic progression in skeletal muscle satellite cells. J Cell Sci 119, 1824-1832.

Zannini, M., Francis-Lang, H., Plachov, D., Di Lauro, R., 1992. Pax-8, a paired domain-containing protein, binds to a sequence overlapping the recognition site of a homeodomain and activates transcription from two thyroid-specific promoters. Mol Cell Biol 12, 4230-4241.

Zhang, J., Ko, J.M., Guileyardo, J.M., Roberts, W.C., 2015. A review of spontaneous closure of ventricular septal defect. Proc (Bayl Univ Med Cent) 28, 516-520.

Zhang, Z., Cerrato, F., Xu, H., Vitelli, F., Morishima, M., Vincentz, J., Furuta, Y., Ma, L., Martin, J.F., Baldini, A., Lindsay, E., 2005. Tbx1 expression in pharyngeal

epithelia is necessary for pharyngeal arch artery development. Development 132, 5307-5315.

Zhang, Z., Huynh, T., Baldini, A., 2006. Mesodermal expression of Tbx1 is necessary and sufficient for pharyngeal arch and cardiac outflow tract development. Development 133, 3587-3595.